

Aus dem Bereich Physiologie
Theoretische Medizin und Biowissenschaften
der Medizinischen Fakultät
der Universität des Saarlandes, Homburg/Saar

**ASTROGLIAL GABA_B RECEPTOR DELETION PROTECTS AGAINST
γ-HYDROXYBUTYRIC ACID-INDUCED ABSENCE SEIZURES**

DISSERTATION

ZUR ERLANGUNG DES GRADES EINES DOKTORS DER NATURWISSENSCHAFTEN

**DER MEDIZINISCHEN FAKULTÄT
DER UNIVERSITÄT DES SAARLANDES**

2023

vorgelegt von: Davide Gobbo
geb. am: 07. April 1993 in Cittadella (IT)

Date of oral examination: 04. September 2023

Dean of the faculty: **Univ.-Prof. Dr. med. Michael D. Menger**

Examinants: **Prof. Dr. Frank Kirchhoff** - University of Saarland
Prof. Dr. Jutta Engel - University of Saarland
Prof. Dr. Christian Lohr - University of Hamburg



This project has received funding from the European Union's Horizon 2020 research and innovation programme under the Marie Skłodowska Curie grant agreement No 722053.

EIDESSTATTLICHE ERKLÄRUNG

Ich erkläre hiermit an Eides statt, dass ich die vorliegende Arbeit ohne unzulässige Hilfe Dritter und ohne Benutzung anderer als der angegebenen Hilfsmittel angefertigt habe; die aus anderen Quellen direkt oder indirekt übernommenen Daten und Konzepte sind unter Angabe des Literaturzitats gekennzeichnet.

Bei der Auswahl und Auswertung folgenden Materials haben mir die nachstehend aufgeführten Personen in der jeweils beschriebenen Weise entgeltlich/unentgeltlich geholfen:

Vor- und Nachname: **Fang Lipao** _____ entgeltlich unentgeltlich

Beitrag: **MACs-Sortierung von Astrozyten und Western Blot Analyse (Figure 9)** _____

Vor- und Nachname: **Guo Qilin** _____ entgeltlich unentgeltlich

Beitrag: **Kryostatbetrieb für RNAscope Analyse (Figure 8)** _____

Vor- und Nachname: **Dr. Huang Wenhui** _____ entgeltlich unentgeltlich

Beitrag: **RNAscope Analyse (Figure 8)** _____

Vor- und Nachname: **Dr. Scheller Anja** _____ entgeltlich unentgeltlich

Beitrag: **AxioScan.Z1 Epifluoreszenzmikroskopbetrieb** _____

Weitere Personen waren an der inhaltlich-materiellen Herstellung der vorliegenden Arbeit nicht beteiligt. Insbesondere habe ich hierfür nicht die entgeltliche Hilfe eines Promotionsberaters oder anderer Personen in Anspruch genommen. Niemand hat von mir weder unmittelbar noch mittelbar geldwerte Leistungen für Arbeiten erhalten, die im Zusammenhang mit dem Inhalt der vorgelegten Dissertation stehen.

Die Arbeit wurde bisher weder im In- noch im Ausland in gleicher oder ähnlicher Form einer anderen Prüfungsbehörde vorgelegt.

Ich versichere an Eides Statt, dass ich nach bestem Wissen die reine Wahrheit gesagt und nichts verschwiegen habe.

Die Bedeutung der eidesstattlichen Erklärung und die strafrechtlichen Folgen einer unrichtigen oder unvollständigen eidesstattlichen Erklärung sind mir bekannt.

Ort, Datum _____

Unterschrift der/des Promovierenden _____

TABLE OF CONTENTS

Eidesstattliche Erklärung	i
List of Abbreviations	v
List of Figures	vii
List of Tables	viii
List of Supplementary Materials	ix
Supplementary Figures	ix
Supplementary Tables.....	ix
Supplementary Videos.....	ix
1 ABSTRACT	1
2 GRAPHICAL ABSTRACT	2
3 ZUSAMMENFASSUNG	3
4 INTRODUCTION	4
4.1 Astrocytes at the centre of the neural <i>active milieu</i>	4
4.1.1 <i>E pluribus unum, ex uno plures</i> : astroglial identity and heterogeneity.....	4
4.1.2 CNS homeostasis and astroglial function.....	5
4.1.3 An astroglial point of view on synaptic transmission.....	6
4.1.4 Astrocytic Ca ²⁺ signalling	7
4.2 Epilepsy	10
4.2.1 Absence seizures.....	11
4.3 An astroglial point of view on absence seizures	17
4.3.1 Astrocytes control extracellular space homeostasis.....	17
4.3.2 Glutamatergic and GABAergic astroglial alterations in absence seizures	18
4.3.3 Astroglial Ca ²⁺ signalling in absence seizures: the state of the art	21
5 AIMS OF THE STUDY	22
6 MATERIALS AND METHODS	23
6.1 Materials	23
6.1.1 Reagents.....	23
6.1.2 Consumables	23
6.1.3 Devices.....	23

6.1.4	Buffers.....	24
6.1.5	Enzymes.....	26
6.1.6	Drugs.....	26
6.1.7	Antibodies.....	27
6.1.8	Dyes.....	28
6.1.9	Primers.....	28
6.1.10	Genetically modified mouse lines.....	29
6.1.11	Software.....	30
6.1.12	Graphical elements.....	31
6.2	Methods.....	31
6.2.1	Genotyping.....	31
6.2.2	Tamoxifen treatment.....	32
6.2.3	Tissue collection.....	32
6.2.4	Magnetic cell separation.....	32
6.2.5	Western blot analysis.....	33
6.2.6	Whole body fixation.....	33
6.2.7	Immunohistochemistry.....	33
6.2.8	RNAscope.....	34
6.2.9	Acute slice preparation.....	34
6.2.10	Surgical procedures.....	37
6.2.11	Open field test.....	40
6.2.12	Microscopy.....	41
6.2.13	Data analysis.....	42
6.2.14	Mouse administration and veterinary licenses.....	47
7	RESULTS.....	48
7.1	Astrocyte-specific conditional GABA_BR deletion.....	48
7.2	Astrocytic GABA_BR deletion impairs seizure activity.....	52
7.2.1	The increase in δ power associated with animal inactivity is reduced in cKO mice upon GHB administration.....	52
7.2.2	Functional astroglial GABA _B Rs result in higher incidence of SWDs.....	55
7.3	GHB induces GABA_BR-mediated Ca²⁺ signalling in astrocytes.....	58

7.3.1	GABA _B R-mediated astroglial Ca ²⁺ signals increase in number, amplitude and duration upon GHB application.....	58
7.3.2	The spatiotemporal properties of GHB-induced Ca ²⁺ signalling differ in ctrl and cKO mice <i>ex vivo</i>	60
7.3.3	Neuronal activity contributes to the net effect of GHB on astroglial Ca ²⁺ signalling	64
7.4	<i>In vivo</i> GHB administration results in enhanced astroglial Ca²⁺ activity in both ctrl and cKO mice.....	65
7.4.1	GHB-induced astroglial Ca ²⁺ signals differ in ctrl and cKO in terms of spatial and temporal distribution.....	65
7.4.2	Astroglial GABA _B R deletion reduces and retards the occurrence of hypersynchronous Ca ²⁺ waves.....	69
7.5	cKO mice exhibit fewer SWD-associated motor arrests.....	71
7.5.1	GHB enhanced the freezing behaviour of ctrl mice	71
7.5.2	Home cage analysis revealed reduced immobility in cKO mice	74
8	DISCUSSION.....	75
8.1	The loss of GABA_BRs protects against GHB-induced SWDs and alteration of EEG..	75
8.1.1	Systemic administration of GHB induces 3-6 Hz SWDs associated with higher δ and θ power and reduced γ power.....	75
8.1.2	Astroglial GABA _B R-loss reduces seizure burden and δ -power specific increase	77
8.1.3	Astroglial GABA _B Rs contribute to the pathological network priming at the basis of SWDs	78
8.2	Ca²⁺ response upon GHB administration is mediated by astroglial GABA_BRs.....	82
8.2.1	GHB directly recruits astroglial GABA _B Rs and induces subsequent Ca ²⁺ activity.. ..	82
8.2.2	Astroglial Ca ²⁺ response upon GHB application is shaped by neuronal evoked neurotransmitter release.....	83
8.3	GHB administration induces the appearance of stereotypical hypersynchronous astroglial Ca²⁺ waves <i>in vivo</i>	84
8.4	Astroglial GABA_BR-loss protects against GHB-induced behavioural arrests	86
9	CONCLUSION AND OUTLOOK.....	87
10	APPENDIX	88
11	REFERENCES.....	106
12	ACKNOWLEDGEMENTS	126
13	CURRICULUM VITAE AND LIST OF PUBLICATIONS.....	128

LIST OF ABBREVIATIONS

2P	two-photon	E/I	excitation/inhibition
a.u.	arbitrary unit	EAAT	excitatory amino acid transporter
ACSA	astrocyte cell surface antigen	EDTA	ethylenediaminetetraacetate
ADP	adenosine diphosphate	(E)GFP	(enhanced) green fluorescent protein
AED	anti-epileptic drug	EEG	electroencephalography
ALDH1L1	aldehyde dehydrogenase 1 family member L1	ER	endoplasmic reticulum
AMPA	α -amino-3-hydroxy-5-methyl-4-isoxazolepropionic acid	ERT2	mutant human estrogen receptor ligand-binding domain
AP	anteroposterior	FFT	fast Fourier transform
APH	(\pm)-2-amino-7-phosphonoheptanoic acid	fl	floxed (flanked by loxP sites)
ASD	anti-seizure drug	fMRI	functional magnetic resonance imaging
AQP4	aquaporin 4	FOV	field of view
ATP	adenosine triphosphate	FWHM	full width at half maximum
BBB	blood-brain barrier	GABA	γ -aminobutyric acid
BGT-1	betaine/GABA transporter 1	GABA _A R	GABA _A receptor
BOLD	blood-oxygen-level-dependent	GABA _B R	GABA _B receptor
bp	base pair	GABA _B R1	GABA _B receptor subunit 1
BSA	bovine serum albumin	<i>Gabbr1</i>	GABA _B receptor subunit 1 locus
bw	body weight	GAERS	genetic absence epilepsy rat from Strasbourg
CAE	childhood absence epilepsy	GBL	γ -butyrolactone
cAMP	cyclic adenosine monophosphate	GCaMP	GFP-calmodulin-M13 peptide fusion protein
cDNA	complementary DNA	GFAP	glial fibrillary acidic protein
chr	chromosome	GFP	green fluorescent protein
cKO	conditional knock-out	GHB	γ -hydroxybutyric acid
CNS	central nervous system	GLAST	L-glutamate/L-aspartate transporter
CNXQ	6-cyano-7-nitroquinoxaline-2,3-dione	GLT-1	glutamate transporter-1
Cre	Cre-DNA recombinase	GS	glutamine synthetase
CT	cortico-thalamic	GJ	gap junction
CTCn	cortico-thalamo-cortical network	HBSS	Hank's balanced sodium solution
ctrl	control	hc	hemichannel
Cx	connexin	HEPES	4-(2-hydroxyethyl)-1-piperazineethanesulfonic acid
DAPI	4',6-diamidin-2-phenylindol	HFO	high-frequency oscillations
DCV	dense core vesicle	HRP	horseradish peroxidase
DNA	deoxyribonucleic acid	HS	horse serum
DREADD	designer receptor exclusively activated by designer drugs	HSP	heat shock protein
DV	dorsoventral	Iba1	ionized calcium-adapter molecule 1

InsP3	inositol 1,4,5-trisphosphate	PV	parvalbumin
i.p.	intraperitoneal	PyRAT	Python-based relational animal tracking software
i.v.	intravenous		
IQR	interquartile range	Q	quartile
KI	knock-in	RNA	ribonucleic acid
L-PTZ	low-dose pentylenetetrazole	ROA	region of activity
lsl	floxed STOP sequence	<i>rosa26</i>	reverse oriented splice acceptor clone 26 locus
LSM	laser-scanning microscopy	RT	room temperature
MACs	magnetic cell separation	s.c.	subcutaneous
MBP	myelin basic protein	S100 β	S100 calcium-binding protein β
MFGE8	milk fat globule epidermal growth factor 8	SEM	standard error of the mean
MGI	Mouse Genome Informatics database	<i>Slc1a3</i>	solute carrier family 1 member 3
mGluR	metabotropic glutamate receptor	SLMV	synaptic-like microvesicle
ML	mediolateral	SNAT	sodium-coupled neutral amino acid transporter
mPTP	mitochondrial permeability transition pore	SRB	sulforhodamine B
NCX	Na ⁺ /Ca ²⁺ exchanger	SSp-ctx	primary somatosensory cortex
NMDA	N-methyl-D-aspartate	SWD	spike-wave discharge
(n)REM	(non) rapid eye movement sleep	TAE	Tris-acetate-EDTA buffer
NRT	nucleus reticularis thalami	TAM	tamoxifen
p	p-value	TC	thalamo-cortical
PAP	peripheral astrocyte process	THIP	4,5,6,7-tetrahydroisoxazolo[5,4-c]pyridin-3-ol
PBS	phosphate-buffered saline	Tris	tris(hydroxymethyl)aminoethane
pCAGGS	cytomegalovirus-immediate early enhancer/chicken β -actin/rabbit β -globin hybrid promoter	TRP	transient receptor potential channel
PCR	polymerase chain reaction	TTX	tetrodotoxin
PEN	penicillin	VGCC	voltage-gated Ca ²⁺ channel
(P)FA	(para)formaldehyde	VP	ventral posterior thalamic nucleus
P _i	inorganic phosphate	VRAC	volume-regulated anion channel
PLC	phospholipase C	WAG/Rij	Wistar Albino Glaxo rat from Rijswijk
PNS	peripheral nervous system	WPE	woodchuck hepatitis virus posttranscriptional regulatory element
px	pixel	wt	wild type

LIST OF FIGURES

Figure 1.	Astroglial Ca ²⁺ signalling	9
Figure 2.	Spike-and-wave discharges and the cortico-thalamo-cortical network	12
Figure 3.	Alterations of astroglial glutamatergic and GABAergic signalling in absence seizures.....	20
Figure 4.	Experimental design of acute slice preparation	35
Figure 5.	Focal drug application during 2P-LSM	37
Figure 6.	Telemetric EEG recording in freely moving mice.....	40
Figure 7.	Analysis of GHB-induced freezing in the open field test.....	46
Figure 8.	Cell-specific conditional knock-out of astroglial GABA _B R1	48
Figure 9.	Effective removal of GABA _B Rs from MACs-purified astrocytes.....	50
Figure 10.	GHB-induced spectral alterations differ between ctrl and cKO mice	54
Figure 11.	Spike-wave discharges occur at lower frequency in cKO mice	56
Figure 12.	GHB enhances astroglial Ca ²⁺ signalling in dependence of functional GABA _B Rs	60
Figure 13.	Astroglial Ca ²⁺ signals induced by GHB display higher spatial extension in ctrl mice	61
Figure 14.	GHB induces synchronous Ca ²⁺ activity in astrocytes of ctrl but not of cKO mice	63
Figure 15.	Cortical astroglial Ca ²⁺ signal density increases <i>in vivo</i> in ctrl and not in cKO mice .	67
Figure 16.	GHB evokes larger and more frequent astroglial Ca ²⁺ signals <i>in vivo</i>	68
Figure 17.	<i>In vivo</i> GHB induces synchronous astroglial Ca ²⁺ waves at lower incidence in cKO mice.....	71
Figure 18.	Open field test revealed specific increase of GHB-induced immobility in ctrl mice ..	72
Figure 19.	Upon GHB administration in their home cage cKO mice displayed reduced immobility	74
Figure 20.	Putative contribution of cortical astroglial GABA _B R-signalling in the E/I imbalance underlying absence seizures	81

LIST OF TABLES

Table 1.	Genetic animal models of typical absence seizures.....	14
Table 2.	Chemical models of typical absence seizures.....	15
Table 3.	List of devices.....	24
Table 4.	List of drugs.....	27
Table 5.	Primary antibodies for immunohistochemistry.....	27
Table 6.	Secondary antibodies for immunohistochemistry.....	28
Table 7.	List of dyes	28
Table 8.	Genotyping primers	29
Table 9.	Genetically modified mouse lines	29
Table 10.	PCR reaction protocols.....	32
Table 11.	Glass pipette pulling program.....	36
Table 12.	2P-LSM filter settings for emission wavelength collection.....	41
Table 13.	List of filter sets for automated epifluorescence microscopy with AxioScan.Z1	42
Table 14.	Pipeline and parameters for automated detection and analysis of Ca ²⁺ events.....	43
Table 15.	Parameters for the identification of the mouse hypnogram stages	44
Table 16.	SWD detection protocol in NeuroScore	44
Table 17.	Activity analysis settings in EthoVision XT.....	45

LIST OF SUPPLEMENTARY MATERIALS

SUPPLEMENTARY FIGURES

Supplementary Figure 1.	Astrocytic Ca ²⁺ response to baclofen is reduced in cKO mice.....	88
Supplementary Figure 2.	<i>Ex vivo</i> baseline Ca ²⁺ dynamics differ in ctrl and cKO mice	89
Supplementary Figure 3.	Spectral analysis of GHB-induced EEG alterations	92
Supplementary Figure 4.	Correlation analysis of EEG spectral power and activity after GHB ...	94
Supplementary Figure 5.	Spike-wave discharge heterogeneity	95
Supplementary Figure 6.	GHB modulates astrocytic Ca ²⁺ dynamics indirectly via neuronal activity	98
Supplementary Figure 7.	Absence of excessive cortical cell reactivity after craniotomy.....	99

SUPPLEMENTARY TABLES

Supplementary Table 1.	Two-way ANOVA test results	101
------------------------	----------------------------------	-----

SUPPLEMENTARY VIDEOS

Supplementary Video 1.	<i>Ex vivo</i> 2P-LSM recording of cortical astroglial Ca ²⁺ signalling of ctrl mouse upon GHB focal application.....	102
Supplementary Video 2.	<i>Ex vivo</i> 2P-LSM recording of cortical astroglial Ca ²⁺ signalling of cKO mouse upon GHB focal application.....	103
Supplementary Video 3.	<i>In vivo</i> 2P-LSM recording of cortical astroglial Ca ²⁺ signalling of ctrl mouse upon GHB administration	104
Supplementary Video 4.	<i>In vivo</i> 2P-LSM recording of cortical astroglial Ca ²⁺ signalling of cKO mouse upon GHB administration	105

1 ABSTRACT

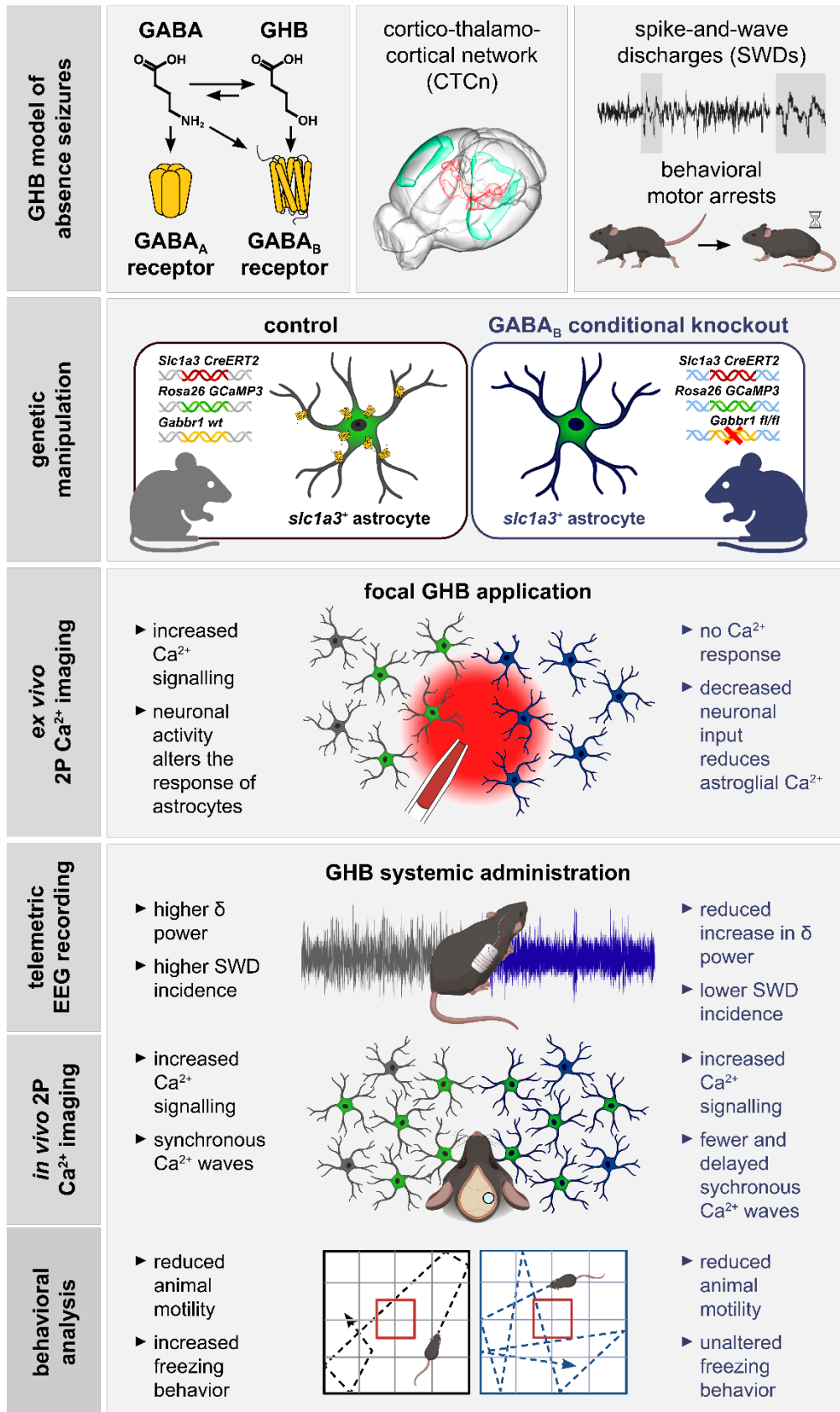
Absence seizures are non-convulsive epileptic events associated with brief loss of consciousness and arising from alterations in GABAergic and glutamatergic synaptic function maintaining the correct excitation-inhibition balance in the brain. Agonists of the metabotropic GABA_B receptor (GABA_BR), including the endogenous metabolite γ -hydroxybutyric acid (GHB), induce or exacerbate absence seizures. Current understanding of the molecular mechanisms underlying absence seizure ictogenesis and propagation is predominantly focused on neuronal networks and so are existing pharmacological interventions. Nevertheless, to date the treatment of absence seizures is still ineffective in almost one-third of the cases.

As active players in neural excitability and plasticity, astrocytes contribute to epileptic network priming and seizure activity. Hence, we investigated the contribution of astroglial GABA_BR and astroglial GABA_BR-mediated Ca²⁺ signalling in the pathological network function of GHB-induced absence seizures in a transgenic mouse model. We induced the astrocyte-specific GABA_BR deletion and expression of the Ca²⁺ indicator GCaMP3 and performed *in vivo* telemetric electroencephalography of freely moving animals, two-photon laser-scanning microscopy of cortical astroglial Ca²⁺ signalling and behavioural analysis of mouse activity upon GHB administration.

Astroglial GABA_BR-deficient mice exhibit reduced seizure burden and experience a reduced and shorter increase in δ -band power upon GHB administration. Also, we found that astroglial GABA_BRs mediate astrocytic Ca²⁺ response upon GHB focal application as well as systemic administration *in vivo*. The loss of astroglial GABA_BRs protects against the emergence of hypersynchronous cortical Ca²⁺ waves upon GHB administration. Moreover, astroglial GABA_BR-deficient mice display significantly less behavioural arrests associated with GHB-induced absence seizures.

In conclusion, these results show that, although not necessary for the occurrence of seizures *per se*, astroglial GABA_BRs contribute to the pathological phenotype associated with absence seizures and exacerbate seizure burden. Therefore, astroglial GABA_BRs and their downstream signalling represent a promising target for future research in epilepsy and possibly for novel pharmacological intervention of absence seizures.

2 GRAPHICAL ABSTRACT



3 ZUSAMMENFASSUNG

Absence-Anfälle, auch Petit-mal Anfälle genannt, sind nicht-convulsive epileptische Ereignisse, die mit paroxysmalem (anfallsartigem) Bewusstseinsverlust einhergehen und auf Veränderungen der GABA- und Glutamat-Wirkung an synaptischen Funktionen zur Aufrechterhaltung des richtigen Erregungs-Hemmungs-Gleichgewichts im Gehirn zurückzuführen sind. Agonisten des metabotropen GABA_B-Rezeptors, wie z.B. die endogene Verbindung γ -Hydroxybuttersäure (GHB), lösen Absence-Anfälle aus oder verstärken sie. Das derzeitige Verständnis der molekularen Mechanismen, die der Entstehung und Ausbreitung von Absence-Anfällen zugrunde liegen, konzentriert sich vorwiegend auf die Aktivität von Nervenzellen, welche aktuell Ziel der bestehenden pharmakologischen Interventionen sind. Dennoch ist die Behandlung von Absence-Anfällen in fast einem Drittel der Fälle unwirksam.

Zur neuronalen Erregbarkeit und Plastizität tragen Astrozyten zur Bahnung epileptischer Netzwerke und zur Anfallsaktivität bei. Daher haben wir in der vorliegenden Arbeit die Rolle des astroglialen GABA_B-Rezeptors und den durch diesen vermittelten intrazellulären Calcium-Anstieg bei der pathologischen Netzwerkfunktion von GHB-induzierten Absence-Anfällen in einem transgenen Mausmodell untersucht. Zur Analyse induzierten wir die Astrozyten-spezifische Deletion des GABA_B-Rezeptors und die Expression des Calcium-Indikators GCaMP3. Wir untersuchten *in vivo* telemetrische Elektroenzephalographie frei beweglicher Tiere, Zwei-Photonen-Mikroskopie der kortikalen astroglialen Calcium-Signalgebung und Verhaltensanalyse der Tieraktivität nach GHB-Injektion durch.

Astrogliale GABA_B-Rezeptor-defiziente Tiere weisen eine geringere Anfallslast auf und zeigen einen geringeren und kürzeren Anstieg der δ -Band-Power bei GHB-Verabreichung. Außerdem fanden wir heraus, dass astrogliale GABA_B-Rezeptoren die astrozytäre Calcium-Antwort sowie nach fokaler GHB-Verabreichung als auch *in vivo* nach systemischer Verabreichung vermitteln und ihr Verlust vor dem Auftreten hypersynchroner kortikaler Calcium-Wellen nach GHB-Verabreichung schützt. Darüber hinaus zeigen astrogliale GABA_B-Rezeptor-defiziente Tiere deutlich weniger Verhaltensstörungen im Zusammenhang mit GHB-induzierten Absence-Anfällen.

Zusammenfassend zeigen diese Ergebnisse, dass astrogliale GABA_B-Rezeptoren, obwohl sie für das Auftreten von Anfällen nicht notwendig sind, zu einem pathologischen Phänotyp beitragen, der mit Abwesenheitsanfällen einhergeht, und die Anfallslast erschweren. Daher stellen astrogliale GABA_B-Rezeptoren und ihre nachgeschalteten Signalwege ein vielversprechendes Ziel für die künftige Forschung auf dem Gebiet der Epilepsie und möglicherweise auch für pharmakologische Interventionen bei Absence-Anfällen dar.

4 INTRODUCTION

The term *glia* derives from the ancient Greek γλία (*glía*, meaning glue) and refers to a plethora of different cells in the central as well as peripheral nervous system (CNS and PNS, respectively) lacking the electrical activity that characterizes neurons (Kettenmann and Ransom, 1995; Kandel et al., 2000). Glial cells, or glia, were first described in an article collection published in 1856 by the pathologist R. Virchow (Virchow, 1856) as connective tissue (*Nervenkitt*) providing mechanical support for neuronal networks (Somjen, 1988). Almost two centuries later, it is now known that glial cells almost outnumber their neuronal counterpart (von Bartheld et al., 2016) and it is widely accepted that they are distinct and active partners in the nervous system contributing to virtually any information processing and functionality of the CNS, which has to be addressed in its whole as an *active milieu* of compartments dynamically interposing and interacting, namely neuronal and glial cells, extracellular space, extracellular matrix and vasculature (Semyanov and Verkhratsky, 2021).

4.1 ASTROCYTES AT THE CENTRE OF THE NEURAL *ACTIVE MILIEU*

4.1.1 *E PLURIBUS UNUM, EX UNO PLURES: ASTROGLIAL IDENTITY AND HETEROGENEITY*

Among glial cells, astrocytes, collectively termed astroglia (von Lenhossék, 1895), are star-shaped cells accounting for 20-40 % of human brain cells (Pelvig et al., 2008; Azevedo et al., 2009; Verkhratsky and Butt, 2013) and occupy with different morphological as well as functional characteristics all CNS regions (Sofroniew and Vinters, 2010). The earliest and the most evident phenotypical classification of astroglia is based on their morphological segregation into protoplasmic and fibrous astrocytes (Cajal, 1909). Protoplasmic astrocytes are mainly restricted to grey matter and are characterized by several main stem branches originating a number of finer processes with a substantial isotropic distribution in space and forming the so called gliapil, which accounts for around 75 % of astrocytic volume (Bindocci et al., 2017). Fibrous astrocytes populate the white matter tissue and exhibit a more elongated morphology with a smaller cell body and many longer but less branched fibre-like processes. Importantly, individual protoplasmic astrocytes occupy distinct anatomical domains with no substantial overlapping in the grey matter (Bushong et al., 2002; Ogata and Kosaka, 2002; Halassa et al., 2007b) and contact simultaneously more than 100.000 neural synapses in rodents and up to two millions in humans (Oberheim et al., 2006). It is likely (but not yet attested) that a similar organization in anatomical domains also occurs in the white matter, where the processes of fibrous astrocytes align along neuronal axons and contact them at the level of the nodes of Ranvier. Although this separation into protoplasmic and fibrous astrocytes is still valid (Verkhratsky and Nedergaard, 2018), astroglia and closely related cell types exist in a number of intermediate forms and display a significant morphological heterogeneity across the CNS (Emsley and Macklis, 2006; Köhler et al., 2021).

Although not necessarily ubiquitously expressed, most studies aiming at segregating astroglial subpopulations based on single astroglial markers have not yet provided conclusive results (Lovatt et al., 2007; Yang et al., 2011; Zhang et al., 2016). Nevertheless, it has been reported that the intermediate filament glial fibrillary acidic protein (GFAP) has a substantial regional variability and it is expressed at higher levels in reactive and fibrous astrocytes (Bignami et al., 1972; Miller and Raff, 1984; Nolte et al., 2001) and that the Ca²⁺ binding glycoprotein S100 β is differentially expressed in protoplasmic and fibrous astrocytes (Ogata and Kosaka, 2002; Emsley and Macklis, 2006). The glutamate transporters EAAT-1 (glutamate aspartate transporter, GLAST) and EAAT-2 (glutamate transporter 1, GLT-1) also display non-overlapping expression patterns across the CNS (Schmitt et al., 1997; Williams et al., 2005; Regan et al., 2007; Jungblut et al., 2012), as it is the case for astrocyte-specific connexin 30 (Cx30) and 43 (Cx43) (Nagy et al., 1999). On the contrary, the majority of astrocytes express key metabolic enzymes such as glutamine synthetase (GS) (Norenberg and Martinez-Hernandez, 1979; Derouiche and Frotscher, 1991; Anlauf and Derouiche, 2013) and the aldehyde dehydrogenase 1 family member L1 (ALDH1L1) (Cahoy et al., 2008) as well as the milk fat globule-epidermal growth factor 8 protein (MFGE8) (Zeisel et al., 2015) and the water channel aquaporin 4 (AQP4) (Nielsen et al., 1997; Nagelhus and Ottersen, 2013).

Beyond the characterization of astroglia in terms of morphology or biochemical markers, several lines of evidence obtained using unbiased single-cell transcriptomics have been accumulating over the last years (Cahoy et al., 2008; Zhang et al., 2014; Tasic et al., 2018) to unravel the basis of astroglial identity and heterogeneity, which in turn reflects an extraordinary functional heterogeneity (Matyash and Kettenmann, 2010; Zhang and Barres, 2010; Oberheim et al., 2012; Khakh and Sofroniew, 2015; Pestana et al., 2020).

4.1.2 CNS HOMEOSTASIS AND ASTROGLIAL FUNCTION

The scientific community is nowadays unanimous in ascribing astroglia an essential function in CNS homeostasis at all organization level, from the molecular and cellular level to the network and organ level (Allen and Barres, 2009; Verkhratsky and Nedergaard, 2018; Semyanov and Verkhratsky, 2021). Astrocytes contact neuronal synapses in correspondence of their terminal processes (or peripheral astrocytic processes, PAPs), soma and primary branches (Schultz et al., 1957; Ventura and Harris, 1999; Reichenbach et al., 2010; Heller and Rusakov, 2017; Gavrillov et al., 2018; Aboufares El Alaoui et al., 2020; Kiyoshi et al., 2020) and are key regulators of K⁺ clearance and redistribution (Somjen, 2002; Kofuji and Newman, 2004; Bellot-Saez et al., 2017; Beckner, 2020). Indeed, given their extensive gap junction (GJ) coupling (Giaume et al., 2010; Giaume et al., 2021), astroglial networks provide a perfect spatial buffering for ions as well as water (Amiry-Moghaddam and Ottersen, 2003; Simard and Nedergaard, 2004; Nagelhus and Ottersen, 2013). Also, astrocytes are involved in neurotransmitter reuptake and recycling (Danbolt, 2001; Schousboe and

Waagepetersen, 2003; Marcaggi and Attwell, 2004; Mahmoud et al., 2019), synaptogenesis and synaptic plasticity (Eroglu and Barres, 2010; Tsai et al., 2012; Risher and Eroglu, 2020) as well as neural metabolic support (Bélanger et al., 2011; Marina et al., 2018). In parallel to that, astroglia contact directly the vasculature (Schafer and Stevens, 2013) through highly plastic structures known as astrocytic endfeet (Kacem et al., 1998; Abbott et al., 2006) and play a key role in the regulation of the blood flow and the blood brain barrier (BBB) (Koehler et al., 2009; Attwell et al., 2010; MacVicar and Newman, 2015; Liu et al., 2018; Marina et al., 2020).

Finally yet importantly, astroglia actively participate in synaptic transmission in virtue of their tight physical association and functional interaction with synapses of the CNS (Araque et al., 1999; Halassa et al., 2007a; Dityatev and Rusakov, 2011; Verkhratsky and Nedergaard, 2014; Caudal et al., 2020; Semyanov and Verkhratsky, 2021) and therefore impact on neural network excitability and balance between excitation and inhibition (E/I) as active information integrators and processors.

4.1.3 AN ASTROGLIAL POINT OF VIEW ON SYNAPTIC TRANSMISSION

Astrocytes were reported to express on their membrane a sophisticated set of ion channels and neurotransmitter transporters as well as virtually any kind of transmitter receptor found in the CNS (Kettenmann and Zorec, 2013). The astroglial membrane receptome includes both ionotropic and metabotropic glutamate receptors (Reiner and Levitz, 2018), namely ionotropic AMPA (Seifert and Steinhäuser, 1995; Matthias et al., 2003; Lalo et al., 2011; Chai et al., 2017) as well as NMDA (Schipke et al., 2001; Lalo et al., 2006; Dzamba et al., 2013) receptors and G protein-coupled metabotropic receptors mGluR3 and mGluR5 (Sun et al., 2013; Panatier and Robitaille, 2016). Both ionotropic GABA_A (MacVicar et al., 1989; Pastor et al., 1995; Vélez-Fort et al., 2012; Mariotti et al., 2016; Perea et al., 2016) and GABA_B (Nilsson et al., 1993; Kang et al., 1998; Charles et al., 2003; Meier et al., 2008) receptors (GABA_AR and GABA_BR, respectively) are expressed by astroglia. Finally, astrocytes expose on their surface, among many others (Verkhratsky and Nedergaard, 2018), P2X and P2Y purinoceptors (Domercq et al., 2006; Lalo et al., 2008; Franke et al., 2012), adenosine receptors (Boison et al., 2010) and nicotinic as well as muscarinic cholinoreceptors (Sharma and Vijayaraghavan, 2001; Araque et al., 2002). Astroglial neurotransmitter and neuropeptide receptors make astrocytes competent cells to sense and react to neural synaptic transmission. Also, they express among others the Na⁺-dependent glutamate transporters GLAST (Storck et al., 1992; Tanaka, 1993) and GLT-1 (Danbolt et al., 1990; Pines et al., 1992), the glutamine transporters SNAT3 and 5 (Bröer and Brookes, 2001; Hertz, 2013), the GABA transporters GAT-3 and GAT-1 and the Na⁺/Cl⁻-dependent betaine/GABA transporter BGT-1 (Minelli et al., 1996; Ribak et al., 1996; De Biasi et al., 1998; Conti et al., 2004) as well as adenosine (Li et al., 2013) and D-serine (Martineau et al., 2014) transporters, which collectively account for astroglial role in neurotransmitter clearance from the synaptic cleft as well as the

homeostasis of the glutamine-glutamate (GABA) and adenosine cycle. Finally, the active role of astrocytes in the control of neural networks relies on their ability to release gliotransmitters in the extracellular space by means of multiple secretory pathways, namely vesicular release, membrane transport or diffusion through membrane channels (Araque et al., 2014; Sahlender et al., 2014; Petrelli and Bezzi, 2016; Papouin et al., 2017; Savtchouk and Volterra, 2018). Astroglial exocytosis revolves around synaptic-like microvesicles (SLMVs, \varnothing 30 - 100 nm) containing glutamate and D-serine (Bezzi et al., 2004; Mothet et al., 2005; Crippa et al., 2006; Jourdain et al., 2007; Martineau et al., 2013; Schwarz et al., 2017) and dense-core vesicles (DCVs, \varnothing 100 - 600 nm) as well as secretory lysosomes (\varnothing 300 - 500 nm) containing ATP (Pangršič et al., 2007; Zhang et al., 2007; Verderio et al., 2012). Transport-mediated gliotransmission includes glutamate release through the cysteine-glutamate antiporter system Xc⁻ (Warr et al., 1999) and reversed EAAT1/2 (Szatkowski et al., 1990) as well as GABA release through reversed GAT1/3 (Héja et al., 2009; Unichenko et al., 2012; Unichenko et al., 2013). The bestrophin-1 and voltage-regulated anion channels (Best-1 and VRAC, respectively) are permeable to glutamate (Takano et al., 2005; Woo et al., 2012) and GABA (Kozlov et al., 2006; Lee et al., 2010; Le Meur et al., 2012) and the ionotropic P2X₇ receptor mediates both glutamate (Duan et al., 2003; Fellin et al., 2006) and ATP (Suadicani et al., 2006) release. Connexin hemichannels are permeable to glutamate (Ye et al., 2003), ATP (Arcuino et al., 2002; Stout et al., 2002; Chever et al., 2014) and possibly GABA (Ransom et al., 2017), whereas pannexin-1 hemichannels mediate ATP release (Suadicani et al., 2012).

4.1.4 ASTROCYTIC Ca²⁺ SIGNALLING

Astroglial response upon neurotransmitter release in the extracellular space concomitant to neural synaptic activity relies among others on intracellular Ca²⁺ oscillations (Verkhratsky et al., 1998; Verkhratsky et al., 2012; Zorec et al., 2012; Volterra et al., 2014; Bazargani and Attwell, 2016; Shigetomi et al., 2016). Ca²⁺ homeostasis and signalling is based on the concerted activity of plasmalemmal and organellar channels, transporters and receptors as well as cytosolic Ca²⁺ binding proteins, which collectively account for the low cytosolic Ca²⁺ concentration ([Ca²⁺]_{in}, 50-150 nM) required for the generation of an electrochemical gradient with the extracellular space ([Ca²⁺]_{ex}, 1.2 mM) and with intracellular compartments topologically equivalent to the extracellular space, such as the lumen of the endoplasmic reticulum (ER; [Ca²⁺]_i, 0.2 - 1 mM) and the mitochondrial matrix ([Ca²⁺]_m, 100-200 nM) (Figure 1). Several lines of evidence indicate that astroglia display spontaneous intracellular Ca²⁺ influx independently of neural firing (Parri et al., 2001; Nett et al., 2002) at least partially deriving from the extracellular space through transient receptor potential (TRP) channels (Shigetomi et al., 2011; Shigetomi et al., 2013b) or from the mitochondrial permeability transition pore (mPTP) (Agarwal et al., 2017). Ca²⁺ enters the cytoplasm upon direct activation of cation-permeable ionotropic receptors, such as P2X, AMPA and NMDA receptors (Seifert and Steinhäuser, 1995; Fumagalli et al., 2003; Lalo et al., 2006; Palygin et al., 2010), as well

as indirectly through voltage-gated Ca^{2+} channels (VGCC) upon depolarization induced by Cl^- -permeable ionotropic GABA_AR (Nilsson et al., 1993; Fraser et al., 1995; Meier et al., 2008). Canonical G_q -coupled metabotropic receptors, such as mGluR5 (Panatier and Robitaille, 2016), as well as P2Y , A_{2b} and A_3 purinoceptors (Bernstein et al., 1998; Pilitsis and Kimelberg, 1998; Chen et al., 2001; Bennett et al., 2003), activate the phospholipase C (PLC)-inositol triphosphate (InsP3) pathway leading to Ca^{2+} release from the ER. Other G-coupled receptors usually associated with the adenylate cyclase (AC)-cyclic adenosine monophosphate (cAMP) pathway, such as GABA_BR (Mariotti et al., 2016; Perea et al., 2016; Nagai et al., 2019) as well as A_1 and A_{2a} receptors (Biber et al., 1997; Doengi et al., 2008), were reported to induce InsP3-dependent intracellular Ca^{2+} oscillations, possibly through promiscuous G_q -coupling, activation of PLC mediated by the $\beta\gamma$ subunit (Boyer et al., 1992; Camps et al., 1992; Pierce et al., 2002) or direct action on InsP3 receptors (Zeng et al., 2003). Finally, glutamate (Schummers et al., 2008; Zhang et al., 2019; Benfey et al., 2021) and GABA (Doengi et al., 2009; Boddum et al., 2016; Matos et al., 2018) transporters can evoke Ca^{2+} increases supposedly through local reduction or reversal of the activity of the $\text{Na}^+/\text{Ca}^{2+}$ exchange (NCX) (Felix et al., 2020).

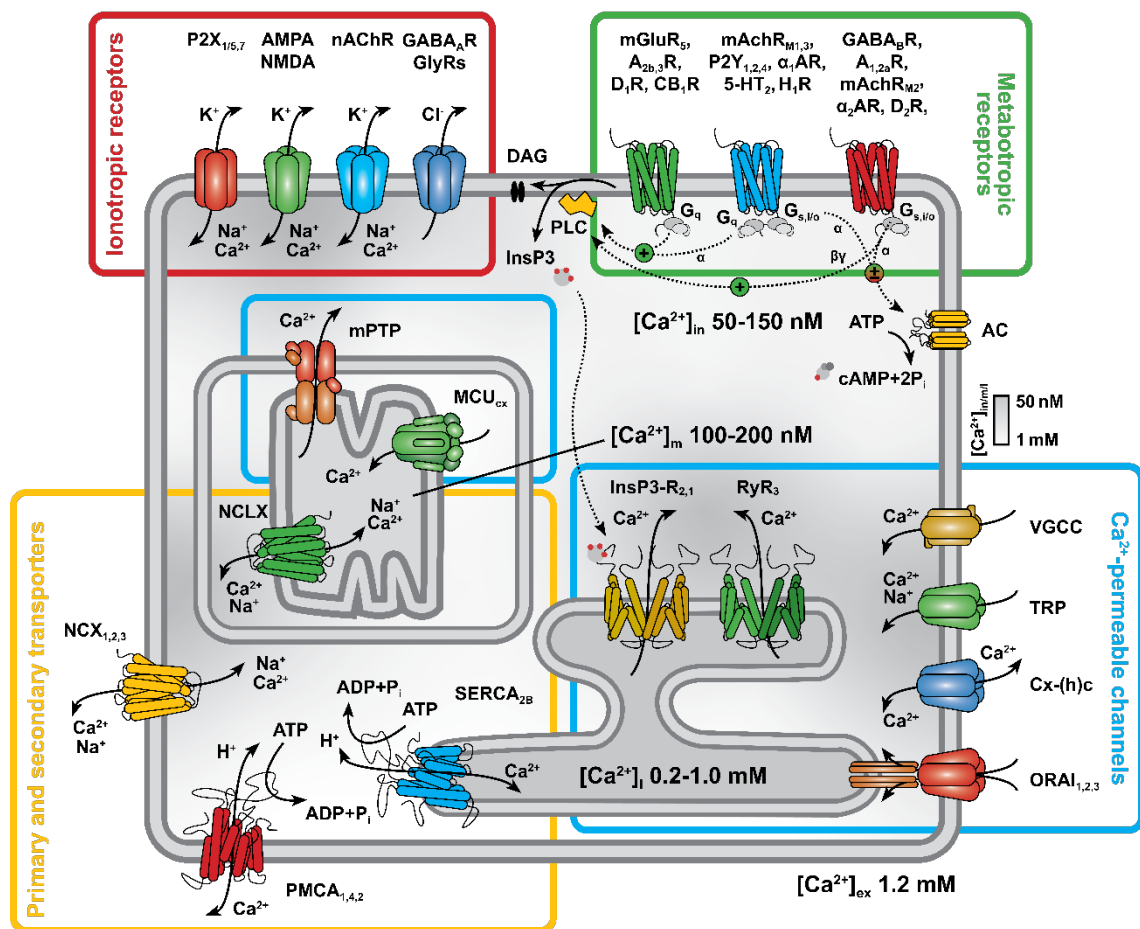


Figure 1. Astroglial Ca²⁺ signalling

5-HT, 5-hydroxytryptamine receptor or serotonin receptor; AC, adenylyl cyclase; ADP, adenosine diphosphate; AMPA, α -amino-3-hydroxy-5-methyl-4-isoxazolepropionic acid receptor; AR, adrenergic receptor; ATP, adenosine triphosphate; CBR, cannabinoid receptor; Cx-(h)c, connexin (hemi)channel; DAG, diacylglycerol; DR, dopamine receptor; GABA_AR, γ -aminobutyric acid receptor A; GABA_BR, γ -aminobutyric acid receptor B; G_{i/o}, inhibitory guanine nucleotide-binding protein; GlyR, glycine receptor; G_q, guanine nucleotide-binding protein of the G_q family; G_s, stimulatory guanine nucleotide-binding protein; HR, histamine receptor; InsP3-R, inositol trisphosphate receptor; mAChR, muscarinic acetylcholine receptor; MCU_{cx}, mitochondrial calcium uniporter complex; mGluR, metabotropic glutamate receptor; mPTP, mitochondrial permeability transition pore; nAChR, nicotinic acetylcholine receptor; NCLX, sodium-lithium-calcium exchanger; NCX, sodium-calcium exchanger; NMDA, N-methyl-D-aspartic acid receptor; ORAI, calcium release-activated calcium channel protein; P2X, P2 purinergic receptor type X; P2Y, P2 purinergic receptor type Y; Pi, inorganic phosphate; PLC, phospholipase C; PMCA, plasma membrane calcium ATPase; RyR, ryanodine receptor; SERCA, sarco/endoplasmic reticulum calcium-ATPase; STIM1, stromal interaction molecule 1; TRP, transient receptor potential channel; VGCC, voltage-gated calcium channel. See 4.1.4 for References.

4.1.4.1 SPATIOTEMPORAL PROPERTIES OF ASTROGLIAL Ca²⁺ SIGNALLING

The complex regulation of astroglial Ca²⁺ homeostasis and signalling gives rise to a variable spatiotemporal organization of Ca²⁺ fluctuations. Most of [Ca²⁺]_{in} transients localize in the gliapil as microdomains (Shigetomi et al., 2010; Di Castro et al., 2011; Kanemaru et al., 2014; Semyanov et al., 2020; Lia et al., 2021), which appear spatially confined (with a diameter of 4-12 μ m) but not necessarily associated to distinct morphological compartments as it is for example the case for perisynaptic leaflets (Shigetomi et al., 2016). Recently, even smaller Ca²⁺ transients (0.07-0.7 μ m²) were recorded in PAPs, suggesting that most of the signals occur at the nanoscopic scale (Arizono et al., 2020). Ca²⁺ signalling in microdomains encompasses both relatively fast (< 1 s) (Di Castro et al., 2011; Stobart et al., 2018) as well as longer (> 3 s) transients (Kanemaru et al., 2014) and are generally independent of larger and longer somatic Ca²⁺ signals. If somatic Ca²⁺ signals almost entirely rely on the PLC-InsP3 pathway, microdomain Ca²⁺ transients, both spontaneous and evoked, are only partially blocked in InsP3R₂^{-/-} animals (Srinivasan et al., 2015; Rungta et al., 2016; Okubo et al., 2019) reflecting alternative mechanisms for Ca²⁺ mobilization in distinct compartments of the cell (Di Castro et al., 2011; Shigetomi et al., 2013a; Zheng et al., 2015). Indeed, around 55 % of PAPs lack ER membranes (Aboufares El Alaoui et al., 2020), suggesting that Ca²⁺ rises originating from the extracellular space and mitochondria are predominant. From the microdomains Ca²⁺ transients can travel across the gliapil to the main processes and soma with a speed of 15 μ m/s (Pasti et al., 1997; Hausteiner et al., 2014; Kanemaru et al., 2014) but are mainly restricted *in vivo* in physiological conditions to one or few adjacent cells, even under sensory stimulation (Wang et al., 2006). Intercellular propagation of Ca²⁺ waves (Scemes and Giaume, 2006) is mediated by either diffusion of InsP3 through GJs (Allbritton et al., 1992; Leybaert and Sanderson, 2001), paracrine signalling via ATP release through connexons, P2X receptors and VRACs (Guthrie et al., 1999;

Arcuino et al., 2002; Anderson et al., 2004) or both (Fiacco and McCarthy, 2006). Whereas InsP3-mediated propagation is relatively fast but more restricted in extension, ATP paracrine signalling is slower but can propagate further in space (Kang and Othmer, 2009). Coordinated Ca^{2+} signals involving entire astroglial syncytia were recorded *in vivo* in awake animals associated with locomotion, arousal and sensory stimulation due to concerted adrenergic input (Ding et al., 2013; Paukert et al., 2014).

While our understanding of the mechanisms underlying astroglial Ca^{2+} elevations and their features is rapidly growing, their downstream impact on cellular as well as network functioning are far from being fully understood (Guerra-Gomes et al., 2017). Nevertheless, several lines of evidence shed new light on the functional role of Ca^{2+} signalling in gliotransmission as well as synaptic modulation and plasticity, network synchronization and neural rhythmicity and up to behavioural outputs such as cognition, emotion, motor and sensory information integration (Oliveira et al., 2015; Allen, 2019; Park and Lee, 2020). The extensive control of CNS homeostasis and physiology at the level of synaptic transmission, network excitability and synchronization makes astrocytes key elements in the mechanisms underlying pathological network alterations, such as epilepsy.

4.2 EPILEPSY

Epilepsy is one of the main neurological disorders next to migraine, stroke and Alzheimer's disease and affects 50 million people all over the world (Beghi et al., 2019; World Health Organization, 2022). Epilepsy is characterized by unprovoked, recurrent seizures resulting from abnormal electric discharge of neural networks (Fisher et al., 2014; Huff and Murr, 2021). Based on their onset, seizures can be classified into focal and generalized seizures (Scheffer et al., 2017). Both seizure types can coexist in the same individual and focal seizures can secondarily develop into generalized seizures. While the individual consciousness can remain unaltered during focal seizures, generalized seizures are always associated with impaired consciousness. Seizure can induce motor symptoms such as muscle tension (tonic) or limpness (atonic), rhythmical jerking movements (clonic) or muscle twitching (myoclonic). Otherwise, they are referred as absence seizures, even though brief myoclonic twitches and automatisms can co-occur. Epileptic seizures display a huge aetiological variability, ranging from structural abnormalities of the CNS, prenatal or perinatal brain damage, genetic or multigenic conditions, strokes, tumors, infections or metabolic disorders, and their aetiology is unknown in almost half of the cases (Schachter et al., 2013). Nevertheless, seizures ultimately result from an abnormal network activity (either hyperactive, hypersynchronous or both) promoted by an imbalance of excitation and inhibition (E/I) at the cellular level. Although only symptomatic, most medical therapies for epilepsy are based on pharmacological treatment with anti-seizure drugs (ASDs, until recently improperly termed anti-epileptic drugs or AEDs) aiming at restoring the correct E/I balance in the CNS and targeting voltage-gated ion channels, glutamatergic

and GABAergic transmission and neurotransmitter release (Sills and Rogawski, 2020). Nevertheless, pharmacological treatments may require several changes in medical regimens within the first years and are ineffective in one third of cases (Schmidt, 2009). Moreover, epilepsy is often accompanied by a broad spectrum of cognitive, behavioural and psychiatric comorbidities not necessarily targeted by ASDs (Tellez-Zenteno et al., 2007; Berg, 2011).

4.2.1 ABSENCE SEIZURES

Absence seizures (also known as petit mal seizures) are generalized non-convulsive seizures and are the only kind of seizures, together with complex partial seizures with impaired consciousness, with no or only subtle motor symptoms (Fisher et al., 2014; Scheffer et al., 2017). Typical absence seizures are associated with brief and sudden impaired consciousness, lack of voluntary movements and responsiveness to external stimuli usually lasting less than 10 seconds (Panayiotopoulos, 2008; Guo et al., 2016). Absence seizures are the only electroencephalographical hallmark of childhood absence epilepsy (CAE) but are to be detected in several other idiopathic generalized epilepsies (Panayiotopoulos et al., 1997; Crunelli and Leresche, 2002; Blumenfeld, 2005a; Camfield and Camfield, 2005; Gardiner, 2005; Matricardi et al., 2014) (Figure 2A). CAE accounts for about 10 % of all childhood epilepsies and has up to 70 % remission rate (Crunelli and Leresche, 2002; Berg et al., 2014). Nevertheless, the first-line medication based on ethosuximide or valproic acid monotherapy is ineffective in 30 % of the cases (Glauser et al., 2013). Moreover, 60 % of the cases involve severe neuropsychiatric comorbid conditions such as impaired attention, learning, memory and cognition (Caplan et al., 2008), which persist despite seizure freedom (Masur et al., 2013) and are often left unaltered or even worsened by common AEDs (Holmes and Noebels, 2016; Cnaan et al., 2017; Crunelli et al., 2020).

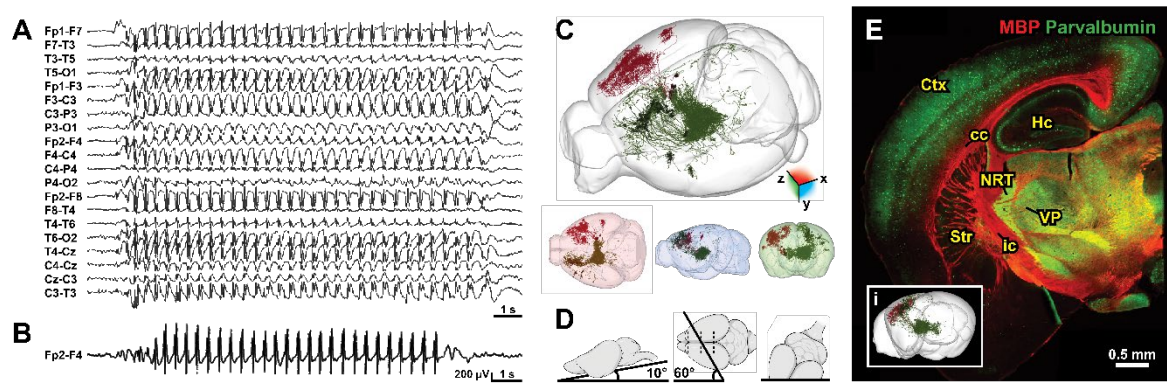


Figure 2. Spike-and-wave discharges and the cortico-thalamo-cortical network

(A) Human ictal electroencephalographical recording (EEG) recorded from an 8-year old child with childhood absence epilepsy (CAE) and displaying 3 Hz spike-and-wave discharges (SWDs) typical of absence seizures. (B) SWDs recorded from an 11-year old child with idiopathic generalized epilepsy with absence statuses. (C) 3D-reconstruction of the mouse cortico-thalamo-cortical network (CTCn) including cortico-thalamic projections from the cortical layer VI (CT, red) and thalamo-cortical neurons from the ventral-posterior nucleus of the thalamus (TC, green) obtained using the database of the MouseLight project (Economio et al., 2016; Winnubst et al., 2019) as in (Shepherd and Yamawaki, 2021). CT and TC components were chosen from opposite hemispheres for easier visualization in C. (D) Schematics of rodent brain preparation for the visualization of intact CTCn adapted from (Agmon and Connors, 1991). (E) CTCn obtained as showed in D and characterized by means of immunocytochemistry of the myelin basic protein (MBP) and parvalbumin, targeting neuronal fibres and the nucleus reticularis thalami enriched in parvalbumin-positive interneurons, respectively. Ctx, cerebral cortex; cc, corpus callosum; Hc, hippocampus; ic, internal capsule; NRT, nucleus reticularis thalami; Str, striatum; VP, ventral-posterior thalamic nucleus. In i, 3D-reconstruction of the CTCn oriented as displayed in the slice preparation for comparison. A, modified with permission from (Cerminara et al., 2012). B, modified with permission from (Panayiotopoulos et al., 2001).

Although with some inter- as well as intraindividual variability (Shi et al., 2019; Crunelli et al., 2020), absence seizures are characterized by generalized bilateral 2.5-4 Hz spike-and-wave discharges (SWDs) with no aura or post-ictal depression (Figure 2B) and corresponding to two functionally coupled states of neuronal excitation and silence in the cortico-thalamo-cortical network (CTCn) (Panayiotopoulos, 1999; Blumenfeld, 2005b; Sitnikova and van Luijtelaa, 2007; Panayiotopoulos, 2008; Terlau et al., 2020) including cortico-thalamic projections (CT) from cortical layer VI, thalamo-cortical neurons (TC) from the ventral posterior nucleus of the thalamus (VP) and projecting to cortical layer V/IV as well as GABAergic neurons from the nucleus reticularis thalami (NRT) (Figure 2C-E). Blood oxygenation level-dependent (BOLD) functional magnetic resonance imaging (fMRI) studies in humans revealed the engagement of cortical networks in correspondence of and preceding SWD appearance in the electroencephalographic trace as well as an increased interictal synchrony in the sensorimotor cortex (Aghakhani et al., 2004; Gotman et al., 2005; Hamandi et al., 2006; Moeller et al., 2008; Bai et al., 2010; Moeller et al., 2010; Bai et al., 2011; Tangwiriyasakul et al., 2018). Although the existence of a unique canonical focal onset or initiation site of absence seizures is still under debate (Meeren et al., 2002; Manning et al., 2004; Polack et al.,

2007; Polack et al., 2009; Lee et al., 2019; Studer et al., 2019), the general consensus agrees on ascribing to cortical networks the role of initiation of SWDs (Crunelli et al., 2020), thus settling the long-lasting controversy between cortical and thalamic components (van Luijtelaar and Sitnikova, 2006; Lüttjohann et al., 2011; van Luijtelaar et al., 2014; Paz and Huguenard, 2015). Nevertheless, induction of seizure activity in the thalamic components is sufficient to initiate SWDs (Avoli, 2012; Lüttjohann and van Luijtelaar, 2015; Sorokin et al., 2017) and necessary for SWD generalization and clinical manifestation (Polack et al., 2007).

4.2.1.1 ANIMAL MODELS OF ABSENCE SEIZURES

Current research on the cellular and synaptic mechanisms underlying SWDs derive from the extensive use of genetic animal models (Table 1), particularly the genetic absence epilepsy rats from Strasbourg (GAERS) and Wistar-Albino-Glaxo rats from Rijswijk (WAG/Rij) (Vergnes et al., 1982; van Luijtelaar and Coenen, 1986; Coenen and Van Luijtelaar, 2003; Depaulis et al., 2006; Sarkisova and van Luijtelaar, 2011; Depaulis et al., 2016) as well as monogenic mouse mutants (Noebels, 1999; Maheshwari and Noebels, 2014). Notably, genetic animal models show higher SWD frequency than human absence seizures and do not show seizure remittance with age but, conversely, tend to aggravate with time in terms of seizure duration and incidence (Pitkänen et al., 2017). Acute absence seizures can also be induced pharmacologically in different animal models (Table 2). Common chemical models of typical absence seizures include penicillin (PEN), low-dose pentylenetetrazole (L-PTZ), gaboxadol (also known as 4,5,6,7-tetrahydroisoxazolo(5,4-c)pyridin-3-ol or THIP) as well as γ -hydroxybutyric acid (GHB) and its precursor γ -butyrolactone (GBL) (Cortez et al., 2016). First insights into SWD ictogenesis collected *in vitro* using thalamic slices (von Krosigk et al., 1993; Bal et al., 1995a, b; Bal et al., 2000; Blumenfeld and McCormick, 2000) or *in vivo* in anesthetized animals (Pinault et al., 1998; Slaght et al., 2002; Polack et al., 2007; Chipaux et al., 2011) have been challenged by recent evidence from non-anesthetized animals (McCafferty et al., 2018; Meyer et al., 2018), which revealed that the ictal firing activity of CT and TC neurons is reduced and that only a small fraction of them are synchronously active at each SWD cycle (eliciting either singles spikes or T-type Ca^{2+} channel-mediated bursts). Conversely, NRT neurons display an increased total and burst firing activity at each SWD cycle.

Model		Type	SWD characteristics	Pharmacological response	Human behaviour recapitulation	References	
GAERS	<i>Rattus norvegicus</i>	polygenic	7-10 Hz, ~ 20 s, from 60 d of age, lifelong, age dependent	ethosuximide, valproic acid, lamotrigine	yes	(Vergnes et al., 1982; Marescaux et al., 1992b; Polack et al., 2007)	
WAG/Rij			7-11 Hz, ~ 5 s, up to 2 min, from 60-80 d of age, lifelong, age dependent			(van Luijtelaar and Coenen, 1986; Drinkenburg et al., 1991; Coenen et al., 1992)	
Tottering	<i>Mus musculus</i>	monogenic	6-7 Hz, 0.3-10 s, from 4 weeks of age, lifelong	ethosuximide, valproic acid	yes (also focal motor seizures and ataxia)	(Kaplan et al., 1979; Noebels and Sidman, 1979; Heller et al., 1983; Fletcher et al., 1996)	
Lethargic			5-7 Hz, 0.6-5 s, from 15 d of age, lifelong				ethosuximide, lamotrigine
Stargazer			6-7 Hz, ~ 6 s, up to 1 min, lifelong	ethosuximide	yes (also ataxia)	(Noebels et al., 1990)	
Mocha			6-7 Hz, lifelong			(Noebels and Sidman, 2007)	
Slow-wave epilepsy			3-4.5 Hz, from 11-14 d of age, lifelong	ethosuximide, valproic acid	yes (also focal motor seizures and ataxia)	(Cox et al., 1997; Papale et al., 2009)	
Ducky			5-7 Hz, 0.6-5 s, lifelong			yes (also ataxia)	(Barclay et al., 2001)
PLC β 4-/-			4-10 Hz, ~ 1 s				yes

Table 1. Genetic animal models of typical absence seizures

GAERS, genetic absence epilepsy rats from Strasbourg; PLC β 4, phospholipase C β 4; WAG/Rij, Wistar-Albino-Glaxo rats from Rijswijk.

Model			Dose	SWD characteristics	Human behaviour recapitulation	References
PEN	cat	i.c., i.m. or i.v.	250-600 kIU/kg	30-90 min after injection, 3-5 Hz, up to 6-8 h	yes	(Fisher and Prince, 1977; Taylor-Courval and Gloor, 1984)
	rodents	i.m.	300-600 kU/kg	multifocal spikes with occasional spontaneous generalized SWDs	only vigilance deficit	(Avoli, 1980)
L-PTZ	rodents	i.p. or s.c.	20-30 g/kg	7-9 Hz, 2-3 s, 2-5 min after injection	yes	(Marescaux et al., 1984; De Deyn et al., 1990; Gale, 1995)
THIP	rat	i.p.	5-10 mg/kg	4-5 Hz, less than 10 s, 20 min after injection	yes	(Fariello and Golden, 1987)
GHB	NHPs	i.v.	200-400 mg/kg	2.5-3 Hz, high-voltage slow waves	yes	(Snead, 1978)
	cat	i.p.	200-400 mg/kg	2-3 Hz, intermittent hypersynchronous bursts and waves		(Winters and Spooner, 1964)
	rat		100-200 mg/kg	5-9 Hz, bursts of hypersynchronous waves at higher dose		(Godschalk et al., 1976, 1977; Kumaresan et al., 2000)
	mouse		100 mg/kg	3-6 Hz		(Ishige et al., 1996)
GBL	NHPs	s.c. or i.v.	200 mg/kg	3 Hz, high-voltage slow waves	yes	(Tenney et al., 2004)
	rat	i.p.	100-200 ^o mg/kg	4-9 Hz, frequency range is dose dependent, 2-5 min after injection, bursts of spikes at higher doses		(Depaulis et al., 1989; Snead, 1992a, b; Tenney et al., 2003)
	mouse		70-150 mg/kg	3-6 Hz, 5-10 min after injection, up to 1 h		(Ishige et al., 1996; Kim et al., 2001; Black et al., 2014)

Table 2. Chemical models of typical absence seizures

GBL, γ -butyrolactone; GHB, γ -hydroxybutyric acid; i.c., intracortical; i.m., intramuscular; i.p., intraperitoneal; i.v., intravenous, L-PTZ, low-dose pentylenetetrazole; NHP, nonhuman primates; PEN, penicillin; s.c. , subcutaneous; SWD, spike-and-wave discharge; THIP, 4,5,6,7-tetrahydroisoxazolo(5,4-c)pyridin-3-ol.

4.2.1.2 γ -HYDROXYBUTYRIC ACID-MODEL OF ABSENCE SEIZURES

γ -hydroxybutyric acid (GHB) is an endogenous brain GABA precursor (Bessman and Fishbein, 1963; Snead and Morley, 1981; Maitre, 1997) originally synthesized from its biologically inactive precursor γ -butyrolactone (GBL) (Laborit et al., 1960; Snead, 1991) and used to induce nonconvulsive generalized seizures in cats, nonhuman primates and rodents (Winters and Spooner, 1964; Roth et al., 1966; Marcus et al., 1967; Snead, 1988). Although with some strain and dose variability (Venzi et al., 2015), systemic administration of 200 mg/kg GHB induces in rats 5-6 Hz

SWDs associated with behavioural arrest, which slowly progress into a hypersynchronous state at a 4-5 Hz frequency (Godschalk et al., 1976, 1977). In mice, 100 mg/kg GHB or 70-100 mg/kg GBL induce 3-6 Hz SWDs for up to 30-60 min after systemic administration (Ishige et al., 1996; Kim et al., 2001). Whereas GHB-induced SWDs are blocked by both ethosuximide and valproate in rats (Kumaresan et al., 2000), only ethosuximide is effective in mice (Ishige et al., 1996). Although the existence of a high affinity ($K_d \sim 100$ nM) putative GHB receptor is still under debate (Benavides et al., 1982; Kaupmann et al., 2003; Wu et al., 2004; Crunelli et al., 2006; Bay et al., 2014), GHB is known to be a weak agonist of GABA_BRs ($K_d \sim 30$ -500 μ M, EC50 ~ 5 mM) (Mathivet et al., 1997; Lingenhoehl et al., 1999), which mediate most GHB-induced behavioural effects, including SWDs (Snead, 1992a, 1996). GHB targets include postsynaptic GABA_BRs on TC neurons (Williams et al., 1995; Connelly et al., 2013) as well as presynaptic GABA_BRs on CT and NRT neurons (Gervasi et al., 2003). In the cortex, GHB is likely to target presynaptic GABA_BRs of both pyramidal neurons and interneurons of layer II/III (Jensen and Mody, 2001; Li et al., 2007). Although most research on GHB-induced facilitation and generation of SWDs has been focused on neuronal targets in the thalamic nuclei, more recent findings revealed that, as for other genetic models of absence seizures, GHB-induced seizure originate from cortical networks (Choi et al., 2010; Lee et al., 2019), urging further research on the effect of GHB administration in cortical networks.

4.2.1.3 GABAERGIC AND GLUTAMATERGIC ALTERATIONS ASSOCIATED WITH SPIKE-AND-WAVE DISCHARGES

The alteration of GABAergic and glutamatergic synaptic functions is a key element of SWD ictogenesis and generalization (Depaulis and Charpier, 2018). The cortical glutamatergic system of genetic models of absence epilepsy is associated with increased expression of glutamate receptors (Kennard et al., 2011; Ngomba et al., 2011a), enhanced NMDA-mediated responses (Pumain et al., 1992; D'Antuono et al., 2006) as well as reduced glutamate uptake (Touret et al., 2007) and increased glutamate concentration (Melø et al., 2006). In parallel to that, cortical GABAergic synaptic transmission is impaired due to reduced GABA_BR expression and function (Merlo et al., 2007; Inaba et al., 2009) and reduced GABA_AR-mediated response to phasic inhibition (D'Antuono et al., 2006; Tan Heneu et al., 2007; Macdonald et al., 2010) as well as GABA_AR expression (Spreafico et al., 1993). On the other hand, tonic inhibition of CT neurons by cortical interneurons results in synchronized and phase-locking discharge and burst firing activity (Chipaux et al., 2011). In the ventral thalamic nuclei, an increased level of extracellular GABA (Richards et al., 1995; Leal et al., 2016) is associated with enhanced tonic GABA_AR-mediated inhibition (Cope et al., 2005; Cope et al., 2009; Errington et al., 2011b). Also, several lines of evidence on alterations of the glutamine-glutamate (GABA) cycle in genetic models of absence seizures (Dutuit et al., 2000; Dufour et al., 2001; Bahi-Buisson et al., 2008) suggest that glutamate availability in the thalamic nuclei is reduced, possibly contributing to the net increase of tonic GABAergic inhibition.

Accordingly, systemic administration of GABA-mimetic drugs (i.e. baclofen, GHB, muscimol or THIP, tiagabine) increases paroxysmal SWDs (Vergnes et al., 1984; Micheletti, 1985; Peeters et al., 1989a; Hosford et al., 1992; Coenen et al., 1995; Hosford and Wang, 1997; van Luijtelaar et al., 2002), whereas GABA receptor antagonists (such as bicuculline, CGP 35348 and SCH 50911) reduce absence seizures via systemic and intrathalamic administration (Peeters et al., 1989a; Hosford et al., 1992; Hosford et al., 1995; Puigcerver et al., 1996; Snead, 1996; Getova et al., 1997; Vergnes et al., 1997). On the other hand, intracerebral injection of NMDA and AMPA increases the number of SWDs, whereas systemic or intracerebral injection of NMDA and AMPA receptor antagonists (i.e. MK-801, APH, CNXQ or kynurenic acid) reduces SWDs (Peeters et al., 1989b; Peeters et al., 1990; Ramakers et al., 1991; Peeters et al., 1994). Notably, intracortical injection of AMPA receptor antagonists reduces SWDs but not their injection in the thalamic nuclei (Citraro et al., 2006). Although the contribution of metabotropic glutamate receptors (mGluRs) to SWDs may be model dependent (Ngomba et al., 2011a; Bazyan and van Luijtelaar, 2013), a number of evidence attributes a protective role to G_q-coupled group I mGluR1 (Ngomba et al., 2011b) and mGluR5 (D'Amore et al., 2013; Celli et al., 2020), whereas activation of G_{i/o}-coupled group II mGluR2/3 (Ngomba et al., 2005) and group III mGluR4 (Ngomba et al., 2008) exacerbates absence seizures.

4.3 AN ASTROGLIAL POINT OF VIEW ON ABSENCE SEIZURES

As active information integrators and processors, astroglia do not only provide mechanical, metabolical and functional support to neural synapses, but they also control synaptic plasticity and transmission, network excitability and E/I balance (Araque et al., 1999; Bazargani and Attwell, 2016; Poskanzer and Molofsky, 2018; Caudal et al., 2020), thus affecting virtually every aspect of the CNS physiology and pathology (Halassa et al., 2007a; von Bartheld et al., 2016; Allen and Lyons, 2018). In the context of epilepsy, astroglia directly affect the pathological priming of neural networks leading to E/I imbalance as well as network aberrant, excessive or excessively synchronous activity and influence the spatial and temporal propagation of seizures. Therefore, they directly impact on the severity and the phenotypical outcome of seizures, thus being ideal candidates for the development of new non-neurocentric drugs (Löscher and Schmidt, 2011; Crunelli et al., 2015; Riquelme et al., 2020). To date, research on astroglial contribution to non-convulsive epileptic activity falls behind with respect to other epileptic forms associated with lower remission rates as well as more obvious, immediate and life-impacting clinical outcomes. Nevertheless, several lines of evidence from the clinics as well as genetic and pharmacological models of SWDs link the activity of astroglial syncytia to CTCn priming, SWD ictogenesis and propagation (Gobbo et al., 2021).

4.3.1 ASTROCYTES CONTROL EXTRACELLULAR SPACE HOMEOSTASIS

Astrocytic networks provide spatial buffering for extracellular K⁺ released during excessive neuronal activity (Haj-Yasein et al., 2011; Kiyoshi et al., 2018; Buskila et al., 2019; Wang et al., 2020). K⁺

uptake is associated with water influx and cellular swelling (Walch et al., 2020), thus impacting on local interstitial osmolarity and network excitability. K^+ and water homeostasis requires intercellular GJ coupling via connexin Cx30 and Cx43 (Wallraff et al., 2006; Bedner et al., 2015). Beyond some general considerations, it is to date still under debate if, how and to which extent astroglial control on the extracellular space homeostasis exactly impacts SWDs. Structural magnetic resonance imaging (MRI) studies revealed that CAE is associated with grey matter volume changes in cortical as well as thalamic regions (Fujiwara et al., 2020; Kim et al., 2020), suggesting some underlying defects in water homeostasis. Also, mutations in the *KCNJ10* gene of the inward-rectifying K^+ channel $K_{i4.1}$ have been associated with forms of childhood epilepsies presenting ataxia and cognitive impairment (Bockenbauer et al., 2009; Scholl et al., 2009; Sicca et al., 2016) and valproic acid treatment was shown to increase the cortical expression of $K_{i4.1}$ in rats (Mukai et al., 2018). The pharmacological block of GJs in genetic animal models of AE revealed the existence of some region as well as model-specificity in the contribution of GJs to SWDs (Manjarrez-Marmolejo and Franco-Pérez, 2016). The broad-spectrum GJ blocker carbenoxolone (CBX) reduces seizure activity in *ex vivo* preparations from mice with spontaneous SWDs (Chang et al., 2013; Gigout et al., 2013) as well as *in vivo* after systemic injection in GAERS rats (Gigout et al., 2006) and injection in the NRT of rats with absence seizures (Proulx et al., 2006). On the contrary, CBX produced no effect on SWDs upon intrathalamic injection in WAG/Rij rats or systemic administration in lethargic mice (Gareri et al., 2005) and even increased SWDs if injected intraperitoneally in WAG/Rij rats (Vincze et al., 2019). Although the interpretation of the results is challenged by its pleiotropic action, the intraventricular injection of the Cx43 specific blocker anandamide (N-arachidonylethanolamine, ANA) also decreased SWDs (Citraro et al., 2013). To note, both CBX and ANA also block connexin hemichannels, thus challenging the attribution of any observed phenotype to the sole GJ coupling (Li et al., 2019; Medina-Ceja et al., 2019).

4.3.2 GLUTAMATERGIC AND GABAERGIC ASTROGLIAL ALTERATIONS IN ABSENCE SEIZURES

Since astrocytes are both GABA- and glutamatergic as well as glutamate- and GABAceptive cells, they exhibit a fundamental control of the E/I balance, possibly reinforcing, integrating or even reversing input signals (Caudal et al., 2020). In the following, we summarize current evidence and speculation on glutamatergic as well as GABAergic alterations observed in absence seizures and ascribed to astroglial pathophysiological phenotype.

In GAERS rats, the expression of cortical astroglial glutamate transporters GLT-1 and GLAST is reduced before seizure development (Dutuit et al., 2002). Also, cellular metabolism and glutamine-glutamate (GABA) cycle are enhanced in cortical astroglia, leading to increased glutamate but decreased GABA labelling (Melø et al., 2006). On the other hand, the expression of thalamic

astroglial glutamate dehydrogenase is increased before and after seizure development (Dutuit et al., 2000), possibly leading to a reduced thalamic glutamate availability. In line with this, pharmacological enhancement of astroglial glutamate catabolism via intraperitoneal injection of branched-chain amino acids and α -ketoisocaproate increased seizure burden (Dufour et al., 2001) and a mutation of the glutamate dehydrogenase gene leading to aberrant glutamate availability has been linked to a case to myoclonic absence epilepsy with irregular SWDs (Bahi-Buisson et al., 2008). Taken together, this suggests that aberrant glutamatergic tone in absence seizures may be, at least partially, mediated by astroglia. Moreover, thalamic astrocytes display Ca^{2+} oscillations in response to glutamatergic CT afferents (Parri et al., 2010; Höft et al., 2014; Copeland et al., 2017). Knowing that astroglia are capable of converting glutamatergic input into tonic GABAergic inhibition (Héja et al., 2019), it is possible that they contribute to the enhanced thalamic GABA level and tonic inhibition associated with absence seizures using a similar mechanism.

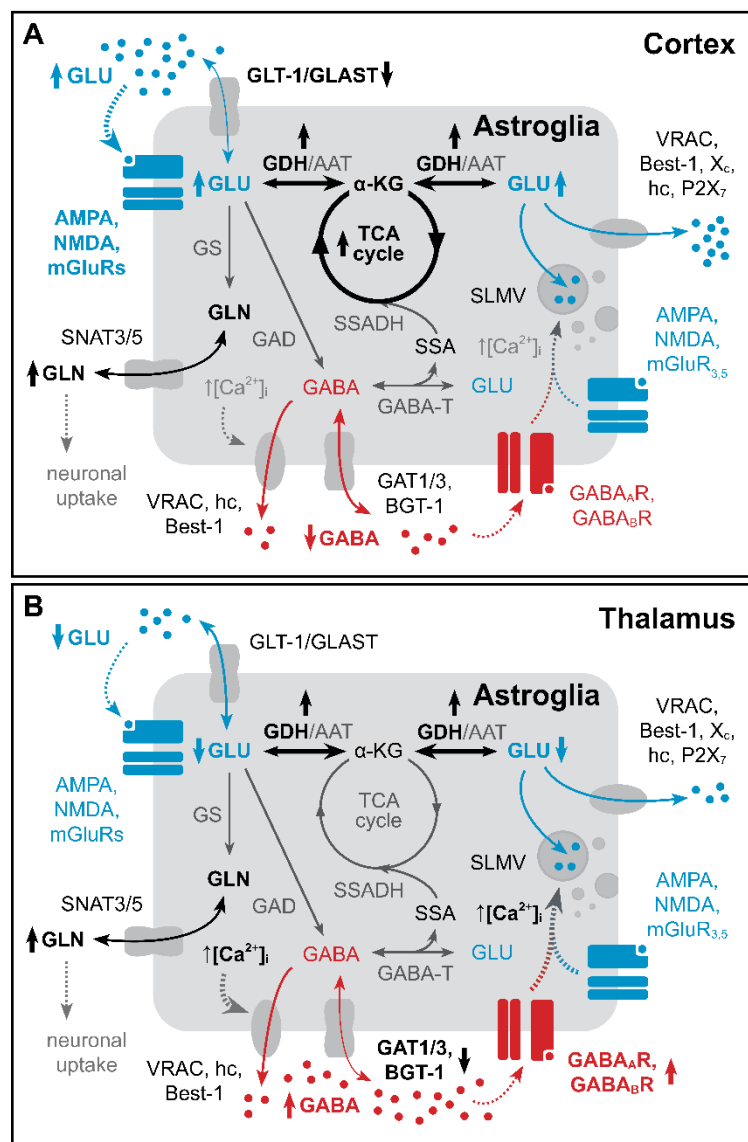


Figure 3. Alterations of astroglial glutamatergic and GABAergic signalling in absence seizures

(A) Cortical and (B) thalamic alterations associated with absence seizures and revolving around astroglial glutamatergic and GABAergic signalling. In the cortex, decrease glutamate transport via GLT-1 and GLAST as well as enhanced astroglial metabolism are associated with increased glutamate and glutamine levels and decreased GABAergic tone. In the thalamus, malfunctions in the GABA transport and increase GDH expression are coupled to reduced glutamate levels and increased GABA tone as well as GABAergic signalling. See 4.3.2 for References.

α -KG, α -ketoglutaric acid; AMPA, α -amino-3-hydroxy-5-methyl-4-isoxazolepropionic acid receptor; Best-1, bestrophin-1 channel; GABA, γ -aminobutyric acid; GABA_AR, γ -aminobutyric acid receptor A; GABA_BR, γ -aminobutyric acid receptor B; GAD, glutamate decarboxylase; GAT, GABA transporter; GABA-T, GABA transaminase; GDH, glutamate dehydrogenase; GLAST, glutamate aspartate transporter; GLN, glutamine; GLT-1, glutamate transporter 1; GLU, glutamate; GS, glutamine synthetase; hc, hemichannel; mGluR, metabotropic glutamate receptor; NMDA, N-methyl-D-aspartic acid receptor; SLMV, synaptic-like microvesicle, SNAT, sodium-coupled neutral amino acid transporter; SSA, succinic semialdehyde; SSADH, succinic semialdehyde dehydrogenase; TCA, tricarboxylic acid; VRAC, volume-regulated anion channel; X_c⁻, cysteine-glutamate transporter system X_c⁻.

To date, there is substantial evidence demonstrating that alterations of astroglial GABAergic signalling contribute to absence seizures. In genetic models of absence epilepsy, malfunctions of the GABA transporter GAT-1 cause the abnormally high GABA levels as well as the altered GABA_AR-mediated tonic inhibition of TC neurons (Richards et al., 1995; Cope et al., 2009; Errington et al., 2011a; Pirttimaki et al., 2013). Given that in the thalamus astroglia are the only cells responsible for GABA uptake (De Biasi et al., 1998), the observed effect is attributed to astrocytes and not to neurons. Accordingly, pharmacological intrathalamic application of GAT inhibitors increases extrasynaptic GABA_AR-mediated tonic inhibition of TC neurons (Herd et al., 2013) and enhances SWDs in GAERS rats (D'Amore et al., 2015). Notably, mutations in the human gene *SLC6A1* coding for GAT-1 leading to reduced GABA uptake are associated with CAE or clinical conditions comprising absence seizures (Dikow et al., 2014; Johannesen et al., 2018; Mattison et al., 2018; Galer et al., 2020; Goodspeed et al., 2020). Astroglial control on GABAergic tone also relies on their capability to release GABA, which in turn can activate neuronal GABA_ARs (Jiménez-González et al., 2011). Notably, in the NRT astrocytes also enhance GABA_AR transmission via endozepine signalling (Christian and Huguenard, 2013). Since thalamic astrocytes also express GABA_ARs (Höft et al., 2014), GABA release may also elicit autocrine and paracrine astroglial activation. Agonists of GABA_BRs such as baclofen and GHB are sufficient to induce absence seizures in rodents and exacerbate them in genetic absence seizure models (Vergnes et al., 1984; Crunelli and Leresche, 1991; Liu et al., 1992; Marescaux et al., 1992a; Manning et al., 2003; Beenhakker and Huguenard, 2010; Bortolato et al., 2010). Although there is plenty of research on neuronal GABA_BR signalling in absence seizures, little is known about the contribution of astroglial GABA_BRs. Nevertheless, application of absence-inducing baclofen and GHB in the thalamus leads to intracellular Ca²⁺ increases in astrocytes independently of neuronal firing activity (Gould et al., 2014), thus suggesting

that astroglia are directly recruited by GABAergic agonists targeting GABA_BRs. Also, astroglial GABA_BR signalling revolving around internal Ca²⁺ oscillations is known to exert multiple function in network modulation, including synaptic transmission (Kang et al., 1998; Serrano et al., 2006; Perea et al., 2016; Covelo and Araque, 2018) and synaptogenesis (Nagai et al., 2019), thus possibly making it a key element in the mechanisms underlying absence seizure development and progression.

4.3.3 ASTROGLIAL Ca²⁺ SIGNALLING IN ABSENCE SEIZURES: THE STATE OF THE ART

Astroglial intracellular Ca²⁺ signalling is connected to neural network activity before and during seizures on many levels. On one hand, excessive network activity leads to excitotoxic spilling of neurotransmitters such as glutamate, GABA and ATP (Carmignoto and Haydon, 2012; Shigetomi et al., 2019), which induce astroglial Ca²⁺ response and gliotransmission, therefore further contributing to network synchronicity and E/I imbalance (Parri et al., 2001; Angulo et al., 2004; Fellin et al., 2004; Tian et al., 2005; Gómez-Gonzalo et al., 2010; Koizumi, 2010; Sasaki et al., 2014; Álvarez-Ferradas et al., 2015; Wellmann et al., 2018). On the other hand, astrocytic Ca²⁺ oscillations were shown to precede and facilitate convulsive seizures *in vivo* (Heuser et al., 2018) and associate with seizure propagation and self-sustain (Gómez-Gonzalo et al., 2010; Kékesi et al., 2015; Losi et al., 2016; Ujita et al., 2017) as well as termination (Seidel et al., 2016). Nevertheless, current research is still far from elucidating astroglial Ca²⁺ contribution to seizure onset, propagation, severity and termination both in mechanistic as well as logical (sufficiency and/or necessity) terms and research on absence seizures is no exception. Yet, several lines of evidence suggest that astroglial Ca²⁺ oscillations influence CTCn function. TC neurons display *ex vivo* NMDA receptor-mediated long lasting inward currents in response to spontaneous astrocytic Ca²⁺ signalling and glutamate release (Parri and Crunelli, 2001; Parri et al., 2001). Also, at least a subpopulation of thalamic astrocytes responds to CT afferents by means of mGluR5 (Parri et al., 2010; Pirttimaki et al., 2011; Pirttimaki and Parri, 2012) and mGluR2 (Copeland et al., 2017) activation, leading to astroglial Ca²⁺ increase, glutamate release and inhibition of presynaptic GABAergic projections from the NRT. Notably, artificial inhibition of Ca²⁺ oscillation in striatal astrocytes leads to GAT-3 functional upregulation resulting in enhanced GABA uptake (Yu et al., 2018). Finally, GHB induces GABA_B receptor-mediated Ca²⁺ signalling in thalamic astrocytes (Gould et al., 2014), but there is to date no evidence about cortical astroglial responses to GHB, neither it is clear if and how GHB-induced GABA_B-mediated Ca²⁺ signalling in astrocytes contribute to the pathology of absence seizures.

5 AIMS OF THE STUDY

Several lines of evidence indicate that the molecular and cellular mechanisms underlying absence seizures include and possibly revolve around alterations in GABAergic signalling. Astroglia, and in particular astrocytic Ca^{2+} response and subsequent gliotransmitter release, are key players in the pathophysiology of epileptic network function. Nevertheless, the contribution of astrocytes to the altered GABAergic transmission and specifically astrocytic GABA_B receptor (GABA_BR)-mediated response have been not fully elucidated in the context of absence seizures.

Therefore, the aim of this work is to investigate the contribution of astrocytic GABA_BRs in the pathological network function associated to absence seizures.

To this aim, we arranged the following work packages:

- **Induce absence seizures in mice with astrocyte-specific conditional GABA_BR deletion**

We took advantage of the γ -hydroxybutyric acid (GHB) acute pharmacological model of absence seizures to induce spike-and-wave discharges (SWDs) in transgenic mice with astrocyte-specific conditional GABA_BR deletion (GABA_BR cKO). The dose-dependency and time-course of GHB-induced effects were evaluated by means of electroencephalography (EEG) of freely moving animals.

- **Assess the impact of GABA_BR deletion on electrical epileptiform activity associated to GHB-induced absence seizures**

Whole-brain continuous telemetric EEG recording synchronized to video monitoring was employed to identify GHB-induced spectral alterations as well as SWD occurrence, duration and spike frequency in freely moving control (ctrl) and cKO mice, thus enabling a correlation analysis between EEG and animal activity.

- **Evaluate cortical astrocytic Ca^{2+} activity in ctrl and cKO mice upon GHB administration**

For the evaluation of astroglial Ca^{2+} signalling, we induced the astrocyte-specific conditional expression of the genetically encoded Ca^{2+} indicator GCaMP3 and recorded astrocytic Ca^{2+} response by means of two-photon laser scanning microscopy (2P-LSM) in acute slice preparations upon GHB focal application and *in vivo* after GHB systemic administration.

- **Monitor animal motor activity and behaviour after GHB administration**

Control and cKO mice were monitored after GHB administration in the open field arena and in their home cage to assess the effect of GABA_BR deletion on animal motor activity and freezing behaviour.

6 MATERIALS AND METHODS

6.1 MATERIALS

6.1.1 REAGENTS

Unless otherwise stated, standard chemicals were purchased from companies like Amersham Biosciences (Freiburg, DE), BD Biosciences (Heidelberg, DE), BioRad (München, DE), Carl Roth (Karlsruhe, DE), Eppendorf (Hamburg, DE), Honeywell Riedel-de-Haën (Hannover, DE), Merck (Darmstadt, DE), Invitrogen (Karlsruhe, DE), Roche (Penzberg, DE), Sigma-Aldrich (Taufkirchen, DE), Thermo Fisher Scientific (Dreieich, DE).

6.1.2 CONSUMABLES

Pipette tips, Sarstedt (Nümbrecht, DE); glass pipettes, VWR International (Darmstadt, DE); borosilicate glass pipettes, Sutter Instrument (Novato, CA, US); syringes and connectors, BD Biosciences (Heidelberg, DE); silicone tubing, Tygon, Saint-Gobain Performance Plastics (Courbevoie, FR), Falcon tubes, Greiner Bio-One (Frickenhausen, DE); Eppendorf reaction tubes, Eppendorf (Hamburg, DE); Venomix canulas, Braun (Melsungen, DE); 96-well PCR reaction-tubes, 4titude (Berlin, DE); 48-well-culture plates, Sarstedt (Nümbrecht, DE); object slides and cover slips, Menzel-Gläser (Braunschweig, DE); gentleMACS C Tubes (Cat. no. 130-093-237), Miltenyi Biotec (Bergisch Gladbach, DE); MACS SmartStrainer (70 μ m, Cat. no. 130-098-462), Miltenyi Biotec (Bergisch Gladbach, DE); MACs MS Columns (Cat. no. 130-042-201), Miltenyi Biotec (Bergisch Gladbach, DE).

6.1.3 DEVICES

Devices used in the generation of the data presented in this work are listed in Table 3.

Device	Manufacturer
Pipettes	Brand (Wertheim, DE)
Mini Star Centrifuge	neoLab (Heidelberg, DE)
Vortex Mixer	VWR International (Darmstadt, DE)
Centrifuge 5804	Eppendorf (Hamburg, DE)
peqSTAR Thermo Cycler	peqlab Biotechnologie Gmbh (Erlangen, DE)
Scales (CPA 8201/CPA 2245)	Sartorius (Göttingen, DE)
Magnetic stirrer C-MAG HS 7	IKA Gmbh (Staufen im Breisgau, DE)
Consort EV231 Power Supply	Merck (Darmstadt, DE)
Quantum gel documentation system	peqlab Biotechnologie Gmbh (Erlangen, DE)
DRS-12 Rocking Shaker	neoLab (Heidelberg, DE)

Surgical instruments	F.S.T. (Heidelberg, DE)
Bead sterilisator	F.S.T. . (Heidelberg, DE)
Robot stereotaxic	Neurostar (Tübingen, DE)
Infrared Thermometer (IRF 260-8S)	Voltcraft (Hirschau, DE)
Water bath WNE14	Memmert Gmbh (Schwabach, DE)
Micropipette Puller P-97	Sutter Instruments (Novato, California, US)
Peristaltic pump LKB P-1	Pharmacia LKB (Uppsala, SE)
Vibratome VT1000S/VT1200S	Leica Biosystems (Wetzlar, DE)
gentleMACS™ Octo Dissociator with Heaters	Miltenyi Biotec (Bergisch Gladbach, DE)
BlueVertical™ PRiME™	SERVA Electrophoresis GmbH (Heidelberg, DE)
ChemiDoc™ MP Gel Imaging Sytem	BioRad (München, DE)
HybEZ™ Hybridization System	Advanced Cell Diagnostics (Newark, CA, US)

Table 3. List of devices

6.1.4 BUFFERS

All buffers were prepared with ultrapure water (ddH₂O) from the MilliQ water purification system (Merck, Darmstadt, DE). All stated concentrations are final working concentration.

Phosphate buffered saline (PBS, pH 7.4)

NaCl	137	mM
KCl	2.7	mM
Na ₂ HPO ₄	10	mM
KH ₂ PO ₄	1.8	mM

Formaldehyde (FA, pH 7.4)

Paraformaldehyde (PFA)	4	% (w/v)
NaH ₂ PO ₄	0.2	M
Na ₂ HPO ₄	0.2	M

Tris-Acetate-EDTA buffer (TAE)

Tris(hydroxymethyl)aminomethane	40	mM
Acetid acid (100%)	20	mM
Ethylendiamintetraacetic acid (EDTA, 0.5 M, pH 8.0)	0.4	mM

Agarose gel in TAE buffer (1x)

Agarose Powder	2	% (w/v)
Ethidium Bromide	0.5	µg/ml

DNA extraction solution (pH 9.5)

KCl	0.25	M
EDTA	0.01	M
Tris-HCl	0.1	M

Neutralization solution in PBS (1x)

Bovine Serum Albumin (BSA)	3	% (w/v)
----------------------------	---	---------

Blocking buffer in PBS (1x)

Horse Serum (HS)	5	% (v/v)
Triton-X-100	0.3	% (v/v)

Cutting solution in ddH₂O (pH 7.4)

NaCl	87	mM
KCl	3	mM
Na ₂ H ₂ PO ₄	1.25	mM
NaHCO ₃	25	mM
Glucose	25	mM
Sucrose	75	mM
MgCl ₂	3	mM
CaCl ₂	0.5	mM
HEPES	5	mM

Incubation solution in ddH₂O (pH 7.4)

NaCl	126	mM
KCl	3	mM
Na ₂ H ₂ PO ₄	1.25	mM
NaHCO ₃	25	mM
Glucose	15	mM
MgCl ₂	1	mM
CaCl ₂	2.5	mM

Perfusion solution in ddH₂O (pH 7.4)

NaCl	126	mM
KCl	3	mM
Na ₂ H ₂ PO ₄	1.25	mM
NaHCO ₃	25	mM
Glucose	15	mM
MgCl ₂	2	mM
CaCl ₂	1	mM

Cortex buffer (pH 7.4)

NaCl	125	mM
KCl	5	mM
Glucose	10	mM
HEPES	10	mM
CaCl ₂	2	mM
MgSO ₄	2	mM

6.1.5 ENZYMES

DreamTaq™ Hot Start Green DNA Polymerase, Thermo Fisher Scientific (Dreieich, DE)

6.1.6 DRUGS

Drugs used in the presented work are listed in Table 4.

Drug	Manufacturer	Working concentration		
Adenosine-5'-triphosphate disodium salt (ATP)	Sigma-Aldrich (Taufkirchen, DE)	100	μM	
(±)-Baclofen	Cayman Chemical (Hamburg, DE)	100	μM	
γ-hydroxybutyric acid sodium salt (GHB)	Unavera ChemLab GmbH (Mittenwald, DE)	0.1-10	mM	(<i>ex vivo</i>)
		70-250	mg/kg	(<i>in vivo</i>)
Ketamine hydrochloride	Serumwerk Bernburg AG (Bernburg, DE)	100	mg/ml	
Miglyol® 812	Caesar & Loretz GmbH (Hilden, DE)			
Tamoxifen	Sigma-Aldrich (Taufkirchen, DE)	10	mg/ml	
Tetrodotoxin Citrate (TTX)	Alomone Labs (Jerusalem, IL)	1	μM	
Xylazine hydrochloride	WDT (Garbsen, DE)	20	mg/ml	

Table 4. List of drugs

6.1.7 ANTIBODIES

6.1.7.1 PRIMARY ANTIBODIES

Primary antibodies used in the presented work are listed in Table 5.

Target	Clonality	Host	Dilution	Manufacturer
α-tubulin	monoclonal	mouse	1:2000	Sigma-Aldrich (Taufkirchen, DE)
c-Fos	polyclonal	guinea pig	1:10000	Synaptic System (Göttingen, DE)
GABAB1	monoclonal	mouse	1:500	Abcam (Cambridge, UK)
GFAP	polyclonal	goat	1:1000	Abcam (Cambridge, UK)
GFP	polyclonal	chicken	1:1000	Invitrogen (Karlsruhe, DE)
Iba1	polyclonal	rabbit	1:1000	Agilent (Santa Clara, US)
MBP	monoclonal	mouse	1:500	BioLegend (San Diego, US)
PV	polyclonal	rabbit	1:1000	Invitrogen (Karlsruhe, DE)
S100β	monoclonal	rabbit	1:500	Abcam (Cambridge, UK)

Table 5. Primary antibodies for immunohistochemistry

6.1.7.2 SECONDARY ANTIBODIES

Secondary antibodies used in the presented work are listed in Table 6.

Host α -target	Conjugated fluorophore	Dilution	Manufacturer
Donkey α -chicken	Alexa Fluor® 488	1:1000	Invitrogen (Karlsruhe, DE)
	Alexa Fluor® 790	1:1000	Invitrogen (Karlsruhe, DE)
Donkey α -goat	Alexa Fluor® 546	1:1000	Invitrogen (Karlsruhe, DE)
Donkey α -guinea pig	Alexa Fluor® 647	1:500	Merck (Darmstadt, DE)
Donkey α -mouse	Alexa Fluor® 488	1:1000	Invitrogen (Karlsruhe, DE)
Donkey α -rabbit	Alexa Fluor® 546	1:1000	Invitrogen (Karlsruhe, DE)
	Alexa Fluor® 790	1:1000	Invitrogen (Karlsruhe, DE)

Table 6. Secondary antibodies for immunohistochemistry

6.1.8 DYES

Dyes used in the presented work are listed in Table 7.

Drug	Manufacturer	Work concentration
4',6-Diamidin-2-phenylindol (DAPI)	Sigma-Aldrich (Taufkirchen, DE)	0.025 μ g/ml
Ethidium Bromide	Carl Roth (Karlsruhe, DE)	10 mg/ml
EasyLadder I (500 Lanes)	Bioline (Neunkirchen, DE)	50 ng/ml
Sulforhodamine B sodium salt	Cayman Chemical (Hamburg, DE)	0.25 mg/ml

Table 7. List of dyes

6.1.9 PRIMERS

Forward and reverse PCR genotyping primers (Roche, Mannheim, DE) are listed in Table 8.

Name	Serial number	Sequence (5' → 3')	Product size (bp)
GABA _B forward	24391	TGGGGTGTGTCCTACATGCAGCGGACGG	742 (KI)
GABA _B reverse	24392	GCTCTTCACCTTTCAACCCAGCCTCAGG CAGGC	526 (wt)
GCaMP3 KI forward	27632	CACGTGATGACAAACCTTGG	
GCaMP3 KI reverse	27496	GGCATTAAAGCAGCGTATCC	245 (KI)
GCaMP3 WT forward	14025	CTCTGCTGCCTCCTGGCTTCT	327 (wt)
GCaMP3 WT reverse	14026	CGAGGCGGATCACAAGCAATA	
GLAST forward	11984	GAGGCACTTGGCTAGGCTCTGAGGA	
GLAST KI reverse	11986	GGTGTACGGTCAGTAAATTGGACAT	400 (KI)
GLAST WT reverse	11985	GAGGAGATCCTGACCGATCAGTTGG	700 (wt)

Table 8. Genotyping primers

6.1.10 GENETICALLY MODIFIED MOUSE LINES

In this work, we made use of the single transgenic mouse lines listed in Table 9 and kept in the C57BL6/N background. Shortly, we took advantage of the Cre^{ERT2}-loxP system to induce the time-controlled and cell-specific knock-out of target genes and expression of reporter proteins (Feil et al., 2009).

Name	Symbol	MGI ID	Reference
TgH (GABA _B R1 ^{fl/fl})	Gabbr1 ^{tm2.1Bet}	3512743	(Haller et al., 2004)
TgH (GLAST-Cre ^{ERT2})	Slc1a3 ^{tm1(cre/ERT2)Mgoe}	3830051	(Mori et al., 2006)
TgH (Rosa 26-CAG-lsl-GCaMP3)	Gt(ROSA)26Sor ^{tm1(CAG-GCaMP3)Dbe}	5659933	(Paukert et al., 2014)

Table 9. Genetically modified mouse lines

CAG, cytomegalovirus-immediate early enhancer/chicken β -actin/rabbit β -globin hybrid promoter; Cre^{ERT2}, inducible Cre DNA recombinase fused to the mutant ligand binding domain of the human estrogen receptor; fl, loxP floxed site; GABA_BR1, GABA_B receptor subunit 1; GLAST, glutamate aspartate transporter; lsl, floxed STOP cassette; MGI, Mouse Genome Informatics database; TgH: genetically modified mouse line via homologous targeted recombination.

In the single transgenic mouse line TgH (GLAST-Cre^{ERT2}), the open reading frame coding for the fusion protein Cre^{ERT2} is knocked into the *Slc1a3* locus and replace the exon II of the L-glutamate/L-aspartate transporter gene (GLAST, chr15qA2) close to the translation initiation site (Mori et al., 2006). The fusion protein Cre^{ERT2} is made up of the Cre DNA recombinase and the mutant ligand binding domain of the human estrogen receptor (Metzger and Chambon, 2001; Seibler et al., 2003;

Feil et al., 2009). As it is the case for the endogenous estrogen receptor, Cre^{ERT2} is confined in the cytosol due to its binding to heat shock proteins (HSPs). On the other hand, it is mostly insensitive to natural ligands, whereas it is highly sensitive to synthetic estrogen antagonists, such as 4-hydroxytamoxifen (Feil et al., 1997; Indra et al., 1999), which enables the translocation to the nucleus after binding and displacement of the HSPs. Here, Cre^{ERT2} mediates DNA recombination in correspondence of target sequences flanked by loxP sites (Sternberg and Hamilton, 1981; Hamilton and Abremski, 1984). In this work, the TgH (GLAST-Cre^{ERT2}) mouse line was crossbred with the TgH (GABA_BR1^{fl/fl}) mouse line, in which two lox511 sites were inserted into the introns flanking the critical exons VII and VIII in the *Gabbr1 locus* (GABABR1, chr17qB1) coding for the metabotropic GABA_B receptor subunit 1 (Haller et al., 2004). Since functional heterodimeric GABA_B receptors require the presence of both subunits, excision of the floxed sequence results in the absence of functional GABA_B receptor on the cellular membrane (Bettler et al., 2004). In addition, we crossbred the Cre^{ERT2} driver line with the TgH (Rosa 26-CAG-lsl-GCaMP3) (Paukert et al., 2014) reporter mouse line carrying the cDNA of the genetically encoded Ca²⁺ indicator GCaMP3 under the control of the cytomegalovirus-immediate early enhancer/chicken β -actin/rabbit β -globin hybrid promoter (pCAGGs) (Niwa et al., 1991) and inserted into the *Rosa26 locus* (chr6qE3) expressed ubiquitously (Friedrich and Soriano, 1991). GCaMP3 consists of a circularly permuted enhanced green fluorescent protein (EGFP) sequence fused with the chicken smooth muscle M13 domain of the myosin light chain kinase and the Ca²⁺-binding calmodulin at its N- and C-termini, respectively (Nakai et al., 2001; Tian et al., 2009). To ensure that the expression of GCaMP3 takes place only in dependence of the Cre^{ERT2} driver, a neomycin STOP cassette floxed by two loxP sites (*lsl*) is inserted upstream of the GCaMP3 cDNA. The expression is enhanced by a downstream Woodchuck hepatitis virus posttranscriptional regulatory element (WPE) (Donello et al., 1998).

In this work, the combined use of the GLAST-Cre^{ERT2} driver line with the floxed *Gabbr1* and the GCaMP3 reporter mouse lines enables the conditional GABA_B receptor (GABA_BR) deletion coupled to the expression of GCaMP3 specifically in GLAST⁺ astrocytes. To this aim, we used animals heterozygous for GLAST-Cre^{ERT2} (*Slc1a3* ct2/wt) and homozygous floxed for the GCaMP3 reporter (*Rosa26 GCaMP3* fl/fl). Control and conditional knock-out animals (cKO) were homozygous non-floxed (*Gabbr1* wt) and floxed (*Gabbr1* fl/fl) for the *Gabbr1 locus*, respectively.

6.1.11 SOFTWARE

For two-photon laser-scanning microscopy image acquisition, the open-source MATLAB-based software application ScanImage® (Vidrio Technologies, Ashburn, VA, USA) (Pologruto et al., 2003) was used. The custom-made MATLAB-based software MSparkles, GraphPad Prism 8 and Microsoft Office Excel 2016 were used for data analysis. Immunohistochemical data were visualized

and modified using the ZEN blue imaging software (Zeiss, Oberkochen, DE) and the ImageJ collection Fiji. Electrophysiological telemetric recordings were performed using the Ponemah software platform (DSI, Data Sciences International, St. Paul, USA). Video monitoring during electrophysiological telemetric recording was performed using MediaRecorder software (Noldus Information Technology, Wageningen, NL). The data analysis of the recordings was performed using NeuroScore (DSI, Data Sciences International, St. Paul, USA). For open field tests, animal recordings were examined and analysed using the software EthoVision XT (v. 11.5, Noldus Information Technology, Wageningen, NL). For figure layout, the Adobe Creative Suite 2021 was used (Adobe InDesign®, Adobe Illustrator®, Adobe Photoshop®). Database research was done using the free internet search service PubMed of the National Center for Biotechnology Information (NCBI).

6.1.12 GRAPHICAL ELEMENTS

The graphical abstract, the brain and skull models in Figure 2D, Figure 4B, the mouse in Figure 6B) and the cells in Figure 20A were generated with Biorender (<https://biorender.com/>).

6.2 METHODS

6.2.1 GENOTYPING

Mouse sample biopsy was conducted between two and three weeks of age in correspondence of pup weaning by the animal caretakers at the animal facility of the Center for Integrative Physiology and Molecular Medicine (CIPMM, Homburg, DE). The sample consisted of either tail (< 0.5 cm) or ear punch ($\varnothing < 0.5$ cm) biopsy and stored at -20 °C. The samples were incubated with 62.5 μ l DNA extraction solution at room temperature (RT) on a shaker (10 min, 700 min^{-1}). After incubation at 95 °C in the water bath for 20 min and subsequent cooling down, 50 μ l neutralization solution were added. For re-genotyping purposes, buccal swap samples were collected from adult animals and processed as previously described with the double amount of DNA extraction solution and neutralization solution. The extracted DNA sample was stored at 4 °C until use. For genotyping, samples were diluted 1:10 in ddH₂O with DreamTaq™ Hot Start Green DNA Polymerase (Thermo Fisher Scientific, Dreieich, DE) and oligonucleotide primers (listed in Table 8). The PCR reactions were run in 96-well PCR plates (4titude, Berlin, DE) in peqSTAR Thermo Cycler (peqlab Biotechnologie GmbH, Erlangen, DE). The details of the PCR reactions are listed in Table 10.

PCR	Hot Start	Loop (35X)			End	
		Annealing	Elongation	Denaturation		
	3 min	30 s	1 min	30 s	30 s	5 min
GABAB		56 °C			56 °C	
GCaMP3	95 °C	58 °C	72 °C	95 C	58 °C	72 °C
GLAST		58 °C			58 °C	

Table 10. PCR reaction protocols

Gel electrophoresis was run on 1-2 % agarose gels submersed in TAE buffer (180 V, 1000 mA, 150 W; 30-50 min) and subsequently exposed using the Quantum Gel documentation system (peQlab Biotechnologie GmbH, Erlangen).

6.2.2 TAMOXIFEN TREATMENT

Tamoxifen was diluted at a concentration of 10 mg/ml in Miglyol® 812 (Caesar & Loretz GmbH, Hilden, DE), aliquoted and stored at 4 °C. Four week-old mice were injected i.p. with tamoxifen at a daily dose of 100 mg/kg body weight for five consecutive days to induce maximal DNA recombination (Jahn et al., 2018). Animals were analysed between four to six weeks after TAM injection to ensure removal of functional GABA_BR from the astroglial membrane.

6.2.3 TISSUE COLLECTION

Animals were anesthetized with ketamine (250 mg/kg body weight) and xylazine (50 mg/kg). Once animals reached a surgical plane of anaesthesia monitored by pedal reflex in response to a firm toe pinch, the heart was exposed by performing a bilateral axillary thoracotomy. The animals were then transcardially perfused with ice-cold sterile Hank's balanced sodium solution without Ca²⁺ and Mg²⁺ (HBSS, Gibco™, Thermo Fisher Scientific, Dreieich, DE) by means of a butterfly needle inserted into the left ventricle. The flow was driven by a peristaltic pump (Pharmacia LKB, Uppsala, SE) and set at a speed of 5 ml/min. The blood was drained off the body through an incision made at the basis of the superior vena cava and visually monitored by the whitening of the liver. The brain cortex and thalamus were dissected one ice-cold HBSS.

6.2.4 MAGNETIC CELL SEPARATION

Magnetic cell separation (MACs) of astrocytes was performed according to the manufacturer's instructions (Miltenyi Biotec, Bergisch Gladbach, DE). The dissected cortex and thalamus were processed for mechanical dissociation and enzymatic degradation of the extracellular matrix as well as cell debris removal using the Adult Brain Dissociation Kit (Cat. no. 130-107-677, Miltenyi Biotec, Bergisch Gladbach, DE) to obtain a single-cell suspension. Astrocytes were MACs-purified from

the single-cell suspension using the Anti-ACSA-2 MicroBead Kit (ACSA, astrocyte cell surface antigen-2, cat. no. 130-097-678, Miltenyi Biotec, Bergisch Gladbach, DE) and stored at -80 °C. The purity of the MACs-purified cells and the enrichment of astrocyte-specific markers was assessed by means of immunocytochemistry and Western blot analysis (see Figure 9).

6.2.5 WESTERN BLOT ANALYSIS

MACs-purified astrocytes were lysed in RIPA buffer (ab156034, 1x, Abcam, Cambridge, UK) supplemented with protease (cOmplete-ULTRA™, 1x, Stock Keeping Unit 5892970001, Roche, Penzberg, DE) and phosphatase inhibitors (PhosSTOP™, 1x, Stock Keeping Unit 4906845001, Roche, Penzberg, DE). Protein samples (5 µg) were boiled for 5-10 min at 95 °C, run with Laemmli sample buffer (1x, cat. no. 1610737, BioRad, München, DE) on precast vertical gels (SERVAGel™ TG PRiME™ 4-20 %, cat. no. 43289.01, SERVA Electrophoresis GmbH, Heidelberg, DE) in denaturing conditions (SERVA Tris-Glycine/LDS Sample Buffer, 1x, cat. no. 42525.01, SERVA Electrophoresis GmbH, Heidelberg, DE) and blotted onto nitrocellulose transfer membranes (0.45 µm, cat. no.-88018, Thermo Fisher Scientific, Dreieich, DE). The membrane was blocked with 5% BSA diluted in 1x TBST (20 mM Tris, 150 mM NaCl. 0.1 % (w/v) Tween® 20) for one hour with agitation. Primary antibody-incubation was performed in blocking buffer overnight at 4 °C with agitation. The following day, membranes were washed with 1x TBST (three times, 10 min each) and incubated with HRP-conjugated anti-mouse secondary antibody (1:2000, A9044, Sigma-Aldrich, Taufkirchen, DE) for one hour at RT with agitation. The membranes were processed with the WesternBright Chemilumineszenz Substrat Quantum kit (art. no. 541015, Biozym Scientific GmbH, Hessisch Oldendorf, DE) and documented with the ChemiDoc™ MP Gel Imaging System (BioRad, München, DE).

6.2.6 WHOLE BODY FIXATION

Animals were anesthetized and perfused with PBS (1x, 15-20 ml) until complete blood draining as described in 6.2.3. The animals were then perfused with 4 % formaldehyde (FA, 25 ml, 5 ml/min). Finally, the brain was dissected and post-fixed in 4 % FA overnight at 4 °C. The brain tissue was stored at 4 °C in 1x PBS or in 0.5 % FA for short and long term use, respectively.

6.2.7 IMMUNOHISTOCHEMISTRY

The fixed brains were cut in 40 µm-thick transversal sections with a vibratome VT1000S (Leica Biosystems, Wetzlar, DE). Free floating slices were collected in 48-well culture plates containing 1x PBS and incubated in blocking buffer containing 5 % (v/v) HS and 0.3 % (v/v) Triton-X-100 for 1 h at RT. The slices were kept on a shaking plate throughout the procedure (12 min⁻¹, DRS-12 Rocking Shaker, neoLab, Heidelberg, DE). Primary antibody-incubation was performed in blocking buffer overnight at 4 °C. The following day, slices were washed with 1x PBS (three times, 10 min each)

and incubated with secondary antibodies and DAPI diluted in 1x PBS for 2 h at RT in the dark. Finally, the slices were washed with 1x PBS (three times, 15 min each) and mounted on glass slides using Eprelia Shandon Immu-Mount solution (Thermo Fisher Scientific, Dreieich, DE).

6.2.8 RNASCOPE

The detection of target RNAs was performed via fluorescence *in situ* hybridization using the RNAscope® Multiplex Fluorescent Kit v2 (cat. no. 323100) according to the manufacturer's instructions (Advanced Cell Diagnostics, Newark, CA; US). After perfusion with freshly prepared 4 % FA (as in 6.2.6), brains were dehydrated by sequential incubation in 10 %, 20 % and 30 % sucrose (one day each) and frozen with liquid nitrogen. After equilibration at -20 °C, 10 µm-thick sections were obtained using a cryostat and mounted on SuperFrost Plus® slides (cat. no. 12-550-15, Thermo Fisher Scientific, Dreieich, DE) for further processing. Pre-treatment and assay were performed using the HybEZ™ Hybridization System (110 Vca, cat. no. 310010, Advanced Cell Diagnostics, Newark, CA; US). Following probes were used: RNAscope® Probe- Mm-Slc1a3 (cat. no. 430781) for *Slc1a3* mRNA; RNAscope® Probe- Mm-Gabbr1- C2 (cat. no. 425181-C2) for *Gabbr1* mRNA. Following fluorophores were used: TSA® Plus fluorescein (1:1500, no. NEL741001KT); TSA® Plus Cyanine 3 (1:1500, no. NEL744001KT, PerkinElmer, Waltham, MA, US). Before proceeding to mounting and storage at 4 °C, slides can be processed similarly as in 6.2.7 for immunohistochemistry.

6.2.9 ACUTE SLICE PREPARATION

For acute brain slice preparation (Figure 4A), 8 to 10-week old mice were euthanized by cervical dislocation followed by decapitation. Right afterwards, the brain was dissected and placed into ice-cooled, carbogen-saturated (5 % CO₂, 95 % O₂) cutting solution. 300 µm-thick sections were cut with a vibratome VT1200S (Leica Biosystems, Wetzlar, DE) using a 0.12 mm/s cutting speed and a 1.9 mm cutting amplitude. They were subsequently placed on a custom-made nylon-basket submerged in incubation solution and kept at 35°C for 30 min. The procedure between decapitation and incubation was performed as fast as possible and in no longer than 10 min for optimal quality of the slice preparation. No more than four slices were collected from each brain in correspondence to the primary somatosensory cortex (SSp-ctx, AP -1.6 ± 0.6) and were cut along the medial sagittal axis to separate the two hemispheres (Figure 4B, C). After incubation the hemislices were recovered with continuous oxygenation for at least 30 min at RT before recording.

6.2.9.1 EX VIVO IMAGING

The hemislices were transferred to a self-made imaging chamber under a custom-made two-photon laser-scanning microscope (2P-LSM) and fixed by stainless steel rings with 1 mm-spaced nylon fibres (Harp Slice Grid HSG-5A; ALA Scientific Instruments Inc., Farmingdale, NY, USA). The

imaging chamber was continuously perfused with oxygenated perfusion solution at a flow rate of 2–5 ml/min with a custom-made perfusion system driven by a peristaltic pump LKB P-1 (Pharmacia LKB, Uppsala, SE). For experiments requiring blockage of neuronal firing activity, hemislices were incubated for 15 min in perfusion solution containing the voltage-gated Na⁺ channel blocker tetrodotoxin (TTX, 1 μM, Alomone Labs, Jerusalem, IL) and continuously perfused with the same solution throughout the recording time. Squared field of views (FOVs, 170 x 170 μm) from the cortical layers II-III of the SSp-ctx were chosen at a depth ranging from 30 to 100 μm from the slice surface and displaying a uniform astroglial distribution (Figure 4D, E). Each FOV was recorded for up to 15 min and each hemisphere was kept in the imaging chamber for up to 30-45 min.

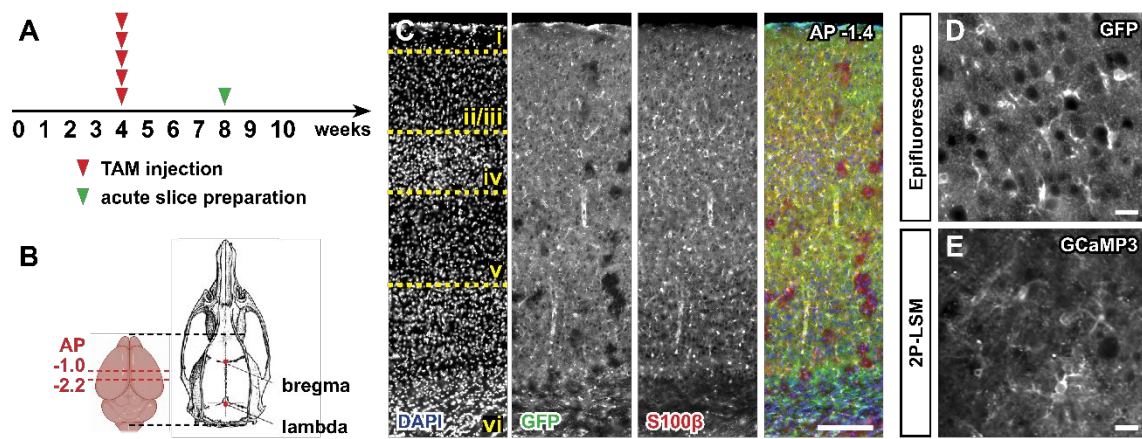


Figure 4. Experimental design of acute slice preparation

(A) Experimental design for tamoxifen (TAM) injection and acute slice preparation. (B) Schematics of mouse anatomical points (bregma and lambda) with respect to mouse skull and brain. 300 μm coronal slices were collected in correspondence of the primary somatosensory cortex (SSp-ctx, indicatively from 1 mm to 2.2 mm posterior to bregma). AP, anteroposterior axis. (C) Immunohistochemistry on 40 μm-thick fixed slices for GFP (detecting GCaMP3, green) and the astroglial marker S100β (red) in the SSp-ctx. DAPI (blue) was used to identify the cortical layers (i-vi). Scale bar, 200 μm. (D-E) Close-up view of the GFP signal from the layer 2/3 of the SSp-ctx and GCaMP3 signal recorded by two-photon laser-scanning microscopy (2P-LSM) from the same region (displayed as arithmetic average of a 5 min recording session). Scale bar, 20 μm. (B), modified from (Ferry et al., 2014).

6.2.9.2 FOCAL DRUG APPLICATION

Focal drug application was performed under the 2P-LSM by means of borosilicate glass pipettes (BF150-86-10, Sutter Instrument, Novato, CA, US) mounted on 3-axis micromanipulator units (LN Mini 25, Luigs & Neumann GmbH, Ratingen, DE) controlled by a SM5 Remote Control station (Luigs & Neumann GmbH, Ratingen, DE) (Figure 5A-B). Pipettes were pulled using a micropipette Puller P-97 (Sutter Instrument, Novato, CA, US) in order to obtain a 5 μm-opening tip (0.5-1 MΩ, see Table 11 for program detail).

Step	Temperature	Pull	Velocity	Delay	Pressure
	° C	arb. unit	arb. unit	ms	arb. unit
1	<i>Ramp</i> - 2	0	35	1	500
2					
3	<i>Ramp</i> - 24	0	24		
4	<i>Ramp</i> - 9	1	28		

Table 11. Glass pipette pulling program

Pulling program for borosilicate glass pipettes (BF150-86-10, Sutter Instrument, Novato, CA, US). *Ramp* refers to the heat value required to melt the glass filament and can be determined by running a *Ramp test* using the micropipette puller. *Ramp* for BF150-86-10 filaments usually ranges between 550 and 600 °C. The units for Pull, Velocity and Pressure are specific for the Puller P-97 (Sutter Instrument, Novato, CA, US). A pressure of 550 arb. units corresponds to 0.136 atm.

The micropipette was filled with 5 µl of the drug of interest solved in perfusion solution containing 5 µg/ml Sulforhodamine B sodium salt (SRB, Cayman Chemical, Hamburg, DE) to monitor the application during the 2P-LSM session. After approaching the slice surface at a 0.5 mm/s speed, the micropipette was positioned in the FOV at lower speed (2 µm/s) with a 25° angle to minimize tissue compression and mechanical insult. Focal application was manually performed by means of 1 ml-syringes (BD Biosciences, Heidelberg, DE) connected to the micropipette head stage via silicon tubes using a constant pressure (1.2-1.5 atm) for 10 s (Figure 5C). The success and extent of the application was monitored during the acquisition as well as in the subsequent data analysis using the SRB signal (Figure 5D-E). The detailed application protocol varied among the different experimental settings (see Results for details) but always included a 4-5 min baseline and at least 2 min between each application. At the end of each application protocol the imaging chamber was washed completely with perfusion solution for 5 min.

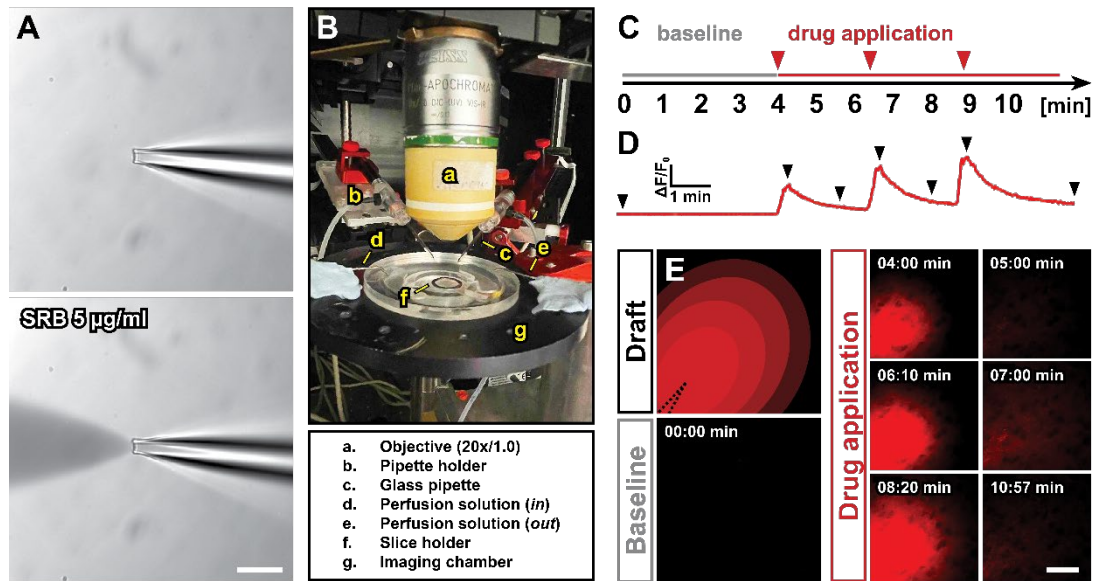


Figure 5. Focal drug application during 2P-LSM

(A) Bright-field image of a glass pipette used for focal drug application before (upper panel) and after (lower panel) releasing saline solution (0.9 % NaCl) containing 5 $\mu\text{g/ml}$ Sulforhodamine B (SRB). Scale bar, 10 μm . (B) Setup for 2P-LSM of acute slice preparations equipped with two 3-axis micromanipulator units enabling focal drug application during image acquisition. (C) Schematics of the protocol for focal drug application including a 4-5 min baseline and consecutive applications at a 2-3 min interval and (D) signal recorded during a representative 2P-LSM session. (E) Draft schematics of the pipette tip and SRB application in the field of view (FOV) and representative time frames (indicated as black arrowheads in D) displaying the temporally and spatially controlled application of SRB. Scale bar, 50 μm .

6.2.10 SURGICAL PROCEDURES

Prior to any surgical procedure, anaesthesia was induced with 5 % isoflurane delivered with O₂ (0.8 l/min) and N₂O (0.4 l/min) using a vaporizer apparatus (Tec3 Selectatec Vaporizers, Harvard Apparatus, Holliston, US) and mice were injected with analgesics (buprenorphine, 0.1 mg/kg, s.c.) and anti-inflammatory drugs (dexamethasone, 0.2 mg/kg, i.p.). Throughout the surgery, mice were kept under 1.5-2 % isoflurane anaesthesia and placed on a heating plate. The body temperature was kept between 36.6-37 °C and monitored using a rectal probe. The corneas were covered with Bepanthen eye ointment (Bayer AG, Leverkusen, DE). To ensure antiseptic conditions, all surgical instruments were sterilized using a Bead sterilisator (F.S.T., Heidelberg, DE) at 300 °C for 5 min and a povidone-iodine solution (Betaisodona®, Mundipharma GmbH, Frankfurt am Main, DE) was applied on affected animal surfaces before and after the surgery. After the surgery the mice were injected with carprofen (5 mg/kg, i.p.) and dexamethasone once per day for three consecutive days and received either buprenorphine (1 mg/kg) or tramadol hydrochloride in the drinking water (400 mg/l, Grünenthal GmbH, Stokenchurch, UK). The mice were monitored continuously till the end of the experiment to ensure the absence of excessive weight loss ($\geq 20\%$), which would require

the forced termination of the experimental procedure. To the scopes of this work, no animal required this intervention.

6.2.10.1 CRANIOTOMY AND WINDOW IMPLANTATION

After exposing the skull, the animals underwent a standard craniotomy (Cupido et al., 2014; Kislin et al., 2014) in correspondence of the SSp-ctx (\varnothing 3-4 mm, centred 1.5-2 mm posterior to bregma, 1.5 mm from the sagittal medial axis). The glass coverslip (\varnothing 3 mm, No. 1.5, Glaswarenfabrik Karl Hecht GmbH, Söndheim v.d. Rhön, DE) and a custom-made holder for head restraining were fixed with dental cement (RelyX™ Unicem 2 Clicker, 3M Deutschland GmbH, Neuss, DE). Animals received the canonical post-surgical care and imaging was performed at least one week after cranial window implantation.

6.2.10.2 *IN VIVO* IMAGING

Ca²⁺ imaging from head-fixed animals was performed using a custom-made two-photon laser-scanning microscope (2P-LSM) setup. Recordings started at least one week after cranial window implantation to enable animal recovery and habituation according to adapted protocols without water restriction (Guo et al., 2014; Kislin et al., 2014). During image acquisition (5-15 min), animals were maintained head-fixed under light isoflurane anaesthesia (0.5 % isoflurane) delivered by means of a custom-made nose mask. During head fixation, drug administration and in between recording sessions the animals received 1.5 % isoflurane anaesthesia. Each imaging session lasted up to 1 h and was interrupted at any sign of animal discomfort. Squared FOVs (256 x 256 μ m) were chosen at a depth ranging from 50 to 150 μ m from the dura mater and displaying a uniform astroglial distribution. Drugs administered during the imaging session were solved in isotonic saline solution (NaCl 0.9 %, Braun, Melsungen, DE) containing 5 μ g/ml SRB to monitor the effective delivery through the circulatory system.

6.2.10.3 EEG TRANSMITTER IMPLANT AND RECORDING

In vivo electroencephalography (EEG) was performed using implantable ETA-F10 transmitters (DSI PhysioTel® ETA-F10, Harvard Biosciences, US), which enable continuous telemetric monitoring of EEG, temperature and animal activity (Figure 6). The ETA-F10 transmitter (2.0 x 1.0 x 0.5 cm) is connected to two insulated wires that are wrapped around the transmitter body before starting the surgical procedure and are fixed with non-absorbable silk suture (Braintree Scientific, Braintree, US). The transmitter was placed in a subcutaneous pouch in the animal flank and the insulated wires are run subcutaneously to the implantation site on the skull surface. The wire extremities (0.5 mm) were deprived of their insulation, inserted in the brain as depth intracortical electrodes at a 90° angle with the cortical surface (bilaterally 1.6 mm from the sagittal medial axis and 3.4 mm posterior to bregma) and fixed with cyanoacrylate and dental cement (RelyX™ Unicem 2 Clicker, 3M

Deutschland GmbH, Neuss, Germany). For precise positioning and drilling, a Stereotaxic Drill Robot (Neurostar, Tübingen, DE) equipped with exchangeable steel round-shaped tip (\varnothing , 0.9 mm, Hager & Meisinger GmbH, Neuss, DE) was used. The animal skin was closed with an interrupted suture (absorbable suture thread, Eickfil, Eickemeyer, Tuttlingen, DE) and Michel suture clips (F.S.T., Heidelberg, DE) and the animals underwent the canonical post-surgical care. Mouse cages were placed on radio-receiving plates (DSI PhysioTel® RPC-1, Harvard Biosciences, US) connected to an input exchange matrix (DSI PhysioTel® Matrix 2.0, Harvard Biosciences, US) controlled using the Ponemah Software platform (DSI, St. Paul, US). Video monitoring was performed using the MediaRecorder Software (Noldus Information Technology, Wageningen, NL). Recordings started at least one week after the surgery to enable animal recovery and habituation. Each recording includes a baseline of at least 1 h before drug administration (i.p.) and up to 12 h monitoring afterwards. Drug administration was performed at least the end of the recording period, animals were perfused and the brains were collected for immunohistochemistry. ETA-F10 transmitters were cleaned with abundant ddH₂O and incubated 72 h in Tergazyme® (10 g/l, Alconox Inc., White Plains, US).

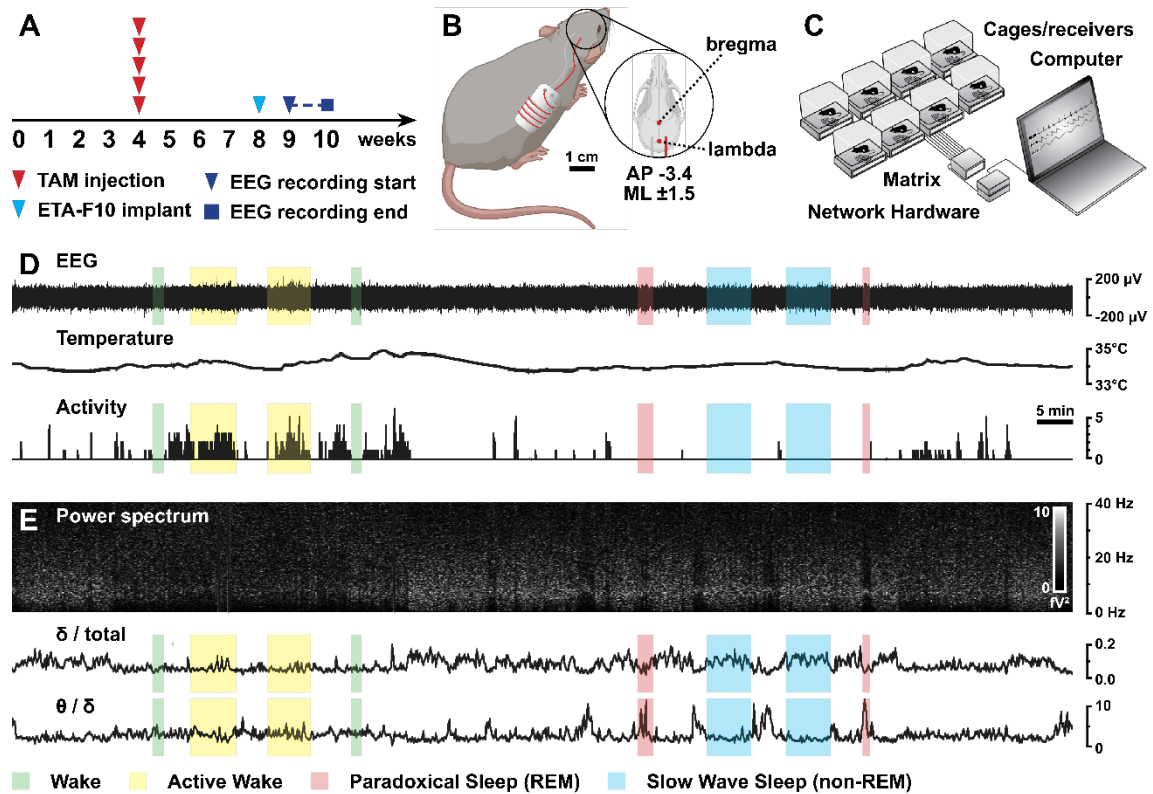


Figure 6. Telemetric EEG recording in freely moving mice

(A) Experimental design for tamoxifen (TAM) injection, ETA-F10 transmitter implant and telemetric *in vivo* electroencephalographical (EEG) recording. (B) Schematics of subcutaneous transmitter implantation and intracortical bilateral electrode positioning with respect to mouse anatomical point bregma. AP, anteroposterior axis; ML, mediolateral axis. (C) Schematic representation of the hardware required for telemetric EEG recording. (D) Representative EEG, temperature and activity traces recorded during a canonical EEG session. (E) Power spectrum analysis of the displayed EEG signal using 10 s-long epochs and color-coded according to the frequency power (upper panel) and derivative power ratios (middle and lower panel) used for the identification of the animal hypnogram stages. δ , 0.5-4 Hz; θ , 4-8 Hz; tot, 0-25 Hz. In D and E, representative bouts of wake, active wake, paradoxical sleep (REM) and slow wave sleep (non-REM) are highlighted. C, modified from *datasci.com* (DSI PhysioTel®, Harvard Biosciences, US).

6.2.11 OPEN FIELD TEST

Behavioural analysis was performed on 8-9 weeks-old mice in the animal facility of the Center for Physiology and Molecular Medicine (CIPMM, Homburg, DE) during the animal light phase approximately between 11 am and 16 pm). Subjects were placed in the behavioural room at least one day before the experimental start for habituation. For open field test analysis (Seibenhener and Wooten, 2015), the arena (50 cm x 50 cm x 35 cm) was evenly illuminated and wiped prior to use and between tests with 70 % ethanol to eliminate olfactory perturbative stimuli. The animals were recorded using a USB webcam placed at a 2 m height from the ground at attached to the ceiling (sampling rate 25 frames/s). For baseline recordings, the animals were placed in the middle of the arena and let move and explore freely for 15 min. One week after, the animals were recorded for 15 min starting 5 min after drug administration (i.p.).

6.2.12 MICROSCOPY

6.2.12.1 TWO-PHOTON LASER SCANNING MICROSCOPY

Images were acquired with a custom-made two-photon laser-scanning microscope (2P-LSM) setup equipped with a mode-locked Ti : sapphire femtosecond pulsed laser (Vision II, Coherent, St. Clara, US), XY-galvanometer-based scanning mirrors (Cambridge Technology, Bedford, US) and a 20x / 1.0 water-immersion objective (W Plan-Apochromat, Zeiss, Oberkochen, DE) using the ScanImage software (Pologruto et al., 2003). The excitation wavelength of the laser was set at 890 nm and the signals were detected by photomultiplier tubes (PMT, H10770PB-40, Hamamatsu Photonics, Hamamatsu, JP). The emission wavelength of GCaMP3 and SRB were opportunely filtered and separated into distinct channels as depicted in Table 12. The laser power under the objective was adjusted from 5 to 30 mW, depending on the focal plane depth. Single focal plane images were acquired with a 2.28 Hz frame rate (1.4 μ s pixel dwell time) and a resolution of 512 x 512 px.

Channel	Dye	Peak emission (nm)	Collected emission (nm)
1	GCaMP3	509 (Tian et al., 2009)	510 - 520
2	SRB	585 (Vichai and Kirtikara, 2006)	630 - 735

Table 12. 2P-LSM filter settings for emission wavelength collection

6.2.12.2 AUTOMATED EPIFLUORESCENCE MICROSCOPY ON FIXED BRAIN SLICES

Fixed and immunostained brain slices were scanned with the automated slide scanner AxioScan.Z1 (Zeiss, Jena, DE) equipped with a LED light source (Colibri 7, Zeiss, Jena, DE) as well as 10x / 0.45 and 20x / 0.8 Plan-Apochromat objectives for pre-focusing and fine-focus image acquisition, respectively. Excitation and emission filter sets are listed in Table 13. Images were recorded in 7 μ m-thick stacks using variance projection settings and offline stitching.

Dye	Excitation (nm)	Beam splitter (nm)	Emission (nm)
DAPI	353	405	410 - 440
Alexa Fluor® 488	493	495	503 - 537
TSA® Plus fluorescein			
Alexa Fluor® 546	553	573	580 - 611
TSA® Plus Cyanine 3			
Alexa Fluor® 647	631	652	661 - 703
Alexa Fluor® 790	752	762	770 - 800

Table 13. List of filter sets for automated epifluorescence microscopy with AxioScan.Z1

6.2.13 DATA ANALYSIS

6.2.13.1 ANALYSIS OF Ca^{2+} IMAGING WITH MSPARKLES

Analysis of Ca^{2+} imaging data was performed using a custom-made detection and analysis software, developed in MATLAB (MSparkles v. 1.8.18) (Stopper et al., 2022). Shortly, fluorescence fluctuations at basal Ca^{2+} concentrations (F_0) were computed along the temporal axes of each individual pixel using a polynomial fitting in a least-squares sense. The range projection of $\Delta F/F_0$ was then used to identify local fluorescence maxima, serving as seed points for simultaneous, correlation-based growing of regions of activity (ROAs). MSparkles automatically computed signal parameters, such as signal amplitude, duration, integrated fluorescence, ROA area and per-ROA signal frequency, which were subsequently averaged per recorded FOV. Pre-processing pipeline and parameters for Ca^{2+} imaging data analysis are presented in Table 14.

Pre-processing

Digital gain (offset)	50 [A.U.]
PURE-LET denoise	(Luisier et al., 2010)
Stack registration	Reference frame = 1 Reference channel = 1
Temporal median filter	Kernel half-size = 2 frames
F_0 computation	
Smoothing (Gaussian filter)	Kernel half-size = 5 px; $\sigma = 2$
Outlier removal on temporal mean/SD	Iterations = 3; $\sigma = 2$
Guidance signal	Order = 6; Optimizer = min. Error
F_0 fit	Polynomial order = 5; Clamp = $[0, +\infty)$

Detection	
Reference	$\Delta F/F_0$
Range image smoothing	$\sigma = 3$; Median filter size = 7
Automated-ROA detection threshold	Detector sensitivity = 95 %
Minimum ROA area	50 px
Correlation threshold	0.5
Analysis	
Sanitary bounds	[-1, 20]
Signal duration calculation	Full-width at half-maximum (FWHM, 50 %)
Sub-signal inclusion [Y/N]	[N]
Minimum peak prominence	0.1
Maximum signal duration	50 s
Synchronicity threshold	0.5 (50 % of simultaneously active ROAs)
Stationarity threshold	10

Table 14. Pipeline and parameters for automated detection and analysis of Ca^{2+} events

6.2.13.2 TELEMETRIC EEG DATA ANALYSIS

Data obtained from the telemetric EEG recordings were visualized and analysed using the software NeuroScore (v. 3.3.9318-1, DSI, Data Sciences International, St. Paul, USA). EEG signal was filtered using a 0.5-200 Hz band pass and a 50 Hz notch filter to remove the power line interference. For power spectrum analysis, following frequency bands were used: α , 8-12 Hz; β , 12-25 Hz; γ , 25-40 Hz; δ , 0.5-4 Hz; θ , 4-8 Hz; high-frequency oscillations (HFO), 40-200 Hz. Absolute spectral powers were calculated by fast Fourier transform (FFT) using 60 s-long epochs. Derivative power ratios were used together with the activity signal to identify the animal hypnogram stages as reported in Table 15.

Stage	activity	σ /total	θ/σ
Wake	low	low	low
Active wake	high	low	low
Paradoxical sleep (REM)	low	high	low
Slow Wave Sleep (non-REM)	low	low	high

Table 15. Parameters for the identification of the mouse hypnogram stages

The detection of spike-wave discharges (SWDs) was performed in the first six hours after γ -hydroxybutyric acid (GHB) administration using a customized detection protocol (Table 16) based on GHB-induced SWDs previously described in C57BL/6 mice (Kim et al., 2001; Black et al., 2014; Lee et al., 2019). Subsequently, the detected signals were manually screened and verified based on the synchronized video monitoring. Behavioural characteristics associated with SWDs include spontaneous behavioural arrest with open eyes, chewing, paroxysms of head and upper limbs as well as slight hypotonia of the neck muscles (Pearce et al., 2014; Jarre et al., 2017).

Spike detection

Detection threshold	Dynamic threshold, 1.5
Maximum ratio	5
Minimum value	adjusted on baseline, 50 - 100 μ V
Spike duration	
Minimum spike duration	1 ms
Maximum spike duration	150 ms
Spike train	
Minimum spike interval	0.1 s
Maximum spike interval	0.4 s
Minimum train duration	0.5 s
Train join interval	3 s
Minimum number of spikes	3

Table 16. SWD detection protocol in NeuroScore

6.2.13.3 OPEN FIELD BEHAVIOURAL ANALYSIS

The videos recorded during the open field test sessions were analysed using the software EthoVision XT (v. 11.5, Noldus Information Technology, Wageningen, NL) (Figure 7). The automatic animal center-point tracking analysis was used to calculate the total distance travelled by the subject (cm), the animal speed (cm/s) as well as the time spent in the centre of the arena (s, defined as the central 25 cm x 25 cm squared region). The non-tracking activity analysis was performed to detect animal freezing by calculating the relative number of pixel displaying changes in their grey scale value between consecutive frames. Parameters used in the activity analysis are listed in Table 17.

Activity settings	
Activity threshold	adjusted on signal-to-noise ratio, 5 - 10
Background noise filter (Y/N)	N
Compression artefact filter (Y/N)	N
Detection Method	Grey scaling
Activity state settings	
Outlier filter	1 sample
Number of states	3
Thresholds	Locomotion above: 1.00 % On-site movement: 0.10-1.00 % Freezing below: 0.10 %
State duration threshold	0.10 s

Table 17. Activity analysis settings in EthoVision XT

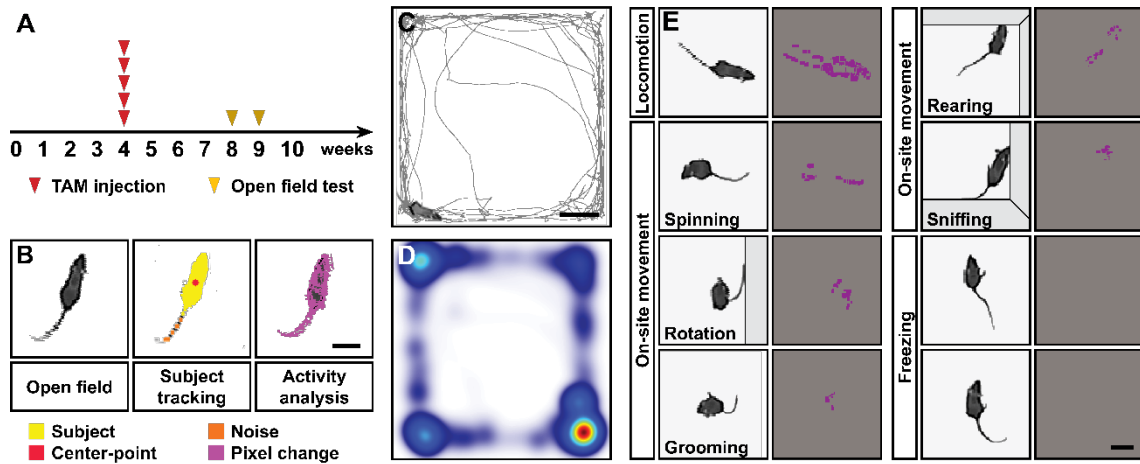


Figure 7. Analysis of GHB-induced freezing in the open field test

(A) Experimental design for tamoxifen (TAM) injection and open field behavioural test (baseline, 8 weeks; saline or GHB injection, 9 weeks). (B) Overview of performed analysis on open field sessions. The tracking analysis (middle panel) enables the detection of the subject body and geometrical centre, the activity analysis (right panel) is based on the identification of pixel display changes in their grey scale value over time. Scale bar, 5 cm. (C) Representative subject trajectory recorded during a canonical 15 min open field session and (D) associated heatmap of the subject position in the arena. Scale bar, 10 cm. (E) Representative time frames and associated pixel change analysis in correspondence of bouts of locomotion, movement without translocation of the subject geometrical centre (on site; e.g. spinning, torso rotation, grooming, rearing, sniffing) and freezing. Scale bar, 5 cm.

6.2.13.4 STATISTICS

Statistical analysis was performed with GraphPad Prism 8. The datasets were preliminary tested for normality using the Shapiro-Wilk normality test and outlier detection was performed using the GraphPad Prism ROUT-method (Q = 1 %). Parametric and non-parametric statistical procedures were performed based on the result of the Shapiro-Wilk normality test and datasets were displayed accordingly as mean \pm standard error of mean (SEM) or median \pm interquartile range (IQR), respectively. Test details are given in the corresponding figure legend. Following *p-values* were used throughout the work: #, $p < 0.1$; *, $p < 0.05$; **, $p < 0.01$; ***, $p < 0.001$.

6.2.14 MOUSE ADMINISTRATION AND VETERINARY LICENSES

Mouse administration was performed with the online database PyRAT (Python-based Relational Animal Tracking, Scionics Computer Innovation GmbH, Dresden, DE). Animals were kept in the animal facility of the Center for Physiology and Molecular Medicine (CIPMM, Homburg, DE). Humidity and temperature were maintained at 45–65 % and 20–24 °C, respectively, and the facility was kept under a 12 h light/dark cycle. All mice received food *ad libitum* (standard autoclaved rodent diet, Ssniff Spezialdiäten, Soest, Germany) and autoclaved tap water. All animal experiments were performed at the University of Saarland (CIPMM, Homburg, DE) in strict accordance with the European and German guidelines for the welfare of experimental animals and approved by the “Landesamt für Gesundheit und Verbraucherschutz” of the state of Saarland in Saarbrücken (DE) (license number 71/2013, 34/2016, 36/2016, 03/2021 and 08/2021). Details about the number of animals used in each experiment are given in the corresponding figure legends.

7 RESULTS

7.1 ASTROCYTE-SPECIFIC CONDITIONAL GABA_BR DELETION

To investigate the contribution of astrocytic GABA_BRs in the pathological network function associated to absence seizure, we took advantage of the Cre^{ERT2}-loxP system (Feil et al., 2009) to induce the time-controlled and cell-specific GABA_BR deletion coupled to the expression of the genetically encoded Ca²⁺ indicator GCaMP3 in GLAST⁺ astrocytes (Figure 8A-C). To this aim, four week-old mice were injected i.p. for five consecutive days with tamoxifen at a daily dose of 100 mg/kg body weight and analysed at least four weeks after injection (Figure 8D).

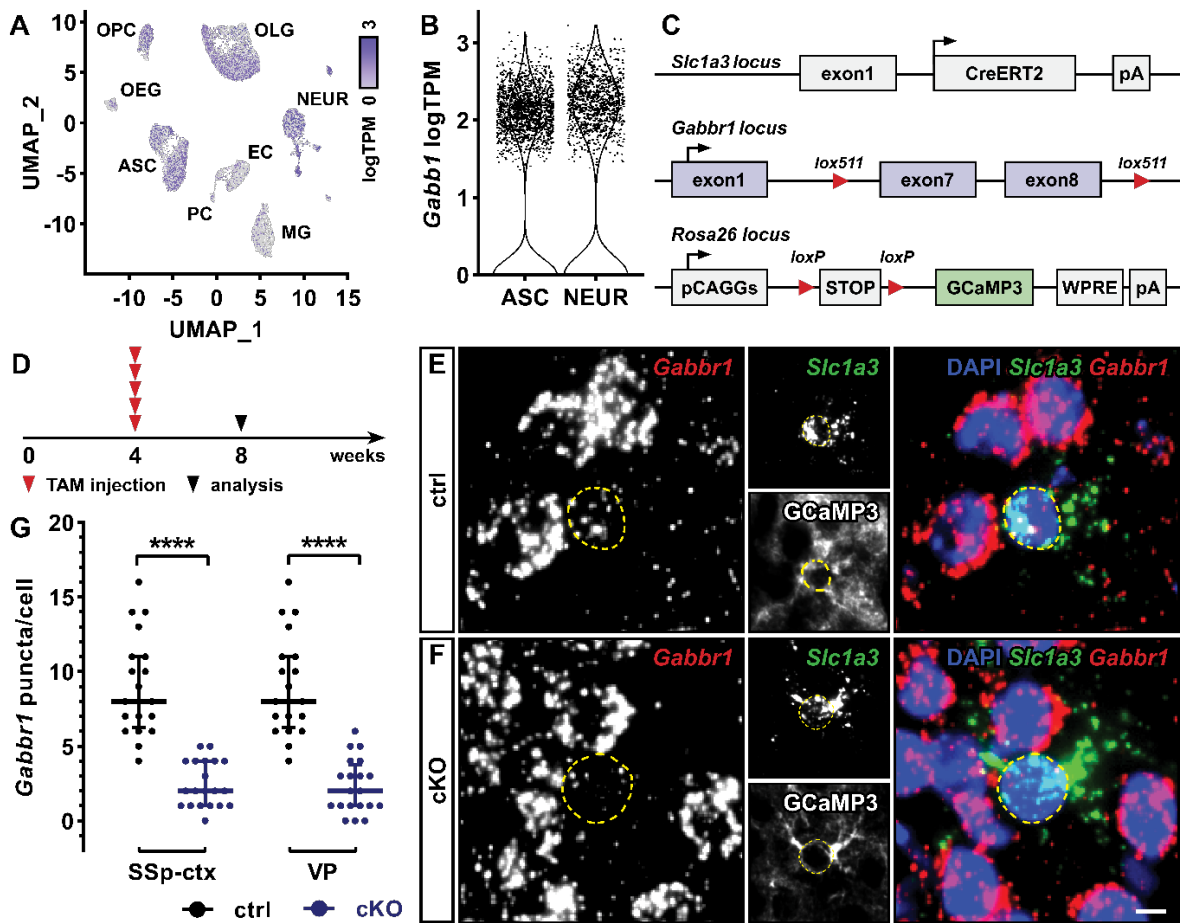


Figure 8. Cell-specific conditional knock-out of astroglial GABA_BR1

(A) Expression level of *Gabbr1* mRNA in across neural cell populations separated by principal component analysis and non-linear dimensional reduction (Stuart et al., 2019). Data were retrieved from the online Gene Expression Omnibus database (GSE129788) and published in (Ximerakis et al., 2019). ASC, astrocytes; EC, ependymal cells; MG, microglia; NEUR, mature neuronal cells; OEG, olfactory ensheathing glia; OLG, oligodendrocytes; OPC, oligodendrocyte-precursor cells; PC, pericytes; TPM, transcripts per million; UMAP, uniform manifold approximation and projection. (B) Violin plot of *Gabbr1* mRNA expression levels in astrocytes (ASC) and mature neuronal cells (NEUR) shown in (A). (C) Schematic representation of genetic knock-in manipulation required for the astrocyte-specific conditional knock-out of the GABA_BR1 subunit coupled to the expression of the genetically-encoded Ca²⁺ indicator GCaMP3 (see 6.1.10 for details). (D)

Experimental design for tamoxifen (TAM) administration and sample collection for RNAscope analysis. **(E-F)** Representative views of astrocytic *Gabbr1* mRNA levels in the primary somatosensory cortex (SSp-ctx) and ventral posterior thalamus (VP) of control (ctrl) and conditional knock-out (cKO) mice. *Gabbr1* mRNA puncta (red) were counted from the soma (DAPI, blue) of recombinant (GCaMP3⁺, white) astrocytes (*Slc1a3* mRNA⁺, green). Scale bar, 5 μ m. **(G)** Quantification of RNAscope analysis of *Gabbr1* mRNA. Data are derived from n = 20 cells (N = 1 animal) and were compared using a Kruskal-Wallis test with Dunn's multiple comparison correction.

We evaluated the effect of the *Gabbr1* conditional knock-out (cKO) by *in situ* hybridization of *Gabbr1* mRNA in the primary somatosensory cortex (SSp-ctx, Figure 8F) and the ventral posterior nucleus of the thalamus (VP; Figure 8G), since both regions are strongly affected by absence seizures and receive the input of GABAergic projections. Four weeks after tamoxifen treatment, *Gabbr1* mRNA levels were reduced by 75 % in both SSp-ctx and VP (****, $p < 0.0001$) with comparable levels between the two regions (ns, $p > 0.99$) (Figure 8G).

To assess the expression of astrocytic GABA_BR subunit 1 (GABBR1) at the protein level, we collected the cortex and thalamus of 8-week-old ctrl and cKO mice and purified astrocytes by magnetic cell separation (MACs, Figure 9A). The enrichment of astrocyte-specific markers and the purity of the MACs-purified cells were assessed by Western blot analysis (Figure 9B-C) and immunocytochemistry (Figure 9D-E), respectively. The expression level of GABBR1 in MACs-purified cells was reduced by 60 % in the cortex (**, $p = 0.001$) and by 50 % in the thalamus (**, $p = 0.003$) of cKO mice (Figure 9H).

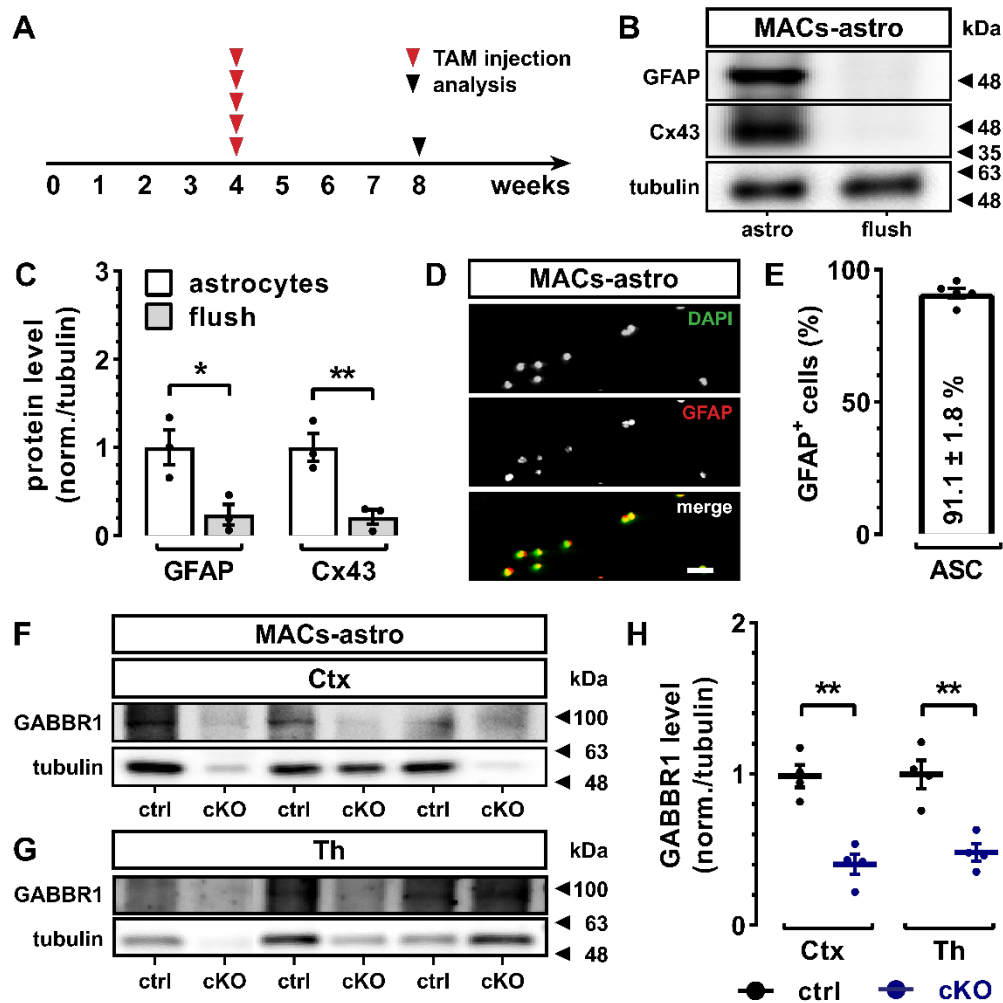


Figure 9. Effective removal of GABA_BRs from MACs-purified astrocytes

(A) Experimental design for tamoxifen (TAM) administration and sample collection for Western blot analysis of MACs-purified astrocytes. (B-C) Enrichment of astrocyte-specific markers GFAP and Cx43 in MACs-purified cells (astro) compared to the relative eluate (flush) visualized by Western blot analysis. (D-E) Cell-population purity cells assessed via GFAP immunocytochemistry. Scale bar, 1 mm. (F-H) Western blot analysis of GABA_B subunit 1 (GABBR1) from MACs-purified astrocytes derived from cortex (Ctx, F) and thalamus (Th, G) of ctrl and cKO mice and relative quantification (H). In C, data are derived from N = 3 animals and were compared using a two-way ANOVA test with Bonferroni's multiple comparison correction. In E, data are derived from N = 4 animals. In H, data are derived from N = 4 animals and were compared using an unpaired t test.

Since astrocytic GABA_BR activation leads to an increase in intracellular Ca²⁺ concentration (Mariotti et al., 2016; Perea et al., 2016; Nagai et al., 2019), we collected acute slices from control (ctrl) and cKO animals and assessed using two-photon laser-scanning microscopy (2P-LSM) astrocytic Ca²⁺ activity in response to the focal application of the GABA_BR-specific agonist baclofen in the SSp-ctx (Supplementary Figure 1A-E). To exclude indirect effects mediated by neuronal GABA_BRs, we incubated slices in the voltage-gated Na⁺ channel blocker tetrodotoxin (TTX) for at least 15 min before slice recording (see Supplementary Figure 2 for a comprehensive evaluation of the effect of TTX on baseline astroglial Ca²⁺ signalling). Ca²⁺ imaging data analysis was performed using a

custom-made detection and analysis software, developed in MATLAB (MSparkles, see for details 6.2.13.1), which identifies regions of activity (ROAs) based on the temporal fluorescence profile of adjacent pixels and extracts fluorescence transients associated to intracellular Ca^{2+} signals (Stopper et al., 2022). After baclofen application, the number of astroglial Ca^{2+} signals occurring per minute (signal density, $[\text{min}^{-1}]$) increased in both control (before, 154 ± 21 ; after, 218 ± 36 ; #, $p = 0.069$) and cKO slices (before, 118 ± 16 ; after, 172 ± 19 ; *, $p = 0.002$) (Supplementary Figure 1F). Nevertheless, astroglial Ca^{2+} signals after baclofen application exhibited reduced spatial extension (ROA area, $[\mu\text{m}^2]$) in cKO slices (30.9 ± 3.9) compared to ctrl slices (43.8 ± 2.6 , *, $p = 0.03$) (Supplementary Figure 1G). Also, baclofen induced an increase in signal amplitude ($[\Delta F/F_0]$) (Supplementary Figure 1H) specifically in ctrl (before, 0.21 ± 0.02 ; after, 0.29 ± 0.02 ; *, $p = 0.03$) and not in cKO slices (before, 0.21 ± 0.01 ; after, 0.23 ± 0.01 ; ns, $p = 0.13$). The same is true for the integrated fluorescence (integral of fluorescence amplitude during the lifetime of the signal, $[\Delta F/F_0]$), which was enhanced specifically in ctrl (before, 1.98 ± 0.17 ; after, 2.73 ± 0.27 ; *, $p = 0.04$) but not in cKO slices (before, 1.94 ± 0.22 ; after, 2.20 ± 0.18 ; ns, $p = 0.53$).

7.2 ASTROCYTIC GABA_BR DELETION IMPAIRS SEIZURE ACTIVITY

Control and cKO animals were injected with γ -hydroxybutyric acid (GHB) at doses ranging from 70 mg/kg to 250 mg/kg and monitored by telemetric electroencephalography (EEG) coupled to video recording in baseline conditions and for six hours after GHB administration. The dosage of GHB was chosen in line with existing literature on GHB administration in mice (see 4.2.1.1 and 4.2.1.2 for details). Since it is already well established that the effect of GHB on the EEG is restricted to the first hour after systemic administration (Ishige et al., 1996; Kim et al., 2001), we evaluated the time course of GHB-response in control and cKO mice within the first hour after application and its dose dependency at the peak of its action (5-20 min after injection) (Figure 10A-B).

7.2.1 THE INCREASE IN δ POWER ASSOCIATED WITH ANIMAL INACTIVITY IS REDUCED IN cKO MICE UPON GHB ADMINISTRATION

In line with previous studies on the kinetics of GHB effects, we found that the systemic administration of GHB induced a transitory change in the spectral power as well a reduction in the animal activity lasting no longer than one hour and peaking within the first 30 min after drug administration (Figure 10C-D). Both control and cKO mice showed an increase in the spectral power in the low-frequency range, in particular in the δ (0.5-4 Hz) and θ (4-8 Hz) range, at different GHB doses (Figure 10E-F, Supplementary Figure 3A-C). In control mice, GHB administration led to up to a four-fold increase in δ relative power at doses ranging between 70 and 200 mg/kg compared to saline injected animals and peaking at a dose of 150 mg/kg (70, *, $p = 0.019$; 100, **, $p = 0.003$; 150, ***, $p < 0.001$; 200, **, $p = 0.003$, 250, ns, $p = 0.194$). On the other hand, cKO mice displayed only a moderate (\sim two-fold) increase in the δ relative power (70-250, ns, $p > 0.1$) with a similar dose-dependency (ns, $p = 0.654$) (Figure 10G). With respect to the relative increase in the θ power, control and cKO mice showed no difference between the groups (ns, $p = 0.628$) as well as the same dose-dependency (ns, $p = 0.931$) (Figure 10H). In parallel to the increase in the power spectrum in the low-frequency range, GHB induced at all tested concentrations a reduction in the γ (25-40 Hz) relative power in both control (70-250, ***, $p < 0.001$) and cKO (70-100, *, $p = 0.031$; 150, *, $p = 0.023$; 200-250, ***, $p < 0.001$) (Figure 10I). In contrast to the increase in δ and θ power, the relative γ power showed a linear negative dependency with the administered GHB dose (***, $p < 0.001$).

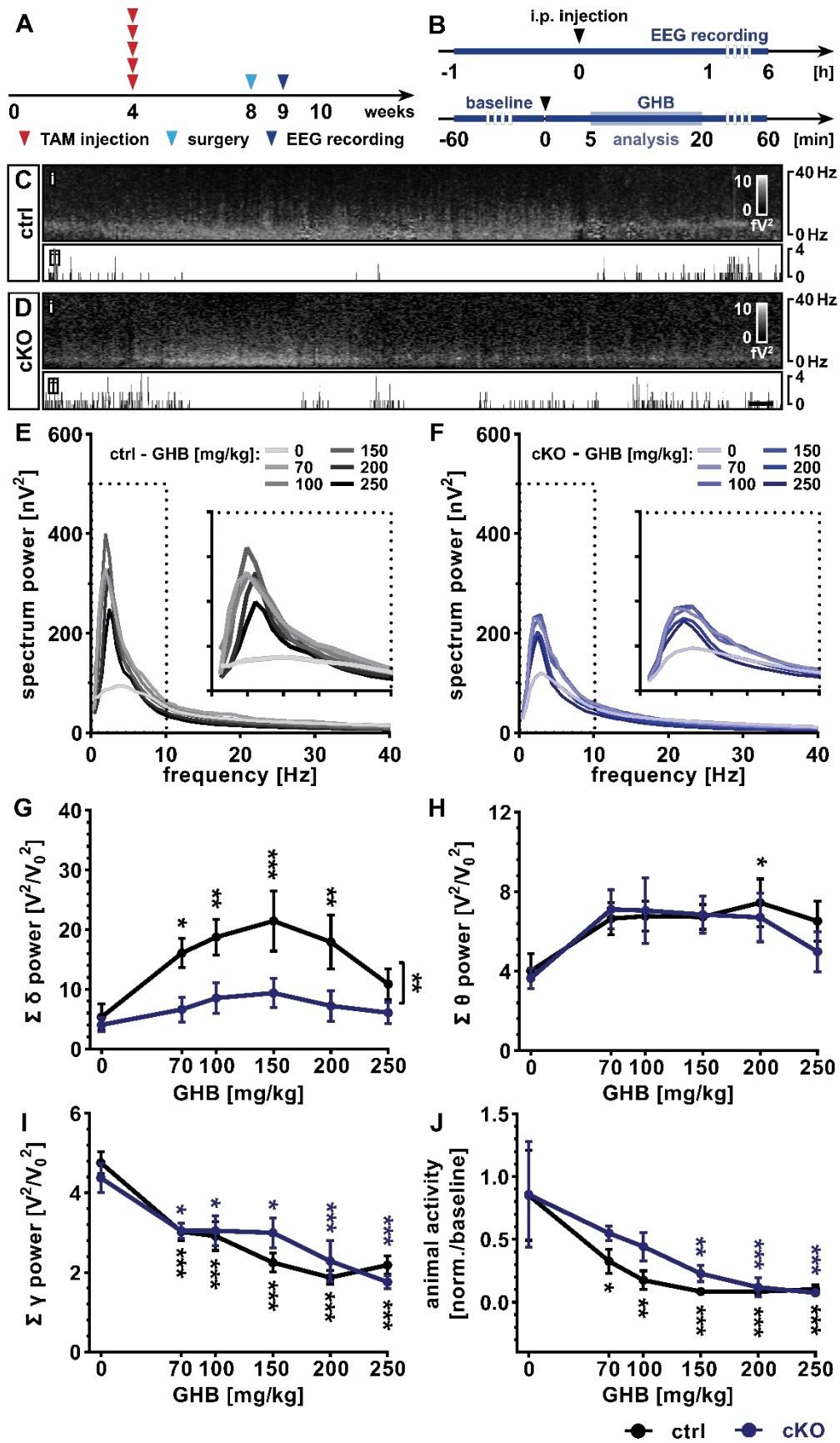


Figure 10. GHB-induced spectral alterations differ between ctrl and cKO mice

(A) Experimental design including tamoxifen (TAM) administration at four weeks of age, depth-electrode implantation for telemetric electroencephalography (EEG) four weeks after and EEG recording of control (ctrl) and conditional knock-out mice (cKO) injected with γ -hydroxybutyric acid (GHB) at doses ranging from 70 to 250 mg/kg or saline (0 mg/kg GHB). (B) Experimental protocol for GHB injection and telemetric EEG recording. Mice were recorded in baseline conditions for one hour, intraperitoneally (i.p.) injected with GHB and recorded for up to 6 hours after GHB injection. (C-D) Representative power spectra of the EEG signal recorded from ctrl (C) and cKO mice (D) injected with 150 mg/kg GHB using 10 s-long epochs and grey-scaled according to the frequency power (0-40 Hz range). The first 60 min after GHB injection are depicted. Scale bar, 2 min. (E-F) Spectral power distribution in the 0.5-40 Hz range (with 1 Hz interval) calculated as mean power over the time interval corresponding to the peak of GHB spectral alterations (5-20 min after i.p. injection). (G-I) Relative change in spectral power in the δ (0.5-4 Hz, G), θ (4-8 Hz, H) and γ (25-40 Hz, I) range in ctrl and cKO mice at different GHB doses and calculated as the cumulative relative spectral power at the peak of GHB effects with respect to baseline conditions. (J) Average animal activity in ctrl and cKO mice at the peak of GHB effects. Data are derived from N = 6-10 animals and were analysed using a two-way ANOVA test with Bonferroni's multiple comparison correction using the genotype and the GHB concentration as independent variables (see Supplementary Table 1 for details).

The spectral alterations in the δ range peak in both control and cKO mice at a dose of 150 mg/kg GHB. Therefore, we chose this dosage to evaluate the temporal profile of the relative spectral power in the δ , θ and γ range after the administration of GHB and confirm that GHB effects followed a kinetic in line with the current knowledge on GHB administration in mice. Indeed, the relative spectrum change in the δ , θ and γ range had similar time-dependencies in control and cKO mice (δ , ns, $p = 0.596$, θ , ns, $p = 0.987$; γ , ns, $p = 0.913$), peaking 5-20 min after GHB administration (Supplementary Figure 3D-F).

Finally, we evaluated the dose-dependency and time-course of the changes in animal activity after GHB administration. Control mice displayed already at the smallest dose of GHB (70 mg/kg) a strong reduction (more than 60 %) in animal activity and a further decrease (~ 90 %) at higher doses (100-250 mg/kg). On the other hand, although reduced, the activity of cKO animals was higher at lower doses of GHB (70-150 mg/kg), whereas it was comparable to control at higher dosage of GHB (200-250 mg/kg) (Figure 10J). Also, the time course of animal activity after 150 mg/kg GHB administration revealed that the reduction in activity, peaking in both control and cKO already 5-10 min after injection, was less prolonged in cKO mice (***, $p < 0.001$), which displayed an increase in activity already 30 min after GHB administration (Supplementary Figure 3G). In particular, we found a strong negative correlation between the animal activity and both δ (ctrl, $r = -0.71$, ****, $p < 0.0001$; cKO, $r = -0.36$, $p = 0.005$) and θ spectral power (ctrl, $r = -0.75$, ****, $p < 0.0001$; cKO, $r = -0.39$, $p = 0.002$) within the first hour after GHB administration, meaning that the animal activity decreases in parallel to the increase in the power spectrum in the low-frequency range. On the contrary, the animal activity positively correlated with the power spectrum in the γ range (ctrl,

$r = 0.77$, ****, $p < 0.0001$; cKO, $r = 0.50$, $p < 0.0001$) as well as the high-frequency oscillation (HFO) range (ctrl, $r = 0.59$, ****, $p < 0.0001$; cKO, $r = 0.50$, $p < 0.0001$) (Supplementary Figure 4).

7.2.2 FUNCTIONAL ASTROGLIAL GABA_BRS RESULT IN HIGHER INCIDENCE OF SWDS

In mice, GHB has been used to induce generalized spike-wave discharges (SWDs) with a 3-6 Hz frequency at doses ranging between 70 and 150 mg/kg (Ishige et al., 1996; Kim et al., 2001; Black et al., 2014; Lee et al., 2019). Accordingly, both control and cKO mice developed SWDs when injected with doses of 70, 100 and 150 mg/kg GHB, as displayed in the representative EEG traces (Figure 11A-D). In order to evaluate the occurrence and the duration of SWDs, we developed a customized detection protocol enabling the detection of any spike train with frequency ranging between 2.5 and 10 Hz (see 6.2.13.2 for details and Supplementary Figure 5C-D for representative SWD magnifications). Compared to baseline conditions, control mice injected with doses of 70-200 mg/kg experienced a five to six-fold increase in SWDs (0, ns, $p = 0.164$; 70, **, $p = 0.005$; 100, ***, $p < 0.001$; 150, **, $p = 0.005$; 200, *, $p = 0.043$; 250, ns, $p = 0.130$) at the peak of GHB action (5-20 min after administration). Similarly, cKO mice displayed an increase in the absolute occurrence of SWDs (0, ns, $p = 0.116$; 70, **, $p = 0.006$; 100, **, $p = 0.009$; 150, *, $p = 0.015$; 200, ns, $p = 0.474$; 250, ns, $p = 0.800$) with a dose-dependency similar to control animals (ns, $p = 0.423$), yet the occurrence of SWDs was reduced compared to controls (**, $p = 0.002$) (Figure 11E). In line with this, the total time spent by control mice in SWDs was higher than baseline conditions at doses of 70 to 250 mg/kg GHB (0, ns, $p = 0.180$; 70, **, $p = 0.003$; 100, **, $p = 0.008$; 150, **, $p = 0.002$; 200, **, $p = 0.006$; 250, ns, $p = 0.120$), whereas only doses of 70 (*, $p = 0.003$) and 100 mg/kg GHB (#, $p = 0.054$) increased the total time spent in SWDs in cKO mice (Figure 11F).

Indeed, the increased time spent in SWDs in controls mainly derived from an increased occurrence of SWDs, since SWD trains displayed a similar duration between control and cKO mice (#, $p = 0.062$), even though SWDs tended to be slightly longer in control mice (Figure 11G). In accordance to previous results obtained from different pharmacological models of absence seizures (see Table 2), the vast majority of the detected SWD trains lasted less than 10 s (ctrl, 96.96 ± 0.79 %; cKO, 98.56 ± 0.52 %) and displayed a substantial uniformity across different GHB doses in both control (70, 2.35 ± 2.40 s; 100, 2.58 ± 2.80 s; 150, 2.98 ± 2.90 s) and cKO mice (70, 1.95 ± 2.22 s; 100, 2.53 ± 2.70 s; 150, 1.94 ± 1.32 s) (Supplementary Figure 5E-F). Also, in line with the analysis of the time course of the spectral changes induced by GHB (Supplementary Figure 3), we found that SWDs progressively accumulate within the first 20 min after GHB administration (Figure 11H).

Finally, we characterized SWDs trains in terms of spike frequency (Supplementary Figure 5G-H). Although rather variable (from 2 Hz up to 10 Hz), the spike frequency of detected SWDs was largely comparable between control (70, 4.70 ± 2.20 s; 100, 4.70 ± 2.30 s; 150, 4.40 ± 2.20 s) and cKO mice

(70, 4.60 ± 2.20 s; 100, 4.50 ± 2.45 s; 150, 4.50 ± 1.83 s) and was in line with previous data obtained in mice (Ishige et al., 1996; Kim et al., 2001).

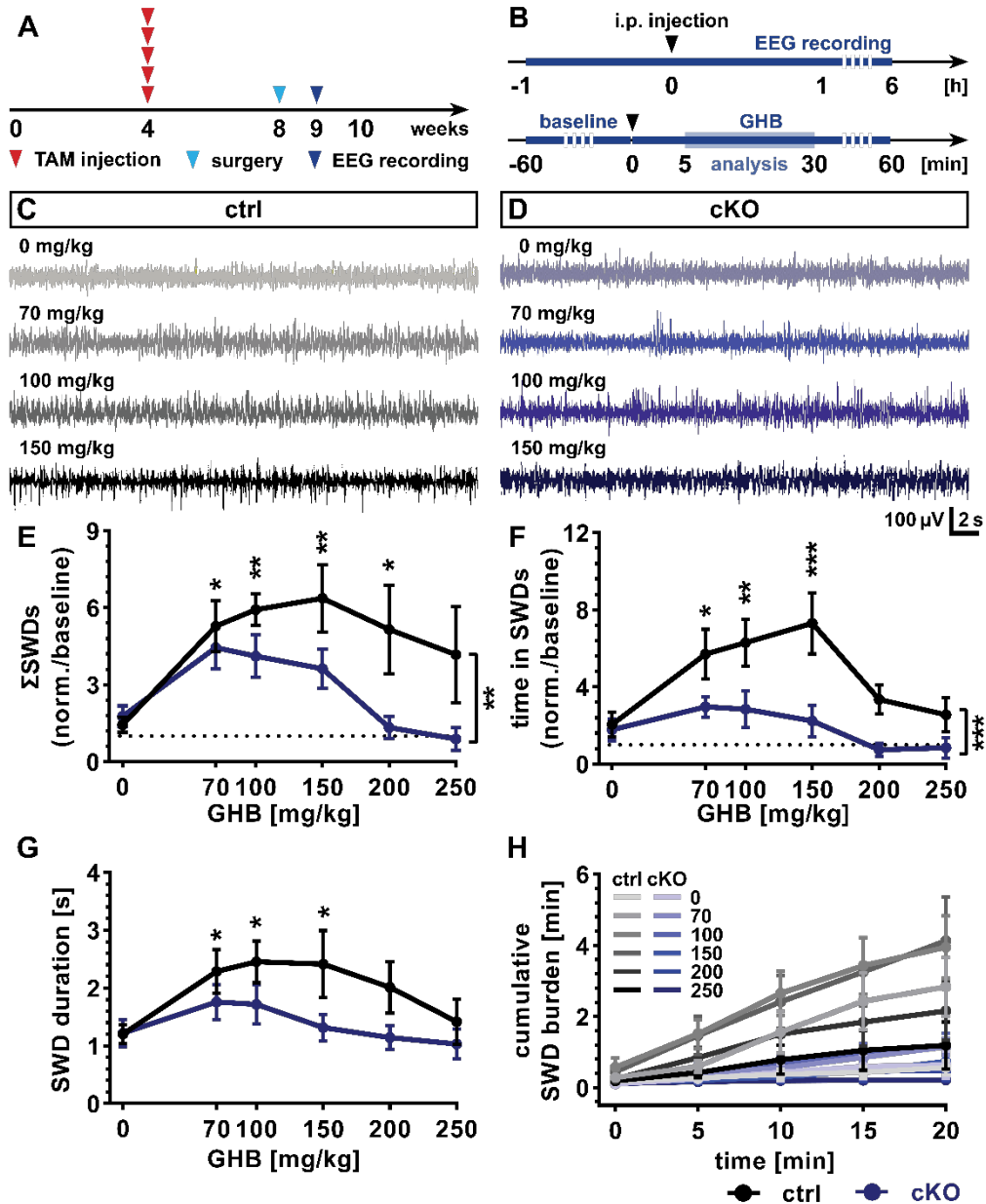


Figure 11. Spike-wave discharges occur at lower frequency in cKO mice

(A) Experimental design including tamoxifen (TAM) administration at four weeks of age, depth-electrode implantation for telemetric electroencephalography (EEG) four weeks after and EEG recording of control (ctrl) and conditional knock-out mice (cKO) injected with γ -hydroxybutyric acid (GHB) at doses ranging from 70 to 250 mg/kg or saline (0 mg/kg GHB). (B) Experimental protocol for GHB injection and telemetric EEG recording. Mice were recorded in baseline conditions for one hour, intraperitoneally (i.p.) injected with GHB and recorded for up to 6 hours after GHB injection. (C-D) Representative EEG traces of ctrl (C) and cKO (D) mice injected with GHB (0 to 150 mg/kg) displaying spike-wave discharges (SWDs). (E-F) Relative number of SWDs (E) and relative total time spent in SWDs (F) in respect to baseline conditions within the time interval corresponding to the peak of GHB action (5-20 min after administration). (G-H) SWD duration (G) and cumulative SWD burden (expressed as cumulative time spent in SWDs, H). (E-H) Data are

derived from N = 6-10 animals and were compared using a two-way ANOVA test with Bonferroni's multiple comparison correction using the genotype and the GHB concentration (**E-G**) or the group and the time (**H**) as independent variables (see Supplementary Table 1 for details).

7.3 GHB INDUCES GABA_BR-MEDIATED CA²⁺ SIGNALLING IN ASTROCYTES

To investigate astroglial Ca²⁺ responses to γ -hydroxybutyric acid (GHB) we collected acute slice preparations from 8-week-old ctrl and cKO animals injected with tamoxifen at four weeks of age to induce GABA_BR deletion and the expression of the genetically encoded Ca²⁺ indicator GCaMP3 in GLAST⁺ astrocytes (Figure 12A-B). *Ex vivo* two-photon laser-scanning microscopy (2P-LSM) of astrocytic Ca²⁺ signalling was performed in layers II/III of the primary somatosensory cortex in baseline conditions as well as upon GHB focal application at doses ranging from 100 μ M to 10 mM (see Supplementary Video 1 and Supplementary Video 2 for representative recordings upon administration of GHB 10 mM in ctrl and cKO mice, respectively). To exclude indirect effects of GHB mediated by neuronal GABA_BRs, the neuronal activity was blocked by using the voltage-gated Na⁺ channel blocker tetrodotoxin (TTX, 1 μ M). The slices were incubated for 15 min in perfusion solution containing TTX and continuously perfused with the same solution throughout the recording session (Figure 12C).

7.3.1 GABA_BR-MEDIATED ASTROGLIAL CA²⁺ SIGNALS INCREASE IN NUMBER, AMPLITUDE AND DURATION UPON GHB APPLICATION

Astroglial Ca²⁺ signals recorded upon application of increasing doses of GHB (0, 0.1, 1 and 10 mM) were characterized in terms of absolute occurrence as well as morphological features of the signal fluorescence profile ($\Delta F/F_0$) plotted over time (namely signal amplitude, duration and integrated fluorescence; Figure 12D-E). GHB induced in cortical astrocytes from ctrl mice an increase in signal density (calculated as average number of signals occurring per minute) compared to baseline at all tested doses (100 μ M, **, $p = 0.003$; 1 mM, *, $p = 0.022$; 10 mM, **, $p = 0.004$), whereas saline application left the astroglial signal density unaltered (ns, $p = 0.124$). Moreover, astroglial signal density increased in parallel to the increase of the dose of GHB peaking at a dose of GHB 10 mM with up to a 3-fold elevation in signal number. On the other hand, GHB did not induce increased signal density in astrocytes from cKO mice at any tested dose (Figure 12F).

Similarly, in ctrl conditions astroglial Ca²⁺ signals displayed a linear increase in signal amplitude upon GHB application compared to baseline (100 μ M, 14.9 ± 4.5 %, **, $p = 0.005$; 1 mM, 17.5 ± 7.2 %, #, $p = 0.060$; 10 mM, 27.3 ± 3.5 %, ***, $p < 0.001$). GABA_BR deletion resulted in the abolishment of GHB-induced increase in signal amplitude (*, $p = 0.020$) (Figure 12G). In terms of signal duration, astroglial signals were longer in ctrl mice upon GHB application compared to baseline (100 μ M, **, $p < 0.001$; 1 mM, *, $p = 0.018$; 10 mM, **, $p = 0.003$) with peak increase at a dose of 10 mM (25.3 ± 4.7 %). Notably, saline application also resulted in longer Ca²⁺ signals (*, $p = 0.027$), therefore suggesting that the increase in astroglial Ca²⁺ signal duration may additionally

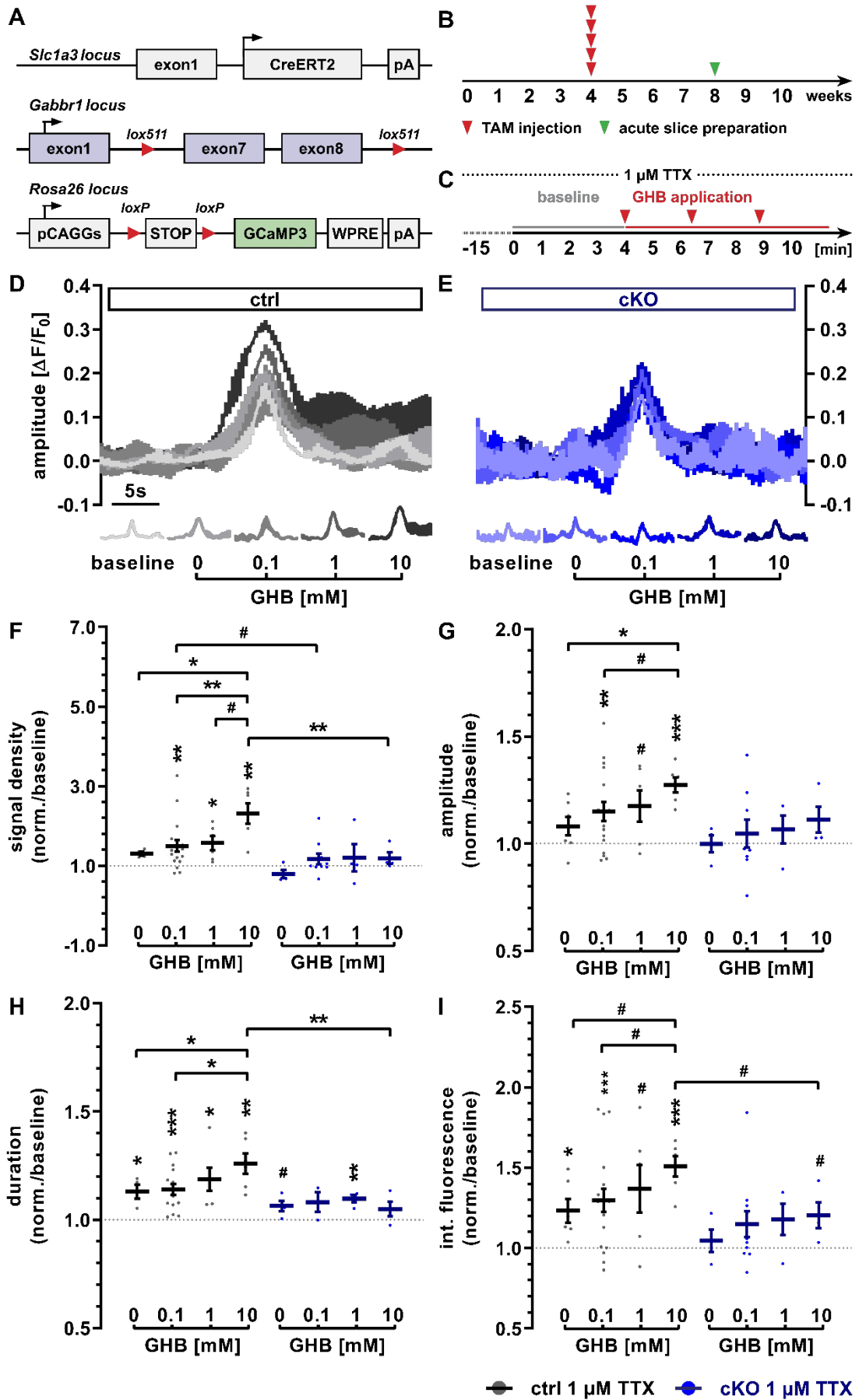


Figure 12. GHB enhances astroglial Ca²⁺ signalling in dependence of functional GABA_BRs

(A) Schematic representation of genetic knock-in manipulation required for the astrocyte-specific conditional knock-out of the GABA_BR1 subunit coupled to the expression of the genetically-encoded Ca²⁺ indicator GCaMP3 (see 6.1.10 for details). (B) Experimental design for tamoxifen (TAM) administration and acute slice preparation for *ex vivo* two-photon laser-scanning microscopy (2P-LSM) analysis of astrocytic Ca²⁺ signalling in the primary somatosensory cortex (SSp-ctx). (C) Slices were continuously perfused with the neuronal blocker tetrodotoxin (TTX, 1 μM) for 15 min before and throughout the recording session. After a 5 min baseline, γ-hydroxybutyric acid (GHB) was focally applied on the field of view (FOV). (D-E) Representative average traces of Ca²⁺ transients recorded in slices from control (ctrl, D) and conditional knock-out (cKO, E) mice upon focal application of saline (0 mM GHB) or GHB (100 μM, 1 mM and 10 mM) and aligned with respect to their signal peak. For each group, four exemplificative signals were used. (F-I) Astrocytic Ca²⁺ signal density (F), amplitude (G), duration (H) and integrated fluorescence (I). Data are derived from n = 4-12 FOVs (from N = 4-10 animals) and were analysed using a two-way ANOVA test using the genotype and the GHB concentration as independent variables (see Supplementary Table 1 for details). Data were normalized on baseline recordings preceding focal GHB application and additionally analysed using a one-sample t test (H₀: $\bar{x}_0=1$).

depend on other factors including photoactivation resulting from the prolonged recording session. In line with this, saline application induced longer Ca²⁺ signals also in cKO mice (#, p = 0.079) with no further increase upon GHB application (Figure 12H). Finally, the integrated fluorescence of the recorded signals was higher at all GHB doses in ctrl mice (100 μM, 29.7 ± 7.3 %, ***, p < 0.001; 1 mM, 36.9 ± 14.9 %, #, p = 0.056; 10 mM, 50.9 ± 6.2 %, ***, p < 0.001) and only slightly increased in correspondence of a dose of 10 mM GHB in cKO mice (#, 20.5 ± 8.0 %, p = 0.083).

7.3.2 THE SPATIOTEMPORAL PROPERTIES OF GHB-INDUCED CA²⁺ SIGNALLING DIFFER IN CTRL AND cKO MICE *EX VIVO*

In parallel to the morphological features of GHB-induced Ca²⁺ signals (namely amplitude, duration and integrated fluorescence), we evaluated their distribution in space and time. First, we analysed the absolute occurrence and the spatial extension of the regions of activity (ROAs) associated with fluctuations in fluorescence intensity over time (Figure 13A-C). Although the number of ROAs emerging per minute (ROA density) was slightly reduced in cKO mice compared to ctrl animal (*, p = 0.011), it was similarly affected by GHB application (ns, p = 0.969). In comparison to the ROA density upon saline application (ctrl, 17.4 ± 1.6 min⁻¹; cKO, 11.5 ± 0.6 min⁻¹), the number of ROAs increased after GHB application with peak at a dose of 100 μM (ctrl, 24.0 ± 1.3 min⁻¹, *, p = 0.023; cKO, 20.0 ± 1.9 min⁻¹, **, p = 0.009) and progressively decreasing at doses of 1 mM (ctrl, 23.5 ± 3.1 min⁻¹, ns, p = 0.101; cKO, 19.7 ± 4.2 min⁻¹, *, p = 0.036) and 10 mM GHB (ctrl, 21.6 ± 1.6 min⁻¹, ns, p = 0.209; cKO, 17.6 ± 3.2 min⁻¹, ns, p = 0.118) (Figure 13D). On the other hand, the ROA area progressively increased in ctrl mice in parallel to the increase of the applied GHB dosage from 37.2 ± 4.2 μm² upon saline application up to 53.9 ± 4.3 μm² (**, p = 0.005), whereas it was almost left unaltered in cKO mice (saline, 9.0 ± 2.0 μm²; GHB 10 mM,

18.0 ± 4.4 μm²; ns, p = 0.200). Notably, the ROA area recorded in acute slice preparations of ctrl mice was larger than cKO mice at all tested doses of GHB as well as in baseline conditions (0-10 mM, ***, p < 0.001) (Figure 13E).

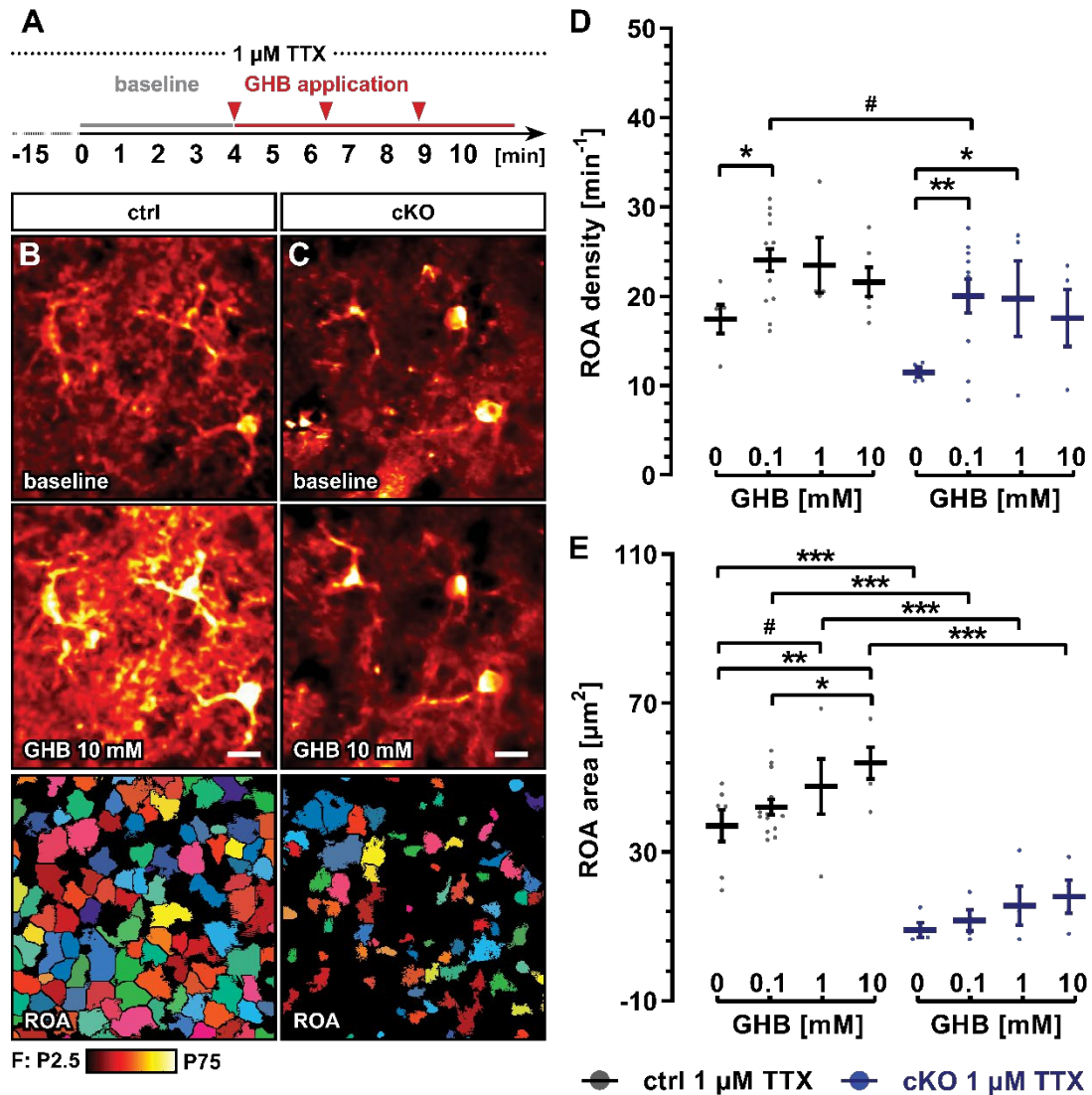


Figure 13. Astroglial Ca²⁺ signals induced by GHB display higher spatial extension in ctrl mice

(A) Experimental design for *ex vivo* two-photon laser-scanning microscopy (2P-LSM) analysis of astrocytic Ca²⁺ signalling upon focal γ -hydroxybutyric acid (GHB) application. (B-C) Representative fields of view (FOVs) from control (ctrl, B) and conditional knock-out (cKO, C) mice before (baseline) and after (GHB 10 mM) focal application of GHB and displayed as maximum intensity projection of the fluorescence intensity over time ($\Delta F/F_0$). The map of extracted regions of activity (ROAs) associated with fluctuations in fluorescence intensity over time (namely a signal) is displayed in the bottom panel. Scale bar, 20 μm. (D-E) Characterization of ROAs in terms of average number of ROAs occurring per minute (ROA density, D) and ROA spatial extension (ROA area, E) upon focal application of saline (0 mM GHB) or GHB (100 μM, 1 mM and 10 mM). Data are derived from n = 4-12 FOVs (from N = 4-10 animals) and were analysed using a two-way ANOVA test using the genotype and the GHB concentration as independent variables (see Supplementary Table 1 for details).

Next, we investigated the signal temporal distribution over the entire recording period and addressed the signal frequency within a given ROA as well as the coincident signal occurrence, calculated as fraction of active ROAs over the total number of ROAs (coincident activity) (Figure 14A-B). The signal frequency in acute slice preparations from ctrl mice displayed a substantial uniformity upon saline ($1.0 \pm 0.1 \text{ min}^{-1}$) and GHB application ($100 \mu\text{M}$, $1.2 \pm 0.1 \text{ min}^{-1}$; $1\text{-}10 \text{ mM}$, $1.0 \pm 0.1 \text{ min}^{-1}$). The same was true for cKO mice, although the signal frequency was higher than ctrl mice for all tested doses of GHB ($0 \mu\text{M}$, $1.4 \pm 0.2 \text{ min}^{-1}$; $100 \mu\text{M}$, $1.3 \pm 0.1 \text{ min}^{-1}$; 1 mM , $1.3 \pm 0.2 \text{ min}^{-1}$; 10 mM , $1.6 \pm 0.2 \text{ min}^{-1}$).

In ctrl mice, focal GHB application resulted in the progressive increase of the coincident activity of astroglial Ca^{2+} signals compared to baseline conditions. In particular, we observed peaks of coincident activity lasting 30 to 60 s directly after each GHB application and increasing in amplitude upon consecutive applications up to a two to five-fold increase compared to baseline conditions. On the other hand, astroglial Ca^{2+} coincident activity did not significantly increase upon GHB application in cKO mice, neither right after the application nor progressively alongside the recording session (Figure 14D-E). In parallel to the evaluation of the temporal profile of the coincident activity over time, we calculated the expected average coincident activity (θ) which would result from a random activation of the ROAs throughout the recording session, thus confirming that the observed coincidence *de facto* reflected a synchronous activation of multiple ROAs (Figure 14E). Notably, in ctrl mice the average coincident activity increased with respect to baseline conditions not only upon GHB focal application ($100 \mu\text{M}$, $55.3 \pm 7.2 \%$, ***, $p < 0.001$; 1 mM , $88.1 \pm 21.2 \%$, **, $p = 0.009$; 10 mM , $158.0 \pm 32.0 \%$, **, $p = 0.004$) but also upon saline application ($47.2 \pm 11.0 \%$, *, $p = 0.024$). Nevertheless, GHB significantly increased astroglial coincident activity beyond the relatively low increase induced by saline (**, $p = 0.004$). In cKO mice, the average coincident astroglial Ca^{2+} activity upon GHB administration was reduced compared to ctrl animals at all tested doses ($100 \mu\text{M}$, #, $p = 0.057$; 1 mM , #, $p = 0.053$; 10 mM , ***, $p < 0.001$) and did not differ with respect to baseline ($100 \mu\text{M}$, $17.7 \pm 1.2 \%$, ns, $p = 0.180$; 1 mM , $30.9 \pm 40.2 \%$, ns, $p = 0.498$; 10 mM , $27.5 \pm 16.8 \%$, ns, $p = 0.200$) (Figure 14F).

focal GHB application corrected to baseline coincident activity. Data are derived from $n = 4-12$ FOVs (from $N = 4-10$ animals) and were analysed using a two-way ANOVA test using the genotype and the GHB concentration as independent variables (see Supplementary Table 1 for details). In **F**, data were additionally analysed using a one-sample t test ($H_0: \bar{x}_0=1$).

7.3.3 NEURONAL ACTIVITY CONTRIBUTES TO THE NET EFFECT OF GHB ON ASTROGLIAL Ca^{2+} SIGNALLING

In the previous sections we addressed whether and to which extent GHB directly activates or alters astroglial Ca^{2+} signalling and how astroglial $GABA_B$ Rs modulate its action using the neuronal blocker tetrodotoxin (TTX). Nevertheless, neurons as well as several other neural cells do express $GABA_B$ Rs (Bettler et al., 2004; Bettler and Tiao, 2006; Zhang et al., 2014), whose activation could contribute to the net effect of GHB application on astroglial Ca^{2+} signalling. Therefore, we performed *ex vivo* two-photon laser-scanning microscopy (2P-LSM) of astrocytic Ca^{2+} signalling upon GHB focal application in absence of TTX (Supplementary Figure 6). Astroglial signal density was differentially affected by GHB (*, $p = 0.019$) with progressively higher signal density in ctrl mice (peaking at a dose of GHB 10 mM, $1.3 \pm 0.2 \text{ min}^{-1}$) and a progressive signal density reduction in cKO conditions (GHB 10 mM, $0.7 \pm 0.1 \text{ min}^{-1}$) (Supplementary Figure 6A). Similarly, astroglial Ca^{2+} signal amplitude displayed a positive correlation with the administered GHB dose in ctrl conditions and a negative correlation in cKO animals (#, $p = 0.074$; Supplementary Figure 6B). On the other hand, the signal duration (ns, $p = 0.431$) and integrated fluorescence (ns, $p = 0.796$) were similarly affected by GHB application (Supplementary Figure 6C-D).

In terms of spatial distribution of the astroglial Ca^{2+} signalling, cKO mice displayed a reduced ROA density (***, $p < 0.001$, Supplementary Figure 6E) as well as ROA area (***, $p < 0.001$, Supplementary Figure 6F) but both parameters were substantially unaffected by GHB application (ROA density, ns, $p = 0.522$; ROA area, ns, $p = 0.709$). A similar consideration applies to the signal frequency, which was higher in ctrl mice (***, $p < 0.001$) but did not differ upon GHB administration at any tested dosage (ns, $p = 0.521$, Supplementary Figure 6G). On the other hand, the coincident activity of astroglial Ca^{2+} signalling recorded from ctrl mice increased with the application of increasing doses of GHB (0 μ M, 1.1 ± 0.0 ; ns, $p = 0.100$; 100 μ M, 1.2 ± 0.2 ; ns, $p = 0.283$; 1 mM, 1.4 ± 0.1 , *, $p = 0.025$; 10 mM, 2.0 ± 0.3 , #, $p = 0.064$) reaching a two-fold increase at a dose of GHB 10 mM. Conversely, in cKO mice GHB induced a reduction in coincident activity compared to saline application (1.5 ± 0.3) at all tested doses (100 μ M, 0.9 ± 0.2 ; *, $p = 0.028$; 1 mM, 1.0 ± 0.2 , #, $p = 0.072$; 10 mM, 0.8 ± 0.1 , *, $p = 0.011$) (Supplementary Figure 6H).

Taken together, these results indicated that astroglial cortical Ca^{2+} response to GHB application is affected by the presence of a functional neuronal network. Therefore, we next aimed at evaluating GHB-induced astroglial Ca^{2+} signalling *in vivo*.

7.4 *IN VIVO* GHB ADMINISTRATION RESULTS IN ENHANCED ASTROGLIAL Ca^{2+} ACTIVITY IN BOTH CTRL AND cKO MICE

To investigate astroglial Ca^{2+} response to γ -hydroxybutyric acid (GHB) administration *in vivo* we performed a cranial window implantation on 8-week-old ctrl and cKO mice to access the primary somatosensory cortex (SSp-ctx). One week after the surgery, we performed two-photon laser-scanning microscopy (2P-LSM) of astrocytic Ca^{2+} signalling upon saline (NaCl 0.9 %, i.p.) and GHB (70 mg/kg, i.p.) administration (Figure 15A). Baseline recording as well as drug administration were performed under 1.5 % isoflurane anaesthesia. Afterwards, the anaesthesia was reduced to 0.5 % for recording of astroglial Ca^{2+} signalling in correspondence of the peak of GHB action (15-30 min after administration) (Figure 15B-D). At the end of the experiment, animals were perfused and processed for immunohistochemistry in order to exclude abnormal or differential glial activation underneath the cranial window (Supplementary Figure 7).

7.4.1 GHB-INDUCED ASTROGLIAL Ca^{2+} SIGNALS DIFFER IN CTRL AND cKO IN TERMS OF SPATIAL AND TEMPORAL DISTRIBUTION

In vivo GHB administration induced in ctrl mice an increased signal density compared to baseline conditions (baseline, $29.9 \pm 4.5 \text{ min}^{-1}$; GHB, $90.4 \pm 18.1 \text{ min}^{-1}$; ***, $p < 0.001$) as well as to saline administration (sal, $50.6 \pm 2.1 \text{ min}^{-1}$; *, $p = 0.019$). On the other hand, cKO mice displayed a reduced signal density compared to ctrl mice ($27.9 \pm 6.3 \text{ min}^{-1}$; ***, $p < 0.001$) and did not experience any signal density increase neither compared to baseline conditions ($5.6 \pm 0.9 \text{ min}^{-1}$; ns, $p = 0.123$) nor to saline administration ($17.9 \pm 6.0 \text{ min}^{-1}$; ns, $p = 0.587$) (Figure 15E). On the other hand, astroglial Ca^{2+} signals displayed a substantial uniformity between ctrl and cKO mice in terms of morphological features associated to their fluorescence profile, namely the signal amplitude, duration and integrated fluorescence. Compared to saline administration (ctrl, $0.22 \pm 0.04 \Delta F/F_0$; cKO, $0.18 \pm 0.03 \Delta F/F_0$), GHB did not induce any difference in signal amplitude in ctrl ($0.20 \pm 0.01 \Delta F/F_0$, ns, $p = 0.429$) or cKO mice ($0.18 \pm 0.01 \Delta F/F_0$, ns, $p = 0.962$) (Figure 15F). Similarly, GHB administration did not alter the signal duration either in ctrl (sal, $6.9 \pm 0.4 \text{ s}$; GHB, $7.4 \pm 0.7 \text{ s}$; ns, $p = 0.584$) nor in cKO animals (sal, $7.6 \pm 0.6 \text{ s}$; GHB, $8.6 \pm 0.6 \text{ s}$; ns, $p = 0.337$) (Figure 15G) and did not induce any change in the integrated signal fluorescence (ctrl: sal, $1.9 \pm 0.3 \Delta F/F_0$; GHB, $2.0 \pm 0.3 \Delta F/F_0$; cKO: sal, $1.8 \pm 0.4 \Delta F/F_0$; GHB, $2.1 \pm 0.3 \Delta F/F_0$) (Figure 15H).

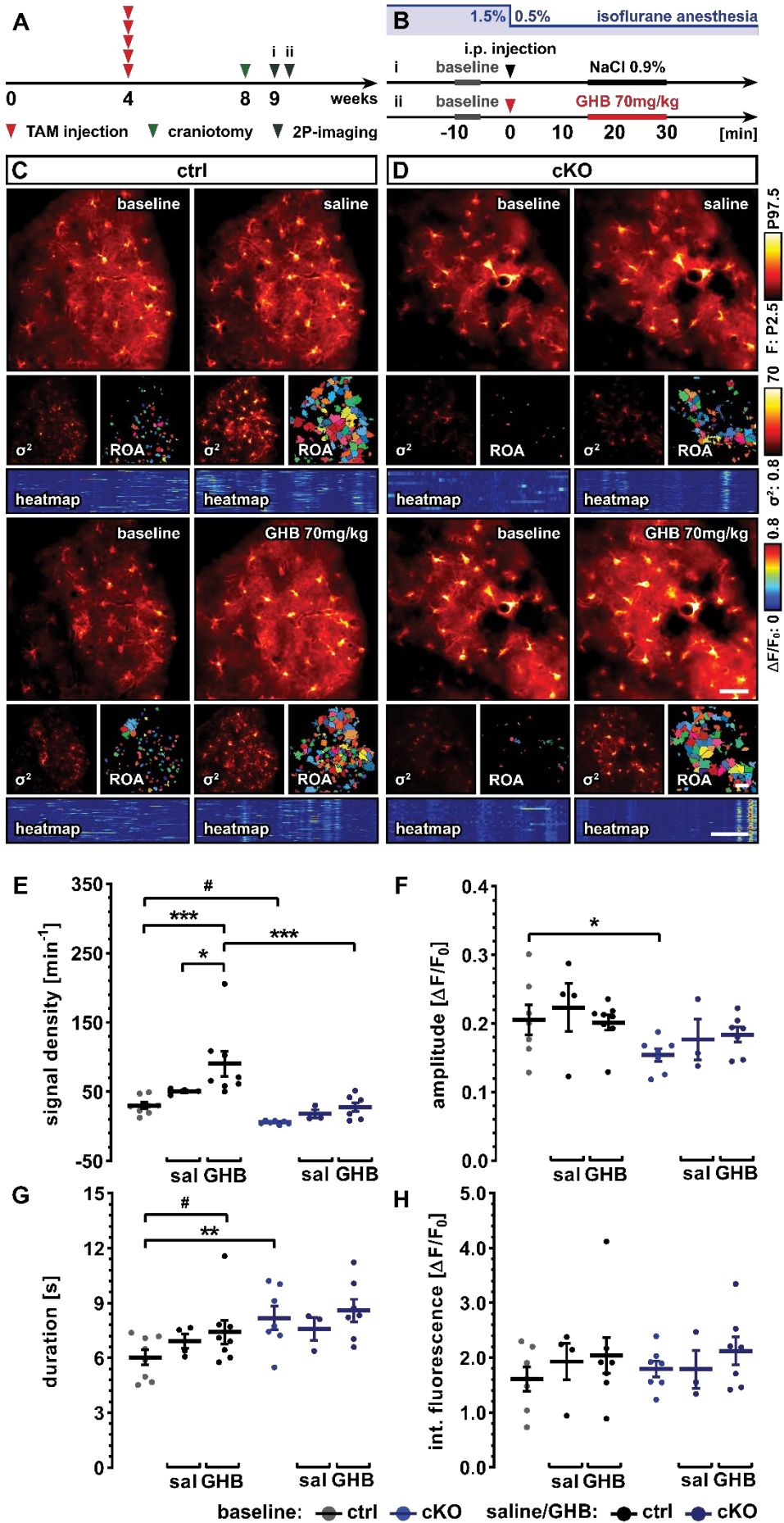


Figure 15. Cortical astroglial Ca²⁺ signal density increases *in vivo* in ctrl and not in cKO mice

(A) Experimental design for tamoxifen (TAM) administration, cranial window implantation on the primary somatosensory cortex (SSp-ctx) and *in vivo* two-photon laser-scanning microscopy (2P-LSM) of astrocytic Ca²⁺ signalling upon saline (NaCl 0.9 %, i) and γ -hydroxybutyric acid (GHB 70 mg/kg, ii) administration. (B) Baseline recordings were collected from control (ctrl) and conditional knock-out (cKO) mice kept under 1.5 % isoflurane anaesthesia. Animals were subsequently injected i.p. with saline or GHB 70 mg/kg and anaesthesia was reduced to 0.5 % for recording of astroglial Ca²⁺ signalling at the peak of GHB action (15-30 min). (C-D) Representative field of views (FOVs) from ctrl (C) and cKO (D) mice in baseline conditions and after saline or GHB application and displayed as maximum intensity projection of the fluorescence intensity over time ($\Delta F/F_0$). The fluorescence intensity variance (σ^2) over the entire recording period as well as the map of regions of activity (ROA) extracted from the representative FOVs are displayed in the middle panel. Scale bar, 20 μ m. In the bottom panel, the heatmap representation of the extracted ROAs with fluctuations in fluorescence intensity over time are included. Scale bar, 1 min. (E-H) Characterization of astrocytic Ca²⁺ signals for ctrl and cKO mice in terms of number of signal occurring per minute (signal density, E), signal amplitude (F), duration (as full-width-at-half-maximum, G) and integrated fluorescence (H). Data are derived from N = 4-10 animals and were analysed using a two-way ANOVA test using the genotype and the treatment as independent variables (see Supplementary Table 1 for details).

The ROA density was similarly affected by GHB *in vivo* administration in ctrl and cKO mice (ns, $p = 0.955$). In particular, the ROA density after GHB administration (ctrl, $23.2 \pm 1.3 \text{ min}^{-1}$; cKO, $13.8 \pm 1.2 \text{ min}^{-1}$) was higher than baseline conditions (ctrl, $13.4 \pm 1.4 \text{ min}^{-1}$; ***, $p < 0.001$; cKO, $4.3 \pm 0.8 \text{ min}^{-1}$, ***, $p < 0.001$) but not than the ROA density after saline injection (ctrl, $21.5 \pm 1.5 \text{ min}^{-1}$; ns, $p = 0.236$; cKO, $8.3 \pm 1.4 \text{ min}^{-1}$, ns, $p = 0.159$). Nevertheless, the ROA density after GHB application was reduced in cKO compared to ctrl animals (***, $p < 0.001$) (Figure 15A-C), whereas the ROA area was comparable (ctrl, $78.4 \pm 12.2 \mu\text{m}^2$; cKO, $76.0 \pm 17.4 \mu\text{m}^2$, ns, $p = 0.875$) (Figure 15D).

With respect to the temporal distribution of astroglial Ca²⁺ signalling *in vivo*, GHB administration induced in ctrl mice an increased signal frequency compared to baseline conditions (baseline, $0.3 \pm 0.1 \text{ min}^{-1}$; GHB, $1.1 \pm 0.1 \text{ min}^{-1}$; ***, $p < 0.001$) as well as to saline administration (sal, $0.6 \pm 0.2 \text{ min}^{-1}$; **, $p = 0.001$). On the other hand, the signal frequency after GHB administration did not increase in cKO mice compared to saline administration (sal, $0.2 \pm 0.1 \text{ min}^{-1}$; GHB, $0.4 \pm 0.1 \text{ min}^{-1}$; ns, $p = 0.577$) and was strongly reduced compared to ctrl mice (***, $p < 0.001$) (Figure 16E). Similarly, the average coincident activity peaked in ctrl mice upon GHB administration (0.08 ± 0.01) compared to baseline conditions (0.05 ± 0.01 , *, $p = 0.010$) and saline administration (0.06 ± 0.01 , ns, $p = 0.114$). Conversely, in cKO animals astroglial Ca²⁺ signals displayed a reduced coincident activity (baseline, 0.02 ± 0.01 ; saline, 0.04 ± 0.01 ; GHB, 0.02 ± 0.01) compared to ctrl mice (***, $p < 0.001$) (Figure 16F).

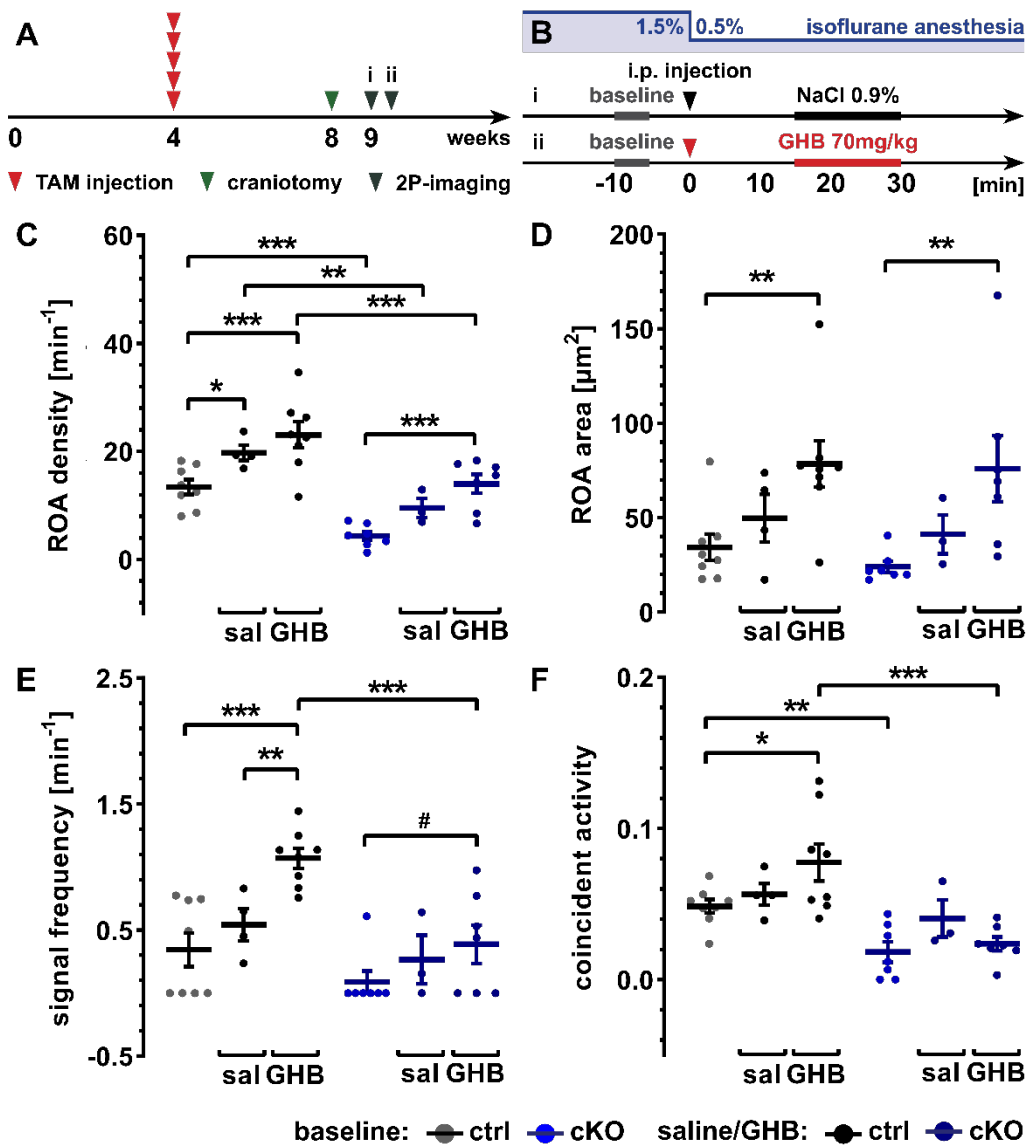


Figure 16. GHB evokes larger and more frequent astroglial Ca^{2+} signals *in vivo*

(A) Experimental design for tamoxifen (TAM) administration, cranial window implantation on the primary somatosensory cortex (SSp-ctx) and *in vivo* two-photon laser-scanning microscopy (2P-LSM) of astrocytic Ca^{2+} signalling upon saline (NaCl 0.9 %, i) and γ -hydroxybutyric acid (GHB 70 mg/kg, ii) administration. (B) Baseline recordings were collected from control (ctrl) and conditional knock-out (cKO) mice kept under 1.5 % isoflurane anaesthesia. Animals were subsequently injected i.p. with saline or GHB 70 mg/kg and anaesthesia was reduced to 0.5 % for recording of astroglial Ca^{2+} signalling at the peak of GHB action (15-30 min). (C-F) Characterization of extracted regions of activity (ROAs) in terms of average number of ROAs occurring per minute (ROA density, C), ROA spatial extension (ROA area, D), average number of signal occurring per ROA per minute (signal frequency, E) and average coincident activity calculated as the fraction of active ROAs over the total number of ROAs (F). Data are derived from N = 4-10 animals and were analysed using a two-way ANOVA test using the genotype and the treatment as independent variables (see Supplementary Table 1 for details).

7.4.2 ASTROGLIAL GABA_BR DELETION REDUCES AND RETARDS THE OCCURRENCE OF HYPERSYNCHRONOUS Ca²⁺ WAVES

So far we limited our analysis of cortical astroglial Ca²⁺ response to the evaluation of general properties associated to single regions of activity (ROAs), which biologically correlate with single spatially-confined Ca²⁺ oscillations. Nevertheless, GHB induced *in vivo* the emergence of large hypersynchronous Ca²⁺ waves encompassing the whole field of view (FOV) beyond the borders of single ROAs. Such waves could be detected in both ctrl (Figure 17C, Supplementary Video 3) and cKO (Figure 17D, Supplementary Video 4) mice. For further characterization, we considered astroglial Ca²⁺ waves which recruited more than half of the ROAs detected in the FOV (namely with a coincident activity greater than 0.5, Figure 17E). In ctrl mice, GHB-induced Ca²⁺ waves displayed a peak coincident activity ranging from 0.58 to 0.70 (0.63 ± 0.02). On the other hand, the Ca²⁺ waves recorded in cKO mice were associated with a wider range of peak coincident activity (from 0.58 to 0.89), resulting in a slightly enhanced average peak coincidence (0.74 ± 0.05 , #, 0.052) (Figure 17F). Conversely, the Ca²⁺ waves recorded ctrl and cKO mice showed no difference in terms of wave duration (ctrl, 7.5 ± 1.0 s; cKO, 8.9 ± 1.2 s; ns, 0384) (Figure 17G).

In order to confirm that these Ca²⁺ waves were specifically induced by GHB administration, we calculated the absolute occurrence of hypersynchronous Ca²⁺ events in ctrl and cKO mice in baseline conditions as well as upon saline and GHB administration at the peak of GHB action. In ctrl mice, hypersynchronous Ca²⁺ waves were almost undetected in both baseline conditions (0.25 ± 0.16 events/15 min) and upon saline application (0.25 ± 0.25). Upon GHB administration, the number of such events increased to 5.25 ± 1.1 events (***, $p < 0.001$). Similarly, in cKO mice the number of hypersynchronous Ca²⁺ waves upon GHB administration (2.86 ± 0.70) was higher than both baseline (0.57 ± 0.37 , *, $p = 0.020$) and saline administration (0.00 ± 0.00 , *, $p = 0.024$) but their absolute occurrence was reduced compared to ctrl animals (**, $p = 0.013$) (Figure 17H). Also, we assessed the cumulative relative frequency of hypersynchronous Ca²⁺ events within the first 45 min upon GHB administration. Such astroglial Ca²⁺ waves appeared earlier (approximately five minutes after GHB i.p. injection) and accumulated faster in ctrl compared to cKO mice (*, $p = 0.015$).

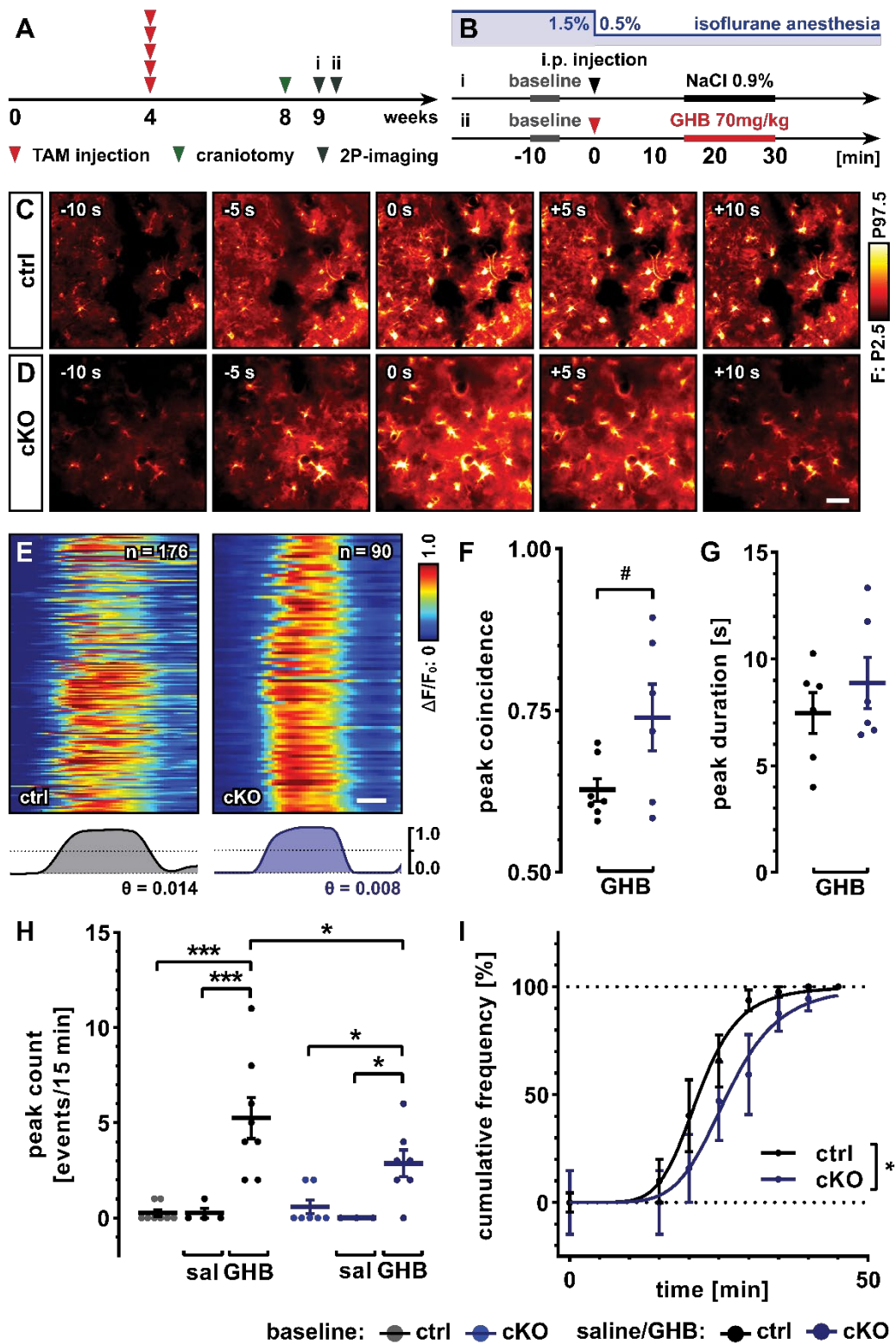


Figure 17. *In vivo* GHB induces synchronous astroglial Ca²⁺ waves at lower incidence in cKO mice

(A) Experimental design for tamoxifen (TAM) administration, cranial window implantation on the primary somatosensory cortex (SSp-ctx) and *in vivo* two-photon laser-scanning microscopy (2P-LSM) of astrocytic Ca²⁺ signalling upon saline (NaCl 0.9 %, i) and γ -hydroxybutyric acid (GHB 70 mg/kg, ii) administration. (B) Baseline recordings were collected from control (ctrl) and conditional knock-out (cKO) mice kept under 1.5 % isoflurane anaesthesia. Animals were subsequently injected i.p. with saline or GHB 70 mg/kg and anaesthesia was reduced to 0.5 % for recording of astroglial Ca²⁺ signalling at the peak of GHB action (15-30 min). (C-D) Representative field of views (FOVs) from ctrl (C) and cKO (D) mice injected with GHB displaying hypersynchronous Ca²⁺ waves (associated with a coincident activity greater than 0.5). The temporal profile of the Ca²⁺ wave is depicted as maximum intensity projection of the fluorescence intensity over time in 5 s-intervals centred at the wave peak. Scale bar, 20 μ m. (E) Heatmap representation of the depicted Ca²⁺ waves in terms of fluorescence intensity over time ($\Delta F/F_0$) as well as corresponding temporal profile of the associated coincident activity. Scale bar, 2 s. θ indicates the coincident activity expected by a random activation of the ROAs alongside the recording session. (F-G) Characterization of the Ca²⁺ waves induced by GHB in terms of peak coincident activity (F) and duration (G). Absolute occurrence of hypersynchronous Ca²⁺ waves in baseline conditions as well as after saline or GHB administration. (H) Cumulative relative frequency of Ca²⁺ waves within the first 45 min after GHB injection. Data are derived from N = 4-10 animals and were analysed using an unpaired t test (F-G) or a two-way ANOVA test using the genotype and the treatment as independent variables (H, see Supplementary Table 1 for details). In I, data were fitted with a sigmoidal curve using a least-squares fitting with no weighting method and compared using the extra-sum-of-squares F test.

7.5 cKO MICE EXHIBIT FEWER SWD-ASSOCIATED MOTOR ARRESTS

Typical absence seizures are associated with brief impairments of consciousness and lack of voluntary movements (which we refer to as immobility or freezing bouts in the following) both in humans (Panayiotopoulos, 2008; Guo et al., 2016) and mice injected with GHB (Ishige et al., 1996; Kim et al., 2001; Meerlo et al., 2004; Black et al., 2014). Therefore, we next assessed motor activity and freezing behaviour upon GHB administration in ctrl and cKO mice.

7.5.1 GHB ENHANCED THE FREEZING BEHAVIOUR OF CTRL MICE

To enable an optimal subject tracking and identification of motor arrests, we performed open field analysis of 8-week-old ctrl and cKO mice injected with saline (NaCl 0.9 %, i.p.) or GHB (70 mg/kg, i.p.) at the peak of GHB action (5-20 min after administration) (Figure 18A-C). Compared to saline-treated mice (ctrl-cKO, 1.00 ± 0.11), both ctrl (0.72 ± 0.14 , ns, $p = 0.165$) as well as cKO mice (0.86 ± 0.16 , ns, $p = 0.501$) showed only a minor reduction in running distance (Figure 18D). On the other hand, ctrl mice were slower after GHB treatment (0.62 ± 0.09) than after saline treatment (1.00 ± 0.11 , #, $p = 0.066$) and were 40 % slower than cKO mice that received GHB (1.04 ± 0.11 , *, $p = 0.048$). Conversely, cKO mice were equally fast upon saline and GHB administration (ns, $p = 0.841$) (Figure 18E). Also, and most importantly, ctrl mice spent more than 50 % more time without moving after GHB injection (1.58 ± 0.10) compared to ctrl mice injected with saline

(1.00 ± 0.08 , ***, $p < 0.001$), whereas no difference was detected in cKO mice (ns, $p = 0.982$) (Figure 18F).

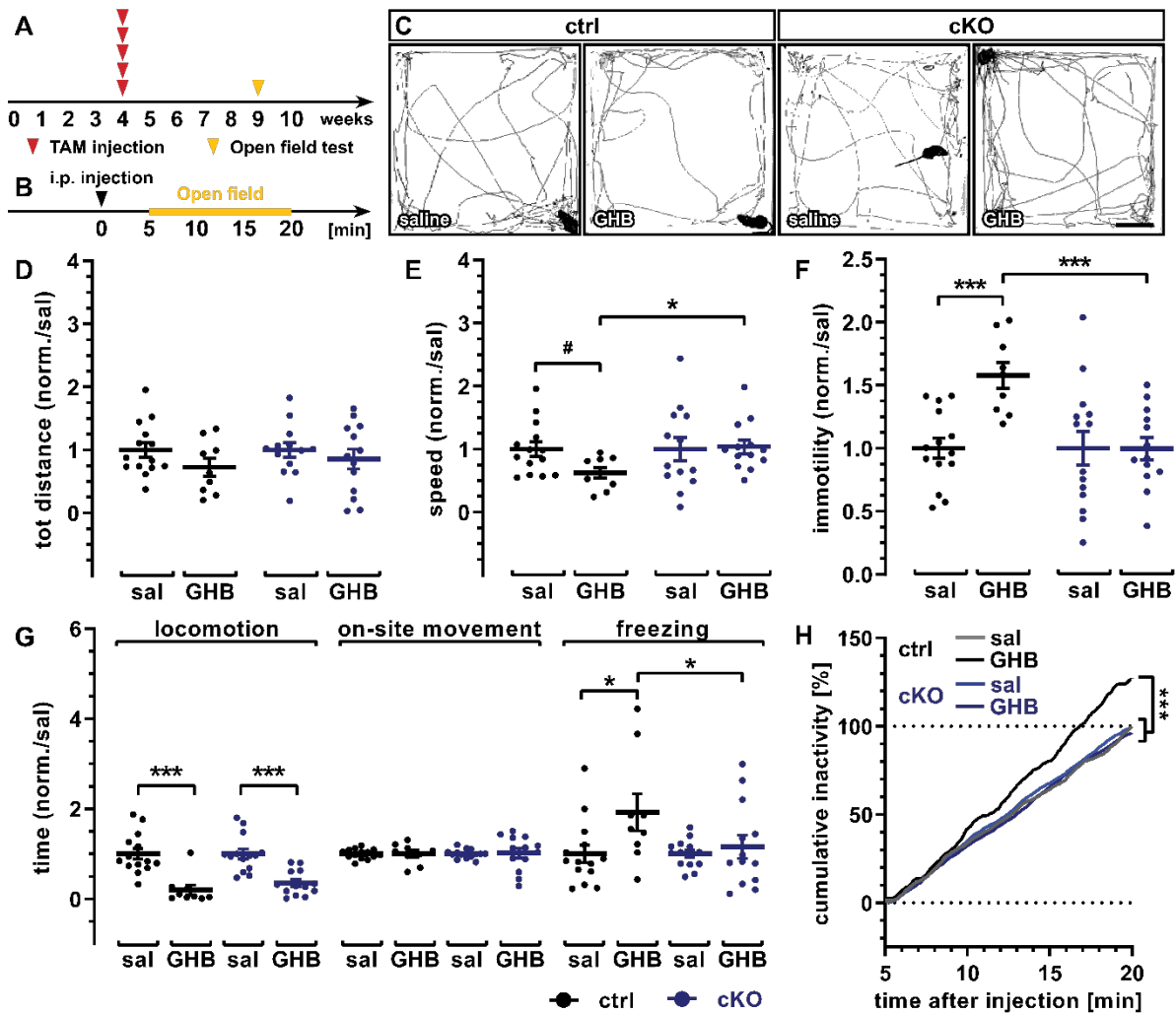


Figure 18. Open field test revealed specific increase of GHB-induced immobility in ctrl mice

(A) Experimental design for tamoxifen (TAM) administration and open field test of animal motor activity. (B) Control (ctrl) and conditional knock-out (cKO) mice injected i.p. with saline (NaCl 0.9 %, sal) or GHB 70 mg/kg (GHB) and placed in the open field arena 5 min after drug administration for 15 min. (C) Representative animal tracking over the recording period obtained using the automatic animal centre-point tracking system (see 6.2.11 for details). Scale bar, 10 cm. (D-F) Total distance covered in the arena within the recording session (D), average subject speed (E) and time spent in absence of translational movement (immobility, F). (G) Relative occurrence of animal behavioural patterns (locomotion, on-site movement and freezing) identified by means of relative pixel change analysis (non-tracking activity analysis, see 6.2.11 for details). (H) Cumulative relative inactivity measured as time spent in absence of movement. Data are derived from N = 9-14 animals and were analysed using a two-way ANOVA test using the genotype and the treatment (D-G) or the group and the time (H) as independent variables (see Supplementary Table 1 for details).

The analysis based on the tracking of the subject within the open field arena can only identify bouts of translational movement (as during locomotion), since it reduces the subject to a centre-point

corresponding to its centre of mass. Therefore, it does not allow to differentiate SWD-associated freezing activity from animal activity not associated with any translation of its centre-point (on-site movements). To do so, we performed an activity analysis based on pixel changes over time which enabled the segregation of bouts of locomotion, on-site movement and freezing activity (see 6.2.11 for details). Both ctrl and cKO mice displayed a strong reduction in locomotion upon GHB treatment (ctrl, 0.20 ± 0.11 ; cKO, 0.35 ± 0.08 ; ***, $p < 0.001$) with no difference between them (ns, $p = 0.358$). Also, we found that GHB treatment did not affect the relative occurrence of bouts of translational immobility associated with on-site movements (ns, $p = 0.887$). The relative occurrence of animal freezing bouts showed an almost two-fold increase in ctrl mice treated with GHB (1.92 ± 0.41) compared to ctrl mice injected with saline (1.00 ± 0.20 , *, $p = 0.011$), whereas no increase in freezing behaviour was detected between cKO mice treated with saline (1.00 ± 0.08) or GHB (1.16 ± 0.26 , ns, $p = 0.614$) (Figure 18G). Moreover, we found that the preferential increase of freezing bouts in ctrl mice injected with GHB started 10 min after GHB administration (Figure 18H), in line with the kinetics of GHB action.

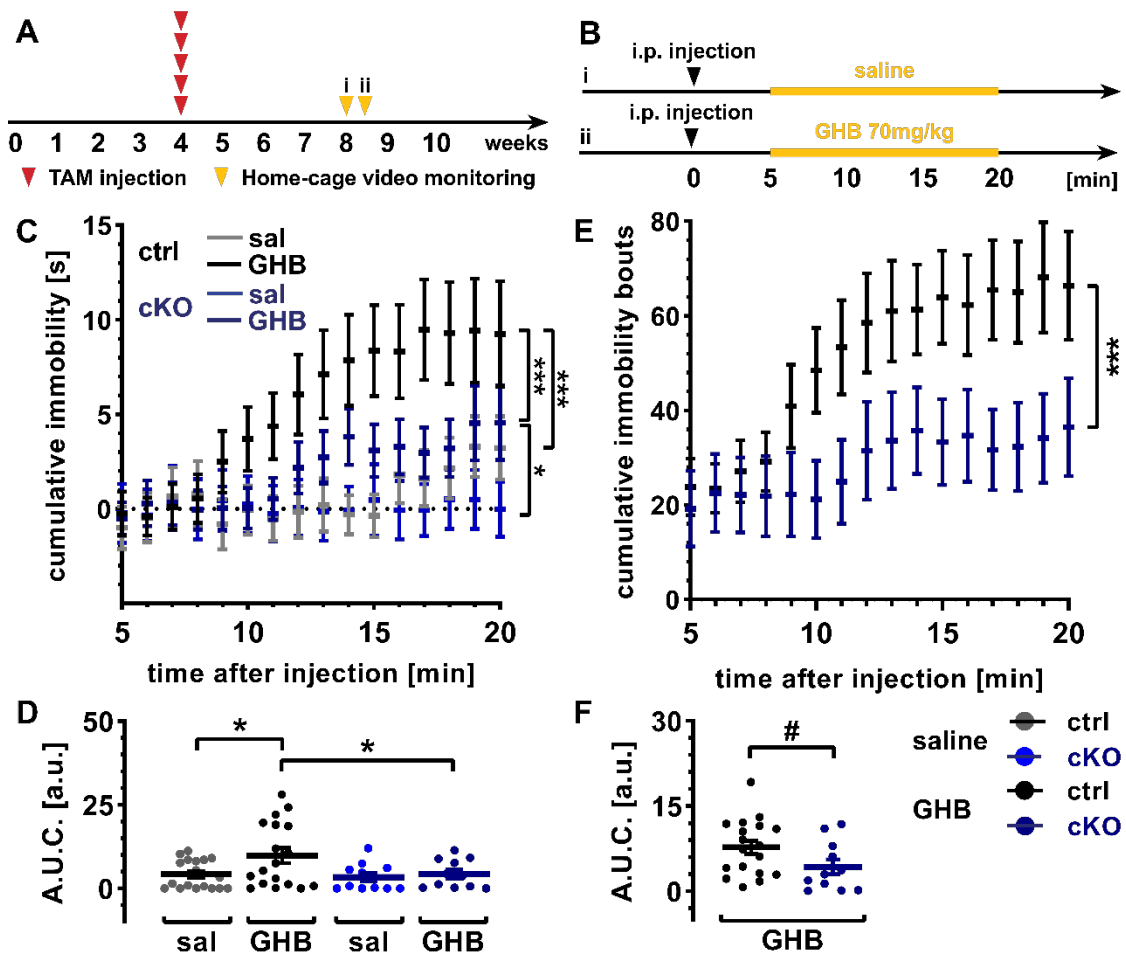


Figure 19. Upon GHB administration in their home cage cKO mice displayed reduced immobility

(A) Experimental design for tamoxifen (TAM) administration and home cage analysis of animal activity upon saline (NaCl 0.9 %, **i**) and GHB 70 mg/kg (**ii**) administration on two consecutive days. (B) Control (ctrl) and conditional knock-out (cKO) mice were injected i.p. with saline (sal) or GHB 70 mg/kg (GHB) and video monitored for up to one hour after injection. Animal immobility was detected as relative pixel change (non-tracking activity analysis, see 6.2.11 for details) during the peak of GHB action (5-20 min after injection). (C-D) Cumulative time spent in absence of movement (C) and total time spent in absence of movement calculated as area under the curve (A.U.C, D). (E-F) Cumulative occurrence of defined immobility bouts represented as function of time (D) and associated A.U.C. (E). Data are derived from N = 11-18 animals and were analysed using a two-way ANOVA test using the group and the time (C, E) or the genotype and the treatment (D) as independent variables (see Supplementary Table 1 for details). In F, data were analysed using an unpaired t test.

7.5.2 HOME CAGE ANALYSIS REVEALED REDUCED IMMOBILITY IN cKO MICE

Finally, we performed video monitoring of ctrl and cKO mice injected with saline (NaCl 0.9 %, i.p.) or γ -hydroxybutyric acid (GHB 70 mg/kg, i.p.) and kept in their home cage throughout the recording session, therefore minimizing stress-induced alterations of animal behaviour. Saline and GHB were administered on two consecutive days and the animal immobility associated with freezing behaviour was detected during the peak of GHB action (5-20 min after injection) (Figure 19A-B). The analysis of the cumulative time spent in correspondence of freezing bouts showed that GHB administration induced an increase in animal freezing behaviour in ctrl (***, $p < 0.001$) as well as cKO mice (*, $p = 0.011$) with respect to saline treatment. The time associated with freezing spent by cKO mice upon GHB administration was reduced compared to ctrl mice treated with GHB (***, $p < 0.001$) (Figure 19C). More specifically, cKO mice experienced around a 30 % increase in freezing activity (ns, $p = 0.729$), whereas ctrl mice displayed more than a 130 % increase (*, $p = 0.011$) (Figure 19D). Although this difference may arise from an increased duration of single bouts of freezing behaviour in ctrl compared to cKO mice, we found that ctrl mice accumulate single immobility bouts earlier and at higher frequency than cKO mice upon GHB administration (***, $p < 0.001$) (Figure 19E). In particular, ctrl mice experienced almost twice as many freezing behaviour bouts compared to cKO mice (#, $p = 0.069$).

8 DISCUSSION

In this work, we investigated the role of astroglial GABA_BRs and their downstream signalling involving intracellular Ca²⁺ increases in the pathological network function of absence seizures induced in mice by systemic administration of γ -hydroxybutyric acid (GHB). Our study included *in vivo* telemetric electroencephalography, two-photon laser-scanning microscopy of astroglial Ca²⁺ signalling and behavioural analysis of animal activity and led to the following key results:

- Astroglial GABA_BR-deficient mice develop less seizures associated with reduced and less prolonged increase in δ -band power upon GHB administration.
- The freezing behaviour and motor activity impairment associated with absence seizures decrease in astroglial GABA_BR-deficient mice.
- GHB evokes astroglial Ca²⁺ increase upon *ex vivo* focal application as well as systemic administration *in vivo*. Astroglial Ca²⁺ response to GHB is mediated by GABA_BRs.
- Astroglial GABA_BR-loss reduces and retards the occurrence of hypersynchronous Ca²⁺ waves upon GHB systemic administration.

8.1 THE LOSS OF GABA_BRS PROTECTS AGAINST GHB-INDUCED SWDS AND ALTERATION OF EEG

8.1.1 SYSTEMIC ADMINISTRATION OF GHB INDUCES 3-6 HZ SWDS ASSOCIATED WITH HIGHER δ AND θ POWER AND REDUCED γ POWER

Systemic injection of GHB at doses ranging from 70 to 200 mg/kg induced a dramatic increase in the δ (0.5-4 Hz) power and a less pronounced increase in θ (4-8 Hz) power peaking within the first 20 min after administration and returning to baseline levels 40 min after injection. The increase in both δ and θ power correlated with the decrease in activity upon GHB administration (δ , $r = 0.723$; θ , $r = 0.756$) and was associated with the identification of defined spike-wave discharge (SWD) trains with a 3-6 Hz frequency range (Q₁, 3.4 Hz; Q₂, 4.6 Hz; Q₃, 5.7 Hz; IQR, 2.3 Hz) and lasting up to ~ 8 s (95th percentile, 8.4 s). Our results are in line with previous work performed in mice with different genetic backgrounds and reporting an increase in spectral power in the 3-6 Hz range, therefore spreading across the δ and θ power range (Ishige et al., 1996; Kim et al., 2001; Vienne et al., 2010; Black et al., 2014). In mice of the inbred strain ddY, the intraperitoneal administration of

100 mg/kg GHB or its prodrug γ -butyrolactone (GBL) at doses of 70 and 100 mg/kg induced 3-6 Hz SWDs which could be partially reduced by both valproate and ethosuximide pre-treatment and displayed the same kinetics that we observed (Ishige et al., 1996). In adult mice with BALB/c background, doses of 50 and 100 mg/kg GBL induced slow waves in the EEG associated with increased relative δ power (lasting less than one hour) and decreased locomotor activity (Vienne et al., 2010). In mice with C57BL/6 background, systemic administration of 70 mg/kg GBL induced 3-5 Hz SWDs (Kim et al., 2001) and doses ranging from 100 to 150 mg/kg GHB (but not 50 mg/kg GHB) increased the spectral power in the δ range (Black et al., 2014). On the other hand, higher doses of GHB (200 to 400 mg/kg) and GBL (200 to 300 mg/kg) induced a state of deep anaesthesia associated with a typical electrical activity displaying burst-suppression patterns (Ishige et al., 1996; Aizawa et al., 1997; Vienne et al., 2010). In line with this, we found no significant increase in the total time with SWDs at the highest doses of GHB tested in this work (namely 200 and 250 mg/kg GHB).

In parallel to the increase in the low-frequency range (δ and θ), we detected a strong reduction in the γ (25-40 Hz) power range as well as in the high-frequency oscillation (HFO, 40-200 Hz) range which robustly correlated with the reduction in animal activity (γ , $r = 0.768$; HFO, $r = 0.608$). To our knowledge, this aspect has not been specifically addressed in the literature, with the exception of the work of Vienne and colleagues (Vienne et al., 2010), who showed a dramatic decrease in relative power density in the γ and HFO range upon injection of a much higher dose of GBL (300 mg/kg). Our finding is in line with the correlation of γ oscillations with large-scale brain network activities, including attention, memory storage and retrieval, learning and other cognitive and motor functions (Başar-Eroglu et al., 1996), which are known to be impaired during absence seizures (Panayiotopoulos, 2008; Guo et al., 2016). Also, the evaluation of the cognitive performance of individuals with childhood absence epilepsy (CAE) as well as juvenile absence epilepsy (JAE) detected attentional deficits in more than one-third of the cases which persisted one year after allocation to monotherapy even despite seizure control (Glauser et al., 2013; Masur et al., 2013; Cnaan et al., 2017). More recently, systematic analysis on the existing literature about absence epilepsy reported lower cognitive performance spreading across different cognitive domains, including attention, executive function, arithmetic achievement, language, learning and memory (Fonseca Wald et al., 2019). To date, follow-up studies on cognitive performance in adulthood in individuals diagnosed with absence epilepsy in their childhood or adolescence are limited in absolute number and sample size. Nevertheless, lower full-scale IQ (Hommet et al., 2001) as well as impaired learning, memory and processing speed (Loughman et al., 2017) have been reported in individuals with a history of CAE or JAE, suggesting that AE may be associated with neurodevelopment impairments.

8.1.2 ASTROGLIAL GABA_BR-LOSS REDUCES SEIZURE BURDEN AND δ -POWER SPECIFIC INCREASE

Astroglial GABA_BR-deletion had a protective effect against GHB-induced spectral power variations of brain waves, SWD burden and animal activity impairment. Most strikingly, GABA_BR-deficient mice showed a reduced increase of the spectral power in the δ range, whereas its kinetics was similar to ctrl mice. Similar to control animals, astroglial GABA_BR-conditional knock-out (cKO) mice experienced comparable alterations of the EEG spectrum in the θ range and a reduction in animal activity upon GHB administration. Nevertheless, cKO mice were more active than control mice at doses of 70 and 100 mg/kg GHB and recovered faster to baseline levels (around 30 min after injection). Interestingly, although still significantly correlated, cKO mice showed a reduced correlation between animal inactivity and the spectral power in the δ and θ range (δ , $r = 0.364$; θ , $r = 0.391$). This suggests that astroglial GABA_BRs contribute not only to the generation of the spectral alteration induced by GHB administration but also to its behavioural manifestation. In virtue of their close functional association to GABAergic interneurons, cortical as well as hippocampal astrocytes are involved in the generation of γ -oscillations (Lee et al., 2014; Mederos and Perea, 2019; Mederos et al., 2021). Astroglial GABA_BR ablation has been linked to a reduced spectral power in the γ range and impaired cognition (Perea et al., 2016; Mederos et al., 2021). In line with this, we also detected a 15 % reduction in γ power in baseline conditions in cKO mice (ctrl, $13.1 \pm 0.2 \mu V^2$; cKO, $11.5 \pm 0.2 \mu V^2$, ***, $p < 0.001$). Upon GHB administration, the spectral power in the γ range was similarly reduced in cKO as in ctrl mice. Nevertheless, the correlation between animal activity and γ - as well as HFO-power was reduced compared to ctrl (γ , $r = 0.498$; HFO, $r = 0.504$).

In cKO mice, the reduced increase in δ -power was associated with a reduced seizure burden, both in terms of absolute occurrence of SWDs as well as time spent in SWD trains. On the other hand, GHB induced-SWDs displayed the same 3-6 Hz frequency range as ctrl mice. Also, although slightly shorter (95th percentile, 6.9 s), SWD trains displayed a comparable duration between ctrl and cKO mice.

Our results therefore suggest that astroglial GABA_BRs are not necessary for the generation of absence seizures and that their deletion from the astrocytic membrane does not alter their electrical properties, including their electroencephalographical profile as well as their specific frequency. Nevertheless, astroglial GABA_BR-loss significantly reduced the number of seizures occurring upon GHB administration, therefore providing evidence for the contribution of astroglial GABA_BRs in the pathological network priming and susceptibility to seizure onset. Alternatively, we cannot exclude that astroglial GABA_BRs are involved in the propagation of SWDs from their focal onset. To rule out this possibility, the employment of multiple depth-electrodes is required and could shine new light on the mechanisms underlying the protective effect of astroglial GABA_BR deletion.

8.1.3 ASTROGLIAL GABA_BRS CONTRIBUTE TO THE PATHOLOGICAL NETWORK PRIMING AT THE BASIS OF SWDS

Our current understanding of the anatomical, cellular as well as molecular substrates of GHB-induced absence seizures is predominantly based on research performed in rats and is not well characterized in mice (Venzi et al., 2015). SWDs arise from synchronous oscillations of the cortico-thalamo-cortical network (CTCn) including the superficial layers (I-IV) of the frontoparietal cortex, the ventral nuclei of the thalamus and the nucleus reticularis thalami (NRT) (Banerjee et al., 1993). Displacement studies with the GABA_BR-specific agonist baclofen showed that GHB is a weak agonist of GABA_BRs with a K_d in the 30-500 μ M range and an EC₅₀ around 5 mM (Maitre, 1997; Mathivet et al., 1997; Lingenhoebl et al., 1999). Evidence from both pharmacological treatment with GABA_BR-agonists and antagonists (Snead, 1992a, 1996; Carter et al., 2005; Carter et al., 2009) as well as from genetic manipulation studies using global GABA_BR knockout mice (Kaupmann et al., 2003) showed that GHB-induced electrical as well as behavioural effects are mediated by GABA_BRs. The existence and molecular identity of GHB receptors (GHBR) with high affinity for GHB ($K_d \sim 100$ nM) (Benavides et al., 1982; Snead, 1994) and not corresponding to GABA_BRs (Maitre, 1997; Kaupmann et al., 2003; Wu et al., 2004) is still under debate. Nevertheless, the existence of GHB as endogenous compound in the brain at a concentration of 1-4 μ M (Doherty et al., 1978; Snead and Morley, 1981) as well as its threshold concentration of 240 μ M required to induce SWDs (Snead, 1991) are in line with a predominant role of GABA_BRs in the induction of the phenotype associate to absence seizures.

In the thalamic nuclei, GHB acts on thalamocortical (TC) neurons via both pre- and postsynaptic mechanisms, including binding to presynaptic GABA_BRs resulting in the reduction of the amplitude of both excitatory postsynaptic potentials (EPSPs) produced by corticothalamic afferents (Emri et al., 1996; Gervasi et al., 2003) and inhibitory postsynaptic potentials (IPSPs) produced by GABAergic afferents from the NRT (Gervasi et al., 2003) as well as binding to postsynaptic GABA_BRs followed by tonic hyperpolarization of TC neurons via opening of K⁺ channels (Williams et al., 1995) and increased tonic GABA_A inhibition (Cope et al., 2009; Connelly et al., 2013). In the cortex, GHB induces the hyperpolarization of both pyramidal cells and interneurons of cortical layers II/III and reduces the amplitude and frequency of miniature EPSPs and IPSPs (Hu et al., 2000; Jensen and Mody, 2001; Li et al., 2007). Since the dose of GHB required to presynaptically induce a reduction of EPSPs is lower in both cortex (300 μ M) and thalamus (100 μ M) compared to the dose required to reduce IPSPs (in the cortex and thalamus, 1 mM and 500 μ M, respectively), it has been speculated that GHB ultimately favors phasic inhibition over phasic excitation (Venzi et al., 2015). To date, there is still some controversy in the identification of the initiation site of GHB-induced absence seizures. Evidence from high-resolution EEG recording from mice injected with 50 mg/kg GBL suggested that absence seizures initiate in the primary somatosensory cortex (Choi et al., 2010).

Nevertheless, intrathalamic administration of both GHB (Snead, 1991) and baclofen (Liu et al., 1992) in rats resulted in similar electrical and behavioral activities to the systemic administration of GHB.

GABA_BRs are widely expressed on neurons throughout the central nervous system (CNS) but also on a number of nonneuronal glial cells, including astrocytes (Nilsson et al., 1993; Kang et al., 1998; Charles et al., 2003; Meier et al., 2008). However, current evidence on the contribution of astroglial GABA_BR-mediated signalling in absence seizures, and in particular in GHB-induced absence seizures, is still limited. In this work, we showed that astrocyte-specific GABA_BR-loss significantly reduced seizure burden and the increase in δ power induced by systemic administration of GHB, therefore suggesting that astroglial GABA_BRs contribute to the pathological network priming at the basis of SWDs. Moreover, our findings might underestimate the contribution of astroglial GABA_BRs to absence seizures since their removal from the astrocytic membrane was not complete in our study. Despite optimization of the tamoxifen injection protocol for genomic DNA recombination in astrocytes (Jahn et al., 2018), we still detected four weeks after treatment the persistence of around 25 % of *Gabbr1* mRNA levels and up to 50 % GABBR1 protein levels in MACs-purified astrocytes, possibly due to a particular membrane stability of astrocytic GABA_BRs. In line with this, *in vitro* studies showed that neuronal GABA_BRs are associated with reduced basal and agonist-induced endocytosis (Fairfax et al., 2004; Balasubramanian et al., 2007) as well as enhanced agonist-induced receptor recycling after internalization (Grampp et al., 2008). It is therefore possible that a stronger reduction of absence seizures may result from a more efficient GABA_BR-removal from the astroglial membrane, which might be achieved by a longer waiting period between tamoxifen treatment and seizure induction or an additional round of tamoxifen treatment. On the other hand, this would result in the use of fully mature adult C57BL6/N mice (Flurkey et al., 2007), which may differ from the model used in this study employing 8- to 9-week-old mice as well as impede the translation of the results to the absence epilepsy phenotype typical of childhood and juvenile phases in humans. Nevertheless, to date most *in vivo* studies of GHB-induced absence seizures in mice share this same limitation since they employ 10- and up to 15-week old animals (Vienne et al., 2010; Black et al., 2014).

Despite its temporal and cell specificity, our approach based on the Cre^{ERT2}-loxP system (Feil et al., 2009) does not provide any regional specificity of the protective effect of astroglial GABA_BR-loss. Given its involvement in the generation and perpetuation of absence seizures, we speculate that astroglial GABA_BRs contribute to the pathological network priming within the CTCn. The specific contribution of astroglial GABA_BRs from different regional components of the CTCn remains elusive. The combined use of TgH (GABA_BR1^{fl/fl}) mice (Haller et al., 2004) with the viral expression of the Cre recombinase under the control of the glial fibrillary acidic protein (GFAP) promoter (pAAV.GFAP.Cre.WPRE.hGH, Addgene # 105550-AAV5) would enable to address this aspect.

Also, given the regional specificity of astroglial control of the excitation/inhibition (E/I) balance (Caudal et al., 2020; Gobbo et al., 2021), this would be crucial to unravel the mechanisms underlying the protective role of astroglial GABA_BR-loss against GHB-induced absence seizures. GABAergic signalling to astrocytes has been linked to glutamate and ATP release leading to presynaptic depression via mGlu2/3 (Andersson et al., 2007) and potentiated inhibitory transmission via NMDA/AMPA receptors (Kang et al., 1998) as well as hetero-synaptic depression via A₁ as well as P2Y receptors (Serrano et al., 2006; Chen et al., 2013; Matos et al., 2018), respectively. In line with this, evidence derived from genetic models of absence epilepsy showed enhanced cortical NMDA-mediated responses (Pumain et al., 1992; D'Antuono et al., 2006) as well as increased extracellular glutamate concentration (Melø et al., 2006) associated with absence seizures. In addition, NMDA and AMPA receptor antagonists reduced the number of SWDs upon systemic or intracerebral injection (Peeters et al., 1989b; Peeters et al., 1990; Ramakers et al., 1991; Peeters et al., 1994) as well as upon intracortical administration (Citraro et al., 2006) and activation of mGlu2/3 exacerbated SWDs (Ngomba et al., 2005). Also, tonic inhibition of CT neurons by cortical interneurons was associated with the emergence of synchronized and phase-locking discharge and burst firing activity (Chipaux et al., 2011) and cortical astrocytes have been shown to specifically respond to tonic (in contrast to phasic) inhibition by means of ATP release, activation of A₁Rs and enhancement of synaptic inhibition (Covelo and Araque, 2018). We therefore speculate that astroglial GABA_BRs mediate the reinforcement of inhibitory or disinhibitory circuits by releasing ATP or glutamate (or both) acting on presynaptic receptors (Figure 20). In line with this, astroglial GABA_BR-loss significantly reduces the seizure burden but is permissive for the occurrence of absence seizures *per se*. To test this hypothesis, the release of glutamate and ATP from cortical astrocytes of ctrl and astroglial GABA_BR-deficient mice could be evaluated *in vivo* by means of membrane-tagged glutamate (Dürst et al., 2019) and ATP sensors (Wu et al., 2022) as well as microdialysis evaluation of gliotransmitter levels in the extracellular space. Whereas the proposed strengthening of inhibitory transmission operated by astrocytes in the cortical networks is in accordance with several lines of evidence, the contribution of a similar mechanism in the ventral thalamic nuclei is controversial. Nevertheless, given the increased levels of extracellular GABA in the thalamus associated with absence seizures (Richards et al., 1995; Leal et al., 2016) and the enhanced tonic GABA_AR-mediated inhibition (Cope et al., 2005; Cope et al., 2009; Errington et al., 2011b), it is very likely that astroglia sense and respond to the enhanced GABAergic tone via gliotransmitter release. Also, astrocytes may further contribute to the enhanced GABAergic inhibition in response to glutamatergic inputs delivered by CT afferents as previously described for hippocampal synapses (Héja et al., 2019).

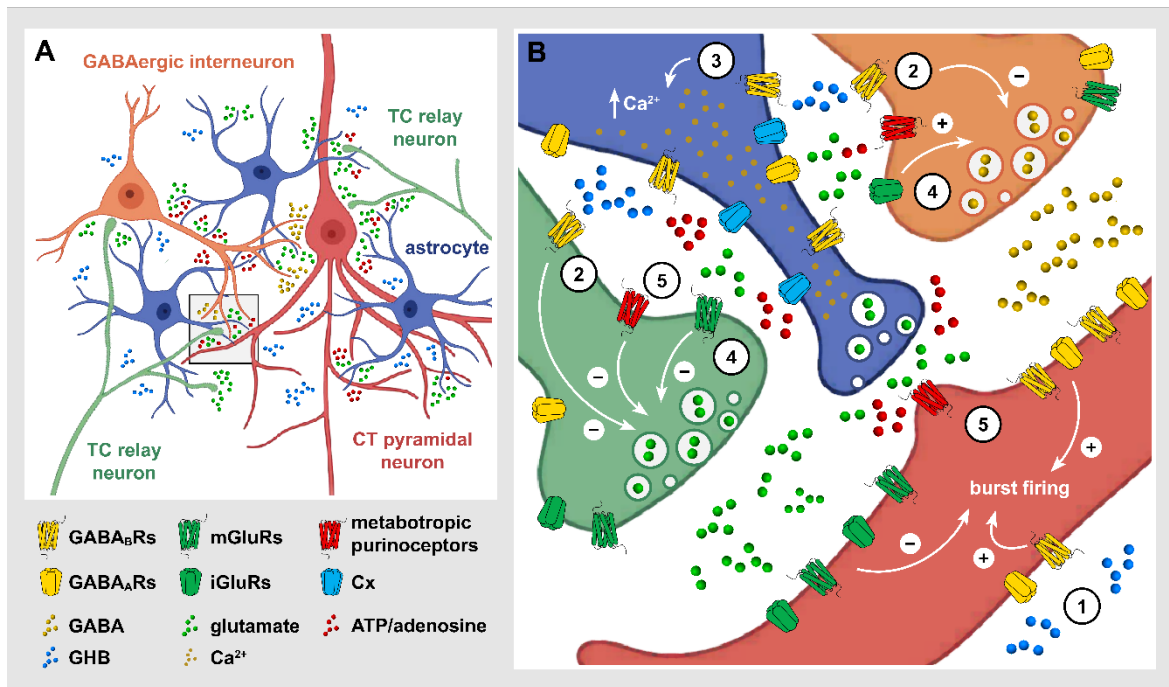


Figure 20. Putative contribution of cortical astroglial GABA_BR-signalling in the E/I imbalance underlying absence seizures

(A) Schematic representation of the cortical cellular components of the cortico-thalamo-cortical network including a cortico-thalamic pyramidal neuron (CT, red), axonal projections of thalamo-cortical relay neurons (TC, in green), GABAergic interneuron (in orange) and astrocytes (in blue). (B) Expanded view of the multi-partite synapse marked in grey in A. γ -hydroxybutyric acid (GHB) induces the hyperpolarization of CT pyramidal neurons via GABA_A and GABA_B receptors (GABA_AR and GABA_BRs, respectively) (1) and acts on presynaptic GABA_BRs (2) inhibiting both glutamate and GABA vesicular release. Ultimately, GHB favors phasic and tonic inhibition over phasic excitation and results in the emergence of burst firing activity in CT neurons. GHB also binds to astroglial GABA_BRs (3) inducing an increase of the intracellular Ca²⁺ concentration and possibly leading to gliotransmitter release, including vesicular release of glutamate and ATP release through connexin hemichannels (Cx). In turn, astroglial glutamate may act on presynaptic ionotropic glutamate receptors (iGluRs, NMDA or AMPA) of cortical interneurons or on presynaptic metabotropic glutamate receptors (mGluRs) of TC projections, resulting in potentiated inhibitory transmission and reduced glutamate release, respectively (4). Similarly, the ATP released from astrocyte may act presynaptically reducing glutamate release from TC projecting neurons as well as postsynaptically potentiating GABAergic inhibition of CT pyramidal neurons (5).

8.2 Ca^{2+} RESPONSE UPON GHB ADMINISTRATION IS MEDIATED BY ASTROGLIAL GABA_B RS

8.2.1 GHB DIRECTLY RECRUITS ASTROGLIAL GABA_B RS AND INDUCES SUBSEQUENT Ca^{2+} ACTIVITY

The intracellular signal transduction of neuronal $G_{i/o}$ -coupled GABA_B Rs including G_α -subunit-mediated inhibition of the adenylyl-cyclase-cAMP pathway as well as the $G_{\beta\gamma}$ -subunit-mediated inhibition of Ca^{2+} channels and activation of inwardly rectifying K^+ channels is well established (Misgeld et al., 1995; Harayama et al., 1998; Couve et al., 2000; Owens and Kriegstein, 2002). On the other hand, the signalling cascade downstream of astroglial GABA_B Rs is still unclear. Recent evidence showed that astroglial GABA_B Rs are $G_{i/o}$ protein-coupled receptors, whose activation results in intracellular Ca^{2+} increase and subsequent gliotransmitter release (Serrano et al., 2006; Mariotti et al., 2016; Perea et al., 2016; Durkee et al., 2019; Nagai et al., 2019). In the context of GHB-induced absence seizures, it has been shown that the focal application of GHB results *ex vivo* in GABA_B R-mediated Ca^{2+} signalling in thalamic astrocytes with a threshold concentration of 250 μM and an ED50 of 1.6 mM (Gould et al., 2014). Adding on this, we provided in this work a comprehensive analysis of cortical astroglial Ca^{2+} signalling upon GHB focal application in acute slice preparations in presence of the neuronal blocker tetrodotoxin (TTX). We took advantage of the astrocyte-specific expression of the genetically encoded Ca^{2+} indicator GCaMP3, which displays higher baseline fluorescence intensity as well as enhanced dynamic range compared to state-of-the-art Ca^{2+} indicators (such as GCaMP6f or GCaMP7) allowing non-invasive and stable Ca^{2+} imaging at the cellular and network level (Podor et al., 2015; Ye et al., 2017). On the other hand, its slower kinetics and reduced Ca^{2+} affinity makes it unfeasible to address fast and subtle Ca^{2+} oscillations at the microdomain level.

GHB induced an increase in astroglial Ca^{2+} signalling in terms of signal number as well as amplitude, duration and integrated fluorescence upon application of doses ranging from 100 μM and up to 10 mM. The increased astroglial Ca^{2+} signalling induced by GHB depends on the presence of functional GABA_B Rs on the astrocytic membrane since cKO mice displayed no significant increase in astroglial Ca^{2+} signalling upon GHB administration at any tested dose. As in the work of Gould and colleagues (Gould et al., 2014), we found a progressive increase of astroglial Ca^{2+} signalling at increasing doses of GHB. On the other hand, we detected an increase in astroglial Ca^{2+} already at a dose of 100 μM GHB compared to baseline conditions. This difference may derive from the fact that our study evaluated astroglial Ca^{2+} signalling occurring within regions of activity (ROAs) associated with fluctuations in fluorescence intensity over time and automatically extracted independently of underlying cellular structures, whereas Gould and colleagues quantified astroglial Ca^{2+} rises as absolute number of Fluo-4 AM-loaded cells displaying somatic Ca^{2+} increase upon GHB application.

In parallel to the increase in astroglial Ca^{2+} signal number as well as amplitude and duration, we found that GHB administration resulted in the occurrence of astroglial Ca^{2+} rises with greater spatial extension as well as higher synchronicity. Once again, this effect was abolished in astroglial GABA_BR -deficient mice. This result is of particular interest in the context of epilepsy research, since the spatiotemporal organization of Ca^{2+} fluctuations impacts the generation of synchronous oscillations of neuronal activity and therefore play a fundamental role in the pathological priming of neural networks as well as in seizure onset, propagation and self-sustain (Gómez-Gonzalo et al., 2010; Kékesi et al., 2015; Losi et al., 2016; Ujita et al., 2017).

Our results revealed that GHB induces the increase of astroglial intracellular Ca^{2+} in a dose dependent manner, in dependence of the presence of functional astroglial GABA_BRs but independent of neuronal firing activity. Notably, we cannot exclude that our findings are not biased by indirect effects resulting from the activation of GABA_BRs expressed on the membrane of other glial cells (Bettler et al., 2004; Bettler and Tiao, 2006) as well as the interference with TTX-independent neuronal mechanisms of neurotransmitter release, such as spontaneous vesicular release or inverse transport (Melom et al., 2013; Kavalali, 2015).

8.2.2 ASTROGLIAL Ca^{2+} RESPONSE UPON GHB APPLICATION IS SHAPED BY NEURONAL EVOKED NEUROTRANSMITTER RELEASE

Although mechanistically relevant, GHB-induced increases in astroglial Ca^{2+} signalling may be practically irrelevant to the generation or propagation of SWDs in the presence of a functional neuronal network. Indeed, we found that the observed cortical astroglial Ca^{2+} response upon GHB focal application was altered in absence of the voltage-gated Na^+ channel blocker tetrodotoxin (TTX). In particular, we observed a significant increase in astroglial Ca^{2+} signal number, amplitude and integrated fluorescence only at the highest dose of GHB tested (namely 10 mM) and we did not detect any difference in terms of spatial extension of the evoked Ca^{2+} signals. Given the inhibitory effect of the activation of neuronal GABA_BRs on neurotransmitter release (Misgeld et al., 1995; Harayama et al., 1998; Couve et al., 2000; Owens and Kriegstein, 2002), our observation could depend on a reduced neurotransmitter release upon GHB administration, which in turn would lead to a reduced evoked Ca^{2+} activity in astrocytes. In line with this, we detected a progressive reduction of astroglial Ca^{2+} properties (signal density, amplitude and area) alongside the increase of the applied dose of GHB in slices from astroglial GABA_BR -deficient mice. These results therefore suggest that in acute slice preparations GHB acts directly on astroglial GABA_BRs inducing an enhanced intracellular Ca^{2+} signalling and reduces neurotransmitter-evoked astroglial Ca^{2+} signals by indirect activation of neuronal GABA_BRs . The combined use of two-photon laser-scanning microscopy (2P-LSM) analysis of astrocytic Ca^{2+} signalling and electrophysiological recording of neighbouring neurons (either via single-cell patch-clamp or local field potential analysis) would confirm this

hypothesis and would possibly enable to temporally segregate direct and indirect effects of GHB on astroglial Ca^{2+} signalling. Notably, despite the concomitant occurrence of these two different mechanisms of action, GHB still induced a progressive increase in astroglial Ca^{2+} signal synchronicity which, once again, was dependent on the presence of functional astroglial GABA_BRs . This suggests that the enhanced synchronous appearance of astroglial intracellular Ca^{2+} oscillations is directly induced by GHB activation of astroglial GABA_BRs and is not affected by indirect alteration of neuronal network activity.

8.3 GHB ADMINISTRATION INDUCES THE APPEARANCE OF STEREOTYPICAL HYPERSYNCHRONOUS ASTROGLIAL Ca^{2+} WAVES *IN VIVO*

In vivo systemic administration of 70 mg/kg GHB induced the specific increase of intracellular Ca^{2+} signalling in cortical astrocytes in ctrl mice, whereas astroglial GABA_BR -deficient mice showed no relative increase compared to saline administration. On the other hand, both ctrl and cKO mice were associated with a substantial uniformity of astroglial Ca^{2+} signal amplitude, duration and integrated fluorescence upon GHB administration. Also, the spatial extension of astroglial Ca^{2+} signalling upon GHB administration was similar between ctrl and cKO mice and only slightly increased compared to astroglial Ca^{2+} signalling upon saline injection. Nevertheless, the signal frequency as well as the synchronicity of astroglial Ca^{2+} signalling was specifically increased in ctrl mice.

Upon GHB administration both ctrl and cKO mice exhibited stereotypical hypersynchronous astroglial Ca^{2+} waves spreading across the entire field of view ($\sim 0.05 \text{ mm}^2$) and engaging all observable astrocytes. These Ca^{2+} events displayed similar amplitude and duration in ctrl and astroglial GABA_BR -deficient mice but occurred at higher frequency in ctrl mice and were absent upon saline administration in both groups. Moreover, the appearance of such astroglial Ca^{2+} waves was retarded in cKO compared to ctrl mice. To our knowledge, stereotypical Ca^{2+} waves have never been described (nor addressed) either in genetic or in pharmacological models of absence seizures. Nevertheless, several studies have been reporting the appearance of stereotypical Ca^{2+} waves during convulsive epileptiform activity (Kang et al., 2005; Tian et al., 2005; Ding et al., 2007; Heuser and Enger, 2021). Interestingly, it has been reported in an *in vivo* model of convulsive seizures that astroglial Ca^{2+} elevations temporally preceded neuronal engagement and that their attenuation results in the reduction of epileptic activity (Heuser et al., 2018). Moreover, blocking of early ictal astrocytic Ca^{2+} signals prevented the spreading of epileptiform activity in mouse entorhinal cortex slices (Gómez-Gonzalo et al., 2010). On the other hand, blocking of astroglial Ca^{2+} signalling *in vivo* during seizures did not affect epileptic discharges in the 4-aminopyridine pharmacological model of convulsive seizures in the rat (Baird-Daniel et al., 2017) and astrocytic Ca^{2+} activity was also associated with spreading depolarization-mediated seizure termination (Seidel et al., 2016). Therefore, current research is still far from understanding the contribution of stereotypical Ca^{2+}

waves to seizure generation, propagation, severity, and termination both in mechanistic and logical (sufficiency and/or necessity) terms.

The propagation of Ca^{2+} signals beyond single astrocytic domains (Scemes and Giaume, 2006; Leybaert and Sanderson, 2012) is mediated by either direct cytoplasmic diffusion of InsP3 through gap junctions (Allbritton et al., 1992; Leybaert and Sanderson, 2001), paracrine signalling via ATP release (Guthrie et al., 1999; Arcuino et al., 2002; Anderson et al., 2004; Fujii et al., 2017) or both (Fiacco and McCarthy, 2006). Since astroglial GABA_B -activation results in the engagement of the InsP3-pathway as well as ATP release, the loss of astroglial GABA_B Rs may impact one or both these phenomena, thus explaining the retarded appearance of stereotypical Ca^{2+} waves. On the other hand, since the occurrence of such hypersynchronous Ca^{2+} waves is not abolished by the loss of astroglial GABA_B Rs, we speculate that their reduced occurrence in cKO mice is probably a consequence of the reduced seizure burden and not its cause. Nevertheless, concomitant animal electroencephalographic monitoring will be required to address the specific temporal correlation between SWD trains and stereotypical Ca^{2+} waves and therefore to draw significant conclusions on their causal association.

8.4 ASTROGLIAL GABA_BR-LOSS PROTECTS AGAINST GHB-INDUCED BEHAVIOURAL ARRESTS

In parallel with the protective effect of astroglial GABA_BR-loss in the reduction of animal activity upon GHB administration, we showed in the present study that astroglial GABA_BR-deficient mice placed in the open field arena were not affected by the induction of behavioural arrests typical of absence seizures (Ishige et al., 1996; Kim et al., 2001; Meerlo et al., 2004; Black et al., 2014). On the other hand, ctrl mice displayed a reduction in average speed and motility as well as an increased time spent in freezing behavioural arrests, which is in line with recent evidence from the open field analysis performed using a genetic mouse model of absence seizures (Cao et al., 2020). Also, we performed the evaluation of animal immobility associated with freezing behaviour in the context of the animal home cage, therefore minimizing stress-induced alterations of animal behaviour. By doing so, we found that the time spent in behavioural arrests as well as the number of defined immobility bouts after systemic administration of GHB were significantly reduced in astroglial GABA_BR-deficient mice. Compared to saline-treated cKO mice, GHB still induced an increase in animal freezing behaviour. Since the kinetics of GHB-induced animal behavioural arrests as well as their dependency on the presence of functional astroglial GABA_BRs are similar to the increase in δ -spectral power and the appearance of SWD trains associated with GHB administration, we conclude that the protective role of astroglial GABA_BR-loss at the behavioural level results from the reduced seizure burden and spectral alteration in the δ range associated with astroglial GABA_BR-loss. These results not only confirm the contribution of astroglial GABA_BRs to the genesis and severity of GHB-induced pathological phenotype but also their validity as putative pharmacological targets for the treatment of absence seizures as well as the phenotypical outcomes associated with absence epilepsy.

9 CONCLUSION AND OUTLOOK

In the present study, we investigated the role of astroglial GABA_BRs and their downstream signalling involving intracellular Ca²⁺ transients in the pathological network function of γ -hydroxybutyric acid (GHB)-induced absence seizures and identified a protective role of astroglial GABA_BR-loss against the disruption of the correct excitation/inhibition (E/I) balance that leads to the pathological priming of the neural networks. Our findings showed that the removal of GABA_BRs from the astrocytic membrane does not abolish the emergence of absence seizures *per se*. Nevertheless, astroglial GABA_BR-deficient mice experienced reduced spectral alterations and seizure burden compared to ctrl mice. Also, they recovered faster from the impairments in motor activity induced by GHB and displayed less behavioural arrests. In parallel to that, we provided evidence that GHB directly engages astroglial GABA_BRs and evokes large synchronous intracellular Ca²⁺ oscillations in the astrocytic syncytium, which may contribute to the disruption of the correct E/I balance in neural networks that leads to seizure activity.

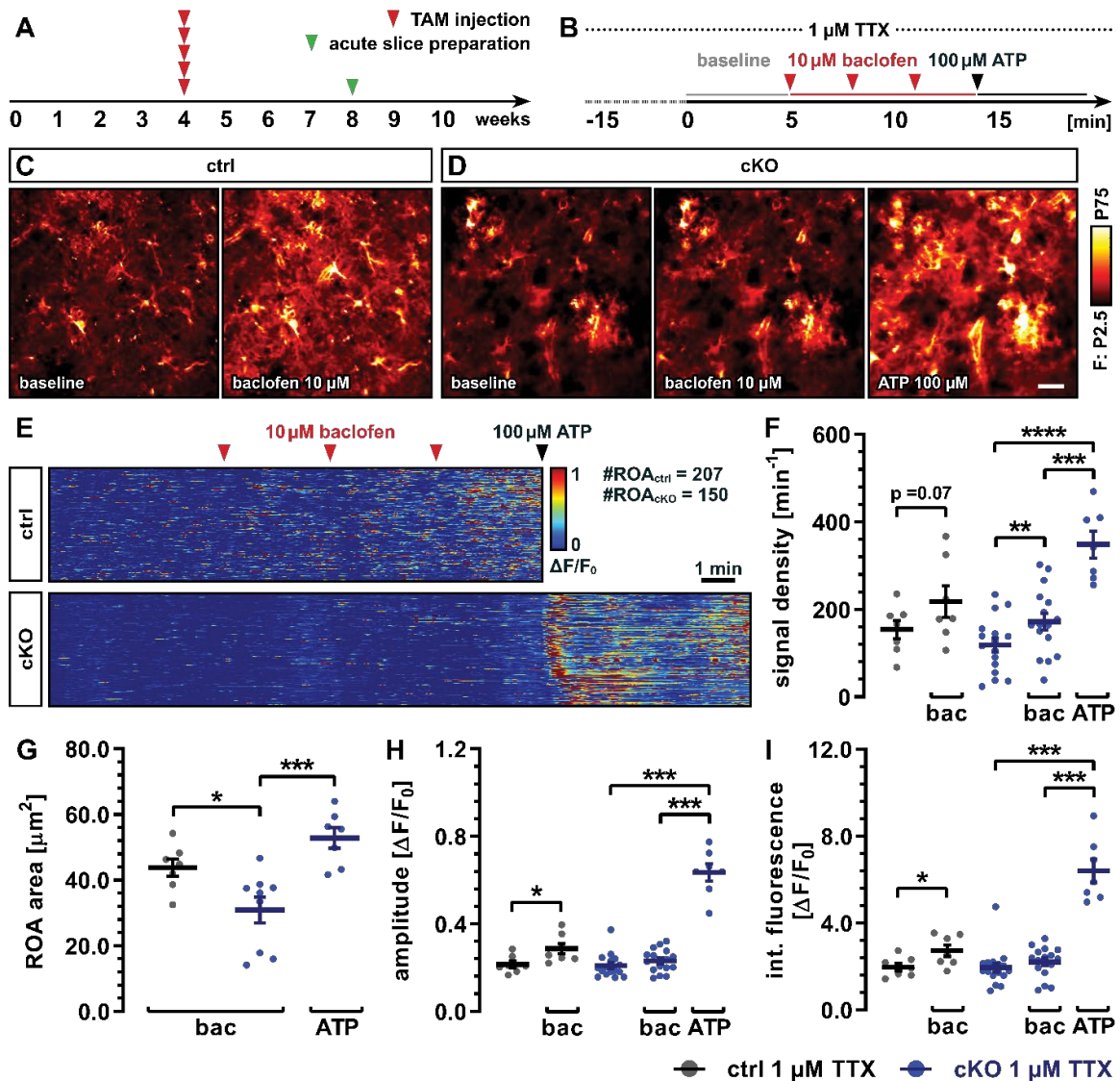
Although the exact mechanisms underlying the contribution of astroglial GABA_BR to the genesis of absence seizures still requires further investigation, our results suggest that astroglial GABA_BRs could mediate the reinforcement of inhibitory or disinhibitory circuits upon GABAergic input by releasing ATP or glutamate acting on presynaptic terminals.

To test this hypothesis, the release of glutamate and ATP from cortical astrocytes of control and astroglial GABA_BR-deficient mice could be evaluated *in vivo* by means of membrane-tagged glutamate (Dürst et al., 2019) and ATP sensors (Wu et al., 2022) as well as microdialysis evaluation of gliotransmitter levels in the extracellular space of both cortical and thalamic components of the cortico-thalamo-cortical network.

The combined use of two-photon laser-scanning microscopy (2P-LSM) of astrocytic Ca²⁺ signalling and multipolar depth-electrode recording would enable the evaluation of the temporal and causal association between SWDs and cortical astroglial Ca²⁺ wave appearance and propagation. Also, region-specific induction of astroglial GABA_BR-loss using adeno-associated viral delivery system would address the contribution of cortical and thalamic astroglial GABA_BRs in the genesis and propagation of spike-wave discharges (SWDs). Finally, we propose that DREADD-based chemogenetic activation of astroglial G_{i/o} pathway could be used to enhance and restore astroglial GABA_BR-signalling in control and conditional knock-out mice, respectively.

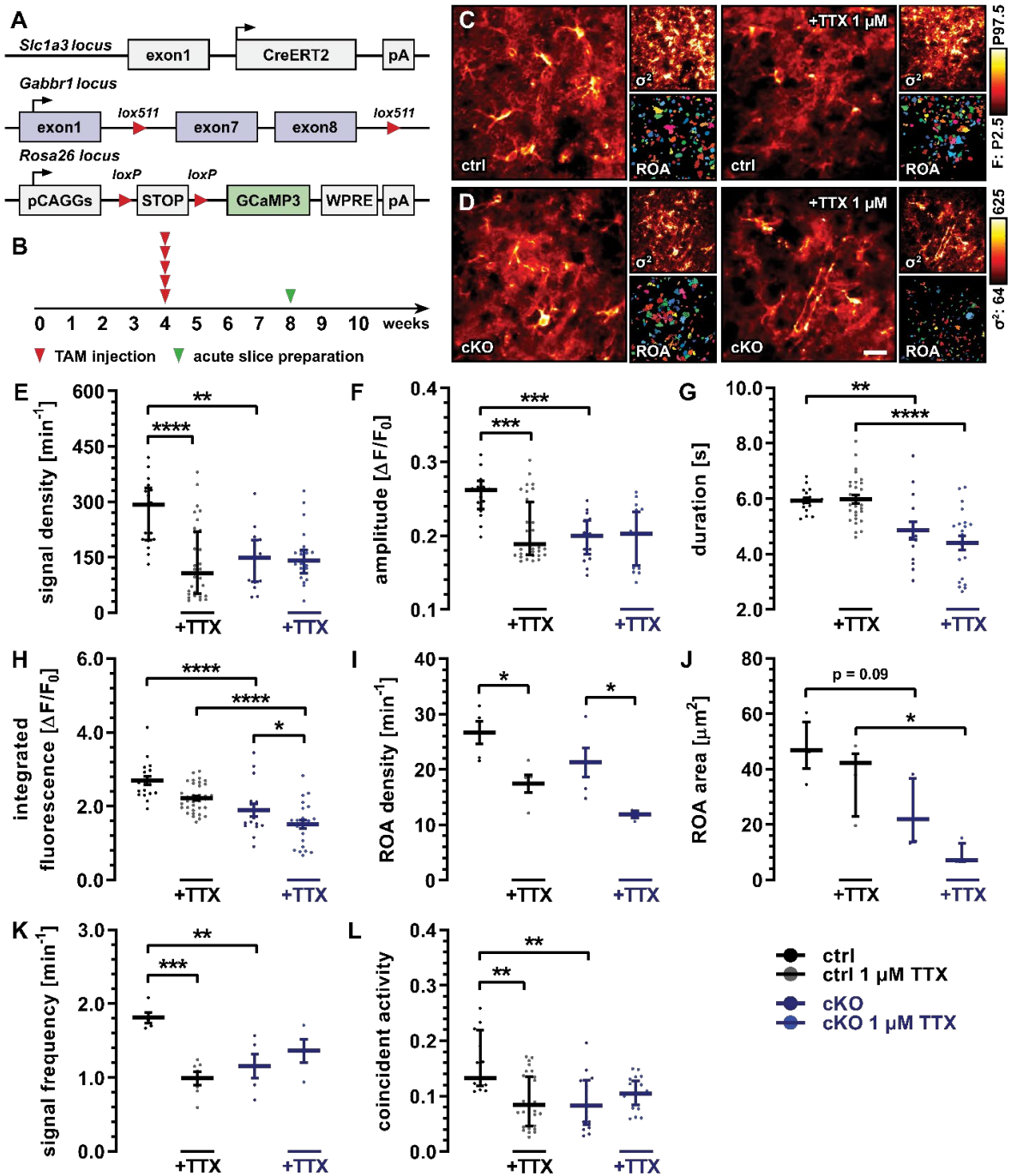
The identification of the mechanisms underlying the contribution of astroglial GABA_BRs to the pathological network function of GHB-induced absence seizures would shine new light on the role of astroglial function in GABAergic alterations at the base of epileptogenesis. Moreover, it would provide fundamental insight into novel therapeutical targets for the treatment of absence epilepsy as well as neurological conditions based on altered excitation/inhibition balance.

10 APPENDIX



Supplementary Figure 1. Astrocytic Ca^{2+} response to baclofen is reduced in cKO mice

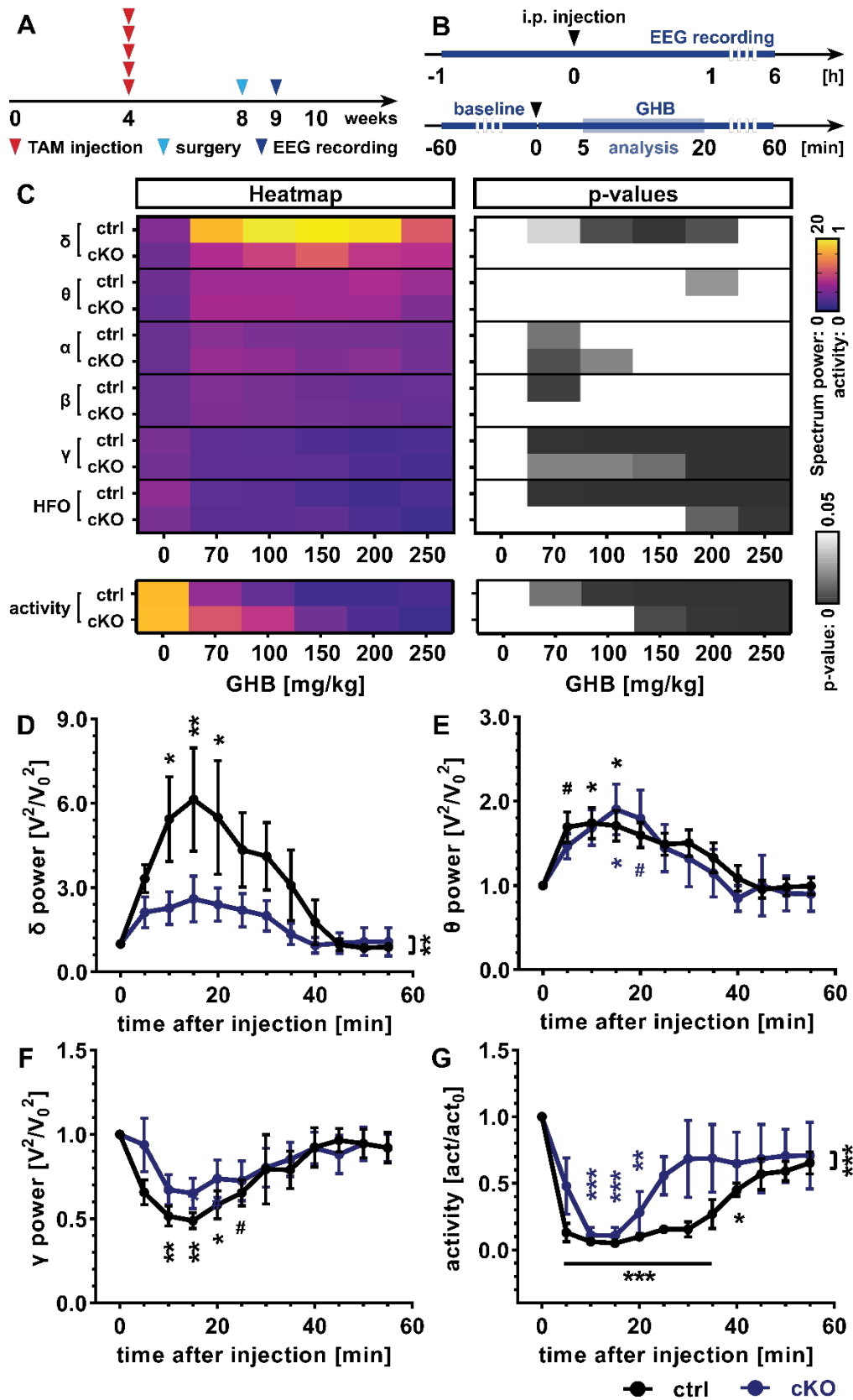
(A) Experimental design for tamoxifen (TAM) administration and acute slice preparation for *ex vivo* two-photon laser-scanning microscopy (2P-LSM) analysis of astrocytic Ca^{2+} signalling. (B) Slices were continuously perfused with the neuronal blocker tetrodotoxin (TTX, 1 μM) for 15 min before and throughout the recording session. After a 5 min baseline, the specific GABA_B receptor agonist baclofen (bac, 10 μM) was focally applied on the field of view (FOV), followed by focal application of adenosine triphosphate (ATP, 100 μM) as positive control. (C-D) Representative FOVs from ctrl (C) and cKO (D) mice displayed as maximum intensity projection of the fluorescence intensity over time ($\Delta F/F_0$). Scale bar, 20 μm . (E) Heatmap representation of extracted regions of activity (ROAs) associated with fluctuations in fluorescence intensity over time. (F) Number of signals occurring per minute in baseline conditions as well as after baclofen or ATP applications. (G) Spatial extension of ROA associated with baclofen as well as ATP application. (H-I) Signal amplitude (as peak fluorescence intensity) and integrated fluorescence intensity in baseline conditions and after baclofen or ATP application. For G-I, data are derived from n = 6-16 FOVs (from N = 3-6 animals) and were analysed using a one-way ANOVA test with Bonferroni's multiple comparison correction.



Supplementary Figure 2. *Ex vivo* baseline Ca²⁺ dynamics differ in ctrl and cKO mice

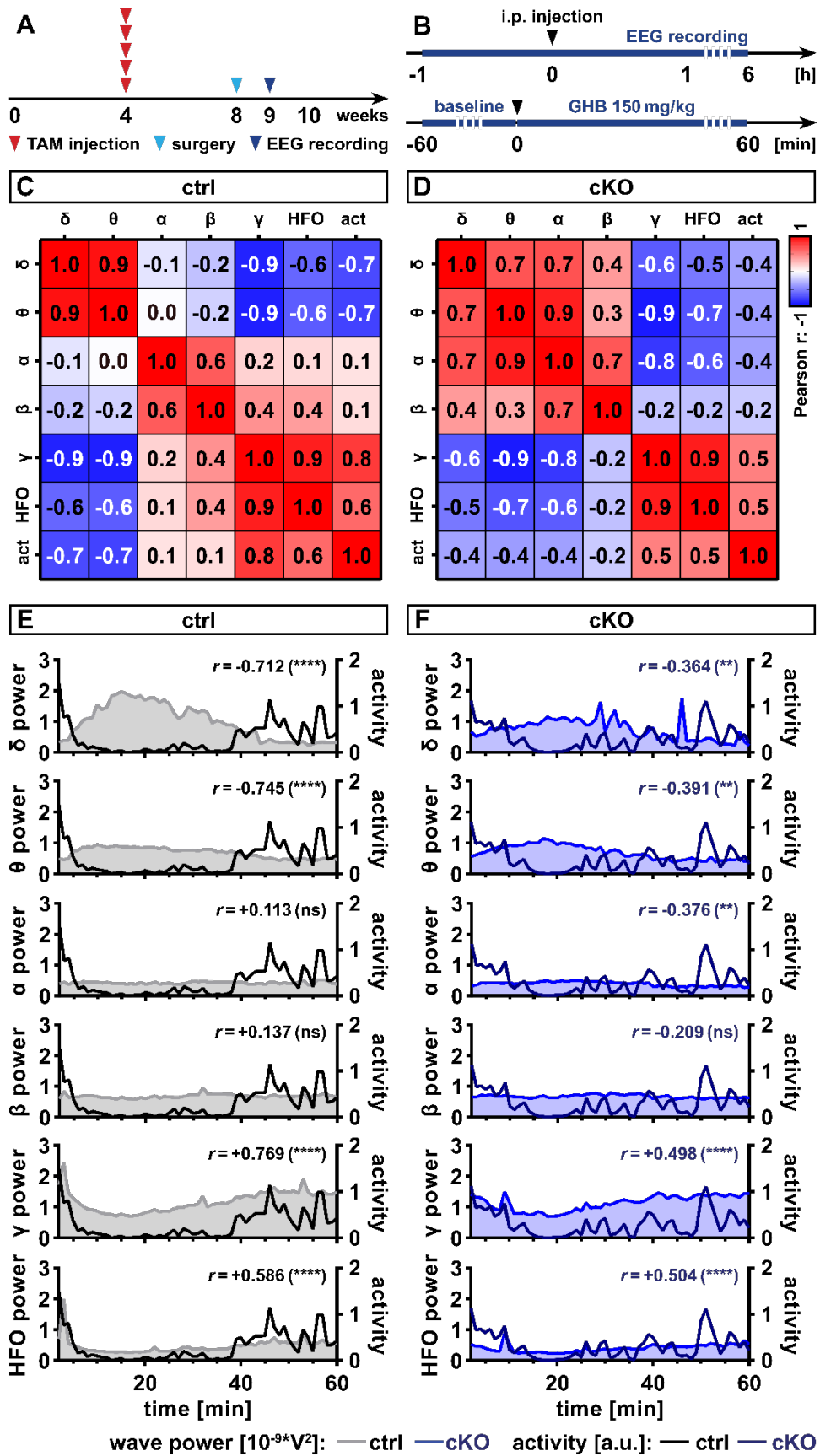
(A) Schematic representation of genetic knock-in manipulation required for the astrocyte-specific conditional knock-out of the GABA_BR1 subunit coupled to the expression of the genetically-encoded Ca²⁺ indicator GCaMP3 (see 6.1.10 for details). (B) Experimental design for tamoxifen (TAM) administration and acute slice preparation for *ex vivo* two-photon laser-scanning microscopy (2P-LSM) analysis of astrocytic Ca²⁺ signalling. Slices were either perfused with standard perfusion solution or perfused with the neuronal blocker tetrodotoxin (TTX, 1 μM) for 15 min before and throughout the recording session. (C-D) Representative field of views (FOVs) from ctrl (C) and cKO (D) mice displayed as maximum intensity projection of the fluorescence intensity over time ($\Delta F/F_0$) as well as its relative variance (σ^2) over the entire recording period and the map of regions of activity (ROA) extracted from the representative FOVs. Scale bar, 20 μm . (E-L) Characterization of astrocytic Ca²⁺ signals for ctrl and cKO mice in terms of number of signal occurring per minute

(signal density, **E**), signal amplitude (**F**), duration (as full-width-at-half-maximum, **G**) and integrated fluorescence (**H**), average number of ROAs occurring per minute (ROA density, **I**), ROA spatial extension (ROA area, **J**), signal frequency on a per-ROA basis (**K**) and coincident activity (as average fraction of active ROAs over the total number of ROAs, **L**). For **D-G** and **K**, data are derived from $n = 15-35$ FOV (from $N = 4-10$ animals); for **H-J**, data are derived from $n = 4-7$ FOVs (from $N = 4-6$ animals). Data were analysed using a one-way ANOVA test with Bonferroni's multiple comparison correction or a Kruskal-Wallis test with Dunn's multiple comparison correction as required.



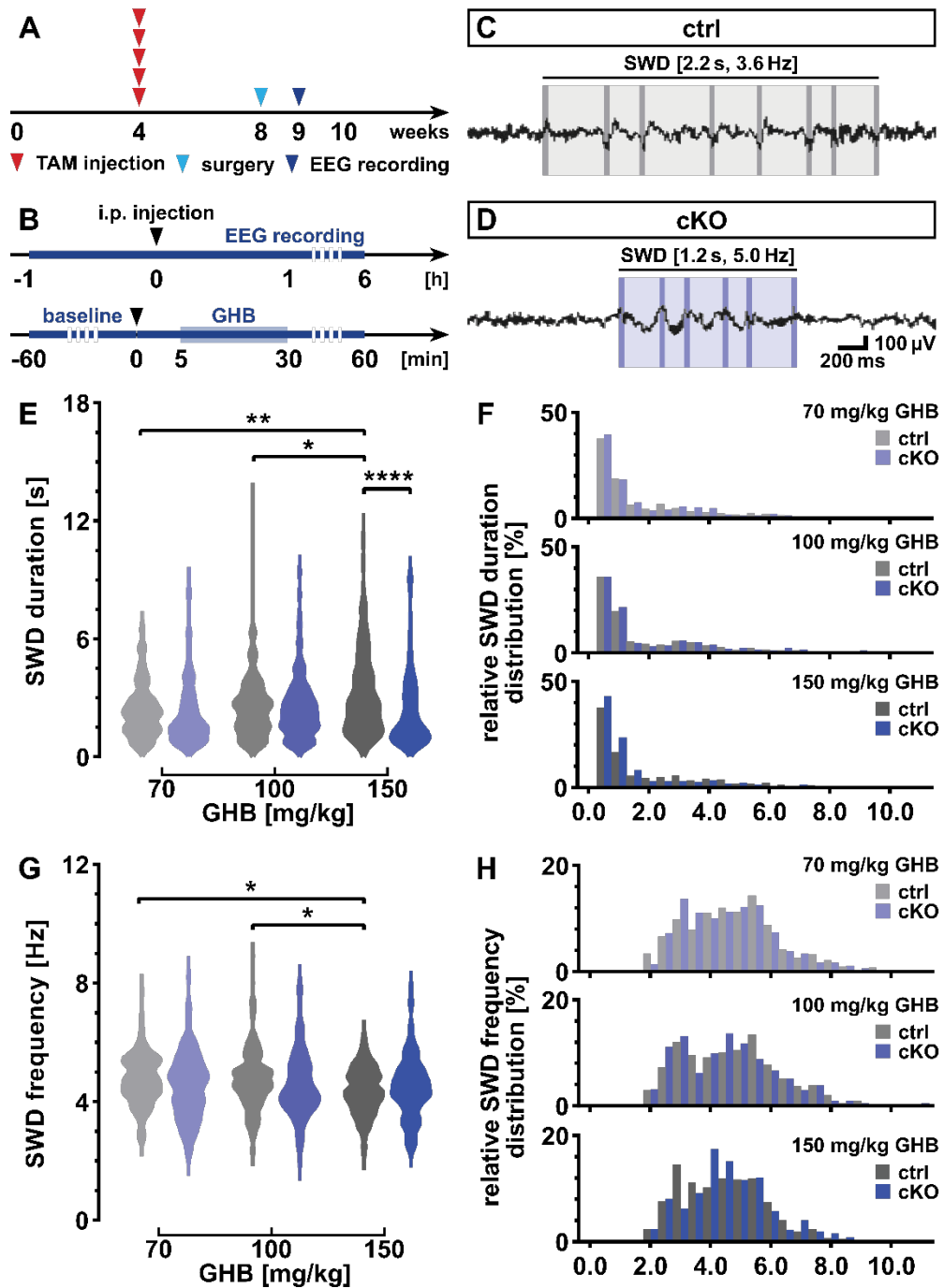
Supplementary Figure 3. Spectral analysis of GHB-induced EEG alterations

(A) Experimental design including tamoxifen (TAM) administration at four weeks of age, depth-electrode implantation for telemetric electroencephalography (EEG) four weeks after and EEG recording of control (ctrl) and conditional knock-out mice (cKO) injected with γ -hydroxybutyric acid (GHB) at doses ranging from 70 to 250 mg/kg or saline (0 mg/kg GHB). (B) Experimental protocol for GHB injection and telemetric EEG recording. Mice were recorded in baseline conditions for one hour, intraperitoneally (i.p.) injected with GHB and recorded for up to 6 hours after GHB injection. (C) Heatmap spectral and activity analysis of GHB-induced alterations at the peak of GHB action (5-20 min after i.p. injection) calculated as relative spectral power and relative activity change compared to baseline conditions, respectively (left panel). Following power bands were used: δ , 0.5-4 Hz; θ , 4-8 Hz; α , 8-12 Hz; β , 12-25 Hz; γ , 25-40 Hz; high-frequency oscillations (HFO), 40-200 Hz. Data were compared on a row-basis to the saline-injected group (0 mg/kg GHB) and p-values associated to the results are depicted as grey-scaled heatmap (right panel). (D-G) Time-course analysis in 5 min bouts of relative δ (D), θ (E) and γ (F) band power and relative activity (G) change of mice injected with 150 mg/kg GHB. Data are derived from N = 6-10 animals and were analysed using a two-way ANOVA test using the genotype and the GHB concentration (C) or time (D-G) as independent variables (see Supplementary Table 1 for details).



Supplementary Figure 4. Correlation analysis of EEG spectral power and activity after GHB

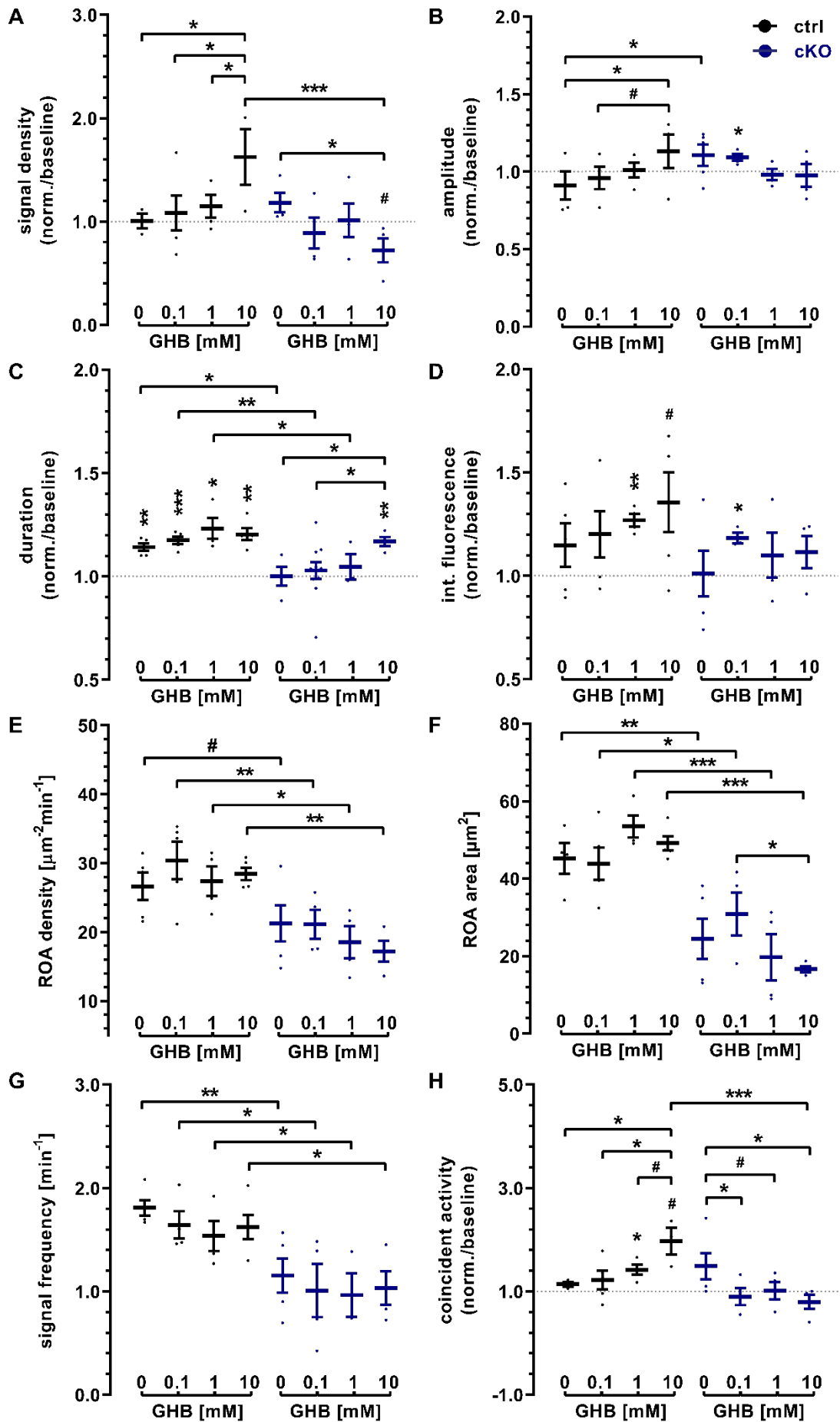
(A) Experimental design including tamoxifen (TAM) administration at four weeks of age, depth-electrode implantation for telemetric electroencephalography (EEG) four weeks after and EEG recording of control (ctrl) and conditional knock-out mice (cKO) injected with γ -hydroxybutyric acid (GHB). (B) Experimental protocol for GHB injection and telemetric EEG recording. Mice were recorded in baseline conditions for one hour, intraperitoneally (i.p.) injected with GHB and recorded for up to 6 hours after GHB injection. (C-D) Correlation matrix of the Pearson correlation coefficients r obtained from pairwise comparisons of spectrum band power and activity count profiles within the first hour after GHB injection for ctrl (C) and cKO (D) mice. Following power bands were used: δ , 0.5-4 Hz; θ , 4-8 Hz; α , 8-12 Hz; β , 12-25 Hz; γ , 25-40 Hz; high-frequency oscillations (HFO), 40-200 Hz. (E-F) Time-course of spectrum band powers after GHB injection overlapped with the associated activity counts for ctrl (E) and cKO (F) mice. Data are derived from N = 6-9 animals.



Supplementary Figure 5. Spike-wave discharge heterogeneity

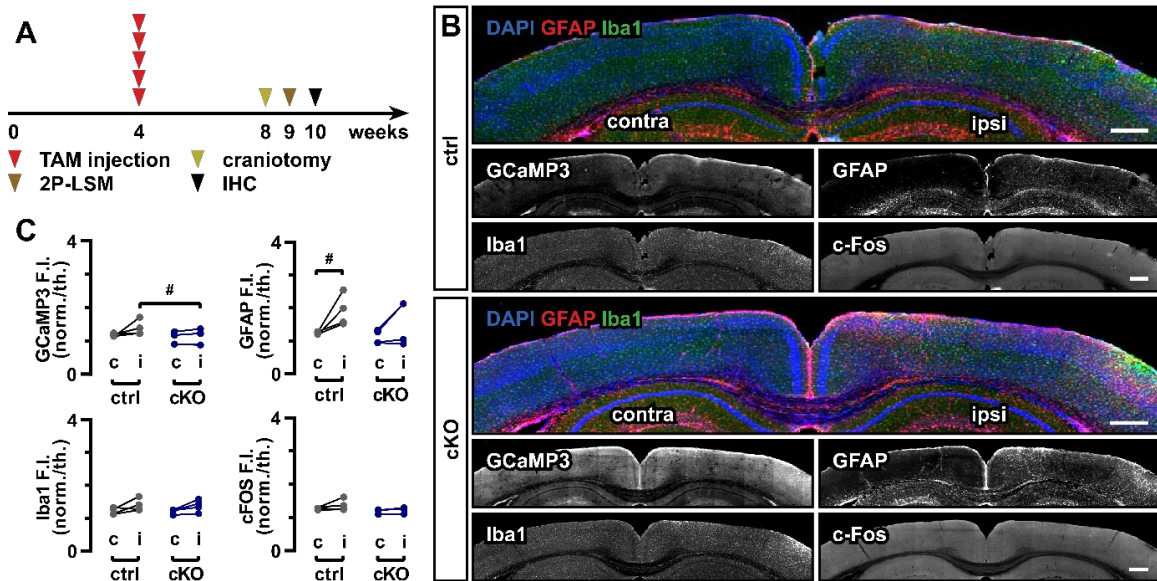
(A) Experimental design including tamoxifen (TAM) administration at four weeks of age, depth-electrode implantation for telemetric electroencephalography (EEG) four weeks after and EEG recording of control (ctrl) and conditional knock-out mice (cKO) injected with γ -hydroxybutyric acid (GHB). (B) Experimental protocol for GHB injection and telemetric EEG recording. Mice were recorded in baseline conditions for one hour, intraperitoneally (i.p.) injected with GHB and recorded for up to 6 hours after GHB injection. (C-D) Representative spike-wave discharge (SWD) traces of ctrl (C) and cKO (D) mice injected with GHB automatically detected using a custom-made NeuroScore detection protocol (see 6.2.13.2 for details). Vertical lines indicate the detected spikes. (E) Duration of SWDs recorded in mice injected with GHB at doses of 70, 100 and 150 mg/kg within the first hour after GHB administration. (F) Relative distribution of SWD duration expressed as percentage using 1 s-wide bins. (G) Spike frequency within SWDs recorded in mice injected with

GHB at doses of 70, 100 and 150 mg/kg within the first hour after GHB administration. **(H)** Relative distribution of SWD frequency expressed as percentage using 1 Hz-wide bins. **(E-H)** Data are derived from N = 6-10 animals. In **E** and **G**, data were represented as violin plot and were compared using a Kruskal-Wallis test with Dunn's multiple comparison correction.



Supplementary Figure 6. GHB modulates astrocytic Ca²⁺ dynamics indirectly via neuronal activity

(**A-D**) Astrocytic Ca²⁺ signal density (**A**), amplitude (**B**), duration (**C**) and integrated fluorescence (**D**) from acute slice preparations of control (ctrl) and conditional knock-out mice (cKO) upon focal application of γ -hydroxybutyric acid (GHB) in absence of the neuronal blocker tetrodotoxin. (**E-H**) Average number of regions of activity (ROAs) occurring per minute (ROA density, **E**), ROA spatial extension (ROA area, **F**), signal frequency on a per-ROA basis (**G**) and coincident activity (as average fraction of active ROAs over the total number of ROAs, **H**). Data are derived from n = 4-5 FOV (from N = 4) and were analysed using a two-way ANOVA test using the genotype and the GHB concentration as independent variables. For **A-D** and **H**, data were normalized on baseline recordings preceding focal GHB application and additionally analysed using a one-sample t test ($H_0: \bar{x}_0=1$).



Supplementary Figure 7. Absence of excessive cortical cell reactivity after craniotomy

(A) Experimental design including tamoxifen (TAM) administration at four weeks of age, craniotomy and cranial window implantation on the primary somatosensory cortex four weeks after, *in vivo* two-photon laser-scanning microscopy (2P-LSM) and immunohistochemistry of brain tissue after perfusion (IHC). (B) Representative views of tissue from control (ctrl) and conditional knock-out (cKO) mice subjected to the experimental protocol depicted in A and stained for GCaMP3 (excluded from the merged view) as well as markers of cell reactivity, namely GFAP (red), Iba1 (green) and c-Fos (excluded from the merged view), to evaluate abnormal cell reaction under the window (ipsilateral side, ipsi) compared to the contralateral side (contra). Scale bar, 500 μ m. (C) Mean fluorescence intensity (F.I.) of GCaMP3, GFAP, Iba1 and c-Fos calculated on the primary somatosensory cortex of the contralateral (c) and ipsilateral (i) hemisphere. Data from $n = 4-8$ slices of $N = 4$ animals and were normalized on the thalamic mean fluorescence intensity of the single channels. Data were analysed using a paired and unpaired t test as required.

Figure	$z = f(x,y)$	x	y	$x*y$
Figure 9I	x, protein y, fraction	p = 0.928	p < 0.001	p = 0.928
Figure 10G		p < 0.001	p = 0.053	p = 0.654
Figure 10H	x, genotype y, concentration	p = 0.628	p = 0.026	p = 0.931
Figure 10I		p = 0.623	p < 0.001	p = 0.346
Figure 10J		p = 0.126	p < 0.001	p = 0.739
Figure 11E		p = 0.002	p = 0.008	p = 0.423
Figure 11F	x, genotype y, concentration	p < 0.001	p < 0.001	p = 0.203
Figure 11G		p = 0.062	p = 0.006	p = 0.729
Figure 11H	x, group y, time	p < 0.001	p < 0.001	p = 0.104
Figure 12F		p < 0.001	p = 0.048	p = 0.230
Figure 12G	x, genotype y, concentration	p = 0.020	p = 0.213	p = 0.951
Figure 12H		p = 0.002	p = 0.547	p = 0.288
Figure 12I		p = 0.010	p = 0.322	p = 0.889
Figure 13D	x, genotype y, concentration	p = 0.011	p = 0.007	p = 0.969
Figure 13E		p < 0.001	p = 0.033	p = 0.842
Figure 14C	x, genotype y, concentration	p < 0.001	p = 0.717	p = 0.041
Figure 14F		p < 0.001	p = 0.004	p = 0.088
Figure 15E		p < 0.001	p < 0.001	p = 0.140
Figure 15F	x, genotype y, treatment	p = 0.023	p = 0.556	p = 0.656
Figure 15G		p = 0.018	p = 0.244	p = 0.511
Figure 15H		p = 0.864	p = 0.336	p = 0.877
Figure 16C		p < 0.001	p < 0.001	p = 0.955
Figure 16D	x, genotype y, treatment	p = 0.498	p < 0.001	p = 0.274
Figure 16E		p < 0.001	p < 0.001	p = 0.155
Figure 16F		p < 0.001	p = 0.081	p = 0.126
Figure 17H	x, genotype y, treatment	p = 0.218	p < 0.001	p = 0.107
Figure 18D	x, genotype y, treatment	p = 0.135	p = 0.218	p = 0.135
Figure 18E		p = 0.687	p = 0.140	p = 0.556

Figure 18F		p = 0.009	p = 0.010	p = 0.009
Figure 18G (locomotion)		p = 0.487	p < 0.001	p = 0.487
Figure 18G (on-site)		p = 0.881	p = 0.887	p = 0.881
Figure 18G (freezing)		p = 0.113	p = 0.026	p = 0.113
Figure 18H	x, group y, time	p < 0.001	p < 0.001	p > 0.999
Figure 19D	x, genotype y, treatment	p = 0.075	p = 0.063	p = 0.182
Figure 19E	x, genotype y, time	p < 0.001	p = 0.001	p = 0.820
Supplementary Figure 3C (δ)		p = 0.017	p = 0.025	p = 0.564
Supplementary Figure 3C (θ)		p = 0.675	p = 0.015	p = 0.924
Supplementary Figure 3C (α)		p = 0.279	p < 0.001	p = 0.771
Supplementary Figure 3C (β)	x, genotype y, concentration	p = 0.760	p < 0.001	p = 0.811
Supplementary Figure 3C (γ)		p = 0.709	p < 0.001	p = 0.310
Supplementary Figure 3C (HFO)		p = 0.799	p < 0.001	p = 0.257
Supplementary Figure 3C (act)		p = 0.153	p < 0.001	p = 0.731
Supplementary Figure 3D		p = 0.001	p = 0.001	p = 0.596
Supplementary Figure 3E	x, genotype	p = 0.485	p < 0.001	p = 0.987
Supplementary Figure 3F	y, time	p = 0.123	p < 0.001	p = 0.913
Supplementary Figure 3G		p < 0.001	p < 0.001	p = 0.552
Supplementary Figure 6A		p = 0.023	p = 0.673	p = 0.019
Supplementary Figure 6B		p = 0.474	p = 0.862	p = 0.074
Supplementary Figure 6C		p < 0.001	p = 0.083	p = 0.431
Supplementary Figure 6D	x, genotype	p = 0.078	p = 0.492	p = 0.796
Supplementary Figure 6E	y, concentration	p < 0.001	p = 0.522	p = 0.573
Supplementary Figure 6F		p < 0.001	p = 0.709	p = 0.060
Supplementary Figure 6G		p < 0.001	p = 0.521	p = 0.993
Supplementary Figure 6H		p = 0.008	p = 0.362	p = 0.008

Supplementary Table 1. Two-way ANOVA test results



Supplementary Video 1. *Ex vivo* 2P-LSM recording of cortical astroglial Ca²⁺ signalling of ctrl mouse upon GHB focal application

Astroglial Ca²⁺ imaging in acute slice preparations of control (ctrl) animal in presence of the neuronal blocker tetrodotoxin (TTX, 1 μ M) upon focal application of γ -hydroxybutyric acid (GHB, 10 mM) using a custom-made two-photon laser-scanning microscope (2P-LSM) setup (see 6.2.12.1 for details).

<https://cloud.hiz-saarland.de/s/mDP2ojXopFZLmzN>



Supplementary Video 2. *Ex vivo* 2P-LSM recording of cortical astroglial Ca²⁺ signalling of cKO mouse upon GHB focal application

Astroglial Ca²⁺ imaging in acute slice preparations of conditional knock-out (cKO) animal in presence of the neuronal blocker tetrodotoxin (TTX, 1 μ M) upon focal application of γ -hydroxybutyric acid (GHB, 10 mM) using a custom-made two-photon laser-scanning microscope (2P-LSM) setup (see 6.2.12.1 for details).

<https://cloud.hiz-saarland.de/s/K28GtMyJ9KBn2WD>



Supplementary Video 3. *In vivo* 2P-LSM recording of cortical astroglial Ca²⁺ signalling of ctrl mouse upon GHB administration

Astroglial Ca²⁺ imaging from head-fixed control (ctrl) animal was performed under light isoflurane anaesthesia (0.5 % isoflurane) after i.p. administration of γ -hydroxybutyric acid (GHB, 70 mg/kg) using a custom-made two-photon laser-scanning microscope (2P-LSM) setup (see 6.2.12.1 for details).

<https://cloud.hiz-saarland.de/s/cRJo9MM7cpyBAPb>



Supplementary Video 4. *In vivo* 2P-LSM recording of cortical astroglial Ca²⁺ signalling of cKO mouse upon GHB administration

Astroglial Ca²⁺ imaging from head-fixed conditional knock-out (cKO) animal was performed under light isoflurane anaesthesia (0.5 % isoflurane) after i.p. administration of γ -hydroxybutyric acid (GHB, 70 mg/kg) using a custom-made two-photon laser-scanning microscope (2P-LSM) setup (see 6.2.12.1 for details).

<https://cloud.hiz-saarland.de/s/TyJgwisskeTpo8F>

11 REFERENCES

- Abbott NJ, Rönnbäck L, Hansson E (2006) Astrocyte-endothelial interactions at the blood-brain barrier. *Nat Rev Neurosci* 7:41-53.
- Aboufares El Alaoui A, Jackson M, Fabri M, de Vivo L, Bellesi M (2020) Characterization of Subcellular Organelles in Cortical Perisynaptic Astrocytes. *Front Cell Neurosci* 14:573944.
- Agarwal A, Wu PH, Hughes EG, Fukaya M, Tischfield MA, Langseth AJ, Wirtz D, Bergles DE (2017) Transient Opening of the Mitochondrial Permeability Transition Pore Induces Microdomain Calcium Transients in Astrocyte Processes. *Neuron* 93:587-605.e587.
- Aghakhani Y, Bagshaw AP, Bénar CG, Hawco C, Andermann F, Dubeau F, Gotman J (2004) fMRI activation during spike-and-wave discharges in idiopathic generalized epilepsy. *Brain* 127:1127-1144.
- Agmon A, Connors BW (1991) Thalamocortical responses of mouse somatosensory (barrel) cortex in vitro. *Neuroscience* 41:365-379.
- Aizawa M, Ito Y, Fukuda H (1997) Pharmacological profiles of generalized absence seizures in lethargic, stargazer and gamma-hydroxybutyrate-treated model mice. *Neurosci Res* 29:17-25.
- Allbritton NL, Meyer T, Stryer L (1992) Range of messenger action of calcium ion and inositol 1,4,5-trisphosphate. *Science* 258:1812-1815.
- Allen NJ (2019) Star Power: Astrocytes Regulate Behavior. *Cell* 177:1091-1093.
- Allen NJ, Barres BA (2009) Neuroscience: Glia - more than just brain glue. *Nature* 457:675-677.
- Allen NJ, Lyons DA (2018) Glia as architects of central nervous system formation and function. *Science* 362:181-185.
- Álvarez-Ferradas C, Morales JC, Wellmann M, Nualart F, Roncagliolo M, Fuenzalida M, Bonansco C (2015) Enhanced astroglial Ca²⁺ signalling increases excitatory synaptic strength in the epileptic brain. *Glia* 63:1507-1521.
- Amiry-Moghaddam M, Ottersen OP (2003) The molecular basis of water transport in the brain. *Nat Rev Neurosci* 4:991-1001.
- Anderson CM, Bergher JP, Swanson RA (2004) ATP-induced ATP release from astrocytes. *J Neurochem* 88:246-256.
- Andersson M, Blomstrand F, Hanse E (2007) Astrocytes play a critical role in transient heterosynaptic depression in the rat hippocampal CA1 region. *J Physiol* 585:843-852.
- Angulo MC, Kozlov AS, Charpak S, Audinat E (2004) Glutamate released from glial cells synchronizes neuronal activity in the hippocampus. *J Neurosci* 24:6920-6927.
- Anlauf E, Derouiche A (2013) Glutamine synthetase as an astrocytic marker: its cell type and vesicle localization. *Front Endocrinol (Lausanne)* 4:144.
- Araque A, Parpura V, Sanzgiri RP, Haydon PG (1999) Tripartite synapses: glia, the unacknowledged partner. *Trends Neurosci* 22:208-215.
- Araque A, Martín ED, Perea G, Arellano JI, Buño W (2002) Synaptically released acetylcholine evokes Ca²⁺ elevations in astrocytes in hippocampal slices. *J Neurosci* 22:2443-2450.
- Araque A, Carmignoto G, Haydon PG, Oliet SHR, Robitaille R, Volterra A (2014) Gliotransmitters Travel in Time and Space. *Neuron* 81:728-739.
- Arcuino G, Lin JH, Takano T, Liu C, Jiang L, Gao Q, Kang J, Nedergaard M (2002) Intercellular calcium signalling mediated by point-source burst release of ATP. *Proc Natl Acad Sci U S A* 99:9840-9845.
- Arizono M, Inavalli VVGK, Panatier A, Pfeiffer T, Angibaud J, Levet F, Ter Veer MJT, Stobart J, Bellocchio L, Mikoshiba K, Marsicano G, Weber B, Oliet SHR, Nägerl UV (2020) Structural basis of astrocytic Ca²⁺ signals at tripartite synapses. *Nat Commun* 11:1906.
- Attwell D, Buchan AM, Charpak S, Lauritzen M, Macvicar BA, Newman EA (2010) Glial and neuronal control of brain blood flow. *Nature* 468:232-243.
- Avoli M (1980) Electroencephalographic and pathophysiologic features of rat parenteral panicillin epilepsy. *Experimental Neurology* 69:373-382.
- Avoli M (2012) A brief history on the oscillating roles of thalamus and cortex in absence seizures. *Epilepsia* 53:779-789.
- Azevedo FA, Carvalho LR, Grinberg LT, Farfel JM, Ferretti RE, Leite RE, Jacob Filho W, Lent R, Herculano-Houzel S (2009) Equal numbers of neuronal and nonneuronal cells make the human brain an isometrically scaled-up primate brain. *J Comp Neurol* 513:532-541.
- Bahi-Buisson N, El Sabbagh S, Soufflet C, Escande F, Boddaert N, Valayannopoulos V, Bellané-Chantelot C, Lascelles K, Dulac O, Plouin P, de Lonlay P (2008) Myoclonic absence epilepsy with photosensitivity and a gain of function mutation in glutamate dehydrogenase. *Seizure* 17:658-664.
- Bai X, Vestal M, Berman R, Negishi M, Spann M, Vega C, Desalvo M, Novotny EJ, Constable RT, Blumenfeld H (2010) Dynamic time course of typical childhood absence seizures: EEG, behavior, and functional magnetic resonance imaging. *J Neurosci* 30:5884-5893.
- Bai X, Guo J, Killory B, Vestal M, Berman R, Negishi M, Danielson N, Novotny EJ, Constable RT, Blumenfeld H (2011) Resting functional connectivity between the hemispheres in childhood absence epilepsy. *Neurology* 76:1960-1967.

- Baird-Daniel E, Daniel AGS, Wenzel M, Li D, Liou JY, Laffont P, Zhao M, Yuste R, Ma H, Schwartz TH (2017) Glial Calcium Waves are Triggered by Seizure Activity and Not Essential for Initiating Ictal Onset or Neurovascular Coupling. *Cereb Cortex* 27:3318-3330.
- Bal T, von Krosigk M, McCormick DA (1995a) Synaptic and membrane mechanisms underlying synchronized oscillations in the ferret lateral geniculate nucleus in vitro. *J Physiol* 483 (Pt 3):641-663.
- Bal T, von Krosigk M, McCormick DA (1995b) Role of the ferret perigeniculate nucleus in the generation of synchronized oscillations in vitro. *J Physiol* 483 (Pt 3):665-685.
- Bal T, Debay D, Destexhe A (2000) Cortical feedback controls the frequency and synchrony of oscillations in the visual thalamus. *J Neurosci* 20:7478-7488.
- Balasubramanian S, Fam SR, Hall RA (2007) GABAB receptor association with the PDZ scaffold Mupp1 alters receptor stability and function. *J Biol Chem* 282:4162-4171.
- Banerjee PK, Hirsch E, Snead OC (1993) gamma-Hydroxybutyric acid induced spike-and-wave discharges in rats: relation to high-affinity [3H]gamma-hydroxybutyric acid binding sites in the thalamus and cortex. *Neuroscience* 56:11-21.
- Barclay J, Balaguero N, Mione M, Ackerman SL, Letts VA, Brodbeck J, Canti C, Meir A, Page KM, Kusumi K, Perez-Reyes E, Lander ES, Frankel WN, Gardiner RM, Dolphin AC, Rees M (2001) Ducky mouse phenotype of epilepsy and ataxia is associated with mutations in the *Cacna2d2* gene and decreased calcium channel current in cerebellar Purkinje cells. *J Neurosci* 21:6095-6104.
- Bay T, Eghorn LF, Klein AB, Wellendorph P (2014) GHB receptor targets in the CNS: focus on high-affinity binding sites. *Biochem Pharmacol* 87:220-228.
- Bazargani N, Attwell D (2016) Astrocyte calcium signalling: the third wave. *Nat Neurosci* 19:182-189.
- Bazyan AS, van Luijelaar G (2013) Neurochemical and Behavioral Features in Genetic Absence Epilepsy and in Acutely Induced Absence Seizures. *ISRN Neurology* 2013:875834.
- Başar-Eroglu C, Strüber D, Schürmann M, Stadler M, Başar E (1996) Gamma-band responses in the brain: a short review of psychophysiological correlates and functional significance. *Int J Psychophysiol* 24:101-112.
- Beckner ME (2020) A roadmap for potassium buffering/dispersion via the glial network of the CNS. *Neurochem Int* 136:104727.
- Bedner P, Dupper A, Hüttmann K, Müller J, Herde MK, Dublin P, Deshpande T, Schramm J, Häussler U, Haas CA, Henneberger C, Theis M, Steinhäuser C (2015) Astrocyte uncoupling as a cause of human temporal lobe epilepsy. *Brain* 138:1208-1222.
- Beenhakker MP, Huguenard JR (2010) Astrocytes as gatekeepers of GABAB receptor function. *J Neurosci* 30:15262-15276.
- Beghi E et al. (2019) Global, regional, and national burden of epilepsy, 1990–2016: a systematic analysis for the Global Burden of Disease Study 2016. *The Lancet Neurology* 18:357-375.
- Bellot-Saez A, Kékesi O, Morley JW, Buskila Y (2017) Astrocytic modulation of neuronal excitability through K. *Neurosci Biobehav Rev* 77:87-97.
- Benavides J, Rumigny JF, Bourguignon JJ, Cash C, Wermuth CG, Mandel P, Vincendon G, Maitre M (1982) High affinity binding sites for gamma-hydroxybutyric acid in rat brain. *Life Sci* 30:953-961.
- Benfey NJ, Li VJ, Schohl A, Ruthazer ES (2021) Sodium-calcium exchanger mediates sensory-evoked glial calcium transients in the developing retinotectal system. *Cell Rep* 37:109791.
- Bennett GC, Ford AP, Smith JA, Emmett CJ, Webb TE, Boarder MR (2003) P2Y receptor regulation of cultured rat cerebral cortical cells: calcium responses and mRNA expression in neurons and glia. *Br J Pharmacol* 139:279-288.
- Berg AT (2011) Epilepsy, cognition, and behavior: The clinical picture. *Epilepsia* 52 Suppl 1:7-12.
- Berg AT, Levy SR, Testa FM, Blumenfeld H (2014) Long-term seizure remission in childhood absence epilepsy: might initial treatment matter? *Epilepsia* 55:551-557.
- Bernstein M, Behnisch T, Balschun D, Reymann KG, Reiser G (1998) Pharmacological characterisation of metabotropic glutamatergic and purinergic receptors linked to Ca²⁺ signalling in hippocampal astrocytes. *Neuropharmacology* 37:169-178.
- Bessman S, Fishbein W (1963) Gamma-hydroxybutyrate, a normal brain metabolite. *Nature* 200:1207-1208.
- Bettler B, Tiao JY (2006) Molecular diversity, trafficking and subcellular localization of GABAB receptors. *Pharmacol Ther* 110:533-543.
- Bettler B, Kaupmann K, Mosbacher J, Gassmann M (2004) Molecular structure and physiological functions of GABA(B) receptors. *Physiol Rev* 84:835-867.
- Bezzi P, Gunderson V, Galbete JL, Seifert G, Steinhäuser C, Pilati E, Volterra A (2004) Astrocytes contain a vesicular compartment that is competent for regulated exocytosis of glutamate. *Nat Neurosci* 7:613-620.
- Biber K, Klotz KN, Berger M, Gebicke-Härter PJ, van Calker D (1997) Adenosine A1 receptor-mediated activation of phospholipase C in cultured astrocytes depends on the level of receptor expression. *J Neurosci* 17:4956-4964.
- Bignami A, Eng LF, Dahl D, Uyeda CT (1972) Localization of the glial fibrillary acidic protein in astrocytes by immunofluorescence. *Brain Res* 43:429-435.

- Bindocci E, Savtchouk I, Liaudet N, Becker D, Carriero G, Volterra A (2017) Three-dimensional Ca²⁺ imaging advances understanding of astrocyte biology. *Science* 356.
- Black SW, Morairty SR, Chen TM, Leung AK, Wisor JP, Yamanaka A, Kilduff TS (2014) GABAB agonism promotes sleep and reduces cataplexy in murine narcolepsy. *J Neurosci* 34:6485-6494.
- Blumenfeld H (2005a) Consciousness and epilepsy: why are patients with absence seizures absent? *Prog Brain Res* 150:271-286.
- Blumenfeld H (2005b) Cellular and network mechanisms of spike-wave seizures. *Epilepsia* 46 Suppl 9:21-33.
- Blumenfeld H, McCormick DA (2000) Corticothalamic inputs control the pattern of activity generated in thalamocortical networks. *J Neurosci* 20:5153-5162.
- Bockenbauer D et al. (2009) Epilepsy, ataxia, sensorineural deafness, tubulopathy, and KCNJ10 mutations. *N Engl J Med* 360:1960-1970.
- Boddum K, Jensen TP, Magloire V, Kristiansen U, Rusakov DA, Pavlov I, Walker MC (2016) Astrocytic GABA transporter activity modulates excitatory neurotransmission. *Nat Commun* 7:13572.
- Boison D, Chen JF, Fredholm BB (2010) Adenosine signalling and function in glial cells. *Cell Death Differ* 17:1071-1082.
- Bortolato M, Frau R, Orrù M, Fà M, Dessì C, Puligheddu M, Barberini L, Pillolla G, Polizzi L, Santoni F, Mereu G, Marrosu F (2010) GABAB receptor activation exacerbates spontaneous spike-and-wave discharges in DBA/2J mice. *Seizure* 19:226-231.
- Boyer JL, Waldo GL, Harden TK (1992) Beta gamma-subunit activation of G-protein-regulated phospholipase C. *J Biol Chem* 267:25451-25456.
- Bröer S, Brookes N (2001) Transfer of glutamine between astrocytes and neurons. *J Neurochem* 77:705-719.
- Burgess DL, Jones JM, Meisler MH, Noebels JL (1997) Mutation of the Ca²⁺ Channel β Subunit Gene *Cchb4* Is Associated with Ataxia and Seizures in the Lethargic (lh) Mouse. *Cell* 88:385-392.
- Bushong EA, Martone ME, Jones YZ, Ellisman MH (2002) Protoplasmic astrocytes in CA1 stratum radiatum occupy separate anatomical domains. *J Neurosci* 22:183-192.
- Buskila Y, Bellot-Saez A, Morley JW (2019) Generating Brain Waves, the Power of Astrocytes. *Front Neurosci* 13:1125.
- Bélanger M, Allaman I, Magistretti PJ (2011) Brain energy metabolism: focus on astrocyte-neuron metabolic cooperation. *Cell Metab* 14:724-738.
- Cahoy JD, Emery B, Kaushal A, Foo LC, Zamanian JL, Christopherson KS, Xing Y, Lubischer JL, Krieg PA, Krupenko SA, Thompson WJ, Barres BA (2008) A transcriptome database for astrocytes, neurons, and oligodendrocytes: a new resource for understanding brain development and function. *J Neurosci* 28:264-278.
- Cajal SR (1909) *Histologie due Systeme Nerveux de l'Homme et des Vertebres*. Paris (FR): Maloine.
- Camfield C, Camfield P (2005) Management guidelines for children with idiopathic generalized epilepsy. *Epilepsia* 46 Suppl 9:112-116.
- Camps M, Carozzi A, Schnabel P, Scheer A, Parker PJ, Gierschik P (1992) Isozyme-selective stimulation of phospholipase C-beta 2 by G protein beta gamma-subunits. *Nature* 360:684-686.
- Cao F, Liu JJ, Zhou S, Cortez MA, Snead OC, Han J, Jia Z (2020) Neuroigin 2 regulates absence seizures and behavioral arrests through GABAergic transmission within the thalamocortical circuitry. *Nat Commun* 11:3744.
- Caplan R, Siddarth P, Stahl L, Lanphier E, Vona P, Gurbari S, Koh S, Sankar R, Shields WD (2008) Childhood absence epilepsy: behavioral, cognitive, and linguistic comorbidities. *Epilepsia* 49:1838-1846.
- Carmignoto G, Haydon PG (2012) Astrocyte calcium signalling and epilepsy. *Glia* 60:1227-1233.
- Carter LP, Koek W, France CP (2009) Behavioral analyses of GHB: receptor mechanisms. *Pharmacol Ther* 121:100-114.
- Carter LP, Wu H, Chen W, Matthews MM, Mehta AK, Hernandez RJ, Thomson JA, Ticku MK, Coop A, Koek W, France CP (2005) Novel gamma-hydroxybutyric acid (GHB) analogs share some, but not all, of the behavioral effects of GHB and GABAB receptor agonists. *J Pharmacol Exp Ther* 313:1314-1323.
- Caudal LC, Gobbo D, Scheller A, Kirchhoff F (2020) The Paradox of Astroglial Ca²⁺ Signals at the Interface of Excitation and Inhibition. *Frontiers in Cellular Neuroscience* 14.
- Celli R, Wall MJ, Santolini I, Vergassola M, Di Menna L, Mascio G, Cannella M, van Lujtelaar G, Pittaluga A, Ciruela F, Bruno V, Nicoletti F, Ngomba RT (2020) Pharmacological activation of mGlu5 receptors with the positive allosteric modulator VU0360172, modulates thalamic GABAergic transmission. *Neuropharmacology* 178:108240.
- Cerminara C, Coniglio A, El-Malhany N, Casarelli L, Curatolo P (2012) Two epileptic syndromes, one brain: childhood absence epilepsy and benign childhood epilepsy with centrotemporal spikes. *Seizure* 21:70-74.
- Chai H, Diaz-Castro B, Shigetomi E, Monte E, Oceau JC, Yu X, Cohn W, Rajendran PS, Vondriska TM, Whitelegge JP, Coppola G, Khakh BS (2017) Neural Circuit-Specialized Astrocytes: Transcriptomic, Proteomic, Morphological, and Functional Evidence. *Neuron* 95:531-549.e539.
- Chang WP, Wu JJ, Shyu BC (2013) Thalamic modulation of cingulate seizure activity via the regulation of gap junctions in mice thalamocingulate slice. *PLoS One* 8:e62952.
- Charles KJ, Calver AR, Jourdain S, Pangalos MN (2003) Distribution of a GABAB-like receptor protein in the rat central nervous system. *Brain Res* 989:135-146.

- Chen J, Tan Z, Zeng L, Zhang X, He Y, Gao W, Wu X, Li Y, Bu B, Wang W, Duan S (2013) Heterosynaptic long-term depression mediated by ATP released from astrocytes. *Glia* 61:178-191.
- Chen Y, Rathbone MP, Hertz L (2001) Guanosine-induced increase in free cytosolic calcium concentration in mouse astrocytes in primary cultures: does it act on an A3 adenosine receptor? *J Neurosci Res* 65:184-189.
- Cheong E, Zheng Y, Lee K, Lee J, Kim S, Sanati M, Lee S, Kim YS, Shin HS (2009) Deletion of phospholipase C beta4 in thalamocortical relay nucleus leads to absence seizures. *Proc Natl Acad Sci U S A* 106:21912-21917.
- Chever O, Lee CY, Rouach N (2014) Astroglial connexin43 hemichannels tune basal excitatory synaptic transmission. *J Neurosci* 34:11228-11232.
- Chipaux M, Charpier S, Polack PO (2011) Chloride-mediated inhibition of the ictogenic neurones initiating genetically-determined absence seizures. *Neuroscience* 192:642-651.
- Choi JH, Koch KP, Poppendieck W, Lee M, Shin HS (2010) High resolution electroencephalography in freely moving mice. *J Neurophysiol* 104:1825-1834.
- Christian CA, Huguenard JR (2013) Astrocytes potentiate GABAergic transmission in the thalamic reticular nucleus via endoepine signalling. *Proc Natl Acad Sci U S A* 110:20278-20283.
- Citraro R, Russo E, Gratteri S, Di Paola ED, Ibbadu GF, Curinga C, Gitto R, Chimirri A, Donato G, De Sarro G (2006) Effects of non-competitive AMPA receptor antagonists injected into some brain areas of WAG/Rij rats, an animal model of generalized absence epilepsy. *Neuropharmacology* 51:1058-1067.
- Citraro R, Russo E, Scicchitano F, van Rijn CM, Cosco D, Avagliano C, Russo R, D'Agostino G, Petrosino S, Guida F, Gatta L, van Luijckelaar G, Maione S, Di Marzo V, Calignano A, De Sarro G (2013) Antiepileptic action of N-palmitoylethanolamine through CB1 and PPAR- α receptor activation in a genetic model of absence epilepsy. *Neuropharmacology* 69:115-126.
- Cnaan A, Shinnar S, Arya R, Adamson PC, Clark PO, Dlugos D, Hirtz DG, Masur D, Glauser TA, Group CAES (2017) Second monotherapy in childhood absence epilepsy. *Neurology* 88:182-190.
- Coenen AM, Van Luijckelaar EL (2003) Genetic animal models for absence epilepsy: a review of the WAG/Rij strain of rats. *Behav Genet* 33:635-655.
- Coenen AM, Blezer EH, van Luijckelaar EL (1995) Effects of the GABA-uptake inhibitor tiagabine on electroencephalogram, spike-wave discharges and behaviour of rats. *Epilepsy Res* 21:89-94.
- Coenen AM, Drinkenburg WH, Inoue M, van Luijckelaar EL (1992) Genetic models of absence epilepsy, with emphasis on the WAG/Rij strain of rats. *Epilepsy Res* 12:75-86.
- Conley JM, Radhakrishnan S, Valentino SA, Tantama M (2017) Imaging extracellular ATP with a genetically-encoded, ratiometric fluorescent sensor. *PLoS One* 12:e0187481.
- Connelly WM, Fyson SJ, Errington AC, McCafferty CP, Cope DW, Di Giovanni G, Crunelli V (2013) GABAB Receptors Regulate Extrasynaptic GABAA Receptors. *J Neurosci* 33:3780-3785.
- Conti F, Minelli A, Melone M (2004) GABA transporters in the mammalian cerebral cortex: localization, development and pathological implications. *Brain Res Brain Res Rev* 45:196-212.
- Cope DW, Hughes SW, Crunelli V (2005) GABAA receptor-mediated tonic inhibition in thalamic neurons. *J Neurosci* 25:11553-11563.
- Cope DW, Di Giovanni G, Fyson SJ, Orbán G, Errington AC, Lorincz ML, Gould TM, Carter DA, Crunelli V (2009) Enhanced tonic GABAA inhibition in typical absence epilepsy. *Nat Med* 15:1392-1398.
- Copeland CS, Wall TM, Sims RE, Neale SA, Nisenbaum E, Parri HR, Salt TE (2017) Astrocytes modulate thalamic sensory processing via mGlu2 receptor activation. *Neuropharmacology* 121:100-110.
- Cortez MA, Kostopoulos GK, Snead OC (2016) Acute and chronic pharmacological models of generalized absence seizures. *J Neurosci Methods* 260:175-184.
- Couve A, Moss SJ, Pangalos MN (2000) GABAB receptors: a new paradigm in G protein signalling. *Mol Cell Neurosci* 16:296-312.
- Covelo A, Araque A (2018) Neuronal activity determines distinct gliotransmitter release from a single astrocyte. *Elife* 7.
- Cox GA, Lutz CM, Yang C-L, Biemesderfer D, Bronson RT, Fu A, Aronson PS, Noebels JL, Frankel WN (1997) Sodium/Hydrogen Exchanger Gene Defect in Slow-Wave Epilepsy Mutant Mice. *Cell* 91:139-148.
- Crippa D, Schenk U, Francolini M, Rosa P, Verderio C, Zonta M, Pozzan T, Matteoli M, Carmignoto G (2006) Synaptobrevin2-expressing vesicles in rat astrocytes: insights into molecular characterization, dynamics and exocytosis. *J Physiol* 570:567-582.
- Crunelli V, Leresche N (1991) A role for GABAB receptors in excitation and inhibition of thalamocortical cells. *Trends Neurosci* 14:16-21.
- Crunelli V, Leresche N (2002) Childhood absence epilepsy: genes, channels, neurons and networks. *Nat Rev Neurosci* 3:371-382.
- Crunelli V, Emri Z, Leresche N (2006) Unravelling the brain targets of gamma-hydroxybutyric acid. *Curr Opin Pharmacol* 6:44-52.

- Crunelli V, Carmignoto G, Steinhäuser C (2015) Novel astrocyte targets: new avenues for the therapeutic treatment of epilepsy. *Neuroscientist* 21:62-83.
- Crunelli V, Lőrincz ML, McCafferty C, Lambert RC, Leresche N, Di Giovanni G, David F (2020) Clinical and experimental insight into pathophysiology, comorbidity and therapy of absence seizures. *Brain* 143:2341-2368.
- Cupido A, Catalin B, Steffens H, Kirchhoff F (2014) Surgical procedures to study microglial motility in the brain and in the spinal cord by in vivo two-photon laser-scanning microscopy. In: *Confocal and Multiphoton Laser-Scanning Microscopy of Neuronal Tissue: Applications and Quantitative Image Analysis* (Bakota L, Brandt R, eds), pp 37-50: Springer.
- D'Amore V, von Randow C, Nicoletti F, Ngomba RT, van Luijtelaar G (2015) Anti-absence activity of mGlu1 and mGlu5 receptor enhancers and their interaction with a GABA reuptake inhibitor: Effect of local infusions in the somatosensory cortex and thalamus. *Epilepsia* 56:1141-1151.
- D'Amore V, Santolini I, van Rijn CM, Biagioni F, Molinaro G, Prete A, Conn PJ, Lindsley CW, Zhou Y, Vinson PN, Rodriguez AL, Jones CK, Stauffer SR, Nicoletti F, van Luijtelaar G, Ngomba RT (2013) Potentiation of mGlu5 receptors with the novel enhancer, VU0360172, reduces spontaneous absence seizures in WAG/Rij rats. *Neuropharmacology* 66:330-338.
- D'Antuono M, Inaba Y, Biagini G, D'Arcangelo G, Tancredi V, Avoli M (2006) Synaptic hyperexcitability of deep layer neocortical cells in a genetic model of absence seizures. *Genes Brain Behav* 5:73-84.
- Danbolt NC (2001) Glutamate uptake. *Prog Neurobiol* 65:1-105.
- Danbolt NC, Pines G, Kanner BI (1990) Purification and reconstitution of the sodium- and potassium-coupled glutamate transport glycoprotein from rat brain. *Biochemistry* 29:6734-6740.
- De Biasi S, Vitellaro-Zuccarello L, Brecha NC (1998) Immunoreactivity for the GABA transporter-1 and GABA transporter-3 is restricted to astrocytes in the rat thalamus. A light and electron-microscopic immunolocalization. *Neuroscience* 83:815-828.
- De Deyn PP, Marescau B, MacDonald RL (1990) Epilepsy and the GABA-hypothesis a brief review and some examples. *Acta Neurol Belg* 90:65-81.
- Depaulis A, Luijtelaar v, G (2006) Characteristics of genetic absence seizures in the rat. In: *Models of seizure and epilepsy* (Pitkanen, A, Schwartzkroin, PA, Moshe, S, eds), pp 233-248: International : Elsevier Academic Press.
- Depaulis A, Charpier S (2018) Pathophysiology of absence epilepsy: Insights from genetic models. *Neurosci Lett* 667:53-65.
- Depaulis A, David O, Charpier S (2016) The genetic absence epilepsy rat from Strasbourg as a model to decipher the neuronal and network mechanisms of generalized idiopathic epilepsies. *J Neurosci Methods* 260:159-174.
- Depaulis A, Snead OC, Marescaux C, Vergnes M (1989) Suppressive effects of intranigral injection of muscimol in three models of generalized non-convulsive epilepsy induced by chemical agents. *Brain Res* 498:64-72.
- Derouiche A, Frotscher M (1991) Astroglial processes around identified glutamatergic synapses contain glutamine synthetase: evidence for transmitter degradation. *Brain Res* 552:346-350.
- Di Castro MA, Chuquet J, Liaudet N, Bhaukaurally K, Santello M, Bouvier D, Tiret P, Volterra A (2011) Local Ca²⁺ detection and modulation of synaptic release by astrocytes. *Nat Neurosci* 14:1276-1284.
- Dikow N, Maas B, Karch S, Granzow M, Janssen JW, Jauch A, Hinderhofer K, Sutter C, Schubert-Bast S, Anderlid BM, Dallapiccola B, Van der Aa N, Moog U (2014) 3p25.3 microdeletion of GABA transporters SLC6A1 and SLC6A11 results in intellectual disability, epilepsy and stereotypic behavior. *Am J Med Genet A* 164A:3061-3068.
- Ding F, O'Donnell J, Thrane AS, Zeppenfeld D, Kang H, Xie L, Wang F, Nedergaard M (2013) alpha(1)-Adrenergic receptors mediate coordinated Ca²⁺ signalling of cortical astrocytes in awake, behaving mice. *Cell Calcium* 54:387-394.
- Ding S, Fellin T, Zhu Y, Lee S-Y, Auberson YP, Meaney DF, Coulter DA, Carmignoto G, Haydon PG (2007) Enhanced astrocytic Ca²⁺ signals contribute to neuronal excitotoxicity after status epilepticus. *Journal of Neuroscience* 27:10674-10684.
- Dityatev A, Rusakov DA (2011) Molecular signals of plasticity at the tetrapartite synapse. *Curr Opin Neurobiol* 21:353-359.
- Doengi M, Deitmer JW, Lohr C (2008) New evidence for purinergic signalling in the olfactory bulb: A2A and P2Y1 receptors mediate intracellular calcium release in astrocytes. *FASEB J* 22:2368-2378.
- Doengi M, Hirnet D, Coulon P, Pape HC, Deitmer JW, Lohr C (2009) GABA uptake-dependent Ca(2+) signalling in developing olfactory bulb astrocytes. *Proc Natl Acad Sci U S A* 106:17570-17575.
- Doherty JD, Hattox SE, Snead OC, Roth RH (1978) Identification of endogenous gamma-hydroxybutyrate in human and bovine brain and its regional distribution in human, guinea pig and rhesus monkey brain. *J Pharmacol Exp Ther* 207:130-139.
- Domercq M, Brambilla L, Pilati E, Marchaland J, Volterra A, Bezzi P (2006) P2Y1 receptor-evoked glutamate exocytosis from astrocytes: control by tumor necrosis factor-alpha and prostaglandins. *J Biol Chem* 281:30684-30696.

- Donello JE, Loeb JE, Hope TJ (1998) Woodchuck hepatitis virus contains a tripartite posttranscriptional regulatory element. *J Virol* 72:5085-5092.
- Drinkenburg WH, Coenen AM, Vossen JM, Van Luijtelaar EL (1991) Spike-wave discharges and sleep-wake states in rats with absence epilepsy. *Epilepsy Res* 9:218-224.
- Duan S, Anderson CM, Keung EC, Chen Y, Swanson RA (2003) P2X7 receptor-mediated release of excitatory amino acids from astrocytes. *J Neurosci* 23:1320-1328.
- Dufour F, Nalecz KA, Nalecz MJ, Nehlig A (2001) Metabolic approach of absence seizures in a genetic model of absence epilepsy, the GAERS: study of the leucine-glutamate cycle. *J Neurosci Res* 66:923-930.
- Durkee CA, Covelo A, Lines J, Kofuji P, Aguilar J, Araque A (2019) G(i/o) protein-coupled receptors inhibit neurons but activate astrocytes and stimulate gliotransmission. *Glia* 67:1076-1093.
- Dutuit M, Touret M, Szymocha R, Nehlig A, Belin MF, Didier-Bazès M (2002) Decreased expression of glutamate transporters in genetic absence epilepsy rats before seizure occurrence. *J Neurochem* 80:1029-1038.
- Dutuit M, Didier-Bazès M, Vergnes M, Mutin M, Conjard A, Akaoka H, Belin MF, Touret M (2000) Specific alteration in the expression of glial fibrillary acidic protein, glutamate dehydrogenase, and glutamine synthetase in rats with genetic absence epilepsy. *Glia* 32:15-24.
- Dzamba D, Honsa P, Anderova M (2013) NMDA Receptors in Glial Cells: Pending Questions. *Curr Neuropharmacol* 11:250-262.
- Dürst CD, Wiegert JS, Helassa N, Kerruth S, Coates C, Schulze C, Geeves MA, Török K, Oertner TG (2019) High-speed imaging of glutamate release with genetically encoded sensors. *Nature Protocols* 14:1401-1424.
- Economu MN, Clack NG, Lavis LD, Gerfen CR, Svoboda K, Myers EW, Chandrashekar J (2016) A platform for brain-wide imaging and reconstruction of individual neurons. *Elife* 5:e10566.
- Emri Z, Antal K, Crunelli V (1996) Gamma-hydroxybutyric acid decreases thalamic sensory excitatory postsynaptic potentials by an action on presynaptic GABAB receptors. *Neurosci Lett* 216:121-124.
- Emsley JG, Macklis JD (2006) Astroglial heterogeneity closely reflects the neuronal-defined anatomy of the adult murine CNS. *Neuron Glia Biol* 2:175-186.
- Eroglu C, Barres BA (2010) Regulation of synaptic connectivity by glia. *Nature* 468:223-231.
- Errington AC, Cope DW, Crunelli V (2011a) Augmentation of Tonic GABA(A) Inhibition in Absence Epilepsy: Therapeutic Value of Inverse Agonists at Extrasynaptic GABA(A) Receptors. *Adv Pharmacol Sci* 2011:790590.
- Errington AC, Gibson KM, Crunelli V, Cope DW (2011b) Aberrant GABA(A) receptor-mediated inhibition in cortico-thalamic networks of succinic semialdehyde dehydrogenase deficient mice. *PLoS One* 6:e19021.
- Fairfax BP, Pitcher JA, Scott MG, Calver AR, Pangalos MN, Moss SJ, Couve A (2004) Phosphorylation and chronic agonist treatment atypically modulate GABAB receptor cell surface stability. *J Biol Chem* 279:12565-12573.
- Fariello RG, Golden GT (1987) The THIP-induced model of bilateral synchronous spike-and-wave in rodents. *Neuropharmacology* 26:161-165.
- Feil R, Wagner J, Metzger D, Chambon P (1997) Regulation of Cre recombinase activity by mutated estrogen receptor ligand-binding domains. *Biochem Biophys Res Commun* 237:752-757.
- Feil S, Valtcheva N, Feil R (2009) Inducible Cre mice. *Methods Mol Biol* 530:343-363.
- Felix L, Delekate A, Petzold GC, Rose CR (2020) Sodium Fluctuations in Astroglia and Their Potential Impact on Astrocyte Function. *Front Physiol* 11:871.
- Fellin T, Pozzan T, Carmignoto G (2006) Purinergic receptors mediate two distinct glutamate release pathways in hippocampal astrocytes. *J Biol Chem* 281:4274-4284.
- Fellin T, Pascual O, Gobbo S, Pozzan T, Haydon PG, Carmignoto G (2004) Neuronal synchrony mediated by astrocytic glutamate through activation of extrasynaptic NMDA receptors. *Neuron* 43:729-743.
- Ferry B, Gervasoni D, Vogt C (2014) Stereotaxic Approach of a Target Structure. In: *Stereotaxic Neurosurgery in Laboratory Rodent.*, pp pp 69-86: Springer, Paris.
- Fiacco TA, McCarthy KD (2006) Astrocyte calcium elevations: properties, propagation, and effects on brain signalling. *Glia* 54:676-690.
- Fisher RS, Prince DA (1977) Spike-wave rhythms in cat cortex induced by parenteral penicillin. II. Cellular features. *Electroencephalography and Clinical Neurophysiology* 42:625-639.
- Fisher RS, Acevedo C, Arzimanoglou A, Bogacz A, Cross JH, Elger CE, Engel J, Forsgren L, French JA, Glynn M, Hesdorffer DC, Lee BI, Mathern GW, Moshé SL, Perucca E, Scheffer IE, Tomson T, Watanabe M, Wiebe S (2014) ILAE official report: a practical clinical definition of epilepsy. *Epilepsia* 55:475-482.
- Fletcher CF, Lutz CM, O'Sullivan TN, Shaughnessy JD, Hawkes R, Frankel WN, Copeland NG, Jenkins NA (1996) Absence epilepsy in tottering mutant mice is associated with calcium channel defects. *Cell* 87:607-617.
- Flurkey K, M. Currer J, Harrison DE (2007) Chapter 20 - Mouse Models in Aging Research. In: *The Mouse in Biomedical Research (Second Edition)* (Fox JG, Davison MT, Quimby FW, Barthold SW, Newcomer CE, Smith AL, eds), pp 637-672. Burlington: Academic Press.

- Fonseca Wald ELA, Hendriksen JGM, Drenthen GS, Kuijk SMJV, Aldenkamp AP, Vles JSH, Vermeulen RJ, Debeij-van Hall MHJA, Klinkenberg S (2019) Towards a Better Understanding of Cognitive Deficits in Absence Epilepsy: a Systematic Review and Meta-Analysis. *Neuropsychol Rev* 29:421-449.
- Franke H, Verkhratsky A, Burnstock G, Illes P (2012) Pathophysiology of astroglial purinergic signalling. *Purinergic Signal* 8:629-657.
- Fraser DD, Duffy S, Angelides KJ, Perez-Velazquez JL, Kettenmann H, MacVicar BA (1995) GABAA/benzodiazepine receptors in acutely isolated hippocampal astrocytes. *J Neurosci* 15:2720-2732.
- Friedrich G, Soriano P (1991) Promoter traps in embryonic stem cells: a genetic screen to identify and mutate developmental genes in mice. *Genes Dev* 5:1513-1523.
- Fujii Y, Maekawa S, Morita M (2017) Astrocyte calcium waves propagate proximally by gap junction and distally by extracellular diffusion of ATP released from volume-regulated anion channels. *Sci Rep* 7:13115.
- Fujiwara H, Tenney J, Kadis DS, Altaye M, Spencer C, Vannest J (2020) Cortical and subcortical volume differences between Benign Epilepsy with Centrottemporal Spikes and Childhood Absence Epilepsy. *Epilepsy Res* 166:106407.
- Fumagalli M, Brambilla R, D'Ambrosi N, Volonté C, Matteoli M, Verderio C, Abbracchio MP (2003) Nucleotide-mediated calcium signalling in rat cortical astrocytes: Role of P2X and P2Y receptors. *Glia* 43:218-203.
- Gale K (1995) Chemoconvulsant seizures: advantages of focally-evoked seizure models. *Ital J Neurol Sci* 16:17-25.
- Galer PD et al. (2020) Semantic Similarity Analysis Reveals Robust Gene-Disease Relationships in Developmental and Epileptic Encephalopathies. *Am J Hum Genet* 107:683-697.
- Gardiner M (2005) Genetics of idiopathic generalized epilepsies. *Epilepsia* 46 Suppl 9:15-20.
- Gareri P, Condorelli D, Belluardo N, Citraro R, Barresi V, Trovato-Salinaro A, Trovato-Salinaro A, Mudò G, Ibbadu GF, Russo E, De Sarro G (2005) Antiabsence effects of carbenoxolone in two genetic animal models of absence epilepsy (WAG/Rij rats and lh/lh mice). *Neuropharmacology* 49:551-563.
- Gavrilov N, Golyagina I, Brazhe A, Scimemi A, Turlapov V, Semyanov A (2018) Astrocytic Coverage of Dendritic Spines, Dendritic Shafts, and Axonal Boutons in Hippocampal Neuropil. *Front Cell Neurosci* 12:248.
- Gervasi N, Monnier Z, Vincent P, Paupardin-Tritsch D, Hughes SW, Crunelli V, Leresche N (2003) Pathway-specific action of gamma-hydroxybutyric acid in sensory thalamus and its relevance to absence seizures. *J Neurosci* 23:11469-11478.
- Getova D, Bowery NG, Spassov V (1997) Effects of GABAB receptor antagonists on learning and memory retention in a rat model of absence epilepsy. *Eur J Pharmacol* 320:9-13.
- Giaume C, Naus CC, Sáez JC, Leybaert L (2021) Glial Connexins and Pannexins in the Healthy and Diseased Brain. *Physiol Rev* 101:93-145.
- Giaume C, Koulakoff A, Roux L, Holcman D, Rouach N (2010) Astroglial networks: a step further in neuroglial and gliovascular interactions. *Nat Rev Neurosci* 11:87-99.
- Gigout S, Louvel J, Pumain R (2006) Effects in vitro and in vivo of a gap junction blocker on epileptiform activities in a genetic model of absence epilepsy. *Epilepsy Res* 69:15-29.
- Gigout S, Louvel J, Rinaldi D, Martin B, Pumain R (2013) Thalamocortical relationships and network synchronization in a new genetic model "in mirror" for absence epilepsy. *Brain Res* 1525:39-52.
- Glauser TA, Cnaan A, Shinnar S, Hirtz DG, Dlugos D, Masur D, Clark PO, Adamson PC, Team CAES (2013) Ethosuximide, valproic acid, and lamotrigine in childhood absence epilepsy: initial monotherapy outcomes at 12 months. *Epilepsia* 54:141-155.
- Gobbo D, Scheller A, Kirchhoff F (2021) From Physiology to Pathology of Cortico-Thalamo-Cortical Oscillations: Astroglia as a Target for Further Research. *Frontiers in Neurology* 12.
- Godschalk M, Dzoljic MR, Bonta IL (1976) Antagonism of gamma-hydroxybutyrate-induced hypersynchronization in the ECoG of the rat by anti-petit mal drugs. *Neurosci Lett* 3:145-150.
- Godschalk M, Dzoljic MR, Bonta IL (1977) Slow wave sleep and a state resembling absence epilepsy induced in the rat by gamma-hydroxybutyrate. *Eur J Pharmacol* 44:105-111.
- Goodspeed K et al. (2020) Current knowledge of SLC6A1-related neurodevelopmental disorders. *Brain Commun* 2:fcaa170.
- Gotman J, Grova C, Bagshaw A, Kobayashi E, Aghakhani Y, Dubeau F (2005) Generalized epileptic discharges show thalamocortical activation and suspension of the default state of the brain. *Proc Natl Acad Sci U S A* 102:15236-15240.
- Gould T, Chen L, Emri Z, Pirttimaki T, Errington AC, Crunelli V, Parri HR (2014) GABA(B) receptor-mediated activation of astrocytes by gamma-hydroxybutyric acid. *Philos Trans R Soc Lond B Biol Sci* 369:20130607.
- Grampp T, Notz V, Broll I, Fischer N, Benke D (2008) Constitutive, agonist-accelerated, recycling and lysosomal degradation of GABA(B) receptors in cortical neurons. *Mol Cell Neurosci* 39:628-637.
- Guerra-Gomes S, Sousa N, Pinto L, Oliveira JF (2017) Functional Roles of Astrocyte Calcium Elevations: From Synapses to Behavior. *Front Cell Neurosci* 11:427.

- Guo JN, Kim R, Chen Y, Negishi M, Jhun S, Weiss S, Ryu JH, Bai X, Xiao W, Feeney E, Rodriguez-Fernandez J, Mistry H, Crunelli V, Crowley MJ, Mayes LC, Constable RT, Blumenfeld H (2016) Impaired consciousness in patients with absence seizures investigated by functional MRI, EEG, and behavioural measures: a cross-sectional study. *Lancet Neurol* 15:1336-1345.
- Guo ZV, Hires SA, Li N, O'Connor DH, Komiyama T, Ophir E, Huber D, Bonardi C, Morandell K, Gutnisky D, Peron S, Xu NL, Cox J, Svoboda K (2014) Procedures for behavioral experiments in head-fixed mice. *PLoS One* 9:e88678.
- Guthrie PB, Knappenberger J, Segal M, Bennett MV, Charles AC, Kater SB (1999) ATP released from astrocytes mediates glial calcium waves. *J Neurosci* 19:520-528.
- Gómez-Gonzalo M, Losi G, Chiavegato A, Zonta M, Cammarota M, Brondi M, Vetri F, Uva L, Pozzan T, de Curtis M, Ratto GM, Carmignoto G (2010) An excitatory loop with astrocytes contributes to drive neurons to seizure threshold. *PLoS Biol* 8:e1000352.
- Haj-Yasein NN, Jensen V, Vindedal GF, Gundersen GA, Klungland A, Ottersen OP, Hvalby O, Nagelhus EA (2011) Evidence that compromised K⁺ spatial buffering contributes to the epileptogenic effect of mutations in the human Kir4.1 gene (KCNJ10). *Glia* 59:1635-1642.
- Halassa MM, Fellin T, Haydon PG (2007a) The tripartite synapse: roles for gliotransmission in health and disease. *Trends in Molecular Medicine* 13:54-63.
- Halassa MM, Fellin T, Takano H, Dong J-H, Haydon PG (2007b) Synaptic islands defined by the territory of a single astrocyte. *Journal of Neuroscience* 27:6473-6477.
- Haller C, Casanova E, Müller M, Vacher CM, Vigot R, Doll T, Barbieri S, Gassmann M, Bettler B (2004) Floxed allele for conditional inactivation of the GABAB(1) gene. *Genesis* 40:125-130.
- Hamandi K, Salek-Haddadi A, Laufs H, Liston A, Friston K, Fish DR, Duncan JS, Lemieux L (2006) EEG-fMRI of idiopathic and secondarily generalized epilepsies. *Neuroimage* 31:1700-1710.
- Hamilton DL, Abremski K (1984) Site-specific recombination by the bacteriophage P1 lox-Cre system. Cre-mediated synopsis of two lox sites. *J Mol Biol* 178:481-486.
- Harayama N, Shibuya I, Tanaka K, Kabashima N, Ueta Y, Yamashita H (1998) Inhibition of N- and P/Q-type calcium channels by postsynaptic GABAB receptor activation in rat supraoptic neurones. *J Physiol* 509 (Pt 2):371-383.
- Haustein MD, Kracun S, Lu XH, Shih T, Jackson-Weaver O, Tong X, Xu J, Yang XW, O'Dell TJ, Marvin JS, Ellisman MH, Bushong EA, Looger LL, Khakh BS (2014) Conditions and constraints for astrocyte calcium signalling in the hippocampal mossy fiber pathway. *Neuron* 82:413-429.
- Heller AH, Dichter MA, Sidman RL (1983) Anticonvulsant sensitivity of absence seizures in the tottering mutant mouse. *Epilepsia* 24:25-34.
- Heller JP, Rusakov DA (2017) The Nanoworld of the Tripartite Synapse: Insights from Super-Resolution Microscopy. *Front Cell Neurosci* 11:374.
- Herd MB, Brown AR, Lambert JJ, Belelli D (2013) Extrasynaptic GABA(A) receptors couple presynaptic activity to postsynaptic inhibition in the somatosensory thalamus. *J Neurosci* 33:14850-14868.
- Hertz L (2013) The Glutamate-Glutamine (GABA) Cycle: Importance of Late Postnatal Development and Potential Reciprocal Interactions between Biosynthesis and Degradation. *Front Endocrinol (Lausanne)* 4:59.
- Heuser K, Enger R (2021) Astrocytic Ca²⁺ Signalling in Epilepsy. *Front Cell Neurosci* 15:695380.
- Heuser K, Nome CG, Pettersen KH, Åbjørnsbråten KS, Jensen V, Tang W, Sprengel R, Taubøll E, Nagelhus EA, Enger R (2018) Ca²⁺ Signals in Astrocytes Facilitate Spread of Epileptiform Activity. *Cereb Cortex* 28:4036-4048.
- Holmes GL, Noebels JL (2016) The Epilepsy Spectrum: Targeting Future Research Challenges. *Cold Spring Harb Perspect Med* 6.
- Hommet C, Billard C, Motte J, Passage GD, Perrier D, Gillet P, Prunier C, Toffol BD, Autret A (2001) Cognitive function in adolescents and young adults in complete remission from benign childhood epilepsy with centro-temporal spikes. *Epileptic Disord* 3:207-216.
- Hosford DA, Wang Y (1997) Utility of the lethargic (lh/lh) mouse model of absence seizures in predicting the effects of lamotrigine, vigabatrin, tiagabine, gabapentin, and topiramate against human absence seizures. *Epilepsia* 38:408-414.
- Hosford DA, Wang Y, Liu CC, Snead OC (1995) Characterization of the antiabsence effects of SCH 50911, a GABA-B receptor antagonist, in the lethargic mouse, gamma-hydroxybutyrate, and pentylentetrazole models. *J Pharmacol Exp Ther* 274:1399-1403.
- Hosford DA, Clark S, Cao Z, Wilson WA, Lin FH, Morrisett RA, Huin A (1992) The role of GABAB receptor activation in absence seizures of lethargic (lh/lh) mice. *Science* 257:398-401.
- Hu RQ, Banerjee PK, Snead OC (2000) Regulation of gamma-aminobutyric acid (GABA) release in cerebral cortex in the gamma-hydroxybutyric acid (GHB) model of absence seizures in rat. *Neuropharmacology* 39:427-439.
- Huff J, Murr N (2021) Seizure. In: (StatPearls, ed): Treasure Island (FL): StatPearls Publishing.
- Héja L, Simon Á, Szabó Z, Kardos J (2019) Feedback adaptation of synaptic excitability via Glu:Na. *Neuropharmacology* 161:107629.

- Héja L, Barabás P, Nyitrai G, Kékesi KA, Lasztóczy B, Toke O, Tárkányi G, Madsen K, Schousboe A, Dobolyi A, Palkovits M, Kardos J (2009) Glutamate uptake triggers transporter-mediated GABA release from astrocytes. *PLoS One* 4:e7153.
- Höft S, Griemsmann S, Seifert G, Steinhäuser C (2014) Heterogeneity in expression of functional ionotropic glutamate and GABA receptors in astrocytes across brain regions: insights from the thalamus. *Philos Trans R Soc Lond B Biol Sci* 369:20130602.
- Inaba Y, D'Antuono M, Bertazzoni G, Biagini G, Avoli M (2009) Diminished presynaptic GABA(B) receptor function in the neocortex of a genetic model of absence epilepsy. *Neurosignals* 17:121-131.
- Indra AK, Warot X, Brocard J, Bornert JM, Xiao JH, Chambon P, Metzger D (1999) Temporally-controlled site-specific mutagenesis in the basal layer of the epidermis: comparison of the recombinase activity of the tamoxifen-inducible Cre-ER(T) and Cre-ER(T2) recombinases. *Nucleic Acids Res* 27:4324-4327.
- Ishige K, Aizawa M, Ito Y, Fukuda H (1996) gamma-Butyrolactone-induced absence-like seizures increase nuclear CRE- and AP-1 DNA-binding activities in mouse brain. *Neuropharmacology* 35:45-55.
- Jahn HM, Kasakow CV, Helfer A, Michely J, Verkhatsky A, Maurer HH, Scheller A, Kirchhoff F (2018) Refined protocols of tamoxifen injection for inducible DNA recombination in mouse astroglia. *Sci Rep* 8:5913.
- Jarre G, Altwegg-Boussac T, Williams MS, Studer F, Chipaux M, David O, Charpier S, Depaulis A, Mahon S, Guillemain I (2017) Building Up Absence Seizures in the Somatosensory Cortex: From Network to Cellular Epileptogenic Processes. *Cereb Cortex* 27:4607-4623.
- Jensen K, Mody I (2001) GHB depresses fast excitatory and inhibitory synaptic transmission via GABA(B) receptors in mouse neocortical neurons. *Cereb Cortex* 11:424-429.
- Johannesen KM et al. (2018) Defining the phenotypic spectrum of SLC6A1 mutations. *Epilepsia* 59:389-402.
- Jourdain P, Bergersen LH, Bhaukaurally K, Bezzi P, Santello M, Domercq M, Matute C, Tonello F, Gundersen V, Volterra A (2007) Glutamate exocytosis from astrocytes controls synaptic strength. *Nat Neurosci* 10:331-339.
- Jungblut M, Tiveron MC, Barral S, Abrahamsen B, Knöbel S, Pennartz S, Schmitz J, Perraut M, Pfrieger FW, Stoffel W, Cremer H, Bosio A (2012) Isolation and characterization of living primary astroglial cells using the new GLAST-specific monoclonal antibody ACSA-1. *Glia* 60:894-907.
- Kacem K, Lacombe P, Seylaz J, Bonvento G (1998) Structural organization of the perivascular astrocyte endfeet and their relationship with the endothelial glucose transporter: a confocal microscopy study. *Glia* 23:1-10.
- Kandel E, Schwartz J, TM. J (2000) *Principles of Neural Science*, Fourth Edition Edition: McGraw-Hill Health Professions Division.
- Kanemaru K, Sekiya H, Xu M, Satoh K, Kitajima N, Yoshida K, Okubo Y, Sasaki T, Moritoh S, Hasuwa H, Mimura M, Horikawa K, Matsui K, Nagai T, Iino M, Tanaka KF (2014) In vivo visualization of subtle, transient, and local activity of astrocytes using an ultrasensitive Ca(2+) indicator. *Cell Rep* 8:311-318.
- Kang J, Jiang L, Goldman SA, Nedergaard M (1998) Astrocyte-mediated potentiation of inhibitory synaptic transmission. *Nat Neurosci* 1:683-692.
- Kang M, Othmer HG (2009) Spatiotemporal characteristics of calcium dynamics in astrocytes. *Chaos* 19:037116.
- Kang N, Xu J, Xu QW, Nedergaard M, Kang J (2005) Astrocytic glutamate release-induced transient depolarization and epileptiform discharges in hippocampal CA1 pyramidal neurons. *Journal of Neurophysiology* 94:4121-4130.
- Kaplan BJ, Seyfried TN, Glaser GH (1979) Spontaneous polyspike discharges in an epileptic mutant mouse (tottering). *Experimental Neurology* 66:577-586.
- Kaupmann K, Cryan JF, Wellendorph P, Mombereau C, Sansig G, Klebs K, Schmutz M, Froestl W, van der Putten H, Mosbacher J, Bräuner-Osborne H, Waldmeier P, Bettler B (2003) Specific gamma-hydroxybutyrate-binding sites but loss of pharmacological effects of gamma-hydroxybutyrate in GABA(B)(1)-deficient mice. *Eur J Neurosci* 18:2722-2730.
- Kavalali ET (2015) The mechanisms and functions of spontaneous neurotransmitter release. *Nature Reviews Neuroscience* 16:5-16.
- Kennard JT, Barmanray R, Sampurno S, Ozturk E, Reid CA, Paradiso L, D'Abaco GM, Kaye AH, Foote SJ, O'Brien TJ, Powell KL (2011) Stargazin and AMPA receptor membrane expression is increased in the somatosensory cortex of Genetic Absence Epilepsy Rats from Strasbourg. *Neurobiol Dis* 42:48-54.
- Kettenmann H, Ransom B (1995) *Neuroglia*, First Edition: Oxford University Press.
- Kettenmann H, Zorec R (2013) Release of gliotransmitters and transmitter receptors in astrocytes. In: *Neuroglia* (Kettenmann H, Ransom B, eds), pp 197-211. New York: Oxford University Press
- Khakh BS, Sofroniew MV (2015) Diversity of astrocyte functions and phenotypes in neural circuits. *Nature Neuroscience* 18:942-952.
- Kim D, Song I, Keum S, Lee T, Jeong MJ, Kim SS, McEnery MW, Shin HS (2001) Lack of the burst firing of thalamocortical relay neurons and resistance to absence seizures in mice lacking alpha(1G) T-type Ca(2+) channels. *Neuron* 31:35-45.

- Kim EH, Shim WH, Lee JS, Yoon HM, Ko TS, Yum MS (2020) Altered Structural Network in Newly Onset Childhood Absence Epilepsy. *J Clin Neurol* 16:573-580.
- Kislina M, Mugantseva E, Molotkov D, Kuleshkaya N, Khirug S, Kirilkin I, Pryazhnikov E, Kolikova J, Toptunov D, Yuryev M, Giniyatullin R, Voikar V, Rivera C, Rauvala H, Khiroug L (2014) Flat-floored air-lifted platform: a new method for combining behavior with microscopy or electrophysiology on awake freely moving rodents. *J Vis Exp*:e51869.
- Kiyoshi C, Aten S, Arzola E, Patterson J, Taylor A, Du Y, Guiher A, Philip M, Camacho EG, Mediratta D, Collins K, Benson E, Kidd G, Terman D, Zhou M (2020) Ultrastructural view of astrocyte-astrocyte and astrocyte-synapse contacts within the hippocampus. In: bioRxiv.
- Kiyoshi CM, Du Y, Zhong S, Wang W, Taylor AT, Xiong B, Ma B, Terman D, Zhou M (2018) Syncytial isopotentiality: A system-wide electrical feature of astrocytic networks in the brain. *Glia* 66:2756-2769.
- Koehler RC, Roman RJ, Harder DR (2009) Astrocytes and the regulation of cerebral blood flow. *Trends Neurosci* 32:160-169.
- Kofuji P, Newman EA (2004) Potassium buffering in the central nervous system. *Neuroscience* 129:1045-1056.
- Koizumi S (2010) Synchronization of Ca²⁺ oscillations: involvement of ATP release in astrocytes. *FEBS J* 277:286-292.
- Kozlov AS, Angulo MC, Audinat E, Charpak S (2006) Target cell-specific modulation of neuronal activity by astrocytes. *Proc Natl Acad Sci U S A* 103:10058-10063.
- Kumaresan S, David J, Joseph T (2000) Comparative profiles of sodium valproate and ethosuximide on electro-behavioural correlates in gamma-hydroxybutyrate and pentylenetetrazol induced absence seizures in rats. *Indian J Physiol Pharmacol* 44:411-418.
- Kékesi O, Ioja E, Szabó Z, Kardos J, Héja L (2015) Recurrent seizure-like events are associated with coupled astroglial synchronization. *Front Cell Neurosci* 9:215.
- Köhler S, Winkler U, Hirrlinger J (2021) Heterogeneity of Astrocytes in Grey and White Matter. *Neurochem Res* 46:3-14.
- Laborit H, Jouany J, Gerard J, Fabiani F (1960) Generalities concerning the experimental study and clinical use of gamma hydroxybutyrate of Na. *Agressologie* 1:397-406.
- Lalo U, Pankratov Y, Kirchhoff F, North RA, Verkhratsky A (2006) NMDA receptors mediate neuron-to-glia signalling in mouse cortical astrocytes. *J Neurosci* 26:2673-2683.
- Lalo U, Palygin O, North RA, Verkhratsky A, Pankratov Y (2011) Age-dependent remodelling of ionotropic signalling in cortical astroglia. *Aging Cell* 10:392-402.
- Lalo U, Pankratov Y, Wichert SP, Rossner MJ, North RA, Kirchhoff F, Verkhratsky A (2008) P2X1 and P2X5 subunits form the functional P2X receptor in mouse cortical astrocytes. *J Neurosci* 28:5473-5480.
- Le Meur K, Mendizabal-Zubiaga J, Grandes P, Audinat E (2012) GABA release by hippocampal astrocytes. *Front Comput Neurosci* 6:59.
- Leal A, Vieira JP, Lopes R, Nunes RG, Gonçalves SI, Lopes da Silva F, Figueiredo P (2016) Dynamics of epileptic activity in a peculiar case of childhood absence epilepsy and correlation with thalamic levels of GABA. *Epilepsy Behav Case Rep* 5:57-65.
- Lee HS, Ghetti A, Pinto-Duarte A, Wang X, Dziewczapolski G, Galimi F, Huitron-Resendiz S, Piña-Crespo JC, Roberts AJ, Verma IM, Sejnowski TJ, Heinemann SF (2014) Astrocytes contribute to gamma oscillations and recognition memory. *Proc Natl Acad Sci U S A* 111:E3343-3352.
- Lee S, Hwang E, Lee M, Choi JH (2019) Distinct Topographical Patterns of Spike-Wave Discharge in Transgenic and Pharmacologically Induced Absence Seizure Models. *Exp Neurobiol* 28:474-484.
- Lee S, Yoon BE, Berglund K, Oh SJ, Park H, Shin HS, Augustine GJ, Lee CJ (2010) Channel-mediated tonic GABA release from glia. *Science* 330:790-796.
- Leybaert L, Sanderson MJ (2001) Intercellular calcium signalling and flash photolysis of caged compounds. A sensitive method to evaluate gap junctional coupling. *Methods Mol Biol* 154:407-430.
- Leybaert L, Sanderson MJ (2012) Intercellular Ca²⁺ waves: mechanisms and function. *Physiol Rev* 92:1359-1392.
- Li B, Gu L, Hertz L, Peng L (2013) Expression of nucleoside transporter in freshly isolated neurons and astrocytes from mouse brain. *Neurochem Res* 38:2351-2358.
- Li Q, Kuhn CM, Wilson WA, Lewis DV (2007) Effects of gamma hydroxybutyric acid on inhibition and excitation in rat neocortex. *Neuroscience* 150:82-92.
- Li Q, Li QQ, Jia JN, Liu ZQ, Zhou HH, Mao XY (2019) Targeting gap junction in epilepsy: Perspectives and challenges. *Biomed Pharmacother* 109:57-65.
- Lia A, Henriques VJ, Zonta M, Chiavegato A, Carmignoto G, Gómez-Gonzalo M, Losi G (2021) Calcium Signals in Astrocyte Microdomains, a Decade of Great Advances. *Front Cell Neurosci* 15:673433.
- Lingenhoehl K, Brom R, Heid J, Beck P, Froestl W, Kaupmann K, Bettler B, Mosbacher J (1999) Gamma-hydroxybutyrate is a weak agonist at recombinant GABA(B) receptors. *Neuropharmacology* 38:1667-1673.

- Liu CY, Yang Y, Ju WN, Wang X, Zhang HL (2018) Emerging Roles of Astrocytes in Neuro-Vascular Unit and the Tripartite Synapse With Emphasis on Reactive Gliosis in the Context of Alzheimer's Disease. *Front Cell Neurosci* 12:193.
- Liu Z, Vergnes M, Depaulis A, Marescaux C (1992) Involvement of intrathalamic GABAB neurotransmission in the control of absence seizures in the rat. *Neuroscience* 48:87-93.
- Losi G, Marcon I, Mariotti L, Sessolo M, Chiavegato A, Carmignoto G (2016) A brain slice experimental model to study the generation and the propagation of focally-induced epileptiform activity. *J Neurosci Methods* 260:125-131.
- Loughman A, Bowden SC, D'Souza WJ (2017) A comprehensive assessment of cognitive function in the common genetic generalized epilepsy syndromes. *Eur J Neurol* 24:453-460.
- Lovatt D, Sonnewald U, Waagepetersen HS, Schousboe A, He W, Lin JH, Han X, Takano T, Wang S, Sim FJ, Goldman SA, Nedergaard M (2007) The transcriptome and metabolic gene signature of protoplasmic astrocytes in the adult murine cortex. *J Neurosci* 27:12255-12266.
- Luisier F, Blu T, Unser M (2010) Fast interscale wavelet denoising of Poisson-corrupted images. *SignalProcessing* 10:415-427.
- Löscher W, Schmidt D (2011) Modern antiepileptic drug development has failed to deliver: ways out of the current dilemma. *Epilepsia* 52:657-678.
- Lüttjohann A, van Luijtelaar G (2015) Dynamics of networks during absence seizure's on- and offset in rodents and man. *Front Physiol* 6:16.
- Lüttjohann A, Zhang S, de Peijper R, van Luijtelaar G (2011) Electrical stimulation of the epileptic focus in absence epileptic WAG/Rij rats: assessment of local and network excitability. *Neuroscience* 188:125-134.
- Macdonald RL, Kang JQ, Gallagher MJ (2010) Mutations in GABAA receptor subunits associated with genetic epilepsies. *J Physiol* 588:1861-1869.
- MacVicar BA, Newman EA (2015) Astrocyte regulation of blood flow in the brain. *Cold Spring Harb Perspect Biol* 7.
- MacVicar BA, Tse FW, Crichton SA, Kettenmann H (1989) GABA-activated Cl⁻ channels in astrocytes of hippocampal slices. *J Neurosci* 9:3577-3583.
- Maheshwari A, Noebels JL (2014) Monogenic models of absence epilepsy: windows into the complex balance between inhibition and excitation in thalamocortical microcircuits. *Prog Brain Res* 213:223-252.
- Mahmoud S, Gharagozloo M, Simard C, Gris D (2019) Astrocytes Maintain Glutamate Homeostasis in the CNS by Controlling the Balance between Glutamate Uptake and Release. *Cells* 8.
- Maitre M (1997) The gamma-hydroxybutyrate signalling system in brain: organization and functional implications. *Prog Neurobiol* 51:337-361.
- Manjarrez-Marmolejo J, Franco-Pérez J (2016) Gap Junction Blockers: An Overview of their Effects on Induced Seizures in Animal Models. *Curr Neuropharmacol* 14:759-771.
- Manning JP, Richards DA, Bowery NG (2003) Pharmacology of absence epilepsy. *Trends Pharmacol Sci* 24:542-549.
- Manning JP, Richards DA, Leresche N, Crunelli V, Bowery NG (2004) Cortical-area specific block of genetically determined absence seizures by ethosuximide. *Neuroscience* 123:5-9.
- Marcaggi P, Attwell D (2004) Role of glial amino acid transporters in synaptic transmission and brain energetics. *Glia* 47:217-225.
- Marcus RJ, Winters WD, Mori K, Spooner CE (1967) EEG and behavioral comparison of the effects of gamma-hydroxybutyrate, gamma-butyrolactone and short chain fatty acids in the rat. *Int J Neuropharmacol* 6:175-185.
- Marescaux C, Vergnes M, Bernasconi R (1992a) GABAB receptor antagonists: potential new anti-absence drugs. *J Neural Transm Suppl* 35:179-188.
- Marescaux C, Vergnes M, Depaulis A (1992b) Genetic absence epilepsy in rats from Strasbourg--a review. *J Neural Transm Suppl* 35:37-69.
- Marescaux C, Micheletti G, Vergnes M, Depaulis A, Rumbach L, Warter JM (1984) A model of chronic spontaneous petit mal-like seizures in the rat: comparison with pentylenetetrazol-induced seizures. *Epilepsia* 25:326-331.
- Marina N, Turovsky E, Christie IN, Hosford PS, Hadjihambi A, Korsak A, Ang R, Mastitskaya S, Sheikhabaie S, Theparambil SM, Gourine AV (2018) Brain metabolic sensing and metabolic signalling at the level of an astrocyte. *Glia* 66:1185-1199.
- Marina N, Christie IN, Korsak A, Doronin M, Brazhe A, Hosford PS, Wells JA, Sheikhabaie S, Humoud I, Paton JFR, Lythgoe MF, Semyanov A, Kasparov S, Gourine AV (2020) Astrocytes monitor cerebral perfusion and control systemic circulation to maintain brain blood flow. *Nat Commun* 11:131.
- Mariotti L, Losi G, Sessolo M, Marcon I, Carmignoto G (2016) The inhibitory neurotransmitter GABA evokes long-lasting Ca²⁺ oscillations in cortical astrocytes. *Glia* 64:363-373.
- Martineau M, Parpura V, Mothet JP (2014) Cell-type specific mechanisms of D-serine uptake and release in the brain. *Front Synaptic Neurosci* 6:12.

- Martineau M, Shi T, Puyal J, Knolhoff AM, Dulong J, Gasnier B, Klingauf J, Sweedler JV, Jahn R, Mothet JP (2013) Storage and uptake of D-serine into astrocytic synaptic-like vesicles specify gliotransmission. *J Neurosci* 33:3413-3423.
- Masur D, Shinnar S, Cnaan A, Shinnar RC, Clark P, Wang J, Weiss EF, Hirtz DG, Glauser TA, Group CAES (2013) Pretreatment cognitive deficits and treatment effects on attention in childhood absence epilepsy. *Neurology* 81:1572-1580.
- Mathivet P, Bernasconi R, De Barry J, Marescaux C, Bittiger H (1997) Binding characteristics of gamma-hydroxybutyric acid as a weak but selective GABAB receptor agonist. *Eur J Pharmacol* 321:67-75.
- Matos M, Bosson A, Riebe I, Reynell C, Vallée J, Laplante I, Panatier A, Robitaille R, Lacaille JC (2018) Astrocytes detect and upregulate transmission at inhibitory synapses of somatostatin interneurons onto pyramidal cells. *Nat Commun* 9:4254.
- Matricardi S, Verrotti A, Chiarelli F, Cerminara C, Curatolo P (2014) Current advances in childhood absence epilepsy. *Pediatr Neurol* 50:205-212.
- Matthias K, Kirchhoff F, Seifert G, Hüttmann K, Matyash M, Kettenmann H, Steinhäuser C (2003) Segregated expression of AMPA-type glutamate receptors and glutamate transporters defines distinct astrocyte populations in the mouse hippocampus. *J Neurosci* 23:1750-1758.
- Mattison KA, Butler KM, Inglis GAS, Dayan O, Boussidan H, Bhambhani V, Philbrook B, da Silva C, Alexander JJ, Kanner BI, Escayg A (2018) SLC6A1 variants identified in epilepsy patients reduce γ -aminobutyric acid transport. *Epilepsia* 59:e135-e141.
- Matyash V, Kettenmann H (2010) Heterogeneity in astrocyte morphology and physiology. *Brain Res Rev* 63:2-10.
- McCafferty C, David F, Venzi M, Lőrincz ML, Delicata F, Atherton Z, Recchia G, Orban G, Lambert RC, Di Giovanni G, Leresche N, Crunelli V (2018) Cortical drive and thalamic feed-forward inhibition control thalamic output synchrony during absence seizures. *Nat Neurosci* 21:744-756.
- Mederos S, Perea G (2019) GABAergic-astrocyte signalling: A refinement of inhibitory brain networks. *Glia* 67:1842-1851.
- Mederos S, Sánchez-Puelles C, Esparza J, Valero M, Ponomarenko A, Perea G (2021) GABAergic signalling to astrocytes in the prefrontal cortex sustains goal-directed behaviors. *Nat Neurosci* 24:82-92.
- Medina-Ceja L, Salazar-Sánchez JC, Ortega-Ibarra J, Morales-Villagrán A (2019) Connexins-Based Hemichannels/Channels and Their Relationship with Inflammation, Seizures and Epilepsy. *Int J Mol Sci* 20.
- Meeren HK, Pijn JP, Van Luijckelaar EL, Coenen AM, Lopes da Silva FH (2002) Cortical focus drives widespread corticothalamic networks during spontaneous absence seizures in rats. *J Neurosci* 22:1480-1495.
- Meerlo P, Westerveld P, Turek FW, Koehl M (2004) Effects of gamma-hydroxybutyrate (GHB) on vigilance states and EEG in mice. *Sleep* 27:899-904.
- Meier SD, Kafitz KW, Rose CR (2008) Developmental profile and mechanisms of GABA-induced calcium signalling in hippocampal astrocytes. *Glia* 56:1127-1137.
- Melom JE, Akbergenova Y, Gavornik JP, Littleton JT (2013) Spontaneous and Evoked Release Are Independently Regulated at Individual Active Zones. *The Journal of Neuroscience* 33:17253.
- Melø TM, Sonnewald U, Touret M, Nehlig A (2006) Cortical glutamate metabolism is enhanced in a genetic model of absence epilepsy. *J Cereb Blood Flow Metab* 26:1496-1506.
- Merlo D, Mollinari C, Inaba Y, Cardinale A, Rinaldi AM, D'Antuono M, D'Arcangelo G, Tancredi V, Ragsdale D, Avoli M (2007) Reduced GABAB receptor subunit expression and paired-pulse depression in a genetic model of absence seizures. *Neurobiol Dis* 25:631-641.
- Metzger D, Chambon P (2001) Site- and time-specific gene targeting in the mouse. *Methods* 24:71-80.
- Meyer J, Maheshwari A, Noebels J, Smirnakis S (2018) Asynchronous suppression of visual cortex during absence seizures in stargazer mice. *Nat Commun* 9:1938.
- Micheletti G (1985) Effects of GABA mimetics and GABA antagonists on spontaneous non-convulsive seizures in Wistar rats. *Epilepsy and GABA receptor antagonists* 3:129-137.
- Miller RH, Raff MC (1984) Fibrous and protoplasmic astrocytes are biochemically and developmentally distinct. *J Neurosci* 4:585-592.
- Minelli A, DeBiasi S, Brecha NC, Zuccarello LV, Conti F (1996) GAT-3, a high-affinity GABA plasma membrane transporter, is localized to astrocytic processes, and it is not confined to the vicinity of GABAergic synapses in the cerebral cortex. *J Neurosci* 16:6255-6264.
- Misgeld U, Bijak M, Jarolimek W (1995) A physiological role for GABAB receptors and the effects of baclofen in the mammalian central nervous system. *Prog Neurobiol* 46:423-462.
- Moeller F, LeVan P, Muhle H, Stephani U, Dubeau F, Siniatchkin M, Gotman J (2010) Absence seizures: individual patterns revealed by EEG-fMRI. *Epilepsia* 51:2000-2010.
- Moeller F, Siebner HR, Wolff S, Muhle H, Granert O, Jansen O, Stephani U, Siniatchkin M (2008) Simultaneous EEG-fMRI in drug-naïve children with newly diagnosed absence epilepsy. *Epilepsia* 49:1510-1519.

- Mori T, Tanaka K, Buffo A, Wurst W, Kühn R, Götz M (2006) Inducible gene deletion in astroglia and radial glia--a valuable tool for functional and lineage analysis. *Glia* 54:21-34.
- Mothet JP, Pollegioni L, Ouanounou G, Martineau M, Fossier P, Baux G (2005) Glutamate receptor activation triggers a calcium-dependent and SNARE protein-dependent release of the gliotransmitter D-serine. *Proc Natl Acad Sci U S A* 102:5606-5611.
- Mukai T, Kinboshi M, Nagao Y, Shimizu S, Ono A, Sakagami Y, Okuda A, Fujimoto M, Ito H, Ikeda A, Ohno Y (2018) Antiepileptic Drugs Elevate Astrocytic Kir4.1 Expression in the Rat Limbic Region. *Front Pharmacol* 9:845.
- Nagai J, Rajbhandari AK, Gangwani MR, Hachisuka A, Coppola G, Masmanidis SC, Fanselow MS, Khakh BS (2019) Hyperactivity with Disrupted Attention by Activation of an Astrocyte Synaptogenic Cue. *Cell* 177:1280-1292.e1220.
- Nagelhus EA, Ottersen OP (2013) Physiological roles of aquaporin-4 in brain. *Physiol Rev* 93:1543-1562.
- Nagy JI, Patel D, Ochalski PA, Stelmack GL (1999) Connexin30 in rodent, cat and human brain: selective expression in gray matter astrocytes, co-localization with connexin43 at gap junctions and late developmental appearance. *Neuroscience* 88:447-468.
- Nakai J, Ohkura M, Imoto K (2001) A high signal-to-noise Ca(2+) probe composed of a single green fluorescent protein. *Nat Biotechnol* 19:137-141.
- Nett WJ, Oloff SH, McCarthy KD (2002) Hippocampal astrocytes in situ exhibit calcium oscillations that occur independent of neuronal activity. *J Neurophysiol* 87:528-537.
- Ngomba RT, Santolini I, Salt TE, Ferraguti F, Battaglia G, Nicoletti F, van Luijckelaar G (2011a) Metabotropic glutamate receptors in the thalamocortical network: strategic targets for the treatment of absence epilepsy. *Epilepsia* 52:1211-1222.
- Ngomba RT, Biagioni F, Casciato S, Willems-van Bree E, Battaglia G, Bruno V, Nicoletti F, van Luijckelaar EL (2005) The preferential mGlu2/3 receptor antagonist, LY341495, reduces the frequency of spike-wave discharges in the WAG/Rij rat model of absence epilepsy. *Neuropharmacology* 49 Suppl 1:89-103.
- Ngomba RT, Ferraguti F, Badura A, Citraro R, Santolini I, Battaglia G, Bruno V, De Sarro G, Simonyi A, van Luijckelaar G, Nicoletti F (2008) Positive allosteric modulation of metabotropic glutamate 4 (mGlu4) receptors enhances spontaneous and evoked absence seizures. *Neuropharmacology* 54:344-354.
- Ngomba RT, Santolini I, Biagioni F, Molinaro G, Simonyi A, van Rijn CM, D'Amore V, Mastroiacovo F, Olivieri G, Gradini R, Ferraguti F, Battaglia G, Bruno V, Puliti A, van Luijckelaar G, Nicoletti F (2011b) Protective role for type-1 metabotropic glutamate receptors against spike-and-wave discharges in the WAG/Rij rat model of absence epilepsy. *Neuropharmacology* 60:1281-1291.
- Nielsen S, Nagelhus EA, Amiry-Moghaddam M, Bourque C, Agre P, Ottersen OP (1997) Specialized membrane domains for water transport in glial cells: high-resolution immunogold cytochemistry of aquaporin-4 in rat brain. *J Neurosci* 17:171-180.
- Nilsson M, Eriksson PS, Rönnbäck L, Hansson E (1993) GABA induces Ca²⁺ transients in astrocytes. *Neuroscience* 54:605-614.
- Niwa H, Yamamura K, Miyazaki J (1991) Efficient selection for high-expression transfectants with a novel eukaryotic vector. *Gene* 108:193-199.
- Noebels JL (1999) Single-gene models of epilepsy. *Adv Neurol* 79:227-238.
- Noebels JL, Sidman RL (1979) Inherited epilepsy: spike-wave and focal motor seizures in the mutant mouse tottering. *Science* 204:1334-1336.
- Noebels JL, Sidman RL (2007) Persistent hypersynchronization of neocortical neurons in the mocha mutant of mouse. *Journal of Neurogenetics* 21:253-256.
- Noebels JL, Qiao X, Bronson RT, Spencer C, Davisson MT (1990) Stargazer: a new neurological mutant on chromosome 15 in the mouse with prolonged cortical seizures. *Epilepsy Research* 7:129-135.
- Nolte C, Matyash M, Pivneva T, Schipke CG, Ohlemeyer C, Hanisch UK, Kirchhoff F, Kettenmann H (2001) GFAP promoter-controlled EGFP-expressing transgenic mice: a tool to visualize astrocytes and astrogliosis in living brain tissue. *Glia* 33:72-86.
- Norenberg MD, Martinez-Hernandez A (1979) Fine structural localization of glutamine synthetase in astrocytes of rat brain. *Brain Res* 161:303-310.
- Oberheim NA, Goldman SA, Nedergaard M (2012) Heterogeneity of astrocytic form and function. *Methods in molecular biology (Clifton, NJ)* 814:23-45.
- Oberheim NA, Wang X, Goldman S, Nedergaard M (2006) Astrocytic complexity distinguishes the human brain. *Trends in Neurosciences* 29:547-553.
- Ogata K, Kosaka T (2002) Structural and quantitative analysis of astrocytes in the mouse hippocampus. *Neuroscience* 113:221-233.
- Okubo Y, Kanemaru K, Suzuki J, Kobayashi K, Hirose K, Iino M (2019) Inositol 1,4,5-trisphosphate receptor type 2-independent Ca. *Glia* 67:113-124.

- Oliveira JF, Sardinha VM, Guerra-Gomes S, Araque A, Sousa N (2015) Do stars govern our actions? Astrocyte involvement in rodent behavior. *Trends Neurosci* 38:535-549.
- Owens DF, Kriegstein AR (2002) Is there more to GABA than synaptic inhibition? *Nat Rev Neurosci* 3:715-727.
- Palygin O, Lalo U, Verkhatsky A, Pankratov Y (2010) Ionotropic NMDA and P2X1/5 receptors mediate synaptically induced Ca²⁺ signalling in cortical astrocytes. *Cell Calcium* 48:225-231.
- Panatier A, Robitaille R (2016) Astrocytic mGluR5 and the tripartite synapse. *Neuroscience* 323:29-34.
- Panayiotopoulos CP (1999) Typical absence seizures and their treatment. *Arch Dis Child* 81:351-355.
- Panayiotopoulos CP (2008) Typical absence seizures and related epileptic syndromes: assessment of current state and directions for future research. *Epilepsia* 49:2131-2139.
- Panayiotopoulos CP, Koutroumanidis M, Giannakodimos S, Agathonikou A (1997) Idiopathic generalised epilepsy in adults manifested by phantom absences, generalised tonic-clonic seizures, and frequent absence status. *J Neurol Neurosurg Psychiatry* 63:622-627.
- Panayiotopoulos CP, Ferrie CD, Koutroumanidis M, Rowlinson S, Sanders S (2001) Idiopathic generalised epilepsy with phantom absences and absence status in a child. *Epileptic Disord* 3:63-66.
- Pangršič T, Potokar M, Stenovec M, Kreft M, Fabbretti E, Nistri A, Pryazhnikov E, Khiroug L, Giniatullin R, Zorec R (2007) Exocytotic release of ATP from cultured astrocytes. *J Biol Chem* 282:28749-28758.
- Papale LA, Beyer B, Jones JM, Sharkey LM, Tufik S, Epstein M, Letts VA, Meisler MH, Frankel WN, Escayg A (2009) Heterozygous mutations of the voltage-gated sodium channel SCN8A are associated with spike-wave discharges and absence epilepsy in mice. *Hum Mol Genet* 18:1633-1641.
- Papouin T, Dunphy J, Tolman M, Foley JC, Haydon PG (2017) Astrocytic control of synaptic function. *Philos Trans R Soc Lond B Biol Sci* 372.
- Park K, Lee SJ (2020) Deciphering the star codings: astrocyte manipulation alters mouse behavior. *Exp Mol Med* 52:1028-1038.
- Parri HR, Crunelli V (2001) Pacemaker calcium oscillations in thalamic astrocytes in situ. *Neuroreport* 12:3897-3900.
- Parri HR, Gould TM, Crunelli V (2001) Spontaneous astrocytic Ca²⁺ oscillations in situ drive NMDAR-mediated neuronal excitation. *Nat Neurosci* 4:803-812.
- Parri HR, Gould TM, Crunelli V (2010) Sensory and cortical activation of distinct glial cell subtypes in the somatosensory thalamus of young rats. *Eur J Neurosci* 32:29-40.
- Pasti L, Volterra A, Pozzan T, Carmignoto G (1997) Intracellular calcium oscillations in astrocytes: a highly plastic, bidirectional form of communication between neurons and astrocytes in situ. *J Neurosci* 17:7817-7830.
- Pastor A, Chvátal A, Syková E, Kettenmann H (1995) Glycine- and GABA-activated currents in identified glial cells of the developing rat spinal cord slice. *Eur J Neurosci* 7:1188-1198.
- Paukert M, Agarwal A, Cha J, Doze VA, Kang JU, Bergles DE (2014) Norepinephrine controls astroglial responsiveness to local circuit activity. *Neuron* 82:1263-1270.
- Paz JT, Huguenard JR (2015) Microcircuits and their interactions in epilepsy: is the focus out of focus? *Nat Neurosci* 18:351-359.
- Pearce PS, Friedman D, Lafrancois JJ, Iyengar SS, Fenton AA, Maclusky NJ, Scharfman HE (2014) Spike-wave discharges in adult Sprague-Dawley rats and their implications for animal models of temporal lobe epilepsy. *Epilepsy Behav* 32:121-131.
- Peeters BW, van Rijn CM, Vossen JM, Coenen AM (1989a) Effects of GABA-ergic agents on spontaneous non-convulsive epilepsy, EEG and behaviour, in the WAG/RIJ inbred strain of rats. *Life Sci* 45:1171-1176.
- Peeters BW, Van Rijn CM, Van Luijckelaar EL, Coenen AM (1989b) Antiepileptic and behavioural actions of MK-801 in an animal model of spontaneous absence epilepsy. *Epilepsy Res* 3:178-181.
- Peeters BW, van Rijn CM, Vossen JM, Coenen AM (1990) Involvement of NMDA receptors in non-convulsive epilepsy in WAG/Rij rats. *Life Sci* 47:523-529.
- Peeters BW, Ramakers GM, Vossen JM, Coenen AM (1994) The WAG/Rij rat model for nonconvulsive absence epilepsy: involvement of nonNMDA receptors. *Brain Res Bull* 33:709-713.
- Pelvig DP, Pakkenberg H, Stark AK, Pakkenberg B (2008) Neocortical glial cell numbers in human brains. *Neurobiol Aging* 29:1754-1762.
- Perea G, Gómez R, Mederos S, Covelo A, Ballesteros JJ, Schlosser L, Hernández-Vivanco A, Martín-Fernández M, Quintana R, Rayan A, Díez A, Fuenzalida M, Agarwal A, Bergles DE, Bettler B, Manahan-Vaughan D, Martín ED, Kirchhoff F, Araque A (2016) Activity-dependent switch of GABAergic inhibition into glutamatergic excitation in astrocyte-neuron networks. *Elife* 5.
- Pestana F, Edwards-Faret G, Belgard TG, Martirosyan A, Holt MG (2020) No Longer Underappreciated: The Emerging Concept of Astrocyte Heterogeneity in Neuroscience. *Brain Sciences* 10:168.
- Petrelli F, Bezzi P (2016) Novel insights into gliotransmitters. *Curr Opin Pharmacol* 26:138-145.
- Pierce KL, Premont RT, Lefkowitz RJ (2002) Seven-transmembrane receptors. *Nat Rev Mol Cell Biol* 3:639-650.

- Pilitsis JG, Kimelberg HK (1998) Adenosine receptor mediated stimulation of intracellular calcium in acutely isolated astrocytes. *Brain Res* 798:294-303.
- Pinault D, Leresche N, Charpier S, Deniau JM, Marescaux C, Vergnes M, Crunelli V (1998) Intracellular recordings in thalamic neurones during spontaneous spike-and-wave discharges in rats with absence epilepsy. *J Physiol* 509 (Pt 2):449-456.
- Pines G, Danbolt NC, Bjørås M, Zhang Y, Bendahan A, Eide L, Koepsell H, Storm-Mathisen J, Seeberg E, Kanner BI (1992) Cloning and expression of a rat brain L-glutamate transporter. *Nature* 360:464-467.
- Pirttimäki T, Parri HR, Crunelli V (2013) Astrocytic GABA transporter GAT-1 dysfunction in experimental absence seizures. *J Physiol* 591:823-833.
- Pirttimäki TM, Parri HR (2012) Glutamatergic input-output properties of thalamic astrocytes. *Neuroscience* 205:18-28.
- Pirttimäki TM, Hall SD, Parri HR (2011) Sustained neuronal activity generated by glial plasticity. *J Neurosci* 31:7637-7647.
- Pitkänen, A, Buckmaster, PS, Galanopoulou, AS, Moshé, SL (2017) *Models of seizures and epilepsy*: Cambridge: Academic Press.
- Podor B, Hu YL, Ohkura M, Nakai J, Croll R, Fine A (2015) Comparison of genetically encoded calcium indicators for monitoring action potentials in mammalian brain by two-photon excitation fluorescence microscopy. *Neurophotonics* 2:021014.
- Polack PO, Mahon S, Chavez M, Charpier S (2009) Inactivation of the somatosensory cortex prevents paroxysmal oscillations in cortical and related thalamic neurons in a genetic model of absence epilepsy. *Cereb Cortex* 19:2078-2091.
- Polack PO, Guillemain I, Hu E, Deransart C, Depaulis A, Charpier S (2007) Deep layer somatosensory cortical neurons initiate spike-and-wave discharges in a genetic model of absence seizures. *J Neurosci* 27:6590-6599.
- Pologruto TA, Sabatini BL, Svoboda K (2003) ScanImage: flexible software for operating laser scanning microscopes. *Biomedical engineering online* 2:13.
- Poskanzer KE, Molofsky AV (2018) Dynamism of an Astrocyte In Vivo: Perspectives on Identity and Function. *Annu Rev Physiol* 80:143-157.
- Proulx E, Leshchenko Y, Kokarotseva L, Khokhotva V, El-Beheiry M, Snead OC, Perez Velazquez JL (2006) Functional contribution of specific brain areas to absence seizures: role of thalamic gap-junctional coupling. *Eur J Neurosci* 23:489-496.
- Puigcerver A, van Luijckelaar EL, Drinkenburg WH, Coenen AL (1996) Effects of the GABAB antagonist CGP 35348 on sleep-wake states, behaviour, and spike-wave discharges in old rats. *Brain Res Bull* 40:157-162.
- Pumain R, Louvel J, Gastard M, Kurcewicz I, Vergnes M (1992) Responses to N-methyl-D-aspartate are enhanced in rats with petit mal-like seizures. *J Neural Transm Suppl* 35:97-108.
- Ramakers GM, Peeters BW, Vossen JM, Coenen AM (1991) CNQX, a new non-NMDA receptor antagonist, reduces spike wave discharges in the WAG/Rij rat model of absence epilepsy. *Epilepsy Res* 9:127-131.
- Ransom CB, Ye Z, Spain WJ, Richerson GB (2017) Modulation of Tonic GABA Currents by Anion Channel and Connexin Hemichannel Antagonists. *Neurochem Res* 42:2551-2559.
- Regan MR, Huang YH, Kim YS, Dykes-Hoberg MI, Jin L, Watkins AM, Bergles DE, Rothstein JD (2007) Variations in promoter activity reveal a differential expression and physiology of glutamate transporters by glia in the developing and mature CNS. *J Neurosci* 27:6607-6619.
- Reichenbach A, Derouiche A, Kirchhoff F (2010) Morphology and dynamics of perisynaptic glia. *Brain Research Reviews* 63:11-25.
- Reiner A, Levitz J (2018) Glutamatergic Signalling in the Central Nervous System: Ionotropic and Metabotropic Receptors in Concert. *Neuron* 98:1080-1098.
- Ribak CE, Tong WM, Brecha NC (1996) GABA plasma membrane transporters, GAT-1 and GAT-3, display different distributions in the rat hippocampus. *J Comp Neurol* 367:595-606.
- Richards DA, Lemos T, Whitton PS, Bowery NG (1995) Extracellular GABA in the ventrolateral thalamus of rats exhibiting spontaneous absence epilepsy: a microdialysis study. *J Neurochem* 65:1674-1680.
- Riquelme J, Wellmann M, Sotomayor-Zárate R, Bonansco C (2020) Gliotransmission: A Novel Target for the Development of Antiseizure Drugs. *Neuroscientist* 26:293-309.
- Risher WC, Eroglu C (2020) Chapter 3 - Astrocytes and synaptogenesis. In: *Synapse Development and Maturation* (Rubenstein J, Rakic P, Chen B, Kwan KY, Cline HT, Cardin J, eds), pp 55-75: Academic Press.
- Roth RH, Delgado JM, Giarman NJ (1966) Gamma-butyrolactone and gamma-hydroxybutyric acid. II. The pharmacologically active form. *Int J Neuropharmacol* 5:421-428.
- Rungta RL, Bernier LP, Dissing-Olesen L, Groten CJ, LeDue JM, Ko R, Drissler S, MacVicar BA (2016) Ca²⁺ transients in astrocyte fine processes occur via Ca²⁺ influx in the adult mouse hippocampus. *Glia* 64:2093-2103.
- Sahlender DA, Savtchouk I, Volterra A (2014) What do we know about gliotransmitter release from astrocytes? *Philos Trans R Soc Lond B Biol Sci* 369:20130592.

- Sarkisova K, van Luijtelaaar G (2011) The WAG/Rij strain: A genetic animal model of absence epilepsy with comorbidity of depression. *Progress in Neuro-Psychopharmacology and Biological Psychiatry* 35:854-876.
- Sasaki T, Ishikawa T, Abe R, Nakayama R, Asada A, Matsuki N, Ikegaya Y (2014) Astrocyte calcium signalling orchestrates neuronal synchronization in organotypic hippocampal slices. *J Physiol* 592:2771-2783.
- Savtchouk I, Volterra A (2018) Gliotransmission: Beyond Black-and-White. *J Neurosci* 38:14-25.
- Scemes E, Giaume C (2006) Astrocyte calcium waves: what they are and what they do. *Glia* 54:716-725.
- Schachter SC, Osborne Shafer P, Sirven JI (2013) What Causes Epilepsy and Seizures? In: <https://www.epilepsy.com/learn/about-epilepsy-basics/what-causes-epilepsy-and-seizures>.
- Schafer DP, Stevens B (2013) Phagocytic glial cells: sculpting synaptic circuits in the developing nervous system. *Curr Opin Neurobiol* 23:1034-1040.
- Scheffer IE, Berkovic S, Capovilla G, Connolly MB, French J, Guilhoto L, Hirsch E, Jain S, Mathern GW, Moshé SL, Nordli DR, Perucca E, Tomson T, Wiebe S, Zhang YH, Zuberi SM (2017) ILAE classification of the epilepsies: Position paper of the ILAE Commission for Classification and Terminology. *Epilepsia* 58:512-521.
- Schipke CG, Ohlemeyer C, Matyash M, Nolte C, Kettenmann H, Kirchhoff F (2001) Astrocytes of the mouse neocortex express functional N-methyl-D-aspartate receptors. *FASEB J* 15:1270-1272.
- Schmidt D (2009) Drug treatment of epilepsy: options and limitations. *Epilepsy Behav* 15:56-65.
- Schmitt A, Asan E, Püschel B, Kugler P (1997) Cellular and regional distribution of the glutamate transporter GLAST in the CNS of rats: nonradioactive in situ hybridization and comparative immunocytochemistry. *J Neurosci* 17:1-10.
- Scholl UI, Choi M, Liu T, Ramaekers VT, Häusler MG, Grimmer J, Tobe SW, Farhi A, Nelson-Williams C, Lifton RP (2009) Seizures, sensorineural deafness, ataxia, mental retardation, and electrolyte imbalance (SeSAME syndrome) caused by mutations in KCNJ10. *Proc Natl Acad Sci U S A* 106:5842-5847.
- Schousboe A, Waagepetersen HS (2003) Role of astrocytes in homeostasis of glutamate and GABA during physiological and pathophysiological conditions. In: *Advances in Molecular and Cell Biology*, pp 461-474: Elsevier.
- Schultz R, Maynard E, Pease D (1957) Electron microscopy of neurons and neuroglia of cerebral cortex and corpus callosum. *Am J Anat* 100:369-407.
- Schummers J, Yu H, Sur M (2008) Tuned responses of astrocytes and their influence on hemodynamic signals in the visual cortex. *Science* 320:1638-1643.
- Schwarz Y, Zhao N, Kirchhoff F, Bruns D (2017) Astrocytes control synaptic strength by two distinct v-SNARE-dependent release pathways. *Nat Neurosci* 20:1529-1539.
- Seibenhener ML, Wooten MC (2015) Use of the Open Field Maze to measure locomotor and anxiety-like behavior in mice. *J Vis Exp*:e52434.
- Seibler J, Zevnik B, Küter-Luks B, Andreas S, Kern H, Hennek T, Rode A, Heimann C, Faust N, Kauselmann G, Schoor M, Jaenisch R, Rajewsky K, Kühn R, Schwenk F (2003) Rapid generation of inducible mouse mutants. *Nucleic Acids Res* 31:e12.
- Seidel JL, Escartin C, Ayata C, Bonvento G, Shuttleworth CW (2016) Multifaceted roles for astrocytes in spreading depolarization: A target for limiting spreading depolarization in acute brain injury? *Glia* 64:5-20.
- Seifert G, Steinhäuser C (1995) Glial cells in the mouse hippocampus express AMPA receptors with an intermediate Ca²⁺ permeability. *Eur J Neurosci* 7:1872-1881.
- Semyanov A, Verkhratsky A (2021) Astrocytic processes: from tripartite synapses to the active milieu. *Trends Neurosci* 44:781-792.
- Semyanov A, Henneberger C, Agarwal A (2020) Making sense of astrocytic calcium signals - from acquisition to interpretation. *Nat Rev Neurosci* 21:551-564.
- Serrano A, Haddjeri N, Lacaille JC, Robitaille R (2006) GABAergic network activation of glial cells underlies hippocampal heterosynaptic depression. *J Neurosci* 26:5370-5382.
- Sharma G, Vijayaraghavan S (2001) Nicotinic cholinergic signalling in hippocampal astrocytes involves calcium-induced calcium release from intracellular stores. *Proc Natl Acad Sci U S A* 98:4148-4153.
- Shepherd GMG, Yamawaki N (2021) Untangling the cortico-thalamo-cortical loop: cellular pieces of a knotty circuit puzzle. *Nat Rev Neurosci* 22:389-406.
- Shi Q, Zhang T, Miao A, Sun J, Sun Y, Chen Q, Hu Z, Xiang J, Wang X (2019) Differences Between Interictal and Ictal Generalized Spike-Wave Discharges in Childhood Absence Epilepsy: A MEG Study. *Front Neurol* 10:1359.
- Shigetomi E, Patel S, Khakh BS (2016) Probing the Complexities of Astrocyte Calcium Signalling. *Trends Cell Biol* 26:300-312.
- Shigetomi E, Kracun S, Sofroniew MV, Khakh BS (2010) A genetically targeted optical sensor to monitor calcium signals in astrocyte processes. *Nature Neuroscience* 13:759-U143.
- Shigetomi E, Saito K, Sano F, Koizumi S (2019) Aberrant Calcium Signals in Reactive Astrocytes: A Key Process in Neurological Disorders. *Int J Mol Sci* 20.
- Shigetomi E, Tong X, Kwan KY, Corey DP, Khakh BS (2011) TRPA1 channels regulate astrocyte resting calcium and inhibitory synapse efficacy through GAT-3. *Nat Neurosci* 15:70-80.

- Shigetomi E, Jackson-Weaver O, Huckstepp RT, O'Dell TJ, Khakh BS (2013a) TRPA1 channels are regulators of astrocyte basal calcium levels and long-term potentiation via constitutive D-serine release. *J Neurosci* 33:10143-10153.
- Shigetomi E, Bushong EA, Hausteiner MD, Tong X, Jackson-Weaver O, Kracun S, Xu J, Sofroniew MV, Ellisman MH, Khakh BS (2013b) Imaging calcium microdomains within entire astrocyte territories and endfeet with GCaMPs expressed using adeno-associated viruses. *Journal of General Physiology* 141:633-647.
- Sicca F, Ambrosini E, Marchese M, Sforza L, Servetini I, Valvo G, Brignone MS, Lanciotti A, Moro F, Grottesi A, Catacuzzeno L, Baldini S, Hasan S, D'Adamo MC, Franciolini F, Molinari P, Santorelli FM, Pessia M (2016) Gain-of-function defects of astrocytic Kir4.1 channels in children with autism spectrum disorders and epilepsy. *Sci Rep* 6:34325.
- Sills GJ, Rogawski MA (2020) Mechanisms of action of currently used antiseizure drugs. *Neuropharmacology* 168:107966.
- Simard M, Nedergaard M (2004) The neurobiology of glia in the context of water and ion homeostasis. *Neuroscience* 129:877-896.
- Sitnikova E, van Luijckelaar G (2007) Electroencephalographic characterization of spike-wave discharges in cortex and thalamus in WAG/Rij rats. *Epilepsia* 48:2296-2311.
- Slaght SJ, Leresche N, Deniau JM, Crunelli V, Charpier S (2002) Activity of thalamic reticular neurons during spontaneous genetically determined spike-and-wave discharges. *J Neurosci* 22:2323-2334.
- Snead OC (1978) Gamma hydroxybutyrate in the monkey. I. Electroencephalographic, behavioral, and pharmacokinetic studies. *Neurology* 28:636-642.
- Snead OC (1988) gamma-Hydroxybutyrate model of generalized absence seizures: further characterization and comparison with other absence models. *Epilepsia* 29:361-368.
- Snead OC (1991) The gamma-hydroxybutyrate model of absence seizures: correlation of regional brain levels of gamma-hydroxybutyric acid and gamma-butyrolactone with spike wave discharges. *Neuropharmacology* 30:161-167.
- Snead OC (1992a) Evidence for GABAB-mediated mechanisms in experimental generalized absence seizures. *Eur J Pharmacol* 213:343-349.
- Snead OC (1992b) Pharmacological models of generalized absence seizures in rodents. *J Neural Transm Suppl* 35:7-19.
- Snead OC (1994) The ontogeny of [3H]gamma-hydroxybutyrate and [3H]GABAB binding sites: relation to the development of experimental absence seizures. *Brain Res* 659:147-156.
- Snead OC (1996) Antiabsence seizure activity of specific GABAB and gamma-Hydroxybutyric acid receptor antagonists. *Pharmacol Biochem Behav* 53:73-79.
- Snead OC, Morley BJ (1981) Ontogeny of gamma-hydroxybutyric acid. I. Regional concentration in developing rat, monkey and human brain. *Brain Res* 227:579-589.
- Sofroniew MV, Vinters HV (2010) Astrocytes: biology and pathology. *Acta Neuropathologica* 119:7-35.
- Somjen GG (1988) Nervenkitz: notes on the history of the concept of neuroglia. *Glia* 1:2-9.
- Somjen GG (2002) Ion regulation in the brain: implications for pathophysiology. *Neuroscientist* 8:254-267.
- Sorokin JM, Davidson TJ, Frechette E, Abramian AM, Deisseroth K, Huguenard JR, Paz JT (2017) Bidirectional Control of Generalized Epilepsy Networks via Rapid Real-Time Switching of Firing Mode. *Neuron* 93:194-210.
- Spreafico R, Mennini T, Danober L, Cagnotto A, Regondi MC, Miari A, De Blas A, Vergnes M, Avanzini G (1993) GABAA receptor impairment in the genetic absence epilepsy rats from Strasbourg (GAERS): an immunocytochemical and receptor binding autoradiographic study. *Epilepsy Research* 15:229-238.
- Srinivasan R, Huang BS, Venugopal S, Johnston AD, Chai H, Zeng H, Golshani P, Khakh BS (2015) Ca(2+) signalling in astrocytes from *Ip3r2(-/-)* mice in brain slices and during startle responses in vivo. *Nat Neurosci* 18:708-717.
- Sternberg N, Hamilton D (1981) Bacteriophage P1 site-specific recombination. I. Recombination between loxP sites. *J Mol Biol* 150:467-486.
- Stobart JL, Ferrari KD, Barrett MJP, Glück C, Stobart MJ, Zuend M, Weber B (2018) Cortical Circuit Activity Evokes Rapid Astrocyte Calcium Signals on a Similar Timescale to Neurons. *Neuron* 98:726-735.e724.
- Stopper G, Caudal LC, Rieder P, Gobbo D, Felix L, Everaerts K, Bai X, Stopper L, Rose CR, Scheller A, Kirchhoff F (2022) Novel algorithms for improved detection and analysis of fluorescent signal fluctuations. [bioRxiv:2022.08.2003.502593](https://doi.org/10.1101/2022.08.2003.502593).
- Storck T, Schulte S, Hofmann K, Stoffel W (1992) Structure, expression, and functional analysis of a Na(+)-dependent glutamate/aspartate transporter from rat brain. *Proc Natl Acad Sci U S A* 89:10955-10959.
- Stout CE, Costantin JL, Naus CC, Charles AC (2002) Intercellular calcium signalling in astrocytes via ATP release through connexin hemichannels. *J Biol Chem* 277:10482-10488.
- Stuart T, Butler A, Hoffman P, Hafemeister C, Papalexi E, Mauck WM, Hao Y, Stoeckius M, Smibert P, Satija R (2019) Comprehensive Integration of Single-Cell Data. *Cell* 177:1888-1902.e1821.
- Studer F, Laghouati E, Jarre G, David O, Pouyatos B, Depaulis A (2019) Sensory coding is impaired in rat absence epilepsy. *J Physiol* 597:951-966.

- Suadicani SO, Brosnan CF, Scemes E (2006) P2X7 receptors mediate ATP release and amplification of astrocytic intercellular Ca²⁺ signalling. *J Neurosci* 26:1378-1385.
- Suadicani SO, Iglesias R, Wang J, Dahl G, Spray DC, Scemes E (2012) ATP signalling is deficient in cultured Pannexin1-null mouse astrocytes. *Glia* 60:1106-1116.
- Sun W, McConnell E, Pare JF, Xu Q, Chen M, Peng W, Lovatt D, Han X, Smith Y, Nedergaard M (2013) Glutamate-dependent neuroglial calcium signalling differs between young and adult brain. *Science* 339:197-200.
- Szatkowski M, Barbour B, Attwell D (1990) Non-vesicular release of glutamate from glial cells by reversed electrogenic glutamate uptake. *Nature* 348:443-446.
- Takano T, Kang J, Jaiswal JK, Simon SM, Lin JH, Yu Y, Li Y, Yang J, Dienel G, Zielke HR, Nedergaard M (2005) Receptor-mediated glutamate release from volume sensitive channels in astrocytes. *Proc Natl Acad Sci U S A* 102:16466-16471.
- Tan Heneu O, Reid Christopher A, Single Frank N, Davies Philip J, Chiu C, Murphy S, Clarke Alison L, Dibbens L, Krestel H, Mulley John C, Jones Mathew V, Seeburg Peter H, Sakmann B, Berkovic Samuel F, Sprengel R, Petrou S (2007) Reduced cortical inhibition in a mouse model of familial childhood absence epilepsy. *Proceedings of the National Academy of Sciences* 104:17536-17541.
- Tanaka K (1993) Expression cloning of a rat glutamate transporter. *Neurosci Res* 16:149-153.
- Tangwiriyasakul C, Perani S, Centeno M, Yaakub SN, Abela E, Carmichael DW, Richardson MP (2018) Dynamic brain network states in human generalized spike-wave discharges. *Brain* 141:2981-2994.
- Tasic B et al. (2018) Shared and distinct transcriptomic cell types across neocortical areas. *Nature* 563:72-78.
- Taylor-Courval D, Gloor P (1984) Behavioral alterations associated with generalized spike-and-wave discharges in the EEG of the cat. *Exp Neurol* 83:167-186.
- Tellez-Zenteno JF, Patten SB, Jetté N, Williams J, Wiebe S (2007) Psychiatric comorbidity in epilepsy: a population-based analysis. *Epilepsia* 48:2336-2344.
- Tenney JR, Marshall PC, King JA, Ferris CF (2004) fMRI of generalized absence status epilepticus in conscious marmoset monkeys reveals corticothalamic activation. *Epilepsia* 45:1240-1247.
- Tenney JR, Duong TQ, King JA, Ludwig R, Ferris CF (2003) Corticothalamic modulation during absence seizures in rats: a functional MRI assessment. *Epilepsia* 44:1133-1140.
- Terlau J, Yang JW, Khastkhodaei Z, Seidenbecher T, Luhmann HJ, Pape HC, Lüttjohann A (2020) Spike-wave discharges in absence epilepsy: segregation of electrographic components reveals distinct pathways of seizure activity. *J Physiol* 598:2397-2414.
- Tian GF, Azmi H, Takano T, Xu QW, Peng WG, Lin J, Oberheim N, Lou NH, Wang XH, Zielke HR, Kang J, Nedergaard M (2005) An astrocytic basis of epilepsy. *Nature Medicine* 11:973-981.
- Tian L, Hires SA, Mao T, Huber D, Chiappe ME, Chalasani SH, Petreanu L, Akerboom J, McKinney SA, Schreiner ER, Bargmann CI, Jayaraman V, Svoboda K, Looger LL (2009) Imaging neural activity in worms, flies and mice with improved GCaMP calcium indicators. *Nat Methods* 6:875-881.
- Touret M, Parrot S, Denoroy L, Belin MF, Didier-Bazes M (2007) Glutamatergic alterations in the cortex of genetic absence epilepsy rats. *BMC Neurosci* 8:69.
- Tsai HH, Li H, Fuentealba LC, Molofsky AV, Taveira-Marques R, Zhuang H, Tenney A, Murnen AT, Fancy SP, Merkle F, Kessaris N, Alvarez-Buylla A, Richardson WD, Rowitch DH (2012) Regional astrocyte allocation regulates CNS synaptogenesis and repair. *Science* 337:358-362.
- Ujita S, Sasaki T, Asada A, Funayama K, Gao M, Mikoshiba K, Matsuki N, Ikegaya Y (2017) cAMP-Dependent Calcium Oscillations of Astrocytes: An Implication for Pathology. *Cereb Cortex* 27:1602-1614.
- Unichenko P, Myakhar O, Kirischuk S (2012) Intracellular Na⁺ concentration influences short-term plasticity of glutamate transporter-mediated currents in neocortical astrocytes. *Glia* 60:605-614.
- Unichenko P, Dvorzhak A, Kirischuk S (2013) Transporter-mediated replacement of extracellular glutamate for GABA in the developing murine neocortex. *Eur J Neurosci* 38:3580-3588.
- van Luijtelaar EL, Coenen AM (1986) Two types of electrocortical paroxysms in an inbred strain of rats. *Neurosci Lett* 70:393-397.
- van Luijtelaar EL, Drinkenburg WH, van Rijn CM, Coenen AM (2002) Rat models of genetic absence epilepsy: what do EEG spike-wave discharges tell us about drug effects? *Methods Find Exp Clin Pharmacol* 24 Suppl D:65-70.
- van Luijtelaar G, Sitnikova E (2006) Global and focal aspects of absence epilepsy: the contribution of genetic models. *Neurosci Biobehav Rev* 30:983-1003.
- van Luijtelaar G, Behr C, Avoli M (2014) Is there such a thing as "generalized" epilepsy? *Adv Exp Med Biol* 813:81-91.
- Ventura R, Harris KM (1999) Three-dimensional relationships between hippocampal synapses and astrocytes. *J Neurosci* 19:6897-6906.
- Venzi M, Di Giovanni G, Crunelli V (2015) A critical evaluation of the gamma-hydroxybutyrate (GHB) model of absence seizures. *CNS Neurosci Ther* 21:123-140.

- Verderio C, Cagnoli C, Bergami M, Francolini M, Schenk U, Colombo A, Riganti L, Frassoni C, Zuccaro E, Danglot L, Wilhelm C, Galli T, Canossa M, Matteoli M (2012) TI-VAMP/VAMP7 is the SNARE of secretory lysosomes contributing to ATP secretion from astrocytes. *Biol Cell* 104:213-228.
- Vergnes M, Boehrer A, Simler S, Bernasconi R, Marescaux C (1997) Opposite effects of GABAB receptor antagonists on absences and convulsive seizures. *Eur J Pharmacol* 332:245-255.
- Vergnes M, Marescaux C, Micheletti G, Depaulis A, Rumbach L, Warter JM (1984) Enhancement of spike-and-wave discharges by GABA-mimetic drugs in rats with spontaneous petit-mal-like epilepsy. *Neurosci Lett* 44:91-94.
- Vergnes M, Marescaux C, Micheletti G, Reis J, Depaulis A, Rumbach L, Warter JM (1982) Spontaneous paroxysmal electroclinical patterns in rat: A model of generalized non-convulsive epilepsy. *Neuroscience Letters* 33:97-101.
- Verkhatsky A, Butt A (2013) Neuroglia: Definition, Classification. Evolution, Numbers, Development *Glial Physiology and Pathophysiology*:73-104.
- Verkhatsky A, Nedergaard M (2014) Astroglial cradle in the life of the synapse. *Philos Trans R Soc Lond B Biol Sci* 369:20130595.
- Verkhatsky A, Nedergaard M (2018) Physiology of Astroglia. *Physiol Rev* 98:239-389.
- Verkhatsky A, Orkand RK, Kettenmann H (1998) Glial calcium: homeostasis and signalling function. *Physiol Rev* 78:99-141.
- Verkhatsky A, Rodríguez JJ, Parpura V (2012) Calcium signalling in astroglia. *Mol Cell Endocrinol* 353:45-56.
- Vichai V, Kirtikara K (2006) Sulforhodamine B colorimetric assay for cytotoxicity screening. *Nat Protoc* 1:1112-1116.
- Vienne J, Bettler B, Franken P, Tafti M (2010) Differential effects of GABAB receptor subtypes, γ -hydroxybutyric Acid, and Baclofen on EEG activity and sleep regulation. *J Neurosci* 30:14194-14204.
- Vincze R, Péter M, Szabó Z, Kardos J, Héja L, Kovács Z (2019) Connexin 43 Differentially Regulates Epileptiform Activity in Models of Convulsive and Non-convulsive Epilepsies. *Front Cell Neurosci* 13:173.
- Virchow R (1856) Über das granulirte Aussehen der Wandungen des Gehirnaventrikels. In: *Gesammelte Abhandlungen zur wissenschaftlichen Medizin*, pp 885-891. Frankfurt.
- Volterra A, Liaudet N, Savtchouk I (2014) Astrocyte Ca^{2+} signalling: an unexpected complexity. *Nat Rev Neurosci* 15:327-335.
- von Bartheld CS, Bahney J, Herculano-Houzel S (2016) The search for true numbers of neurons and glial cells in the human brain: A review of 150 years of cell counting. *J Comp Neurol* 524:3865-3895.
- von Krosigk M, Bal T, McCormick DA (1993) Cellular mechanisms of a synchronized oscillation in the thalamus. *Science* 261:361-364.
- von Lenhossék M (1895) Die Stützzellen des Rückenmarkes. In: *Der Feinere Bau des Nervensystems im Lichte neuerer Forschung*, Second Edition (Kornfeld BNFsMBH, ed), pp 176-247.
- Vélez-Fort M, Audinat E, Angulo MC (2012) Central role of GABA in neuron-glia interactions. *Neuroscientist* 18:237-250.
- Walch E, Murphy TR, Cuvelier N, Aldoghmi M, Morozova C, Donohue J, Young G, Samant A, Garcia S, Alvarez C, Bilas A, Davila D, Binder DK, Fiacco TA (2020) Astrocyte-Selective Volume Increase in Elevated Extracellular Potassium Conditions Is Mediated by the Na. *ASN Neuro* 12:1759091420967152.
- Wallraff A, Köhling R, Heinemann U, Theis M, Willecke K, Steinhäuser C (2006) The impact of astrocytic gap junctional coupling on potassium buffering in the hippocampus. *J Neurosci* 26:5438-5447.
- Wang F, Qi X, Zhang J, Huang JH (2020) Astrocytic modulation of potassium under seizures. *Neural Regen Res* 15:980-987.
- Wang X, Lou N, Xu Q, Tian G-F, Peng WG, Han X, Kang J, Takano T, Nedergaard M (2006) Astrocytic Ca^{2+} signalling evoked by sensory stimulation in vivo. *Nature Neuroscience* 9:816-823.
- Warr O, Takahashi M, Attwell D (1999) Modulation of extracellular glutamate concentration in rat brain slices by cystine-glutamate exchange. *J Physiol* 514 (Pt 3):783-793.
- Wellmann M, Álvarez-Ferradas C, Maturana CJ, Sáez JC, Bonansco C (2018) Astroglial Ca^{2+} -Dependent Hyperexcitability Requires P2Y1 Purinergic Receptors and Pannexin-1 Channel Activation in a Chronic Model of Epilepsy. *Front Cell Neurosci* 12:446.
- Williams SM, Sullivan RK, Scott HL, Finkelstein DI, Colditz PB, Lingwood BE, Dodd PR, Pow DV (2005) Glial glutamate transporter expression patterns in brains from multiple mammalian species. *Glia* 49:520-541.
- Williams SR, Turner JP, Crunelli V (1995) Gamma-hydroxybutyrate promotes oscillatory activity of rat and cat thalamocortical neurons by a tonic GABAB, receptor-mediated hyperpolarization. *Neuroscience* 66:133-141.
- Winnubst J et al. (2019) Reconstruction of 1,000 Projection Neurons Reveals New Cell Types and Organization of Long-Range Connectivity in the Mouse Brain. *Cell* 179:268-281.e213.
- Winters W, Spooner C (1964) A neurophysiological comparison of gamma-hydroxybutyrate with pentobarbital in cats. *Electroencephalogram Clin Neurophysiol* 18:287-229.

- Woo DH, Han KS, Shim JW, Yoon BE, Kim E, Bae JY, Oh SJ, Hwang EM, Marmorstein AD, Bae YC, Park JY, Lee CJ (2012) TREK-1 and Best1 channels mediate fast and slow glutamate release in astrocytes upon GPCR activation. *Cell* 151:25-40.
- World Health Organization (2022) Epilepsy. In. www.who.int/news-room/fact-sheets/detail/epilepsy.
- Wu Y, Ali S, Ahmadian G, Liu CC, Wang YT, Gibson KM, Calver AR, Francis J, Pangalos MN, Carter Snead O (2004) Gamma-hydroxybutyric acid (GHB) and gamma-aminobutyric acidB receptor (GABABR) binding sites are distinctive from one another: molecular evidence. *Neuropharmacology* 47:1146-1156.
- Wu Z, He K, Chen Y, Li H, Pan S, Li B, Liu T, Xi F, Deng F, Wang H, Du J, Jing M, Li Y (2022) A sensitive GRAB sensor for detecting extracellular ATP in vitro and in vivo. *Neuron* 110:770-782.e775.
- Ximerakis M, Lipnick SL, Innes BT, Simmons SK, Adiconis X, Dionne D, Mayweather BA, Nguyen L, Niziolek Z, Ozek C, Butty VL, Isserlin R, Buchanan SM, Levine SS, Regev A, Bader GD, Levin JZ, Rubin LL (2019) Single-cell transcriptomic profiling of the aging mouse brain. *Nat Neurosci* 22:1696-1708.
- Yang Y, Vidensky S, Jin L, Jie C, Lorenzini I, Frankl M, Rothstein JD (2011) Molecular comparison of GLT1+ and ALDH1L1+ astrocytes in vivo in astroglial reporter mice. *Glia* 59:200-207.
- Ye L, Haroon MA, Salinas A, Paukert M (2017) Comparison of GCaMP3 and GCaMP6f for studying astrocyte Ca²⁺ dynamics in the awake mouse brain. *PLoS One* 12:e0181113.
- Ye ZC, Wyeth MS, Baltan-Tekkok S, Ransom BR (2003) Functional hemichannels in astrocytes: a novel mechanism of glutamate release. *J Neurosci* 23:3588-3596.
- Yu X, Taylor AMW, Nagai J, Golshani P, Evans CJ, Coppola G, Khakh BS (2018) Reducing Astrocyte Calcium Signalling In Vivo Alters Striatal Microcircuits and Causes Repetitive Behavior. *Neuron* 99:1170-1187.e1179.
- Zeisel A, Muñoz-Manchado AB, Codeluppi S, Lönnerberg P, La Manno G, Juréus A, Marques S, Munguba H, He L, Betsholtz C, Rolny C, Castelo-Branco G, Hjerling-Leffler J, Linnarsson S (2015) Cell types in the mouse cortex and hippocampus revealed by single-cell RNA-seq. *Science* 347:1138-1142.
- Zeng W, Mak DO, Li Q, Shin DM, Foskett JK, Muallem S (2003) A new mode of Ca²⁺ signalling by G protein-coupled receptors: gating of IP₃ receptor Ca²⁺ release channels by Gbetagamma. *Curr Biol* 13:872-876.
- Zhang RW, Du WJ, Prober DA, Du JL (2019) Müller Glial Cells Participate in Retinal Waves via Glutamate Transporters and AMPA Receptors. *Cell Rep* 27:2871-2880.e2872.
- Zhang Y, Barres BA (2010) Astrocyte heterogeneity: an underappreciated topic in neurobiology. *Curr Opin Neurobiol* 20:588-594.
- Zhang Y, Chen K, Sloan SA, Bennett ML, Scholze AR, O'Keefe S, Phatnani HP, Guarnieri P, Caneda C, Ruderisch N, Deng S, Liddelow SA, Zhang C, Daneman R, Maniatis T, Barres BA, Wu JQ (2014) An RNA-sequencing transcriptome and splicing database of glia, neurons, and vascular cells of the cerebral cortex. *J Neurosci* 34:11929-11947.
- Zhang Y, Sloan SA, Clarke LE, Caneda C, Plaza CA, Blumenthal PD, Vogel H, Steinberg GK, Edwards MS, Li G, Duncan JA, Cheshier SH, Shuer LM, Chang EF, Grant GA, Gephart MG, Barres BA (2016) Purification and Characterization of Progenitor and Mature Human Astrocytes Reveals Transcriptional and Functional Differences with Mouse. *Neuron* 89:37-53.
- Zhang Z, Chen G, Zhou W, Song A, Xu T, Luo Q, Wang W, Gu XS, Duan S (2007) Regulated ATP release from astrocytes through lysosome exocytosis. *Nat Cell Biol* 9:945-953.
- Zheng K, Bard L, Reynolds JP, King C, Jensen TP, Gourine AV, Rusakov DA (2015) Time-Resolved Imaging Reveals Heterogeneous Landscapes of Nanomolar Ca²⁺ in Neurons and Astroglia. *Neuron* 88:277-288.
- Zorec R, Araque A, Carmignoto G, Haydon PG, Verkhratsky A, Parpura V (2012) Astroglial excitability and gliotransmission: an appraisal of Ca²⁺ as a signalling route. *Asn Neuro* 4:103-119.

12 ACKNOWLEDGEMENTS

Firstly, I would like to thank my supervisor Prof. Frank Kirchhoff for welcoming me in the group, challenging and supporting me throughout my PhD project. To you goes my deepest appreciation for trusting me and believing in me and my capabilities. It has been an amazing journey through science and the world.

I thank Prof. Jutta Engel for accepting to read and review my work.

I am thankful to Prof. Vincenzo Crunelli for the scientific discussion and guidance within my project. I would like to express my most sincere gratitude to Dr. Giorgio Carmignoto for the invaluable support and consideration since the beginning of my scientific carrier.

I would like to thank the European Union's Horizon 2020 Research and Innovation Programme for funding this project (Marie Skłodowska-Curie grant agreement No. 722053) along with the Deutsche Forschungsgemeinschaft DFG (SFB 894, SFB 1158, SPP 1757).

I thank all the current and former member of the Kirchhoff group and everybody that visited us through the years. Each of you made my life in the lab a constant grow and I cherish every day I had the chance to spend with you.

I would like to particularly thank Anja Scheller for the constant support and guidance and for being at my side against any challenge, from the smallest problem to the biggest doubt. My appreciation goes also to Wenhui Huang and Xianshu Bai for helping me and being unaware scientific role models. It has been a pleasure to work with you. I also thank Na Zhao for keeping an eye on me and supporting me in the moments of need.

I would like to thank my one and only co-first ESR Laura Caudal for everything that we shared during our PhDs and for everything that we still share beyond the lab and beyond science. Thank you Lipao Fang and Qilin Guo for your help with my work and for being a constant source of positivity in the lab: Liu Qing, thank you for being there when I needed a break, even just for a minute. A very special thank you goes to the Dream Team Emeline Buttigieg and Phillip Rieder, who always managed to make the bad days good and the good days better. I could not wish for better company for my journey!

I would like to thank all those who entered my life through the glass windows of the lab and did not leave. Thank you Erika Meyer, Mariza Bortolanza and Naielly Rodrigues da Silva for sharing your authenticity and warmth in everything that we did together. Thank you to Elisa Damo, with whom I share and will share forever an unbreakable bond.

Once again I thank each and every member of the Kirchhoff lab for these last years together and the wonderful team spirit, not only the people above listed but also many many others, including

Gebhard Stopper, Ahmad Lotfinia, Yasser Medlej, Michael Schweigmann, Rhea Seth, Frank Rhode, Daniel Schauenburg and Ute Legler.

I would like to thank all my closest friends all around the world that never failed to make me feel their support and their vicinity through the years. To you goes my greatest appreciation and affection for your unconditional friendship.

Ich möchte Thorsten für seine ständige Unterstützung in der letzten und schwierigsten Phase dieser Reise danken, dafür, dass er mein Anker ist und mir ermöglicht, die Welt mit anderen Augen zu sehen. Ihm gelten meine Zuneigung und meine Dankbarkeit.

Vorrei infine ringraziare la mia famiglia, mio fratello Francesco e i miei genitori Anny e Enzo, che mi hanno permesso di raggiungere questo traguardo con il loro costante supporto e il loro amore incondizionato.

A voi dedico questo lavoro, poiché voi lo avete reso possibile.

13 CURRICULUM VITAE AND LIST OF PUBLICATIONS

The curriculum vitae was removed from the electronic version of the doctoral thesis for reasons of data protection

